IRE
Transactions
on ANTENNAS and PROPAGATION

Volume AP-7 JULY, 1959 Number 3

Published Quarterly

TABLE OF CONTENTS

CONTRIBUTIONS

COMMUNICATIONS

PUBLISHED BY THE
ofessional Group on Antennas and Propagation

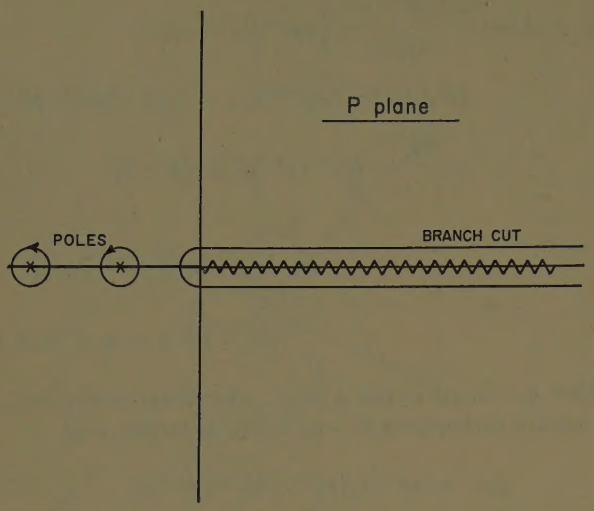

Fig. 2—Path of integration.

$$p_1^2 + q_1^2 = \epsilon_r - 1 \tag{20}$$

$$\frac{K_1(Kaq_1)}{q_1K_0(Kaq_1)} + \frac{\epsilon_r J_1(Kap_1)}{p_1J_0(Kap_1)} = 0. \tag{21}$$

Eqs. (16) and (17) agree exactly with the $TM_{0,1}$ surface wave term given by Schelkunoff.[4] Eqs. (20) and (21) are deduced from $p'-p=K^2(\epsilon_r-1)$ and $g(p)=0$ for $Kp_1=p'^{1/2}$ and $Kq_1=jp^{1/2}$.

The integration of $G(\rho, \rho', p)$ around its branch cut yields the continuous set of modes. It is clear that the integrations along the top and bottom of the branch cut can be combined and simplified since the only change in crossing the branch cut is a jump of 2π in the phase angle of p. The resulting combined integral has exactly the form of

$$\int_0^\infty \phi(\lambda, \rho)\phi(\lambda', \rho)d\lambda$$

after a change of variable $\lambda=p^{1/2}$ and $\lambda'=p'^{1/2}$, where the path of integration is understood to be underneath the branch cut from 0 to ∞. Thus the continuous set of modes is as follows:

$$\phi(\lambda, \rho) = \frac{N_0(\lambda a)J_1(\lambda\rho) - J_0(\lambda a)N_1(\lambda\rho) - \dfrac{\lambda' J_0(\lambda' a)}{\epsilon_r \lambda J_1(\lambda' a)}\left[N_1(\lambda a)J_1(\lambda\rho) - J_1(\lambda a)N_1(\lambda\rho)\right]}{\left(X\dfrac{2\pi}{\lambda}\right)^{1/2}} \quad \text{for } \rho > a, \tag{22}$$

$$\phi(\lambda, \rho) = \frac{2J_1(\lambda'\rho)}{\pi\lambda a J_1(\lambda' a)\left(X\dfrac{2\pi}{\lambda}\right)^{1/2}} \quad \text{for } \rho < a, \tag{23}$$

[4] S. A. Schelkunoff, "Electromagnetic Waves," D. Van Nostrand Book Co., Inc., New York, N. Y., pp. 425–428; 1943.

where

$$X = \left[H_0^{(1)}(\lambda a) - \frac{\lambda' J_0(\lambda' a)}{\epsilon_r \lambda J_1(\lambda' a)} H_1^{(1)}(\lambda a)\right] \cdot \left[H_0^{(2)}(\lambda a) - \frac{\lambda' J_0(\lambda' a)}{\epsilon_r \lambda J_1(\lambda' a)} H_1^{(2)}(\lambda a)\right]. \tag{24}$$

When $\epsilon_r=1$, the $G(\rho, \rho', p)$ has no pole. Therefore ψ does not have the descrete set of modes. The modes exhibited in (22) and (23) reduce immediately to the well-known Fourier-Bessel transform.

Hence,

$$\psi(\nu, \rho) = \frac{J_1(\nu, \rho)}{\left(\dfrac{2\pi}{\nu}\right)^{1/2}}. \tag{25}$$

Knowing the functions ϕ and ψ, we can rewrite (1) and (2) formally as,

$$\left.\begin{aligned} H_\phi &= I_1(z)\phi_1(\rho) + \int_0^\infty I(\lambda, z)\phi(\lambda, \rho)d\lambda \qquad (26)\\ \epsilon E_\rho &= V_1(z)\phi_1(\rho) + \int_0^\infty V(\lambda, z)\phi(\lambda, p)d\lambda \qquad (27)\end{aligned}\right\} \text{ for } z < 0,$$

and

$$\left.\begin{aligned} H_\phi &= \int_0^\infty I'(\nu, z)\psi(\nu, \rho)d\nu \qquad (28)\\ E_\rho &= \int_0^\infty V'(\nu, z)\psi(\nu, \rho)d\nu \qquad (29)\end{aligned}\right\} \text{ for } z > 0.$$

The Variational Expression for the Terminal Admittance

If the representation given in (26)–(29) is used in Maxwell's equations written as in (3) and (4), one finds immediately that V, I, V', and I' must satisfy the following equations:

$$\left.\begin{aligned} \frac{dV_1}{dz} &= -j\frac{K^2(1+q_1^2)}{\omega\epsilon_0} I_1 \qquad (30a)\\ \frac{dI_1}{dz} &= -j\omega\epsilon_0 V_1 \qquad (30b)\end{aligned}\right\} \text{ for } z < 0,$$

$$\left.\begin{aligned} \frac{dV(\lambda, z)}{dz} &= -j\frac{K^2-\lambda^2}{\omega\epsilon_0} I(\lambda, z) \qquad (31a)\\ \frac{dI(\lambda, z)}{dz} &= -j\omega\epsilon_0 V(\lambda, z) \qquad (31b)\end{aligned}\right\} \text{ for } z < 0,$$

and

$$\frac{dV'(\nu, z)}{dz} = -j\frac{K^2 - \nu^2}{\omega\epsilon_0} I'(\nu, z) \quad \text{for } z > 0, \tag{32a}$$

$$\frac{dI'(\nu, z)}{dz} = -j\omega\epsilon_0 V'(\nu, z) \tag{32b}$$

plus the boundary condition that $I(\lambda, z)$, $V(\lambda, z)$, $I'(\nu, z)$, and $V'(\nu, z)$ must represent outgoing waves at $z=0$. Therefore,

$$I_1(z) = I_1(0)\cos\left[Kz(1+q_1^2)^{1/2}\right] - j\frac{\omega\epsilon_0}{K(1+q_1^2)^{1/2}} V_1(0)\sin\left[Kz(1+q_1^2)^{1/2}\right] \tag{33a}$$

$$I(\lambda, z) = -\frac{\omega\epsilon_0}{(K^2-\lambda^2)^{1/2}} V(\lambda, 0)\exp\left\{j(K^2-\lambda^2)^{1/2}z\right\} \quad \text{for } z < 0 \tag{33b}$$

$$I'(\nu, z) = \frac{\omega\epsilon_0}{(K^2-\nu^2)^{1/2}} V'(\nu, 0)\exp\left\{-j(K^2-\nu^2)^{1/2}z\right\} \quad \text{for } z > 0. \tag{34}$$

The complete solution to our problem is obtained if the following continuity condition for E_ρ and H_ϕ at $z=0$ are met:

$$I_1(0)\phi_1(\rho) + \int_0^\infty I(\lambda, 0)\phi(\lambda, \rho)d\lambda = \int_0^\infty I'(\nu, 0)\psi(\nu, \rho)d\nu \tag{35}$$

$$V_1(0)\frac{\phi_1(\rho)}{\epsilon(\rho)} + \int_0^\infty V(\lambda, 0)\frac{\phi(\lambda, \rho)}{\epsilon(\rho)}d\lambda = \int_0^\infty V'(\nu, 0)\psi(\nu, \rho)d\nu. \tag{36}$$

These two integral equations are very hard to solve.

$$I_1(0)\phi_1(\rho) = \int_0^\infty I'(\nu, 0)\psi(\nu, \rho)d\nu - \int_0^\infty I(\lambda, 0)\phi(\lambda, \rho)d\lambda$$
$$= \int_0^\infty \frac{\omega\epsilon_0}{(K^2-\nu^2)^{1/2}} V'(\nu, 0)\psi(\nu, \rho)d\nu + \int_0^\infty \frac{\omega\epsilon_0}{(K^2-\lambda^2)^{1/2}} V(\lambda, 0)\phi(\lambda, \rho)d\lambda \tag{37}$$

but,

$$V'(\nu, 0) = \int_0^\infty E_\rho(0, \rho')\psi(\nu, \rho')2\pi\rho'd\rho \tag{38}$$

$$V(\lambda, 0) = \int_0^\infty E_\rho(0, \rho')\phi(\lambda, \rho')2\pi\rho'd\rho'. \tag{39}$$

Hence,

$$I_1(0)\phi_1(\rho) = \int_0^\infty \Lambda E_\rho(0, \rho')2\pi\rho'd\rho' \tag{40}$$

where

$$\Lambda = \int_0^\infty \frac{\omega\epsilon_0}{(K^2-\nu^2)^{1/2}}\psi(\nu, \rho)\psi(\nu, \rho')d\nu + \int_0^\infty \frac{\omega\epsilon_0}{(K^2-\lambda^2)^{1/2}}\phi(\lambda, \rho)\phi(\lambda, \rho')d\lambda \tag{41}$$

is the dyadic kernel of (40).

Operating both sides of (40) with $\int_0^\infty E\rho(0, \rho)2\pi\rho d\rho$, one obtains

$$I_1(0)V_1(0) = \int_0^\infty E_\rho(0, \rho)2\pi\rho d\rho \int_0^\infty \Lambda E_\rho(0, \rho')2\pi\rho'd\rho. \tag{42}$$

However,

$$V_1(0) = \int_0^\infty E_\rho(0, \rho)\phi_1(\rho)2\pi\rho d\rho. \tag{43}$$

Therefore

$$\frac{I_1(0)}{V_1(0)} = \mathcal{Y}_{11}(0) = \frac{\displaystyle\int_0^\infty \frac{\omega\epsilon_0}{(K^2-\lambda^2)^{1/2}}\left[\int_0^\infty E_\rho(0, \rho)\phi(\lambda, \rho)2\pi\rho d\rho\right]^2 d\lambda + \int_0^\infty \frac{\omega\epsilon_0}{(K^2-\nu^2)^{1/2}}\left[\int_0^\infty E_\rho(0, \rho)\psi(\nu, \rho)2\pi\rho d\rho\right]^2 d\nu}{\left[\displaystyle\int_0^\infty \phi_1(\rho)E_\rho(0, \rho)2\pi\rho d\rho\right]^2}. \tag{44}$$

Therefore, a variation expression for the terminal admittance, $I_1(0)/V_1(0)$, will be set up based on (35).

Eq. (35) can be rewritten as

This is a variational expression for the terminal admittance, $\mathcal{Y}_{11}(0)$. It is the extremum for the exact unknown field $E_\rho(0, \rho)$ and independent of the amplitude

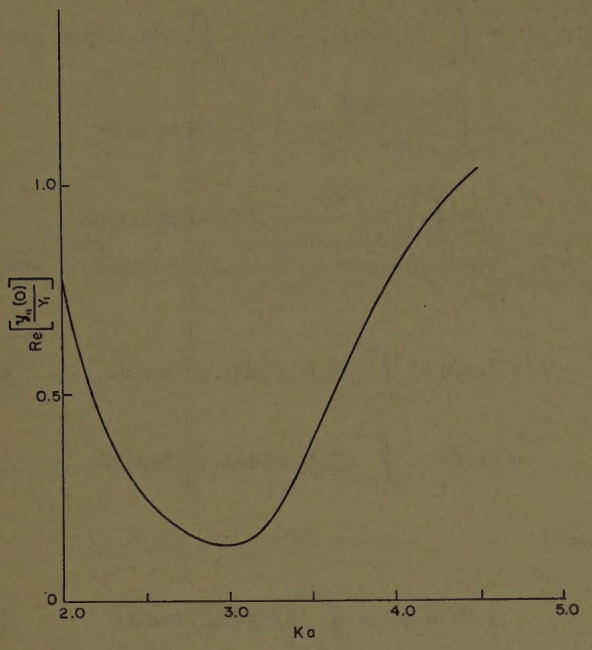

Fig. 3—Plot of the conductance.

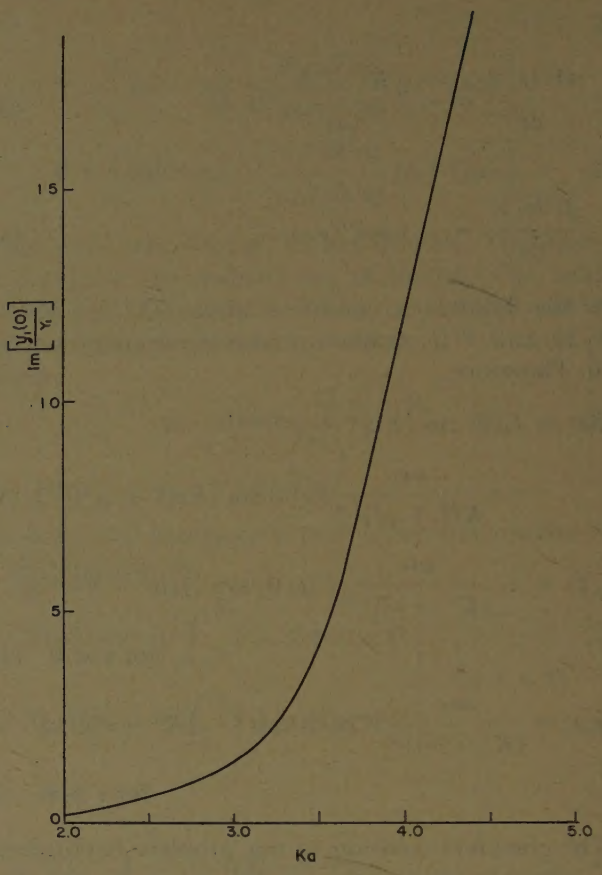

Fig. 4—Plot of the susceptance.

of $E_\rho(0, \rho)$. If a trial field is inserted, the error in the admittance would be of higher order than the error of the field.

We assume here that the field $E_\rho(0, \rho)$ is the field of the $TM_{0,1}$ surface wave. Then,

$$\begin{aligned} \mathcal{Y}_{11}(0) &= \int_0^\infty \frac{\omega\epsilon_0}{(K^2 - \nu^2)^{1/2}} \left[\int_0^\infty \psi(\nu, \rho) \frac{\phi_1(\rho)}{\epsilon(\rho)} 2\pi\rho d\rho \right]^2 d\nu \\ &= \frac{8(Ka)^3}{\pi K^2 N^2} \left(\frac{\epsilon_0}{\mu_0}\right)^{1/2} \int_0^\infty \frac{x}{(K^2a^2 - x^2)^{1/2}} \left\{ \frac{Kaq_1K_0(Kaq_1)J_1(x) + xK_1(kaq_1)J_0(x)}{x^2 + K^2a^2q_1^2} \right. \\ &\quad \left. + \frac{Kaq_1K_0(Kaq_1)J_1(x) + \frac{x}{\epsilon_r} K_1(Kaq_1)J_0(x)}{x^2 - K^2a^2p_1^2} \right\}^2 dx. \end{aligned} \tag{45}$$

Eq. (45) is numerically computed for $\epsilon_r = 2.49$, for various values of Ka. Its final numerical results are shown vs Ka in Figs. 3 and 4 for

$$\text{Real}\left[\left(\frac{\mu_0(1 + q_1^2)}{\epsilon_0}\right)^{1/2} \mathcal{Y}_{11}(0)\right]$$

and

$$\text{Imag}\left\{\left[\frac{\mu_0(1 + q_1^2)}{\epsilon_0}\right]^{1/2} \mathcal{Y}_{11}(0)\right\}$$

respectively, where

$$Y_1 = \left[\frac{\epsilon_0}{\mu_0(1 + q_1^2)}\right]^{1/2}.$$

Y_1 is the characteristic impedance of the ϕ_1 mode along the dielectric rod [see (30)].

Radiation from Slot Arrays on Cones*

R. F. GOODRICH†, R. E. KLEINMAN†, A. L. MAFFETT‡, C. E. SCHENSTED†, K. M. SIEGEL†, M. G. CHERNIN§, H. E. SHANKS§, AND R. E. PLUMMER§

Summary—A method is obtained for determining far field patterns, sidelobes as well as the main beam, for an array of slots on the surface of a cone. It is found that accurate results can be obtained for a single slot by using geometric optics for the main beam and an extension of Fock theory for fields in the shadow region. The tip contribution is computed by physical optics and, for reasonably thin cones, is found to be negligible. The array pattern is obtained by appropriately summing the single slot fields. To test the validity of the method and to test the ease with which computations could be performed, a radiation pattern from a linear array of 65 slots on the surface of a cone was computed and compared with experiment. The agreement is excellent.

The major theoretical part of this paper is the generalization and simplification of Fock theory as applied to the surface of a cone.

I. The Far Field of a Slot on a Cone

TO find the radiation pattern of a single infinitesimal slot located on the surface of a cone we make use of 1) the equivalence of a magnetic dipole and an infinitesimal slot, 2) the reciprocity theorem, and 3) the locally-plane nature of the wave fronts of the dipole's far field; then, solve the equivalent problem of finding the field induced by an incident plane electromagnetic wave of arbitrary polarization and direction of incidence on the cone surface at the point at which the slot is to be located.

Without loss of generality, we confine the direction of incidence to lie in the x-z plane as illustrated in Fig. 1.

The direction in which the incident field propagates is given by

$$\hat{k} = -\sin\theta\hat{\imath}_x - \cos\theta\hat{\imath}_z.$$

We assume that the time dependence of all fields is e^{-ikct} and shall not explicitly exhibit this factor. We write the incident magnetic field at r as

$$H_i = H_0\hat{p}e^{ik\cdot r}$$

where $\hat{p}$ is the polarization, H_0 is the magnitude, and $k = k\hat{k}$, $k = 2\pi/\lambda$.

The magnetic field induced at a point on the cone surface is treated as a quantity having two dominant contributions, *i.e.*

$$H_s(\hat{p}) \approx H_1(\hat{p}) + H_2(\hat{p}). \tag{1}$$

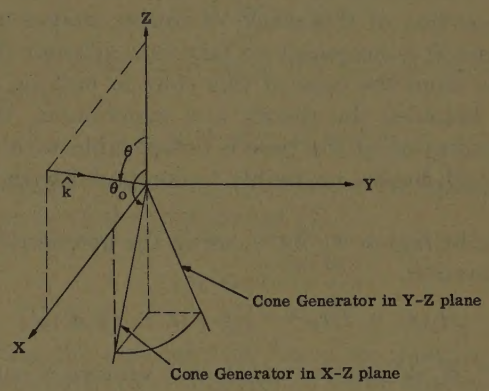

Fig. 1—Geometry.

One of these contributions, $H_1(\hat{p})$, arises from energy which either impinges directly upon the point or, if the point of interest is not in the illuminated region, travels to this point along a geodesic from the shadow boundary. This contribution we call the "geometric optics" term if the point is in the illuminated region and the "creeping wave" term if the point is in the shadow region. Thus, depending on whether or not the point at which we are calculating the induced field is directly illuminated by the incident wave, this contribution is denoted by

$$H_1(\hat{p}) \equiv {}_gH_1(\hat{p}) \quad \text{or} \quad H_1(\hat{p}) \equiv {}_cH_1(\hat{p}),$$

the subscript g denoting geometric optics and the subscript c denoting creeping wave. The other of these contributions, $H_2(\hat{p})$, consists of energy which is scattered by the tip of the cone to the point of interest. This contribution we call the "tip" term without regard to whether the point of interest is in the lit or shadow region.

We use different approximation techniques to evaluate each of these contributions. ${}_gH_1(\hat{p})$ is obtained, of course, by use of geometric optics, *i.e.*, the field on the surface in the lit region is given by twice the tangential component of the incident field. ${}_cH_1(\hat{p})$ is obtained by extending the work of V. A. Fock as described in Section II. $H_2(\hat{p})$ is obtained from the physical optics result.[1] By physical optics, we mean the field obtained by utilizing the geometric optics approximation in the Kirchhoff-Huygens integral representation of the scattered magnetic field. These approximations are subject to the limitation that the point at which we evaluate the field be many wavelengths distant from the tip. This require-

* Manuscript received by the PGAP, July 7, 1958; revised manuscript received February 2, 1959. This paper, in part, summarizes portions of "Studies in Radar Cross Sections XXVII—Calculated Far Field Patterns from Slot Arrays on Conical Shapes," R. E. Doll, R. F. Goodrich, R. E. Kleinman, A. L. Maffett, C. E. Schensted, and K. M. Siegel, University of Michigan, Rept. No. 2713-1-F; February, 1958. This work was performed under Air Force contracts AF33(038)-28634 and AF33(600)-36192.

† University of Michigan, Ann Arbor, Mich.

‡ Bendix Systems Div., Bendix Aviation Corp., Ann Arbor, Mich. Formerly with the University of Michigan.

§ Hughes Aircraft Co., Culver City, Calif.

[1] R. F. Goodrich, R. E. Kleinman, A. L. Maffett, N. E. Reitlinger, C. E. Schensted, and K. M. Siegel, "Radiation and Scattering from Simple Shapes II," Presented at Congrès International Circuits et Antennas Hyperfréquences, Paris, France; October 21–28, 1957.

ment is to assure that the characteristic dimensions of the region of the cone near the point at which the field is evaluated be large in respect to the wavelength.

In applying these approximate methods below we will find that the tip contribution H_2 is negligible with respect to the other terms, H_1, in the specific cases considered. Furthermore, we note that since the experimental portion of this work, of course, makes use of a finite cone, it is necessary to take into account the contribution from the base of this cone in making a comparison between the theory and experiment. We find the contribution of the base is comparable with that of the tip and, hence, negligible as compared with the H_1 terms.

In the lit region we have, using the geometric optics approximation,

$$_oH_1(\hat{p}) = 2H_0e^{ik\cdot r'}[(\hat{p}\cdot\hat{r}')\hat{r}' + (\hat{p}\cdot\hat{\phi}')\hat{\phi}'] \qquad (2)$$

where $\hat{r}'$, $\hat{\theta}'$, $\hat{\phi}'$ are the usual unit vectors in spherical coordinates evaluated on the surface of the cone

$$\hat{r}' = \sin\theta_0\cos\phi\hat{\imath}_x + \sin\theta_0\sin\phi\hat{\imath}_y + \cos\theta_0\hat{\imath}_z$$
$$\hat{\phi}' = -\sin\phi\hat{\imath}_x + \cos\phi\hat{\imath}_z$$
$$\hat{\theta}' = \cos\theta_0\cos\phi\hat{\imath}_x + \cos\theta_0\sin\phi\hat{\imath}_y - \sin\theta_0\hat{\imath}_z$$

and $r' = r'\hat{r}'$.

In the shadow region we have, from Section II,

$$_cH_1(\hat{p}) = H_0\Big\{\sum_{n=0}^{N} e^{i\Phi_n}g(\xi_n)(\hat{p}\cdot\hat{q}_\parallel)(\hat{r}'\cos X_n - \hat{\phi}'\sin X_n) + (i/m_n)f(\xi_n)(\hat{p}\cdot\hat{q}_\perp)(\hat{r}'\sin X_n + \hat{\phi}'\cos X_n) + \sum_{n=1}^{N'} e^{i\Phi_n'}[g(\xi_n')(\hat{p}\cdot\hat{q}_\parallel)(\hat{r}'\cos X_n' - \hat{\phi}'\sin X_n') + (1/m_n')f(\xi_n')(\hat{p}\cdot\hat{q}_\perp)(\hat{r}'\sin X_n' + \hat{\phi}'\cos X_n')]\Big\} \qquad (3)$$

where

$$X_n = (2\pi n + \phi - \phi_s)\sin\theta_0 + \psi,$$
$$X_n' = (2\pi n - \phi - \phi_s)\sin\theta_0 + \psi$$
$$\Phi_n = kr'\sin X_n,$$
$$\Phi_n' = kr'\sin X_n',$$
$$N = \text{lub}\,\{n \mid X_n \le \pi/2\},$$
$$N' = \text{lub}\,\{n \mid X_n' \le \pi/2\},$$
$$\xi_n = \left(\frac{kr'\cos X_n\sin\theta_0}{2\sec^2\theta_0}\right)^{1/3}(2\pi n + \phi - \phi_s),$$
$$\xi_n' = \left(\frac{kr'\cos X_n'\sin\theta_0}{2\sec^2\theta_0}\right)^{1/3}(2\pi n - \phi - \phi_s),$$
$$m_n = \left(-\frac{kr'\tan\theta_0}{2\cos^2 X_n}\right)^{1/3}, \qquad m_n' = \left(-\frac{kr'\tan\theta_0}{2\cos^2 X_n'}\right)^{1/3},$$
$$\phi_s = \cos^{-1}\left(\frac{\tan\theta_0}{\tan\theta}\right), \qquad \psi = \sin^{-1}\left(-\frac{\cos\theta}{\cos\theta_0}\right),$$
$$\hat{q}_\perp = \hat{\theta}'\big|_{\phi=\phi_s}, \qquad \hat{q}_\parallel = \hat{q}_\perp\times\hat{k},$$

and f and g are the tabulated Fock functions.[2] Finally, we have for the tip term,

$$H_2(\hat{p}) = \frac{ikH_0e^{ikr'}}{2\pi r'}[(\hat{r}'\cdot\hat{p})f - (\hat{r}'\cdot f)\hat{p}] \qquad (4)$$

where

$$f = \frac{2\sin\theta_0}{k^2}\Big\{-Q^{-3/2}\arctan\left(\frac{Q^{1/2}\sin\alpha}{q\cos\alpha + b}\right)\cdot(b\cos\theta_0\hat{\imath}_x + c\cos\theta_0\hat{\imath}_y + q\sin\theta_0\hat{\imath}_z) + \frac{\sin\alpha}{Q[(q + b\cos\alpha)^2 - c^2\sin^2\alpha]}\cdot(\cos\theta_0(q^2 - c^2 + qb\cos\alpha)\hat{\imath}_x + c\cos\theta_0(b + q\cos\alpha)\hat{\imath}_y + \sin\theta_0[bq + (b^2 + c^2)\cos\alpha]\hat{\imath}_z)\Big\}$$

$$q = \cos\theta_0(\cos\theta_0 + \cos\theta),$$
$$b = \sin\theta_0(\cos\phi\sin\theta_0 + \sin\theta)$$
$$c = \sin^2\theta_0\sin\phi,$$
$$Q = q^2 - b^2 - c^2,$$

and

$$\alpha = \arccos\left(\frac{\tan\theta_0}{\tan\theta}\right).$$

If there is no shadow, *i.e.* $\theta < \pi - \theta_0$, the expression f becomes,

$$f = -\frac{2\sin^2\theta_0\cos\theta_0}{Q^{3/2}}(\hat{r}' - \hat{k}').$$

Eqs. (2), (3), and (4), together with (1), give an approximate value for $H_s(\hat{p})$, the magnetic field induced by a plane wave at a point on the surface of a cone. In order to apply the reciprocity theorem we need the comparable expression for the field induced by a magnetic dipole located far from the cone. We obtain this immediately from $H_s(\hat{p})$ by recognizing that the far field of that magnetic dipole which can be written as $C(e^{ikR}e^{ik\cdot r}/R)\,\hat{p}$, where $\hat{p}$ has no radial component, is the same as the field of a plane wave of polarization $\hat{p}$ if we replace H_0, the magnitude of the plane wave, with $C(e^{ikR}/R)$; R, of course, is the distance of the dipole from the origin.[3] If we denote by $H_{1,2}'(\hat{p})$ the expressions obtained by replacing H_0 by $C(e^{ikR}/R)$ in the expressions for $H_{1,2}(\hat{p})$, given by (2), (3), and (4), then

$$H_s'(\hat{p}) = H_1'(\hat{p}) + H_2'(\hat{p}) \qquad (5)$$

represents the field induced on the cone surface by a magnetic dipole oriented along $\hat{p}$ far from the cone.

The far field radiated by a magnetic dipole on a cone is expressed in terms of the field induced on the surface

[2] "Tables of Fock Functions," Air Force Cambridge Research Center, Antenna Laboratory (to be published).

[3] R. F. Goodrich, R. E. Kleinman, A. L. Maffett, N. E. Reitlinger, C. E. Schensted, and K. M. Siegel, "Radiation and Scattering from Simple Shapes I," Presented at Congrès International Circuits et Antennas Hyperfréquences, Paris, France; October 21–28, 1957.

by a dipole far from the cone as follows,[3]

$$H_R = (H_s'(\hat{p}_1)\cdot\hat{m})\hat{p}_1 + (H_s'(\hat{p}_2)\cdot\hat{m})\hat{p}_2 \qquad (6)$$

where $\hat{m}$ is the direction of the dipole on the surface and $H_s'(\hat{p}_{1,2})$ are given by (5). Note that it is necessary to solve the reciprocal problem for two distinct dipole orientations $\hat{p}_1$ and $\hat{p}_2$, where $\hat{p}_1$ and $\hat{p}_2$ can be used as a basis for the transverse electromagnetic field.

Eq. (6) gives the radiated field at $(R, \theta, 0)$ due to a magnetic dipole located at (r', θ_0, ϕ) with orientation $\hat{m}(r', \theta_0, \phi)$ in terms of $\hat{p}_{1,2}(\theta, 0)$. We note that by replacing ϕ by $(\phi'-\phi)$ in (6) we obtain the radiated field at (R, θ, ϕ) due to a dipole at (r', θ_0, ϕ') with orientation $\hat{m}(r', \theta_0, \phi')$ in terms of $\hat{p}_{1,2}(\theta, \phi)$. It has been shown[4] that we can use the field radiated from a magnetic dipole on a surface to represent the field radiated from a slot of small but finite length, $L(L\ll\lambda)$, with a voltage V_0 impressed across the slot. In the present case, this is accomplished if, in the components of (6), we replace C by $ikV_0L/4\pi$. Let us denote by (6′) the result of replacing ϕ by $(\phi'-\phi)$ and C by $ikV_0L/4\pi$ in (6) and by H_R' the field thus represented.

H_R', then, is the field radiated from a slot located on the surface of a cone. To find the far field radiated by an array of slots we evaluate the field radiated by each slot using (6′) and then sum these results. We assume that interactions are negligible in the far field, at least for interslot distances of practical interest.

II. Fock Theory Applied to the Cone

Here we obtain an approximate method of determining the field on the surface of a perfectly conducting semi-infinite cone which has been illuminated by a plane electromagnetic wave. In particular we take the direction of incidence to be such that not all of the cone surface is illuminated and find the field on that part of the surface which lies in the shadow and which is far from the tip, *i.e.*, ${}_eH_1(\hat{p})$ of Section I. The approach is that of Franz[5] and Fock[6] generalized after an idea of Keller.[7]

We take a plane electromagnetic wave incident on a perfectly conducting semi-infinite cone. We take the direction of incidence to be such that part of the cone is shadowed and apply the Franz-Fock theory to determine the field induced on the surface of the cone in the shadow and far from the tip. The term "far from the tip" will be made more precise below and indicated as a requirement for the application of the theory.

Using the coordinate system illustrated in Fig. 1 the equation of the cone can be given as

$$\theta = \theta_0, \qquad \theta_0 > \pi/2. \qquad (7)$$

The plane wave incident in the x-z plane making an angle $\theta(\theta>\pi-\theta_0)$ with the cone axis, is again characterized by the unit vector

$$\hat{k} = -\sin\theta\hat{i}_x - \cos\theta\hat{i}_z. \qquad (8)$$

This fixes the shadow boundaries which are solutions of

$$\hat{k}\cdot\nabla f = 0 \qquad (9)$$

where $f=0$ is the equation of the cone, *i.e.* in Cartesian coordinates

$$f = x^2 + y^2 - z^2\tan^2\theta_0. \qquad (10)$$

Denoting $\phi = \pm\phi_s$ as the equations of the shadow boundaries we have the solutions of (9)

$$\cos\phi_s = \frac{\tan\theta_0}{\tan\theta}. \qquad (11)$$

Taking the viewpoint of Franz we consider the field in the shadow as arising from a wave launched at the shadow boundary and propagating along a geodesic according to the prescription of Fock. This makes more precise the condition on the distance from the tip. We now require the radius of curvature everywhere along the geodesic to be much larger than a wavelength. In Fock's notation

$$\left(\frac{kR}{2}\right)^{1/3} \gg 1 \qquad (12)$$

where R is the radius of curvature and $k=2\pi/\lambda$ with λ, the wavelength.

Our first step is to find the geodesics, the curvatures, and finally the generalized arguments of Fock's functions.

We need the equation of the geodesic $r=r(\phi)$ which starts at some point $r=r_s$, $\phi=\phi_s$ on the shadow boundary and, at this point, has the unit tangent vector $\hat{T}=\hat{k}$. (In this section r will denote radial distance on the surface, primes denoting differentiation.)

The geodesic is given by the equations

$$\begin{cases} \hat{r}\cdot\dfrac{d^2r}{ds^2} = 0 \\ \hat{\phi}\cdot\dfrac{d^2r}{ds^2} = 0 \end{cases} \quad \text{or} \quad \begin{cases} r'' - r\sin^2\theta_0\phi'^2 = 0 \\ r\phi'' + 2r'\phi' = 0 \end{cases} \qquad (13)$$

where s is the path length along the geodesic and the primes indicate differentiation with respect to s. From the second equation of (13) we have

$$\frac{\phi''}{\phi'} = -2\frac{r'}{r} \qquad (14)$$

which has the solution

$$\phi' = \frac{\alpha}{r^2} \qquad (15)$$

where α is to be determined. Now

$$s = \int^{\phi}\left(r^2\sin^2\theta_0 + \left(\frac{dr}{d\phi}\right)^2\right)^{1/2} d\phi \qquad (16)$$

[4] R. F. Goodrich, A. L. Maffett, N. E. Reitlinger, C. E. Schensted, and K. M. Siegel, "Studies in Radar Cross Sections XXII—Elementary Slot Radiators." University of Michigan, Rept. No. 2472-13-T; November, 1956.

[5] W. Franz, "On the Green's Functions of the Cylinder and the Sphere," *Z. Naturf.*, vol. 9a, pp. 705–716; March, 1954.

[6] V. A. Fock, "The field of a plane wave near the surface of a conducting body," *J. of Physics*, vol. 10, pp. 399–409; 1946.

[7] J. B. Keller, "Diffraction by a convex cylinder," IRE Trans.

so that

$$\frac{d\phi}{ds} = \phi' = \left(r^2 \sin^2\theta_0 + \left(\frac{dr}{d\phi}\right)^2\right)^{-1/2}. \tag{17}$$

Equating this to (15) we find

$$\frac{dr}{d\phi} = \frac{r}{\alpha}\sqrt{r^2 - \alpha^2 \sin^2\theta_0}. \tag{18}$$

This has the solution

$$r = \alpha \sin\theta_0 \sec\left[(\phi - \phi_s)\sin\theta_0 + \Psi\right]. \tag{19}$$

where Ψ is also to be determined.

Applying the condition $r = r_s$ at $\phi = \phi_s$ we have

$$\alpha = r_s \frac{\cos\Psi}{\sin\theta_0}. \tag{20}$$

The tangent vector is given by

$$\hat{T} = \frac{dr}{ds} = \hat{r}\frac{dr}{ds} + r\frac{d\hat{r}}{ds}. \tag{21}$$

which, making use of the above, becomes

$$\hat{T} = \hat{r}\sin\left[(\phi - \phi_s)\sin\theta_0 + \Psi\right] + \hat{\phi}\cos\left[(\phi - \phi_s)\sin\theta_0 + \Psi\right] \tag{22}$$

Now imposing the condition $\hat{T} = \hat{k}$ at $\phi = \phi_s$, $r = r_s$ we have

$$\sin\Psi = -\frac{\cos\theta}{\cos\theta_0}. \tag{23}$$

Finally

$$\begin{cases} r = r_s \cos\Psi \sec\left[(\phi - \phi_s)\sin\theta_0 + \Psi\right] \\ \Psi = \sin^{-1}\left(-\dfrac{\cos\theta}{\cos\theta_0}\right). \end{cases} \tag{24}$$

The radius of curvature is given by

$$\frac{1}{R} = \left|\frac{d\hat{n}}{ds}\cdot\hat{T}\right|, \tag{25}$$

where $\hat{n}$ is the unit normal at the point in question. Since $\hat{n} = \hat{\theta}$,

$$\frac{d\hat{n}}{ds} = -\frac{\cos\theta_0}{\sin\theta_0}\frac{r_s\cos\Psi}{r^2}\hat{\phi}. \tag{26}$$

Thus, using the above expression for $\hat{T}$,

$$\frac{1}{R} = -\frac{r_s^2}{r^3}\cos^2\Psi\cot\theta_0. \tag{27}$$

We take the generalized argument of the Fock functions in the shadow to be

$$\xi = \int_0^s \left(\frac{kR}{2}\right)^{1/3}\frac{ds}{R}. \tag{28}$$

Substituting and performing the integration,

$$\xi = \left(\frac{kr_s}{2}\frac{\cos\Psi\sin\theta_0}{\sec^2\theta_0}\right)^{1/3}(\phi - \phi_s). \tag{29}$$

Finally we anticipate our need for the path length,

$$s = r\sec\Psi\sin\left[(\phi - \phi_s)\sin\theta_0\right]. \tag{30}$$

We now apply the Fock theory. We fix on a point r, ϕ in the shadow and determine the contribution to the field at this point arising from the wave launched at r_s, ϕ_s where r_s satisfies (24) with these fixed r, ϕ.

If the incident magnetic field is perpendicular to the surface at r_s, ϕ_s then, according to Fock, the field at r, ϕ due to the surface wave launched at r_s, ϕ_s will be tangent to the geodesic and given by

$$H_T = e^{iks}\frac{i}{m}f(\xi). \tag{31}$$

where s is the path length and

$$m = \left(\frac{kR}{2}\right)^{1/3}$$

$$\xi = \left(\frac{kr_s}{2}\cos\Psi\frac{\sin\theta_0}{\sec^2\theta_0}\right)(\phi - \phi_s).$$

Otherwise, if the incident magnetic field is tangent to the surface at r_s, ϕ_s the field will be perpendicular to the geodesic and given by

$$H_\perp = e^{iks}g(\xi) \tag{32}$$

The functions f and g are given by Fock as

$$g(\xi) = \frac{1}{\sqrt{\pi}}\int_\Gamma \frac{e^{i\xi t}}{w'(t)}dt \tag{33}$$

$$f(\xi) = \frac{1}{\sqrt{\pi}}\int_\Gamma \frac{e^{i\xi t}}{w(t)}dt \tag{34}$$

where

$$w(t) = \frac{1}{\sqrt{\pi}}\int_{\Gamma'} e^{zt - 1/3z^3}dz \tag{35}$$

and the prime indicates differentiation with respect to t. The contours are shown in Fig. 2.

We need the projection of the magnetic polarization, $\hat{p}$, onto the perpendicular and tangent directions at the shadow boundary in order to apply the above method of computing the field. We designate these directions at the shadow boundary by

$$\begin{cases} \hat{q}_\perp = \cos\theta_0\cos\phi_s\hat{\imath}_x + \cos\theta_0\sin\phi_s\hat{\imath}_y - \sin\theta_0\hat{\imath}_z \\ \hat{q}_\parallel = \hat{q}_\perp \times \hat{k}. \end{cases} \tag{36}$$

Hence, with the incident $\hat{p}$ polarization, the field H_T is multiplied by $(\hat{p}\cdot\hat{q}_\perp)$ while the field $H_\perp$ is multiplied by $(\hat{p}\cdot\hat{q}_\parallel)$.

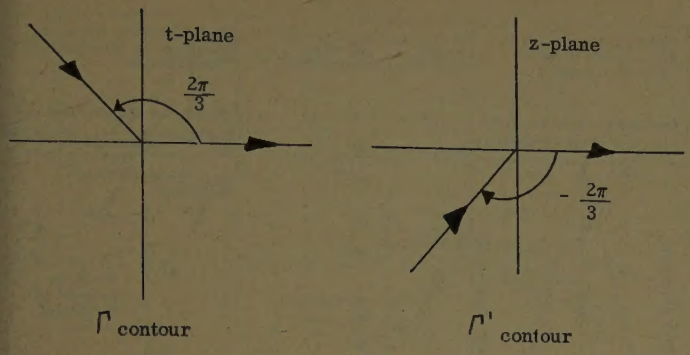

Fig. 2—Contours of integration.

There will be a contribution from each geodesic path satisfying the boundary conditions and passing through a given point. We enumerate these.

Let the point in question be specified by r, ϕ where $\phi_s \leq \phi \leq \pi$. Then, given the direction of incidence we have the possible geodesics

$$r = r_s^{(n)} \cos \Psi \sec [(2\pi n + \phi - \phi_s) \sin \theta_0 + \Psi], \quad n = 0, 1, \cdots \quad (37)$$

$$r = r_s^{(n')} \cos \Psi \sec [(2\pi n' - \phi - \phi_s) \sin \theta_0 + \Psi], \quad n = 1, 2, \cdots \quad (37')$$

These are to be solved for $\{r_s^{(n)}\}$ and $\{r_s^{(n')}\}$, where we note the first set terminates at n such that

$$(2\pi n + \phi - \phi_s) \sin \theta_0 + \Psi \geq \frac{\pi}{2} \quad (38)$$

while the second terminates at n' such that

$$(2\pi n' - \phi - \phi_s) \sin \theta_0 + \Psi \geq \frac{\pi}{2}. \quad (38')$$

Corresponding to these will be the sets $\{\xi_n\}$ and $\{\xi_n'\}$ as well as the path lengths $\{s_n\}$, $\{s_n'\}$.

Since, in general, the shadow boundary does not coincide with the phase front of the incident radiation we take account of the phase by inserting the factor $e^{ik \cdot r_s^{(n)}}$ or $e^{ik \cdot r_s^{(n')}}$ in each case. This gives a total phase of

$$\Phi_n = k \cdot r_s^{(n)} + ks^{(n)} \quad (39)$$

or

$$\Phi_{n'} = k \cdot r_s^{(n')} + ks^{(n')}. \quad (39')$$

These are explicitly

$$\begin{cases} \Phi_n = kr \sin [(2\pi n + \phi - \phi_s) \sin \theta_0 + \Psi] \\ \Phi_{n'} = kr \sin [(2\pi n' - \phi - \phi_s) \sin \theta_0 + \Psi]. \end{cases} \quad (40)$$

Since we will need to add the various contributions vectorially we choose to facilitate this by resolving the components of the field on the surface in the $\hat{\phi}$ and $\hat{r}$ directions. Now the field H_T lies along the tangent vector

$$\hat{T} = \hat{r} \sin [(\phi - \phi_s) \sin \theta_0 + \Psi] + \hat{\phi} \cos [(\phi - \phi_s) \sin \theta_0 + \Psi] \quad (41)$$

while the field $H\perp$ lies along the vector

$$\hat{\theta} \times \hat{T} = -\hat{\phi} \sin [(\phi - \phi_s) \sin \theta_0 + \Psi] + \hat{r} \cos [(\phi - \phi_s) \sin \theta_0 + \Psi]. \quad (42)$$

These explicitly give the $\hat{r}$ and $\hat{\phi}$ components. Finally, we find the total contributions. On the surface at the point r, ϕ we have, for incident polarization $\hat{p}$,

$$\begin{aligned} {}_cH_1(\hat{p}) = \hat{r} \Big[& \sum_{n=0} e^{i\Phi_n} \{ (\hat{p} \cdot \hat{q}_\parallel) g(\xi_n) \cos X_n \\ & + (\hat{p} \cdot \hat{q}_\perp)(i/m_n) f(\xi_n) \sin X_n \} \\ & + \sum_{n=1} e^{i\Phi_{n'}} \{ (\hat{p} \cdot \hat{q}_\parallel) g(\xi_{n'}) \cos X_{n'} \\ & + (\hat{p} \cdot \hat{q}_\perp)(i/m_{n'}) f(\xi_{n'}) \sin X_{n'} \} \Big] \\ + \hat{\phi} \Big[& \sum_{n=0} e^{i\Phi_n} \{ (\hat{p} \cdot \hat{q}_\perp)(i/m_n) f(\xi_n) \cos X_n \\ & - (\hat{p} \cdot \hat{q}_\parallel) g(\xi_n) \sin X_n \} \\ & + \sum_{n=1} e^{i\Phi_{n'}} \{ (\hat{p} \cdot \hat{q}_\perp (i/m_{n'}) f(\xi_{n'}) \cos X_{n'} \\ & - (\hat{p} \cdot \hat{q}_\parallel) g(\xi_{n'}) \sin X_{n'} \} \Big] \end{aligned} \quad (43)$$

where we have put

$$\begin{aligned} X_n &= (2\pi n + \phi - \phi_s) \sin \theta_0 + \Psi \\ X_{n'} &= (2\pi n' - \phi - \phi_s) \sin \theta_0 + \Psi. \end{aligned} \quad (44)$$

III. Far Field of a Particular Array of Slots on a Cone

The technique described in Section I has been applied to the problem of finding the far field radiation patterns of a linear array of 65 transverse slots lying along a generator of a 30° (full angle) cone. In this problem we had $\theta_0 = 165°$ and, for convenience, chose the generator on which the slots were located to be given by $\phi' = 0°$. Then $\hat{m} = \hat{i}_y$ for all slots. The first slot was located 16λ from the tip and the slots were spaced 0.4λ apart. Thus, in (6'), the only quantity that varied from slot to slot was r'; explicitly $r' = 16\lambda$ for the first slot and $r' = 16\lambda + 0.4\lambda(n-1)$ for the nth slot. We will denote by r_n' the distance from the tip to the nth slot ($r_n' = 16\lambda + 0.4\lambda(n-1)$) and thus $H_R'(n)$ is the far field radiated by the nth slot as given by (6'). To completely set the problem, it is necessary to specify the relative phases (or phase differences) of the fields of any two slots. This was done by requiring that the slots be phased so as to produce main beam positions, θ_B, of 10°, 30°, 50° and 70° from the extension of the cone axis. Explicitly, the far field, H, for the 65 slot array was computed from the following

$$H = \sum_{n=1}^{65} H_R'(n) e^{ikr_{n'} \cos (\theta_B - \theta_0)}. \quad (45)$$

Exhibiting all the variables

$$H_R'(n) = H_R'(R, \theta, \phi, r_n', \theta_0, \phi_s, \hat{p}_1, \hat{p}_2, \hat{m})$$

where

(R, θ, ϕ) = field point,
(r_n', θ_0, ϕ_s) = slot position = $(16\lambda + 0.4\lambda(n-1),\ 165°,\ 0°)$,
$\hat{p}_1$ and $\hat{p}_2$ were chosen, for convenience, to be $\hat{\theta}$ and $\hat{\phi}$ respectively, and $\hat{m} = \hat{i}_y$.

As pointed out above, computations were performed for four different main beam directions, $\theta_B = 10°$, 30°, 50° and 70°. For each beam direction field patterns were obtained on two "cuts":

1) a conical cut where the field point is restricted to lie on a cone whose axis is the extension of the generator containing the slots and which has a half-angle equal to $15° + \theta_B$, and
2) a plane cut where the field point is restricted to lie in the plane of the generator containing the slots and the axis of the cone.

These cuts are displayed in Fig. 3. Fig. 4 shows which approximate value of $H_1'(\hat{p})$ (*i.e.*, ${}_gH_1'(\hat{p})$ or ${}_cH_1'(\hat{p})$) is employed for each value of (θ, ϕ), the field point position. The expression for the tip contribution, $H_2'(\hat{p})$, was employed everywhere except in the transition region which in this case is the neighborhood of the point $\theta = 15°$, $\phi = 180°$.

A description of the experimental technique which was used to measure field patterns for this example is given in the Appendix.

In carrying out the computations indicated in (45), terms of the form

$$\sum_{n=1}^{65} H_{1,2}'(\hat{p}) e^{ikr_n' \cos(\theta_B - \theta_0)}$$

occurred. While the expressions involving ${}_gH_1'(\hat{p})$ and $H_2'(\hat{p})$ were summable as geometric series, the corresponding term involving ${}_cH_1'(\hat{p})$ was not so easily handled. In the computations, the following technique was employed. The sum was put in the form

$$\sum_{n=0}^{N} F(n) e^{ian}.$$

Then, by approximating $F(n)$ by the expression $F(0)\,[F(N)/F(0)\,]^{n/N}$, we again could sum as a geometric series, *i.e.*,

$$\sum_{n=0}^{N} F(n) e^{ian} \approx F(0) \left[\frac{1 - [F(N)/F(0)]^{(N+1)/N} e^{ia(N+1)}}{1 - [F(N)/F(0)]^{1/N} e^{ia}} \right]. \quad (46)$$

IV. Comparison Between Theory and Experiment

Plane Cut

The theroretical values of the field on the plane cut were computed according to the following procedure for each main beam direction. In the lit region, where ${}_gH_1'(\hat{p})$ was used, only relative maxima were found to determine an envelope, except in the vicinity of the main beam where the abscissa of the minima were noted. In the shadow region, where ${}_cH_1'(\hat{p})$ was used, values were computed at 10° intervals in θ. The tip contribution was found to be negligible almost everywhere, affecting only the ordinates of the minima of ${}_gH_1'(\hat{p})$. The experimental results were obtained continuously in θ and are presented together with the theoretical points in Fig. 5 through Fig. 8. The power in each component is plotted in db below the main beam power as a function of θ.

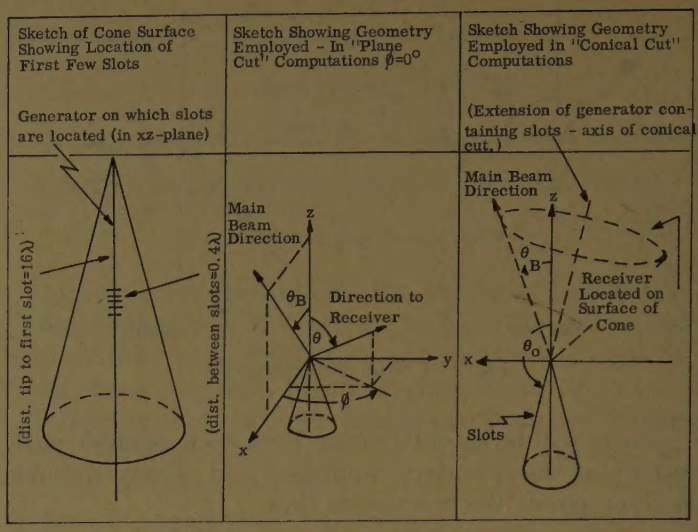

Fig. 3—Geometry used in the analysis of the 65-slot problem.

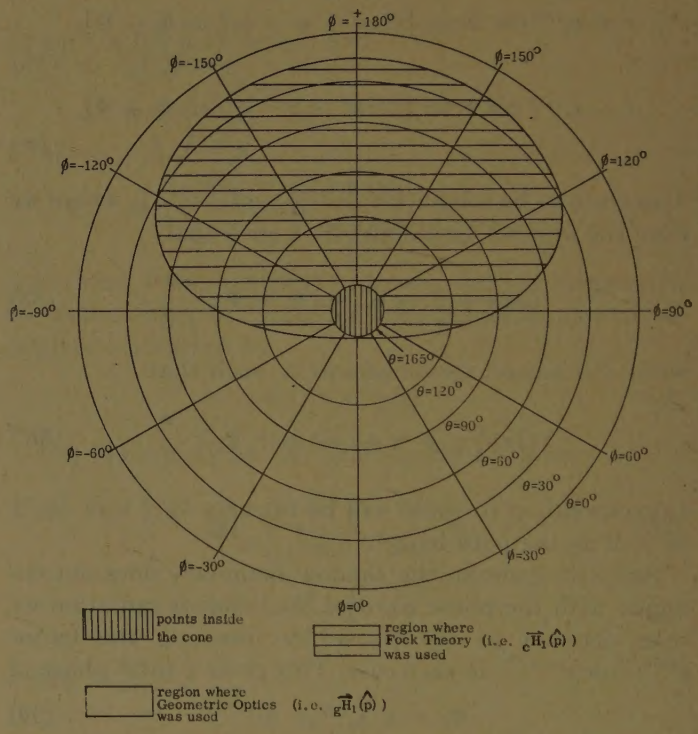

Fig. 4—Applicability of approximation techniques as a function of the field point (receiver position).

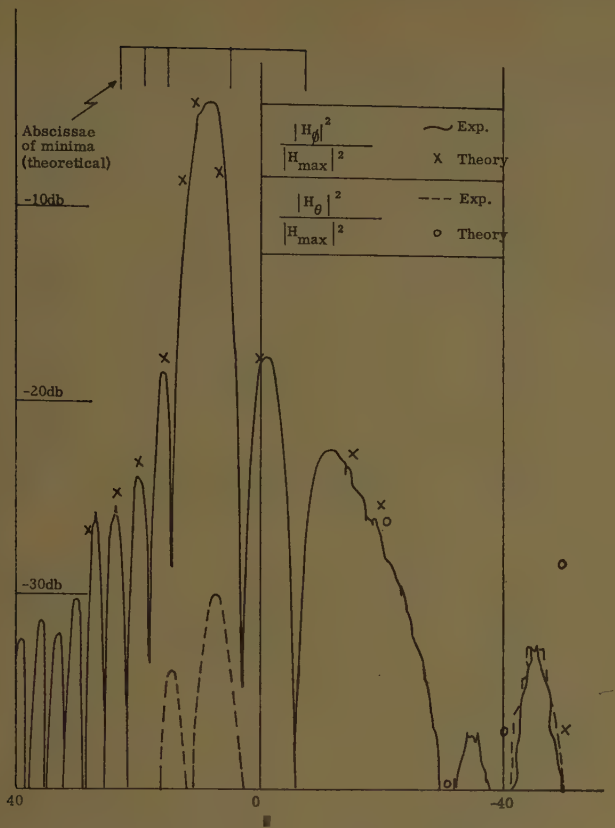

Fig. 5—Comparison between theory and experiment for a plane cut ($\theta_B=10°$, $\phi=0°$).

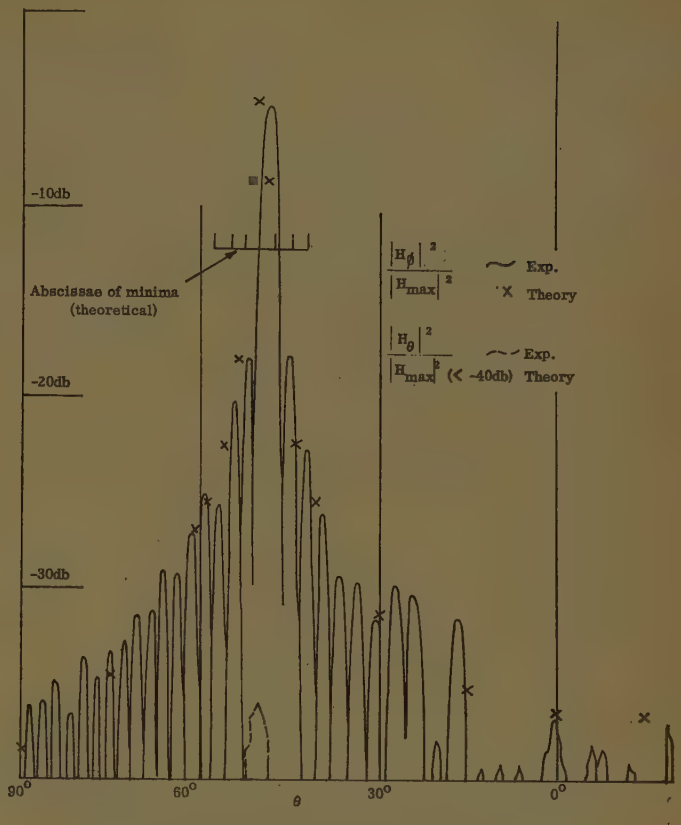

Fig. 7—Comparison between theory and experiment for a plane cut ($\theta_B=50°$, $\phi=0°$).

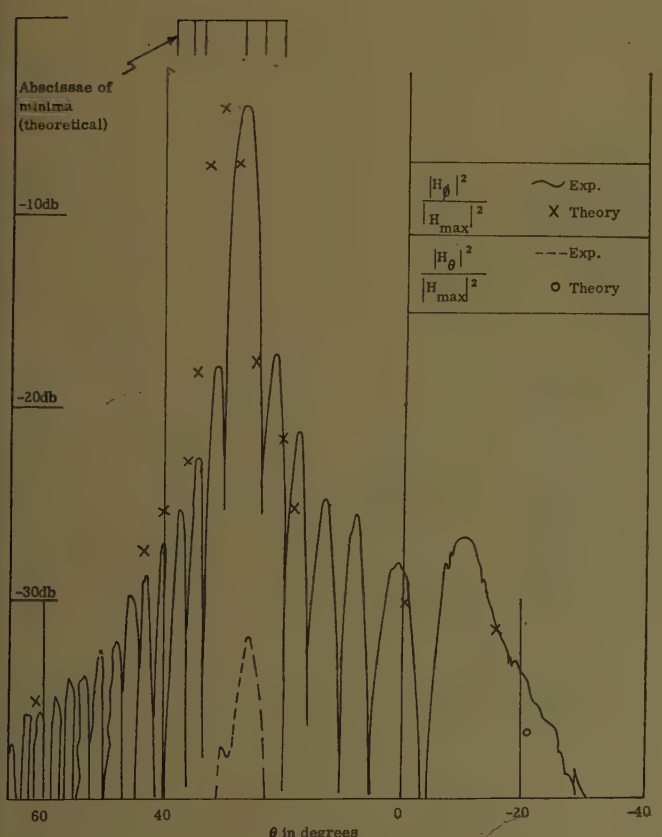

Fig. 6—Comparison between theory and experiment for a plane cut ($\theta_B=30°$, $\phi=0°$).

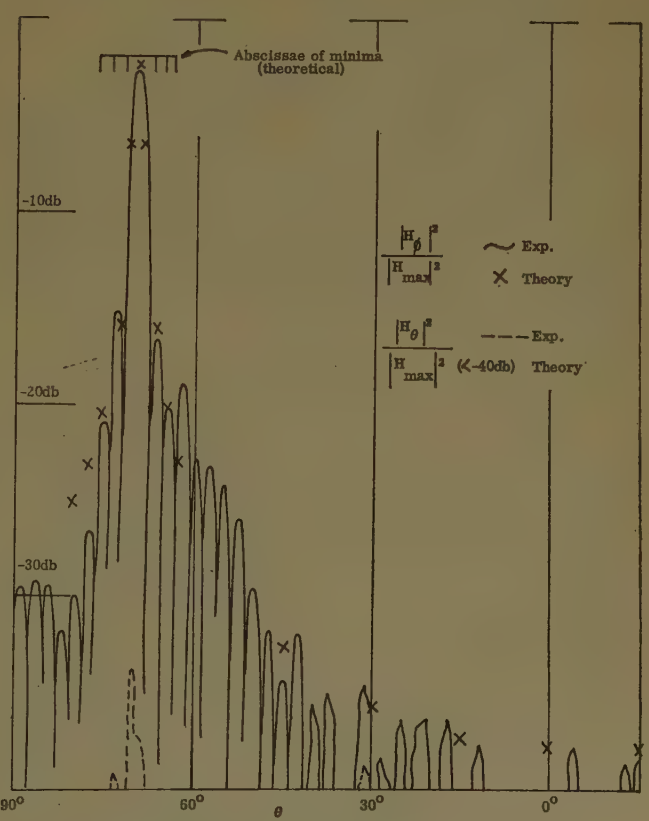

Fig. 8—Comparison between theory and experiment for a plane cut ($\theta_B=70°$, $\phi=0°$).

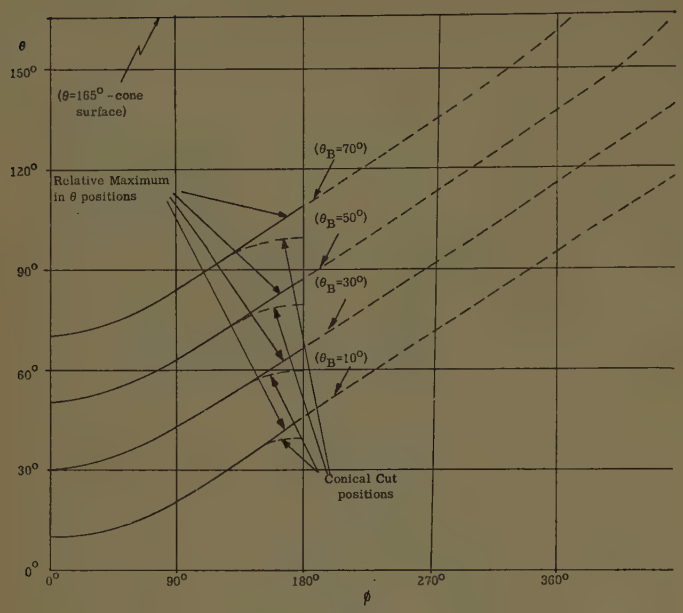

Fig. 9—The relative maximum in θ for a given ϕ and main beam direction θ_B.

Conical Cut

The theoretical values of the field on the conical cut were obtained in the following manner for each main beam direction. In the lit region, since ${}_{\theta}H_1'(\hat{p})$ varied essentially as a $\cos^2$ curve, only a few points were necessary to indicate the theoretical curve. In the shadow region, values of ${}_{c}H_1'(\hat{p})$ were computed at 5° intervals in ϕ. The appropriate θ values were determined from the following equation,

$$\sin\theta_0 \sin\theta \cos\phi + \cos\theta_0 \cos\theta = \cos(\theta_0 - \theta_B). \quad (47)$$

The tip contribution again was found to be negligible. The experimental results were obtained for a given ϕ value by determining the relative maximum in θ. This departs from the conical cut in the shadow. The relative maximum in θ for a given ϕ and main beam direction θ_B is given by (47) in the illuminated region and by the following equation in the shadow

$$\theta_B + \pi - \theta_0 = \cos^{-1}(-\cos\theta/\cos\theta_0) - [\phi - \cos^{-1}(\tan\theta_0/\tan\theta)]\sin\theta_0. \quad (48)$$

This departure from the conical cut is illustrated in Fig. 9 showing θ as a function of $|\phi|$ for both the conical cut and the relative maximum positions. In Fig. 9 the locus of the relative maximum in θ is continued until it reaches the cone surface, $\theta = 165°$, however, for $\phi > 180°$ the field is dominated by that arising at the other shadow boundary.

Keeping in mind the fact that the experimental values, near $\phi = 180°$, refer to points displaced from the conical cut, the experimental results together with the theoretically computed points are presented in Fig. 10 through Fig. 13. As before, each component is normalized with respect to the main beam maximum.

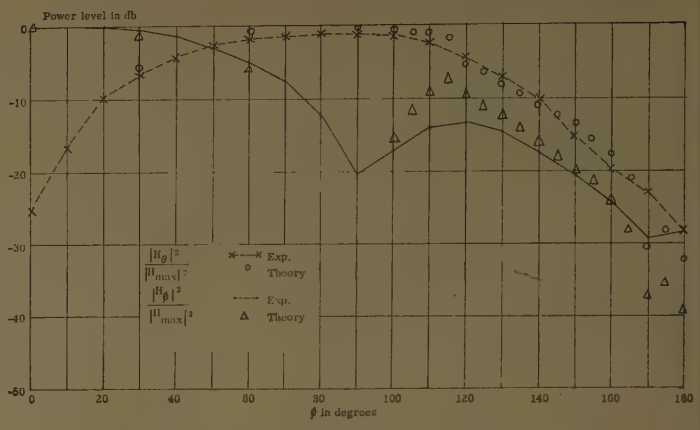

Fig. 10—Comparison between theory and experiment for a conical cut ($\theta_B = 10°$).

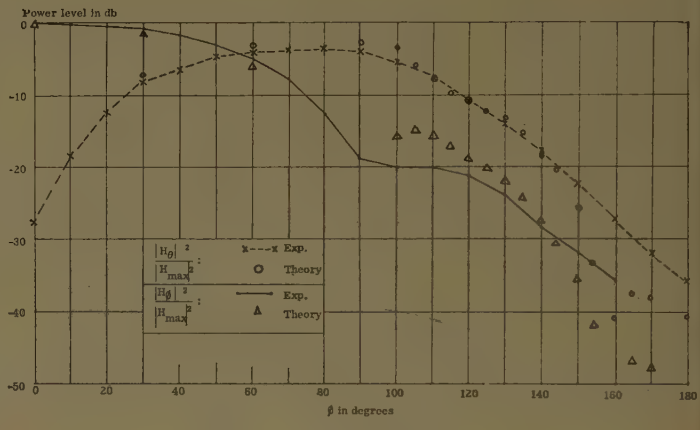

Fig. 11—Comparison between theory and experiment for a conical cut ($\theta_B = 30°$).

The agreement or lack of agreement between the experimental results and the application of the Fock theory to a cone tends to be obscured in the case of the 65-slot array. For this reason we have made a comparison for the case of a single slot on a cone. The cone used was of angle $\theta_0 = 170°$ with the slot transverse and 20 wavelengths from the tip. With the coordinates as in Fig. 14 the receiver was placed at $\theta = 90°$ and the pattern taken continuously for $0 \leq \phi \leq 360$. The range we are interested in for the comparison with the Fock approximation is for $90° \leq \phi \leq 270°$. Because of the experimental limitations, only the ranges $90° \leq \phi \leq 120°$ and $240° \leq \phi \leq 270°$ can be used for the comparison. These limitations are that the signal on the side opposite the slot becomes so weak as to be obscured by the extraneous scatterers on the experimental range.

The Fock expression used is that of (43) taking only the terms $n = 0$ and $n' = 1$. The values of the parameters are

$$\theta_0 = 170°$$
$$\hat{p} = \hat{\imath}y$$
$$r = 20\lambda$$

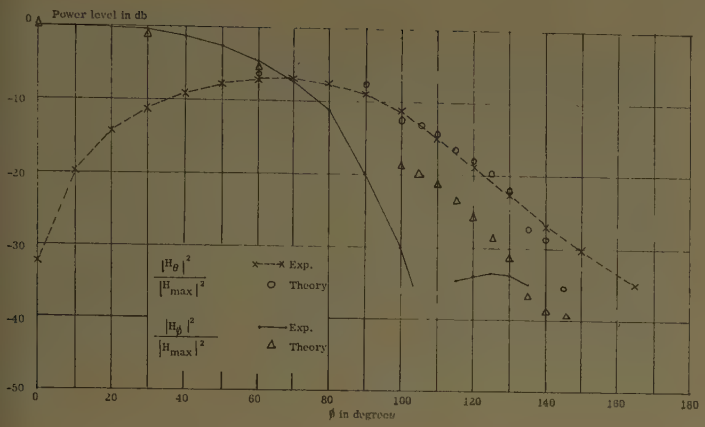

Fig. 12—Comparison between theory and experiment for a conical cut ($\theta_B = 50°$).

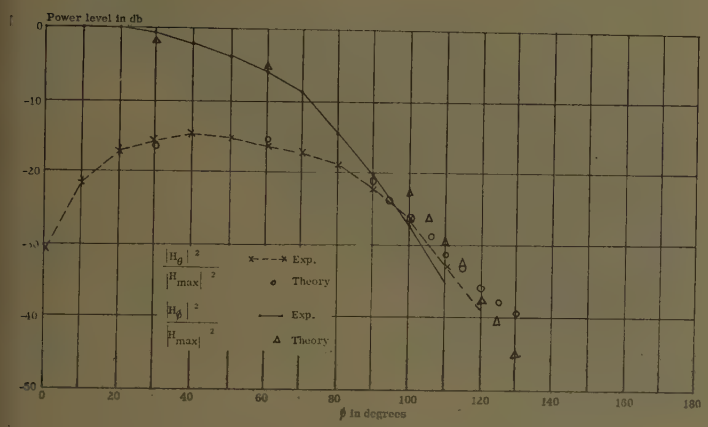

Fig. 13—Comparison between theory and experiment for a conical cut ($\theta_B = 70°$).

so that

$$ {}_cH_\phi = e^{i\Phi_0}\left\{\frac{i}{m_0} f(\xi_0)\cos\theta_0\cos X_0 + g(\xi_0)\sin\theta_0\sin X_0\right\} $$

$$ + e^{i\Phi_1}\left\{\frac{i}{m_1'} f(\xi_1')\cos\theta_0\cos X_1' + g(\xi_1')\sin\theta_0\sin X_1'\right\}. $$

We plot $|{}_cH_\phi|^2$ along with the experimental curve in Fig. 15. The results are in db below the value at the shadow boundary.

As a concluding remark, it is felt that a detailed discussion of discrepancies between the theoretical and experimental results would serve only to obscure the main result of the comparison; the comparison shows that the theoretical approximations described in Sections I and II can be used successfully to predict radiation patterns from arrays of slots on a cone. These techniques are applicable to an arbitrary number of arbitrarily oriented slots (sufficiently far from each other and the tip) on a cone. Comparable approximations for other surfaces will be available, following the same procedure, as other extensions of the Fock technique are obtained.

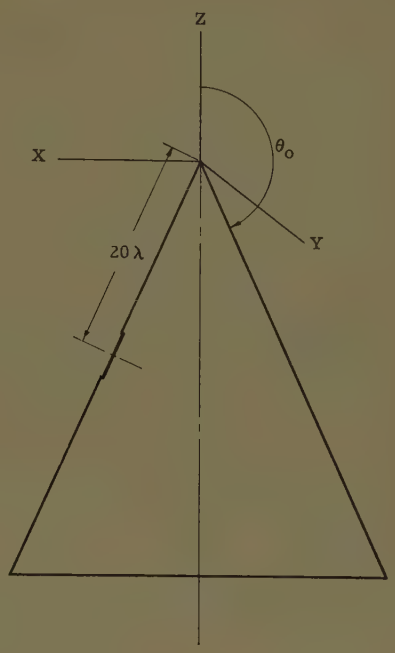

Fig. 14—Cone geometry for the single slot.

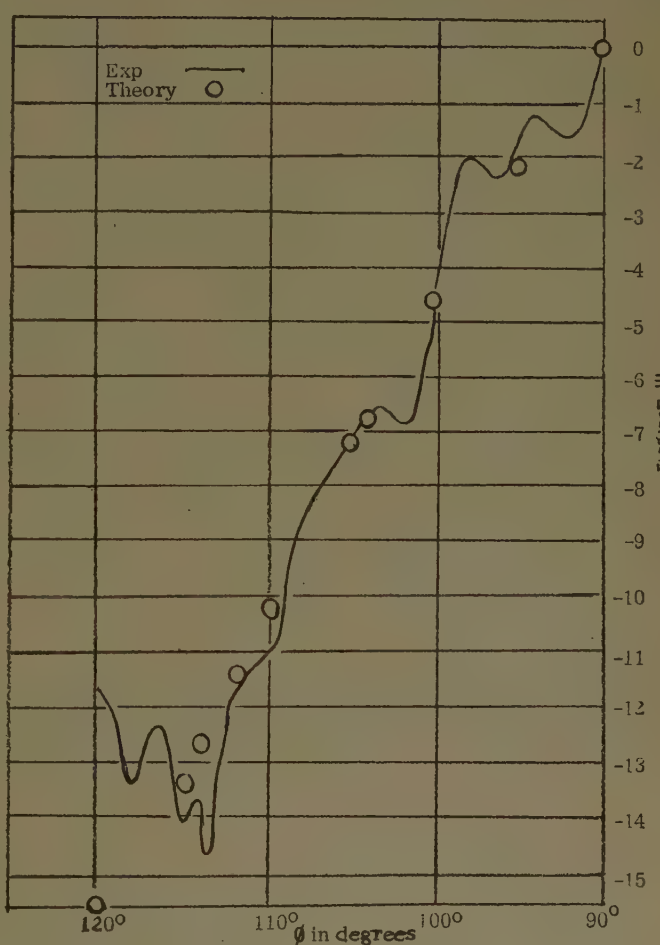

Fig. 15—Comparison between theory and experiment for a single slot and the conical cut ($\theta_B = 90°$).

Appendix

The experimental program to verify the theoretical pattern calculations for a linear array on a cone could logically have followed either of two possible paths. The first of these consists of utilizing a single array with means provided for adjusting the phase progression so that all four beam positions could be realized. An alternate approach would be based on using a number of arrays each of limited scan capacity, in order to place the beam at the stipulated positions. Unfortunately a wide angle scanning array having appropriate dimensions was not available for use in these experiments and as a result the second approach was necessary.

For the 10° and 30° beam positions, an array of purely transverse nonresonant slots, positioned in the broadwall of rectangular waveguide, was fabricated. With a slot spacing of 0.4λ and at a frequency of 9375 mc. the beam from this array was very close to the required 30° from the cone axis. By partially filling the waveguide with a dielectric of modest constant (polystyrene, $\epsilon=2.5$) the beam was shifted to the 10° position.

This technique proved adequate for these scan angles. However, because of the basic endfire nature of this type of array it could not be used for the 50° and 70° cases and still retain the correct slot spacing. It thus became necessary to relax the requirement on pure transverse slots and to design an array of slightly inclined slots in the narrow wall of rectangular guide. The artifice of alternating the slot inclination results in an array with inherent broadside characteristics. Two arrays based on this technique were constructed. By using standard guide dimension and loading with a dielectric of constant $\epsilon=1.2$ (Eccofoam) the 50° position was realized. For the 70° case it was necessary to reduce the standard X-band guide width to 0.8 inch and to load the guide with Teflon $\epsilon=2.1$. Fig. 16 shows a section of inclined narrow wall slots used to obtain impedance data for the array design. Also seen in this photograph are the dielectric loading slabs and the metallic insert used to reduce the guide width. The inclination of the slots used in these arrays tends to introduce additional cross-polarized radiation. However, for the slot tilt angles used (10° maximum) this contribution was negligible.

In order to ascertain the effect of a conical ground plane on the radiation pattern of these arrays they were mounted in a channel on a 30° cone such that they were flush with the cone surface. For all conditions the first slot of each array was located a distance 16λ from the cone tip. This cone was attached to a rotatable platform with angular calibration and the platform in turn mounted on the receiving end of an 800-foot pattern range. A typical array mounted on the cone in pattern taking position is shown in Fig. 17. The calibrated platform allowed any azimuthal positioning of the cone and the rotation of the receiving mount led to the θ pattern dependence in this azimuthal plane.

Although the mechanical tolerances and cone alignment (boresighting) were not held to rigid dimensional specifications, the resulting patterns, as displayed earlier, are consistent with the accuracies necessary to verify the theoretical results.

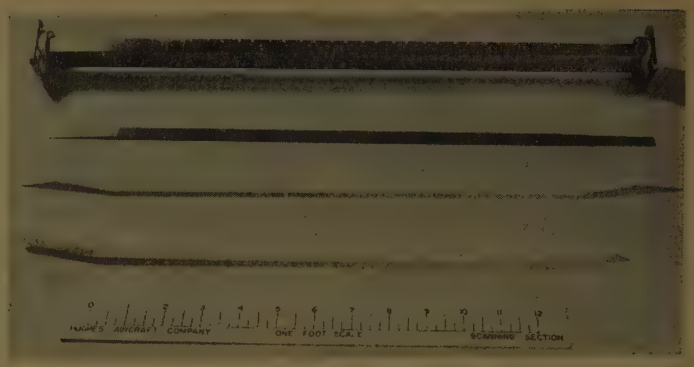

Fig. 16—Inclined slot test section.

Fig. 17—Typical linear array mounted on cone.

A Study of Spherical Reflectors as Wide-Angle Scanning Antennas*

TINGYE LI†

Summary—**A study is made of spherical reflectors for use as wide-angle scanning antennas. In order to keep the effects of spherical aberration within tolerable limits, the approach of using a restricted aperture is adopted. This approach is suitable for applications requiring very wide angles of scan.**

Experimental results show that the phase error over the illuminated aperture of a spherical reflector should not exceed one-sixteenth of a wavelength. This requirement determines the beamwidth of the primary source. A square-aperture horn with diagonal polarization is found to satisfy the requirements of a suitable feed for the reflector. Secondary patterns of a 10-foot-diameter hemispherical reflector illuminated by this horn at 11.2 kmc have a 3-db beamwidth of 1.76° and a relative sidelobe level of about −20 db throughout a total useful angle of scan of 140°. The measured gain is 39.4 db, which is equivalent to the gain of a uniformly illuminated circular aperture of 31-inch diameter.

Introduction

THE suitability of spherical reflectors for use as wide-angle scanning antennas has been recognized for some time.[1] In order to minimize the effects of spherical aberration, two general approaches have been used. The first approach involves the use of a restricted aperture and a reflector of a sufficiently large radius.[1,2] This approach permits a simple design and is suitable for applications requiring very wide angles of scan. The second approach uses methods of compensation for spherical aberration. These methods include the use of phased line-source feeds,[3] multiple-source feeds,[4,5] auxiliary reflectors,[5,6] or correcting lenses.[7,8] With these methods of compensation a larger aperture can be effectively utilized. However, this is achieved at the expense of some complexity in design and of a reduction in the useful angle of scan.

In applications requiring very wide angles of scan, it is necessary to use a small illuminated aperture as compared with the reflector aperture. In such a case the first approach involving the use of a restricted aperture is applicable. The present study of the spherical reflector includes both theoretical and experimental investigations of this approach. In particular, the experimental work is devoted to the conception and realization of a suitable feed for the spherical reflector.

Theoretical Considerations

When a point source is placed at the focus of a spherical reflector, the reflected wave arising from it does not have a plane wave-front. This phenomenon is known as spherical aberration. The amount of departure of phase from a plane wave is a function of the aperture diameter and of the focal length. This functional relationship can be established by means of geometrical optics.

A hemispherical reflector and its geometry are shown in Fig. 1. A point source is assumed to be located at the

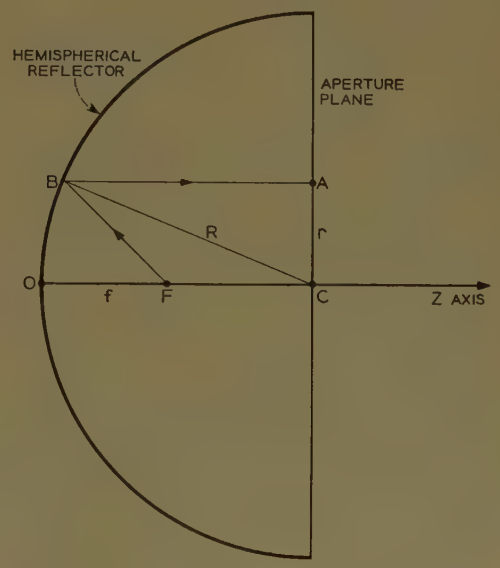

Fig. 1—Geometry of a spherical reflector.

focal point F. FB and BA are typical incident and reflected rays. The total path-length from the focal point F to the aperture plane at A is

$$FB + BA = d = \sqrt{R^2 - r^2} + \sqrt{r^2 + [\sqrt{R^2 - r^2} - (R - f)]^2} \quad (1)$$

where R = radius of the sphere, r = radial distance from the Z axis, and $f = OF$ = focal length. In (1) it is assumed that BA, the reflected ray, is parallel to the Z axis. This approximation is good for the range of variables given by $0 \leq r/R \leq 0.6$ and $0.45 \leq f/R \leq 0.50$.

* Manuscript received by the PGAP, February 10, 1959.
† Bell Telephone Labs., Inc., Holmdel, N. J.

[1] J. Ashmead and A. B. Pippard, "The use of spherical reflectors as microwave scanning aerials," *J. IEE*, vol. 93, pt. IIIA, pp. 627–632; 1946.
[2] A. S. Dunbar, "Applications of the Rayleigh criterion," Symp. on Microwave Optics, McGill Univ., Montreal, Can.; June, 1953.
[3] R. C. Spencer, C. J. Sletten, and J. E. Walsh, "Correction of spherical aberration by a phased line source," *Proc. NEC*, vol. 5, pp. 320–333; 1949.
[4] C. J. Sletten and W. G. Mavroides, "A Method of Side-Lobe Reduction," Naval Res. Lab., Washington, D. C., NRL No. 4043, pp. 1–12; April, 1952.
[5] W. Rotman, "Wide-angle scanning with microwave double-layer pillboxes," IRE TRANS. ON ANTENNAS AND PROPAGATION, vol. AP-6, pp. 96–105; January, 1958.
[6] A. K. Head, "A new form for a giant radio telescope," *Nature*, vol. 179, pp. 692–693; April 6, 1957.
[7] H. B. Devore and H. Iams, "Microwave optics between parallel conducting sheets," *RCA Rev.*, vol. 9, pp. 730–732; December, 1948.
[8] H. N. Chait, "Wide-angle scan radar antenna," *Electronics*, vol. 26, pp. 128–132; January, 1953.

The path-length difference between an axial ray *FOC* and a non-axial ray *FBA* is

$$\Delta = R + f - d. \tag{2}$$

Therefore, the phase error in wavelengths is

$$(\Delta/\lambda) = (R/\lambda)(2 - m - s - \sqrt{1 + m^2 - 2ms}) \tag{3}$$

where $m = 1 - f/R$ and $s = \sqrt{1-(r/R)^2}$. A family of curves for $(\Delta/\lambda)/(R/\lambda)$ is plotted in Fig. 2.

When considering the phase error over a given aperture, the sum of the maximum absolute values of positive and negative phase errors is important. This sum is referred to as the total phase error and is plotted in Fig. 3 as a function of the focal length f for different aperture radii a. The optimum focal length for each aperture is determined by the minimum of each curve. For example, the optimum focal length for an aperture having a diameter equal to the radius of the sphere ($2a = R$) is equal to $0.4665R$. The corresponding total phase error is 0.004206 (R/λ) wavelength, or, 0.02643 (R/λ) radian.

It is of interest to note that the total phase error over a prescribed aperture is least when the phase error at the edge of the aperture is zero. Thus, equating (3) to zero and solving for f, the optimum focal length for an aperture of radius a is found to be

$$f_{op} = \frac{1}{4}(R + \sqrt{R^2 - a^2}). \tag{4}$$

Although this optimum focal length is one for which the total phase error is least over a prescribed aperture, it is not necessarily the focal length that yields the best radiation pattern when the aperture illumination is non-uniform. If the amplitude distribution is tapered, the focal length that yields the best radiation pattern would be somewhat longer. In practice, this can be determined easily by experiment.

It is clear from Fig. 3 that corresponding to a given aperture size there exists a minimum value of total phase error. This means that specification on phase-error tolerance sets the limit on the aperture size. The relationship between the maximum permissible aperture and the total allowable phase error is given by

$$\left(\frac{a}{R}\right)^4_{\max} = 14.7\,\frac{(\Delta/\lambda)_{\text{total}}}{(R/\lambda)}. \tag{5}$$

As an example, consider a spherical reflector having a 10-foot diameter. If the allowable phase error is $\lambda/16$ at 11.2 kmc, the maximum permissible aperture is found to have a diameter of 3.56 feet.

Experimental Studies

The experimental work was conducted using a hemispherical reflector of 10-foot diameter. The reflector is constructed of wood and has a mechanical tolerance of $\pm 1/32$ of an inch. The concave surface of the hemispherical bowl is covered with a coat of silver paint to render it reflecting. A photograph of the reflector is shown in Fig. 4.

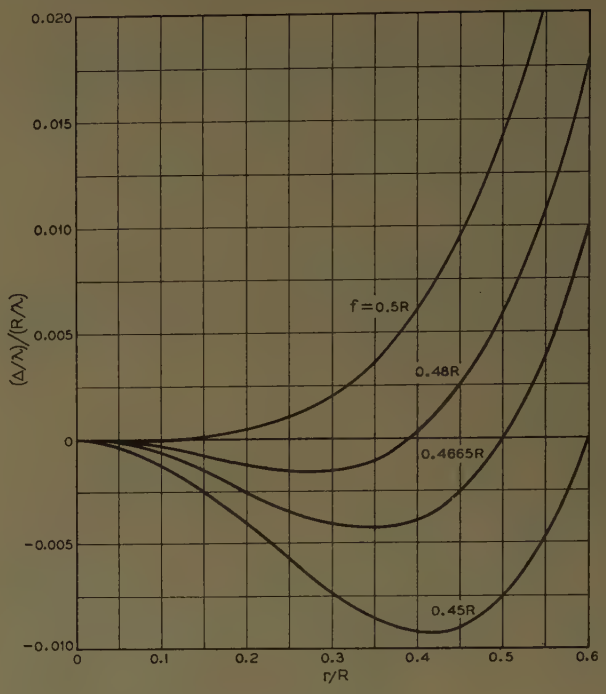

Fig. 2—Phase error over the aperture plane of a spherical reflector.

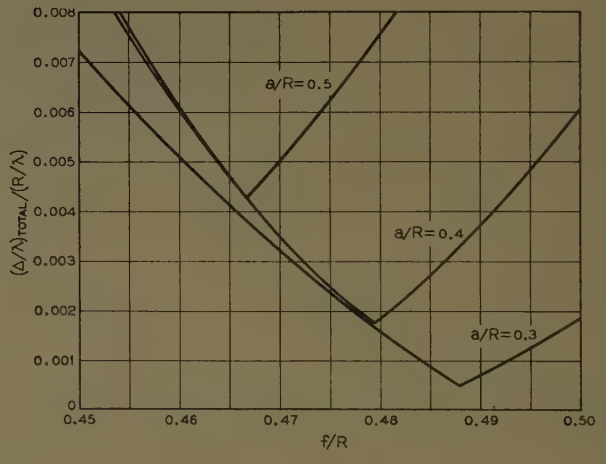

Fig. 3—Total phase error vs focal length for different aperture sizes.

Preliminary experimental studies consisted of taking radiation patterns of the reflector at X-band using several feed horns and different focal lengths. It was found that a suitable feed for the spherical reflector should have a 10-db beamwidth which produces an aperture over which the total phase error is less than $\lambda/16$. Furthermore, its radiation pattern should be rotationally symmetric and its sidelobes should be at least 25 db below peak intensity.

A square-aperture horn with diagonal polarization was found to satisfy the requirements. An exploded view of the horn is shown in Fig. 5. There are two

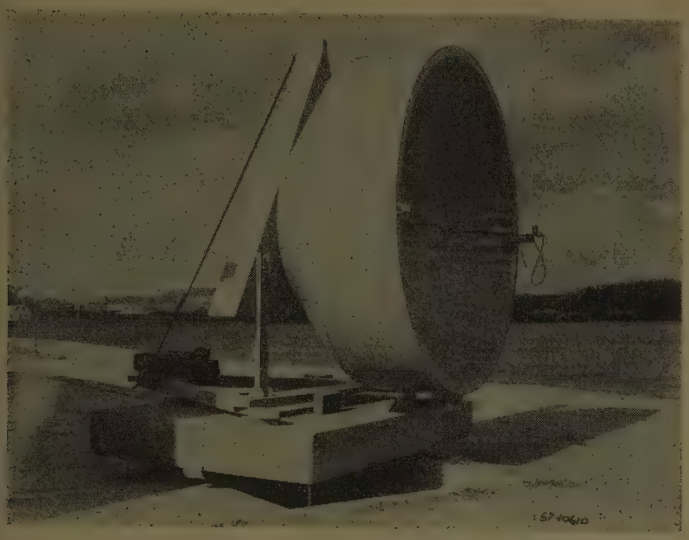

Fig. 4—10-foot diameter spherical reflector.

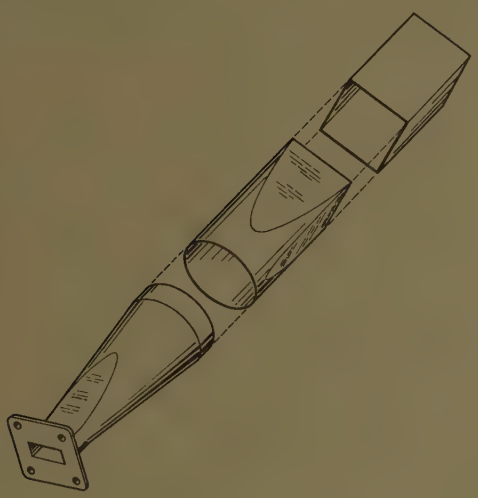

Fig. 5—The square-aperture horn.

transition sections in the horn; the first converts a TE_{10} wave in the rectangular waveguide to a TE_{11} wave in the circular waveguide, the second converts the TE_{11} wave in the circular waveguide to a wave polarized in the diagonal direction of the square waveguide. The diagonally polarized wave in the square waveguide is resolvable into a TE_{10} wave and a TE_{01} wave, both of which are in phase and of equal amplitude. The radiation characteristics of a square-aperture horn having a 3.9 cm by 3.9 cm aperture were measured at 11.2 kmc. Its *H*-, *E*-, and 45°-plane patterns were found to be essentially identical. Its 10-db beamwidth is 76° and all its sidelobe levels are at least 25 db below peak intensity.

Radiation characteristics of the 10-foot spherical reflector illuminated by the square-aperture horn were measured at 11.2 kmc. The radiation patterns in *E*-, *H*-, and 45°-planes for a focal length of 29.5 inches are plotted in Fig. 6. The measured gain is 39.4 db. This is

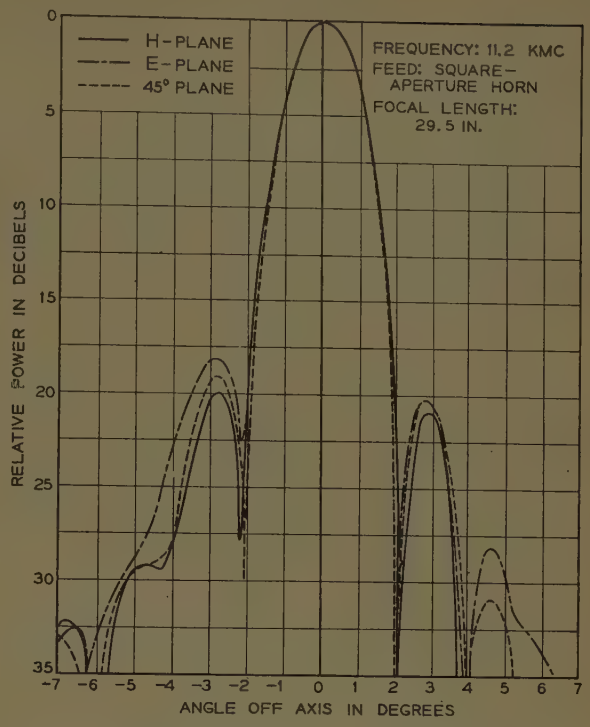

Fig. 6—Radiation patterns of 10-foot spherical reflector.

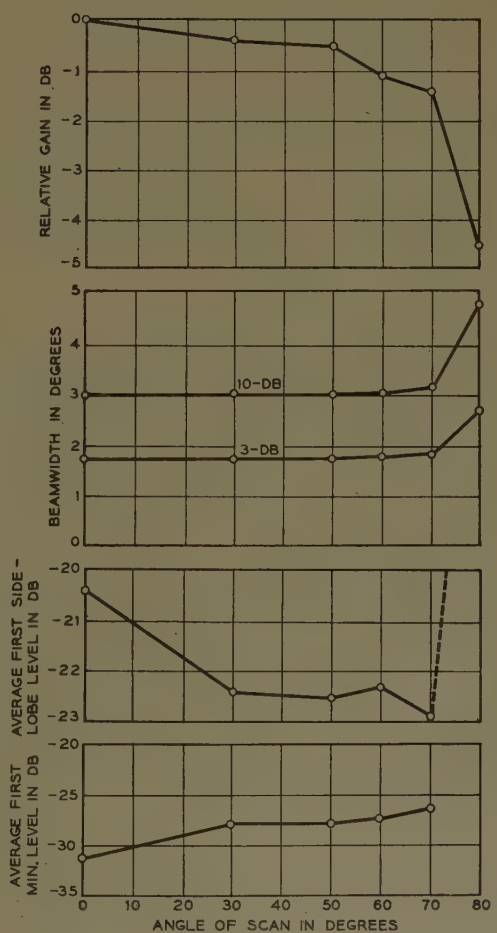

Fig. 7—*H*-plane scanning characteristics of 10-foot spherical reflector.

equivalent to the gain of a uniformly illuminated circular aperture of 31-inch diameter, or a typical paraboloid of 40-inch diameter.

Scanning characteristics of the spherical reflector with the square aperture horn were investigated. A summary of the results is shown graphically in Fig. 7. It is seen that the total useful angle of scan is about 140°. In order to achieve a wider scan, a smaller aperture or a larger reflector must be used.

Conclusion

The spherical reflector is well adapted for use as a wide-angle scanning antenna. By using a restricted aperture and choosing a proper focal point, the effects of spherical aberration can be kept within tolerable limits. The maximum allowable aperture corresponding to a prescribed phase error can be obtained from (5). The focal point that yields the most desirable radiation pattern is best determined experimentally.

Experimental results indicate that the total phase error over the illuminated aperture of the spherical reflector should be held within the $\lambda/16$ limit. This requirement sets an upper limit for the beamwidth of the primary source. A square-aperture horn with an aperture field polarized in the diagonal direction was found to be a suitable primary source. At 11.2 kmc, the radiation patterns of the spherical reflector illuminated by the square-aperture horn showed a 3-db beamwidth of 1.76° and a relative sidelobe level of about −20 db. An absolute gain of 39.4 db was measured and a total useful angle of scan of 140° was achieved. If a larger reflector or a smaller aperture is used, it should be possible to attain a lower sidelobe level and a wider angle of scan.

Acknowledgment

The author wishes to express his appreciation to A. B. Crawford and W. C. Jakes for many stimulating discussions during the course of this investigation. The assistance of W. E. Legg in the experimental phase of the work is also gratefully acknowledged. The hemispherical reflector was built by the carpenter shop personnel of the Holmdel Laboratory.

Analysis and Reduction of Scattering from the Feed of a Cheese Antenna*

W. A. CUMMING†, C. P. WANG‡ AND S. C. LOH†

Summary—**The far field of a cheese antenna can be described in terms of three components: a) one due to the unobstructed aperture field, b) one due to that portion of the primary feed energy not intercepted by the reflector, and c) a scattered component due to the fact that the feed acts as an obstacle in the path of energy emerging from the reflector. This scattered component is usually calculated by considering a perturbation in the aperture field, in the form of an out-of-phase component sufficient to produce zero field in the geometrical shadow region behind the feed. A more exact analysis of a reflector excited by a longitudinally-slotted circular cylinder shows this engineering approach to be satisfactory, provided the out-of-phase component is assumed to exist over an area of width 1.5 times the projected width of the feed. An empirical investigation shows a similar result for a slotted rectangular waveguide feed and for a horn feed. An antenna is described in which the scattered field and the backlobe of the primary feed are made to partially cancel. An additional control over these field components is provided by a series of vanes or waveguides located either side of the feed.**

* Manuscript received by the PGAP, October 21, 1958. Read at IRE Canadian Convention, Toronto, Can., October 8–10, 1958.

† Nat. Res. Council, Radio and Elec. Engrg. Div. Ottawa, Can.
‡ Stanford Electronics Res. Labs., Stanford Univ., Stanford, Calif. Formerly with Natl. Res. Council, Ottawa, Can.

Introduction

THE analysis of a reflector illuminated by a primary radiator shows that the far-field may be considered to consist of three components: a) one due to an unobstructed field distribution over the aperture of the reflector, and determined by the primary feed pattern and focussing properties of the reflector, b) one due to that portion of the primary feed energy which is not intercepted by the reflector, and c) a scattered field component due to the fact that the feed acts as an obstacle in the path of the focussed energy emerging from the reflector. The first two components are readily calculated provided the primary feed pattern, the primary feed gain, and the reflector geometry are known, but the third component is, in general, quite difficult to calculate or measure. The usual engineering analysis[1] treats

[1] S. Silver, "Microwave Antenna Theory and Design," McGraw-Hill Book Co., Inc., New York, N. Y., ch. 6, sec. 6.7, pp. 190–192; 1949.

the scattered field in terms of a perturbation in the unobstructed aperture field caused by the presence of the feed, and assumes a simple perturbation in the form of an out-of-phase component superimposed on the unobstructed aperture field in such a way as to produce zero field in the geometrical shadow region behind the feed.

Since the rear lobe and the scattered field pattern produced by an antenna feed are usually much broader than the secondary pattern of the unobstructed aperture, the effect of these additional fields is to raise the over-all level of spurious or background energy. The effect on the diffraction lobes of the aperture will, of course, depend on the relative phase of the spurious energy. For example, if it is in phase with the main beam it will tend to reduce the odd-order sidelobes and increase the even-order sidelobes, while if it is out-of-phase with the main beam the effect will be reversed. In the case of a paraboloidal reflector illuminated by an electromagnetic horn or similar "point source" feed, it can easily be shown[2] that for a fixed ratio of focal length to diameter, a fixed wavelength, and hence a fixed primary pattern, the ratio of the backlobe field strength to the main beam field strength varies as D^{-1} where D is the reflector diameter. Similarly, by using the simple theory for the scattered field it can be shown[1] that the ratio of scattered field to main beam field for the same conditions varies as D^{-2}. However, in the case of a symmetrical parabolic cylinder illuminated by a line source, and again with the f/D ratio, the wavelength, and the primary pattern fixed, it can be shown that the ratio of the backlobe field strength and scattered field strength to the main beam field strength vary as $D^{-1/2}$ and D^{-1} respectively, and are independent of L, where L is the length of the parabolic cylinder and line source, and D is the reflector width. Thus in both cases the effects of the backlobe and the scattered field are more serious with small antennas, and since this is particularly true for the symmetrical parabolic cylinder, it was chosen for investigation with a view to determining more accurately the magnitude and phase of the scattered field, and also with a view to devising means of reducing it.

Analysis of the Far Field

The configuration assumed for the analysis is shown in Fig. 1. It consists of a parabolic cylinder of focal length f, aperture $D=4f$, and length L. It is illuminated by a magnetic current line source in the form of a narrow slot of angular width ϕ_0 cut in the wall of a hollow circular cylinder of diameter $2a$ and length L. The cylinder axis is located a distance a outside the focal plane, thereby placing the magnetic line source on the

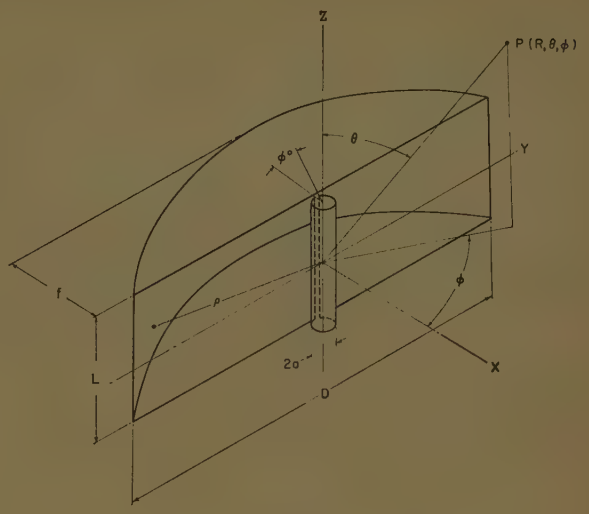

Fig. 1.

focal line. As will be shown, the phase front of the feed with respect to the line source is very nearly cylindrical in the range $90°<\phi<270°$. Assuming a voltage $V\cos(\pi z/L)$ to be impressed across the slot, the total far field was calculated in terms of this voltage by the following steps:

1) The primary pattern was calculated.
2) The unobstructed aperture distribution was calculated from 1).
3) The far-zone pattern was calculated from 2).
4) The scattered field in the region $|\phi|<90°$ was calculated from 2).
5) The backlobe of the primary pattern in the region $|\phi|<90°$ as calculated from 1), and the scattered field from 4), were added to 3).

The Primary Pattern

In order that the cylinder dimensions approximate those of a practical line source feed, the cylinder diameter was chosen so that $ka=(2\pi a)/\lambda=3$. In order that the effects of scattering and of the backlobe be significant, a reflector D of the order of 20λ was selected, the final value being chosen to bring the backlobe in phase with the main lobe. The height of the parabolic cylinder and hence the length of the line source were then chosen to ensure that the entire reflecting surface lay within the cylindrical wave zone of the feed; that is, such that $(L/\lambda)^2>D/2\lambda$, and such that $L/\lambda\gg1$. The value used for both theory and experiment was $L/\lambda=5.73$. As has been pointed out, the value of L was selected so that the reflector lies in the near zone of the feed, thus in the region $90°<\phi<270°$ the primary field E_ϕ^p at distance ρ is given by:[3]

[2] *Ibid.*, ch. 12, sec. 12.5, pp. 428–429.

[3] E. C. Jordan, "Electromagnetic Waves and Radiating Systems," Prentice-Hall, Inc., New York, N. Y., ch. 15, sec. 15.11, pp. 593–596; 1950.

$$E_\phi^p(\rho, \phi, z) = -\frac{jV \cos \frac{\pi z}{L}}{\phi_0 \pi a} \sqrt{\frac{2}{\pi k \rho}}\, e^{-j(k\rho - \pi/4)} \cdot \sum_{n=-o^\circ}^{\infty} \frac{\sin \frac{n\phi_0}{2}}{n H_n^{(2)\prime}(ka)} e^{jn(\phi - \pi/2)}. \quad (1)$$

If the angular width of the slot ϕ_0 is small, so that

$$\frac{\sin \frac{n\phi_0}{2}}{n} \approx \frac{\phi_0}{2},$$

then,

$$E_\phi^p(\rho, \phi, z) = -\frac{jV \cos \frac{\pi z}{L}}{2\pi a} \sqrt{\frac{2}{\pi k \rho}}\, e^{-j(k\rho - \pi/4)} \cdot \sum_{n=0}^{\infty} \epsilon_n j^n \frac{\cos n(\pi - \phi)}{H_n^{(2)\prime}(ka)} \quad (2)$$

where ϵ_n = Neumann's number,
$= 1$, when $n = 0$,
$= 2$, when $n \geq 1$.

In the region of the backlobe, $|\phi| < 90°$, only the far field is of interest, and again assuming ϕ_0 is small, the primary field at a point $P(R,\theta,\phi)$ is given by[4]

$$E_\phi^B(R, \theta, \phi) = -\frac{VL}{2\pi^2 aR} e^{-jkR} \frac{2}{\pi} \cdot \frac{\cos\left(\frac{kL \cos \theta}{2}\right)}{1 - \left(\frac{kL \cos \theta}{\pi}\right)^2} \sum_{n=0}^{\infty} \epsilon_n j^n \frac{\cos n(\pi - \phi)}{H_n^{(2)\prime}(ka \sin \theta)}. \quad (3)$$

Since it is only the field in the principal plane $\theta = 90°$ that is of interest, this can be written,

$$E_\phi^B(R, \theta, \phi) = -\frac{VL}{2\pi^2 aR} e^{-jkR} \frac{2}{\pi} \sum_{n=0}^{\infty} \epsilon_n j^n \frac{\cos n(\pi - \phi)}{H_n^{(2)\prime}(ka)}. \quad (4)$$

Examination of (2) and (4) shows that the variation of E_ϕ^p and E_ϕ^B with respect to ϕ is the same, and the magnitude of this pattern function $f(\phi)$ is plotted in Fig. 2.

The Unobstructed Aperture Distribution

The near field primary energy in the region $90° < \phi < 270°$ is intercepted by the reflector, and provided that the primary phase front in this region is cylindrical, the energy can be focussed to a plane phase front if the axis of the cylindrical phase front is placed on the focal line of the reflector. If $E_\phi^p(\rho, \phi, z)$ is written

$$E_\phi^p(\rho, \phi, z) = E_\phi^p(\rho, \phi, z) e^{j\alpha(\rho, \phi, z)},$$

[4] J. R. Wait, "Radiation characteristics of axial slots on a conducting cylinder," *Wireless Eng.*, vol. 32, pp. 316–323; December, 1955.

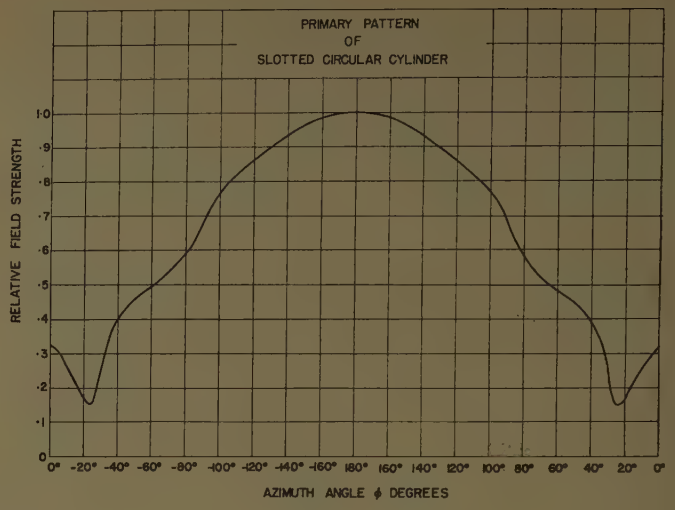

Fig. 2.

then evaluation of (2) shows that $\alpha(\rho, \phi, z)$ has the form

$$\alpha(\rho, \phi, z) = \alpha(\rho, z)\big|_{\phi=180°} - \frac{2\pi a}{\lambda}(1 + \cos \phi) + \Delta_\phi$$

where Δ_ϕ is a small perturbation of the order of 5° to 10°. It is then evident that if the reference for phase is taken to be the slot rather than the center of the cylinder, and further that if Δ_ϕ is neglected, then $\alpha(\rho, \phi, z)$ becomes

$$\alpha(\rho, \phi, z) = \alpha(\rho, z)\big|_{\phi=180°} - \frac{2\pi a}{\lambda}$$

and is thus independent of ϕ in the region $90° < \phi < 270°$, thereby satisfying the condition for a cylindrical phase front. It can therefore be seen that a plane wave will emerge from the reflector if the feed cylinder is located with its axis a distance $x = a$ outside the focal plane, as is shown in Fig. 1.

The equation of the parabola referred to its focus is given by

$$S = \frac{2f}{1 + \cos \psi}$$

where f is the focal length, S is the distance from a point P on the reflector to the focus, and ψ is the angular coordinate of P with respect to the axis of the reflector. The field over the aperture of the reflector can then be obtained quite simply by making use of the reflector equation.[5] Since it has been assumed that the reflector is illuminated by a line source placed at its focus, the emerging rays are parallel, and hence the field remains constant along a reflected ray. The electric field $E_y(y, z)$ in the aperture plane is given by the value of $E_\phi^p(\rho, \phi, z)$ at the corresponding point (ρ, ϕ, z) so that

[5] S. Silver, *op. cit.*, ch. 12, section 12.3, p. 419.

$$|E_y(y,z)| = \frac{V\cos\frac{\pi z}{L}}{2\pi a}\sqrt{\frac{2}{\pi k\rho}} \cdot \left|\sum_{n=0}^{\infty}\epsilon_n j^n \frac{\cos n(\pi-\phi)}{H_n^{(2)\prime}(ka)}\right| \quad (5)$$

where

$$y = \rho\sin\phi, \quad \text{and} \quad \rho = \frac{2f}{1-\cos\phi}.$$

The error which results from defining y and ρ in this manner is small due to the small value of a/f. The phase of the field is very nearly constant over the aperture plane $x=0$ and has a value

$$\text{ARG}\, E_y(y,z) = \alpha(y,z)$$

$$= \text{ARG} - \left\{-je^{-j[2k(f+a)-\pi/4]}\sum_{n=0}^{\infty}\frac{\epsilon_n j^n}{H_n^{(2)\prime}(ka)}\right\} \quad (6)$$

where the additional minus sign is due to the 180° phase shift which occurs on reflection.

The Far Field of the Unobstructed Aperture

The direct computation of the far field, $E_\phi{}^0(R,\theta,\phi)$, from the aperture field, $E_y(y,z)$ is quite difficult due to the nature of the function given in (5). This function is plotted in Fig. 3, and is a reasonable approximation to a much simpler function

$$f(y,z) = A + B\cos\left(\frac{\pi y}{D}\right)$$

where $A=0.5$, and $B=0.5$.

Making use of this approximation, (5) can be written,

$$|E_y(y,z)| = \frac{V\cos\frac{\pi z}{L}}{2\pi a}\sqrt{\frac{2}{\pi kf}}\left|\sum_{n=0}^{\infty}\frac{\epsilon_n j^n}{H_n^{(2)\prime}(ka)}\right| \cdot \left\{0.5+0.5\cos\left(\frac{\pi y}{D}\right)\right\}. \quad (7)$$

The far field in the plane $\theta=90°$ can be readily calculated from the aperture field from the relation[6]

$$E_\phi{}^0(R,\phi) = \frac{j}{2\lambda R}(1-\cos\phi) \cdot e^{-ikR}\int_{-L/2}^{L/2}E_y(z)dz\int_{-D/2}^{D/2}E_y(y)e^{iky\sin\phi}dy. \quad (8)$$

Substituting from (6) and (7) this becomes,

$$E_\phi{}^0(R,\phi) = \frac{jE_m(1+\cos\phi)}{2\lambda R}e^{-ikR}\int_{-L/2}^{L/2}\cdot\cos\frac{\pi z}{L}\,dz\int_{-D/2}^{D/2}\left[0.5+0.5\cos\frac{\pi y}{D}\right]e^{iky\sin\phi}dy \quad (9)$$

[6] S. Silver, *op. cit.*, ch. 6, sect. 6.2, p. 173.

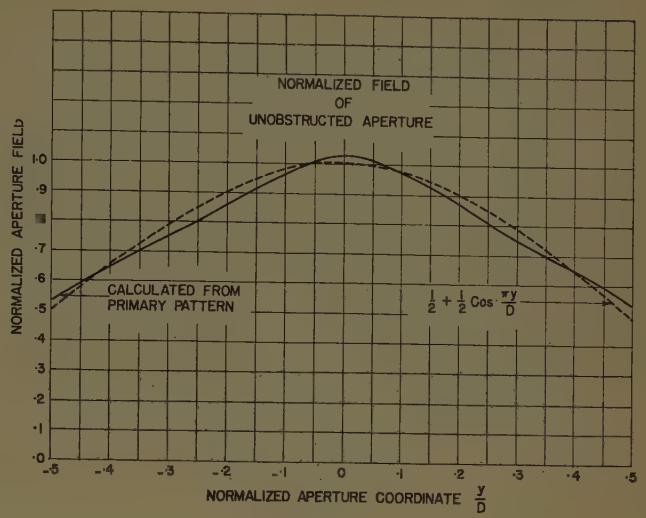

Fig. 3.

where

$$E_m = \frac{V}{2\pi a}\sqrt{\frac{2}{\pi kf}}\left|\sum_{n=0}^{\infty}\frac{\epsilon_n j^n}{H_n^{(2)\prime}(ka)}\right| e^{j\alpha(y,z)}$$

is the maximum value of the aperture field.

Upon integration (9) becomes

$$E_\phi{}^0(R,\phi) = \frac{jE_mLD(1+\cos\phi)}{\pi\lambda R} \cdot e^{-jkR}\left\{\frac{0.5\sin\beta}{\beta}+\frac{1}{\pi}\frac{\cos\beta}{1-(2\beta/\pi)^2}\right\} \quad (10)$$

where $\beta=\pi D\sin\phi/\lambda$.

The secondary pattern function from (10) is plotted in Fig. 4, for a value of $D/\lambda=20$.

The Scattered Field

As has been pointed out earlier, the feed acts as an obstacle in the path of the emerging aperture field $E_y(y,z)$. Due to the separation of the feed and reflector, the energy scattered back into the reflector and then into space can be neglected, but the energy scattered directly into space is quite significant. This can be calculated by assuming first that the incident field in the immediate vicinity of the feed is independent of y, with a value $E_m\cos\pi z/L$, and further assuming that the slot in the feed cylinder has a small effect on the scattering properties of the cylinder. The calculation of the scattered field then becomes one of determining the induced current on the cylinder, subject to the boundary condition that there be no net tangential electric field on the surface of the cylinder. The far-zone electric field produced by the induced current can then be readily calculated.

The scattered magnetic field in the immediate vicinity of the feed can be calculated by Carter's method[7] and gives

[7] P. S. Carter, "Antenna arrays around cylinders," Proc. IRE, vol. 31, pp. 671–693; December, 1943.

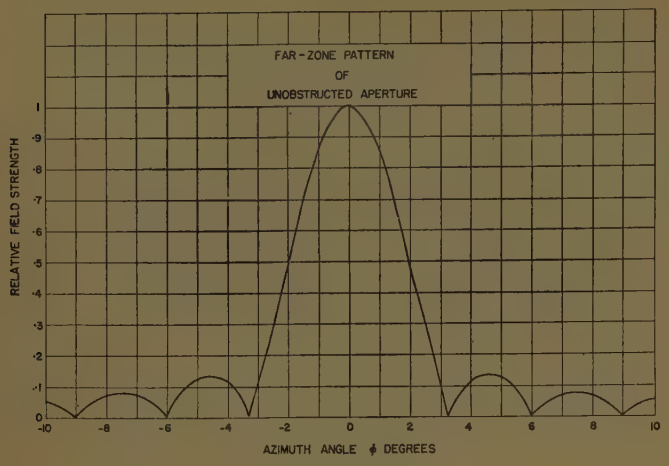

Fig. 4.

$$H_z^s = \sqrt{\frac{\epsilon}{\mu}}\, E_m \cdot \cos\frac{\pi z}{L} \sum_{-\infty}^{\infty} (j)^n \frac{J_n'(ka)}{H_n^{(2)\prime}(ka)} H_n^{(2)}(kR) e^{jn(\pi-\phi)}. \quad (11)$$

The induced surface current on the cylinder is then

$$J_\phi = \vec{n} \times \vec{H}_z^s\big|_{R=a} = \sqrt{\frac{\epsilon}{\mu}}\, E_m \cos\frac{\pi z}{L} \sum_{n=-\infty}^{\infty} (j)^n \cdot \frac{J_n'(ka)}{H_n^{(2)\prime}(ka)} H_n^{(2)}(ka) e^{jn(\pi-\phi)}. \quad (12)$$

The far-zone electric field can be calculated from the induced surface current by means of the relation[8]

$$E^s = -\frac{j\omega\mu}{2\pi R} e^{-jkR} \int_{\text{surf}} \{(\vec{n} \times \vec{H}_z^s) - (\vec{n} \times \vec{H}_z^s)\cdot\vec{R}\} \cdot e^{-jka\cdot R}\, ds \quad (13)$$

where $\vec{n}$ is the exterior normal from a point on the surface. Since only the ϕ-component of the scattered field is significant, this can be written

$$E_\phi^s = -\sqrt{\frac{\epsilon}{\mu}}\, \frac{j\omega\mu}{2\pi R} E_m e^{-jkR} \sum_{-\infty}^{\infty} (j)^n \frac{J_n'(ka)}{H_n^{(2)\prime}(ka)} H_n^{(2)}(ka) \cdot a \int_0^{2\pi} \cos(\phi' - \phi) e^{jn(\pi-\phi)} e^{jka \sin\theta \cos(\phi'-\phi)} d\phi' \cdot \int_{-L/2}^{L/2} \cos\frac{\pi z}{L} e^{jkz\sin\theta} dz \quad (14)$$

where ϕ is the angular co-ordinate of a point on the surface of the cylinder.

In the plane $\theta = 90°$ this becomes

$$E_\phi^s = \frac{kaE_mL}{R} e^{-jkR} \frac{2}{\pi} \sum_{n=0}^{\infty} (-1)^n \frac{\epsilon_n [J_n'(ka)]^2 H_n^{(2)}(ka)}{H_n^{(2)\prime}(ka)} \cdot \cos n(\pi - \phi). \quad (15)$$

[8] S. Silver, *op. cit.*, ch. 5, sect. 5.9, p. 149.

The scattered field has been evaluated for the assumed geometry, and is tabulated in Table I, normalized to the peak field strength $E_\phi^0(R, \phi)\big|_{\phi=0°}$.

TABLE I

TABULATION OF THE FAR FIELD COMPONENTS

ϕ	$\frac{E_\phi^s}{E_\phi^0\|_{\phi=0°}}$	$\frac{E_\phi^B}{E_\phi^0\|_{\phi=0°}}$	$\frac{E_\phi^0}{E_\phi^0\|_{\phi=0°}}$
0°	$-(0.086+j0.023)$	0.047	1
1°	$-(0.086+j0.023)$	0.046_5	0.856
2°	$-(0.086+j0.023)$	0.046	0.472
3°	$-(0.086+j0.023)$	0.046	0.094
4°	$-(0.086+j0.023)$	$0.045+j0.001$	-0.110
5°	$-(0.086+j0.022)$	$0.045+j0.001$	-0.108
6°	$-(0.085+j0.022)$	$0.044+j0.002$	-0.002
7°	$-(0.085+j0.022)$	$0.043+j0.003$	0.073
8°	$-(0.085+j0.022)$	$0.041+j0.003$	0.057
9°	$-(0.084+j0.022)$	$0.040+j0.004$	-0.010
10°	$-(0.084+j0.021)$	$0.038_5+j0.005$	-0.054

The Total Far Field

The total far field is the sum of the fields given in (4), (10), and (15), *i.e.*,

$$E_\phi^T(R, \phi) = E_\phi^0(\phi, R) + E_\phi^B(\phi, R) + E_\phi^s(\phi, R) = \frac{jVLDC}{2\lambda R} e^{-jk[R-\alpha(y,z)]} \cdot \left\{F_0(\phi) - j\frac{4\pi a}{D} F_s(\phi) - j\frac{4}{\pi^2 akDC} e^{-j\alpha(y,z)} F_B(\phi)\right\} \quad (16)$$

where

$$C = \frac{1}{\pi^2 a}\sqrt{\frac{2}{\pi kf}}\left|\sum_{n=0}^{\infty} \epsilon_n \frac{j^n}{H_n^{(2)\prime}(ka)}\right|$$

$$F_0(\phi) = (1+\cos\phi)\left\{\frac{1}{2}\frac{\sin\beta}{\beta} + \frac{1}{\pi}\frac{\cos\beta}{1-\left(\frac{2\beta}{\pi}\right)^2}\right\}$$

$$F_s(\phi) = \sum_{n=0}^{\infty} (-1)^n \epsilon_n \frac{[j_n'(ka)]^2 H_n^{(2)}(ka)}{H_n^{(2)\prime}(ka)} \cos n(\pi - \phi)$$

$$F_B(\phi) = \sum_{n=0}^{\infty} \epsilon_n \frac{j^n \cos n(\pi - \phi)}{H_n^{(2)\prime}(ka)}$$

and the minus sign associated with $F_B(\phi)$ is due to the phase reversal in space between the forward and back lobes of the primary pattern.

It is seen from (16) that the phase of the backlobe relative to the main beam is given by

$$\Delta = -90° - \alpha(y, z) + \text{ARG} \sum_{n=0}^{\infty} \epsilon_n \frac{j^n \cos n(\pi - \phi)}{H_n^{(2)\prime}(ka)} \quad (17)$$

which in the direction $\phi = 0°$ becomes

$$\Delta = -90° - \left\{+90° - 2k(f+a) + 45° + \text{ARG} \sum_{n=0}^{\infty} \epsilon_n \frac{j^n}{H_n^{(2)\prime}(ka)}\right\} + \text{ARG} \sum_{n=0}^{\infty} \epsilon_n \frac{j^n \cos n\pi}{H_n^{(2)\prime}(ka)}. \quad (18)$$

When evaluated for $ka = 3$, this becomes $\Delta = 2k(f+a)$. Thus in order to bring the backlobe into phase with the main beam, f must be chosen so that $2k(f+a) = 2m\pi$. Thus f must have a value

$$\frac{f}{\lambda} = \frac{1}{4\pi}(2m\pi - 2ka).$$

Since the preceding calculations have been based on a value of $f/\lambda = 5$, this value must now be adjusted to

$$\frac{f}{\lambda} = \frac{1}{2\pi}(2\pi \cdot 11 - 6) = 5.022.$$

With f/λ chosen to bring the backlobe in phase with the main beam, the values of the three field components were calculated, and are tabulated in Table I, with all components normalized to the value $E_\phi{}^0(\phi)\big|_{\phi=0°}$. The magnitude of the total field is shown by the calculated points in Fig. 5.

It is of interest to compare the scattered field as shown in Table I with that which would be obtained from the usual theory of aperture blocking.[1] This field has a normalized value

$$\frac{E_\phi{}^s}{E_\phi{}^0\big|_{\phi=0°}} = \frac{2a \sin\left(\frac{\pi a}{\lambda}\sin\phi\right)}{\int_{-D/2}^{D/2} F(y)dy \quad \frac{\pi a}{\lambda}\sin\phi} \quad (19)$$

where $F(y)$ is the unobstructed aperture distribution in the y-direction. For the value $F(y) = 0.5 + 0.5\cos(\pi y/D)$, this becomes

$$\frac{E_\phi{}^s}{E_\phi{}^0\big|_{\phi=0°}} = 2.4(a/d)\frac{\sin\left(\frac{\pi a}{\lambda}\sin\phi\right)}{\frac{\pi a}{\lambda}\sin\phi}.$$

For a value of $\pi a/\lambda = 1.5$, the pattern function is nearly constant, so this becomes,

$$\frac{E_\phi{}^s}{E_\phi{}^0\big|_{\phi=0°}} = 2.4(a/D) = 0.057.$$

Thus the simple theory predicts an out-of-phase scattered field having a constant amplitude of 0.057 in the region of the main beam, while the more exact theory predicts a scattered field of again almost constant amplitude, having a magnitude of 0.089 and a phase of $-195°$ with respect to the main beam.

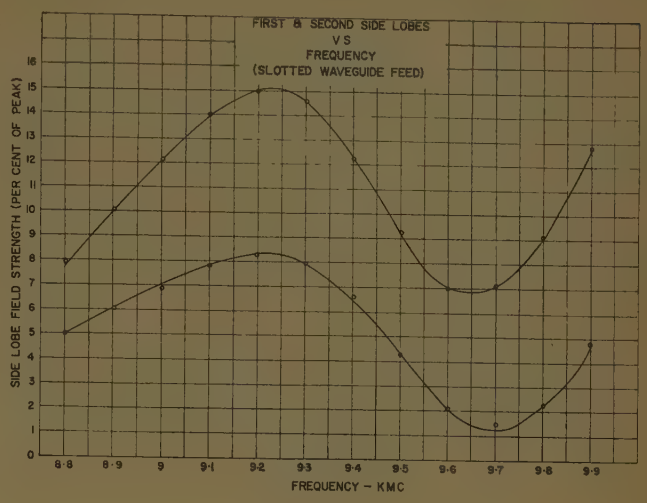

Fig. 5.

Experimental Verification

In order to verify the analysis, a parabolic cylinder of focal length 6.5 inches, aperture 26 inches and height 7.5 inches was constructed. It was illuminated by a cylindrical feed 1.25 inches in diameter, with a series of collinear half-wave slots cut longitudinally in the cylinder wall. As has been pointed out, the theoretical analysis requires that the focal length have a value of 5.022λ in order to bring the backlobe into phase with the main beam. This in turn dictates an operating frequency of 9125 mc.

A measured pattern in the E-plane ($\theta = 90°$) is shown in Fig. 6, together with the theoretical points. It is seen that the agreement between theory and experiment is quite satisfactory.

Examination of the expression for the scattered field, as calculated by the simple theory and by the more exact theory, has shown that they differ mainly in amplitude, with a small phase discrepancy. For the type of feed which has been studied, this suggests that for engineering purposes the simple theory might be modified to give a more accurate result. In fact, if the actual projected width $2a$ of the feed were replaced by an "effective" width approximately 50 per cent greater, then the approximate theory would give a result adequate for most purposes.

Two other types of feed were investigated experimentally in order to extend this concept of an "effective" width. These were a rectangular waveguide of outside dimensions 1 inch $\times \frac{1}{2}$ inch, with shunt slots in the broad face, and an electromagnetic horn of aperture size 5.5 inches $\times$ 1 inch and length 5 inches. The centers of phase were assumed to be at the face of the waveguide and at the mouth of the horn, respectively, and far-zone patterns were measured with these phase centers on the focal line of the parabolic cylinder. In both cases patterns were measured at a number of frequencies, so that the variation in sidelobe level due to the change in the relative phase of the backlobe with frequency could be observed. A curve of the level of the first measured sidelobe and of the second measured sidelobe is shown in

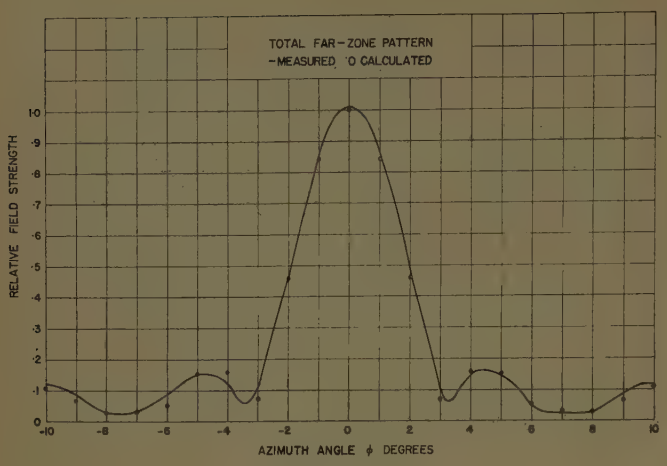

Fig. 6.

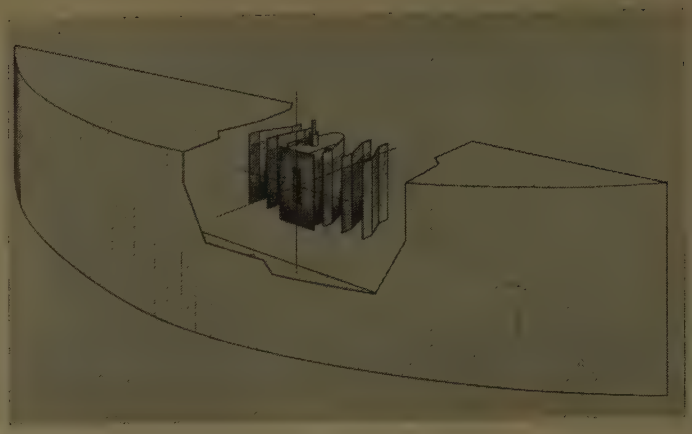

Fig. 7.

Fig. 6 for the slotted rectangular waveguide feed. Let the normalized values of the "ideal" first sidelobe, the "ideal" second sidelobe, the backlobe, and the scattered field, be E_L', E_L'', E_B, and E_s respectively. Then if the maximum and minimum values of the first measured sidelobes are $E_{\max}'$ and $E_{\min}'$, and the maximum and minimum values of the second measured sidelobe are $E_{\max}''$ and $E_{\min}''$, it is easy to see that

$$\frac{E_s + E_B + E_L'}{1 - E_s - E_B} = E_{\max}' \qquad \frac{E_s + E_B + E_L''}{1 - E_s - E_B} = E_{\max}''$$

$$\frac{E_s - E_B + E_L'}{1 - E_s + E_B} = E_{\min}' \qquad \frac{E_s - E_B - E_L''}{1 - E_s + E_B} = E_{\min}''$$

assuming the antenna is properly focussed so that E_L' and E_L'' are 180° out-of-phase. These equations can then be solved to give E_s, E_B, E_L', and E_L''. The values obtained for the slotted waveguide feed were $E_s = 6.5$ per cent, $E_B = 3$ per cent, $E_L' = 4$ per cent, and $E_L'' = 2.75$ per cent; and for the horn feed, $E_s = 6$ per cent, $E_B = 1.8$ per cent, $E_L' = 2.5$ per cent, and $E_L'' = 1$ per cent.

The primary patterns of both feeds were also measured, from which the unobstructed aperture distribution could be calculated. Then by using the measured values of scattered field and the calculated aperture distributions in (19), the "effective" width of the feeds could be calculated. In the case of the rectangular waveguide feed it was found that the ratio of effective width to projected width was 1.18, and in the case of the horn feed, 1.10.

Reduction of Sidelobes

As has been shown, the effect of the backlobe and of the scattered field is to raise the over-all background level of the antenna pattern, an effect that is most serious in the direction of the major sidelobes. Since the patterns of the backlobe and scattered field are similar in shape and quite broad in terms of the main beam, it becomes apparent that if their magnitude could be made equal, the two fields could be made to cancel by appropriate choice of phase, thereby leaving only the "ideal" pattern. This cancellation would of course be frequency-sensitive, and as can be seen from Fig. 6, if the phase is chosen to give cancellation at one frequency, there will be another frequency at which the fields will add. In the interest of obtaining bandwidth it would be desirable to make the fields equal and as small as possible, and to adjust their relative phase for cancellation at midband.

The backlobe of a primary feed can be considered as originating from current flowing back on the outside of the feed. It would be expected that a reduction in these surface currents would be accompanied by a reduction in the backlobe. This is found to be the case, and the reduction in surface current is usually accomplished by means of high impedance resonant chokes placed across the path of current flow.[9] These resonant chokes, of course, tend to reduce further the bandwidth of the antenna.

It has been shown that the scattered field is proportional to the projected width of the feed. It is then obvious that in order to reduce scattering the feed should be made as small as possible, consistent with obtaining the desired primary pattern. One method which has been successfully employed to reduce the scattered field still further is shown in Fig. 7. Here the feed consists of a longitudinal slot or series of slots cut in the narrow wall of a waveguide or cavity. The narrow face is extended either side of the slot to form a ground plane of width 0.35λ. A pair of resonant chokes is located either side of the cavity to suppress the backlobe to a reasonable value. In order to increase the aperture field in the shadow region behind the feed, the feed is tapered on the outside and surrounded by two sets of inclined metal vanes which tend to guide energy into the shadow region. As yet only an empirical investigation of this device has been carried out, but it does appear to reduce the scattered field, and at the same time to modify the primary pattern.

[9] W. H. Watson, "The Physical Principles of Waveguide Transmission and Antenna Systems," Oxford University Press, New York, N. Y., p. 88; 1947.

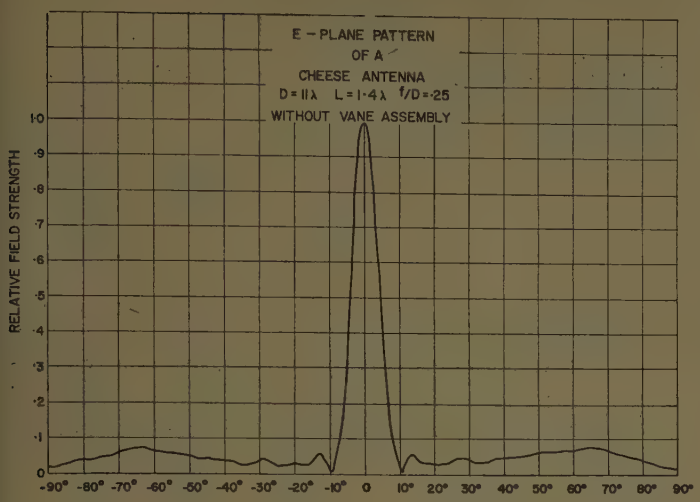

Fig. 8.

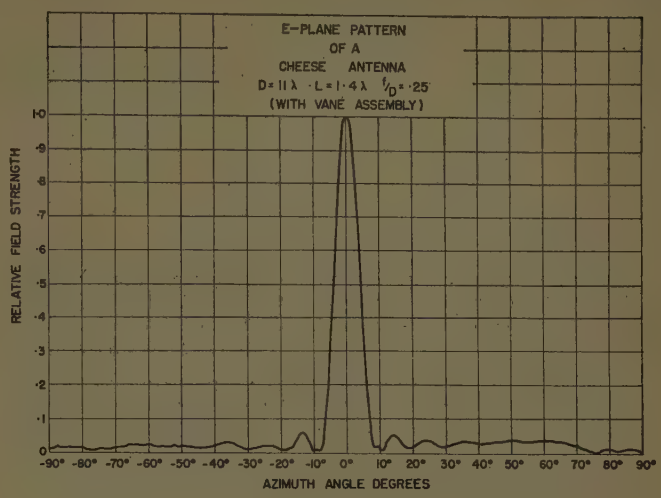

Fig. 9.

The patterns of Figs. 8 and 9 show the extent to which the undesirable effects of the backlobe and scattered field have been reduced for a small cheese antenna of aperture $11\lambda \times 1.4\lambda$ and $f/D = 0.25$. The feed consists of a cavity 0.7λ high $\times 0.6\lambda$ deep $\times 0.25\lambda$ wide. Due to the presence of the chokes and ground plane the exterior width of the feed is 0.35λ. Two sets of plates of height 0.7λ and depth 0.5λ are located either side of the feed, with a total width varying from 1.1λ at the inner face to 1λ at the outer face. The focal length of the reflector was chosen to give the greatest degree of cancellation between the backlobe and scattered field. However, examination of Fig. 8 shows this cancellation to be incomplete. The mean background level in the vicinity of the sidelobes is 4 per cent and the presence of the deep null either side of the main beam suggests that the scattered field predominates. Furthermore, the high level of 7.5 per cent at 65° shows considerable spill-over exists. In Fig. 9 the background level has been reduced to 3 per cent by the addition of the vanes, while the first null has risen. In addition the spill-over level has dropped by 4 per cent, and the sidelobe structure is more clearly defined, indicating a change in primary pattern.

It must again be pointed out that this reduction in background level is frequency-sensitive. In this case, the first sidelobe rose to 10 per cent for a frequency swing of ± 3.75 per cent, at which frequencies calculation shows the backlobe to be in quadrature with the main beam.

Conclusion

It has been shown that the presence of the feed in the aperture of a symmetrical cheese antenna has an effect greater than that predicted by simple theory for the types of feeds investigated. While it is not suggested that the example given in the preceding section shows the best that can be achieved by way of eliminating the undesirable effects of the backlobe and scattered field, it does indicate that a great deal can be done toward making these effects self-cancelling.

On the Phase Velocity of Wave Propagation along an Infinite Yagi Structure*

DIPAK L. SENGUPTA†

Summary—**An approximate expression is derived for the phase velocity of wave propagation along an infinite Yagi structure and its dependence on the various parameters of the structure is discussed in detail. The structure is at first studied qualitatively by applying the transmission line analogy. The problem is next treated from the viewpoints of linear antenna and field theories. It is assumed that a traveling wave is propagating along the axial direction and it induces an axially symmetric and sinusoidal current distribution in each element. The electric field at any point due to this current distribution is calculated by the Hertz vector method. After applying boundary condition to the electric field, an expression for the propagation constant is derived. The results are compared with existing experimental values. The agreement between theory and experiment is found to be within 5 per cent. The accuracy of the expression given is sufficient for practical purposes.**

Introduction

In this paper an approximate expression is derived for the phase velocity of wave propagation along an infinite Yagi structure. An infinite Yagi structure is a periodic structure of parallel and conducting metal rods of finite length which extends to infinity in both directions along the z-axis (Fig. 1). It is assumed that a traveling wave is launched into this structure and it is propagating along the positive z-direction.

Because of its importance in antenna applications, a considerable amount of experimental work on this type of structure has recently been done by Ehrenspeck and Poehler[1] and Spector.[2] They found that when excited properly, the long Yagi structure can support a traveling wave and they have measured the velocity of propagation along the structure. In the following investigation an approximate expression for the phase velocity is derived by applying the ideas of linear antenna and field theories. The theoretical expression is then compared with the existing experimental results.

It can be shown[3] that once the phase velocity is known the complete design of a long Yagi antenna can be carried out by applying the traveling wave ideas.

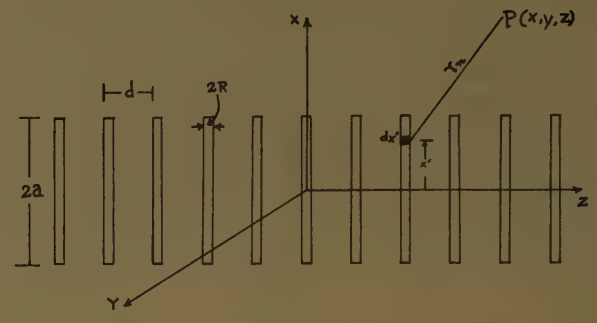

Fig. 1—Geometrical representation of the infinite Yagi structure, showing the system of co-ordinates used.

Method of Analysis

The analysis is divided into two parts. First, the structure is studied from the viewpoint of transmission line analogy. Although this is a crude analysis which fails to offer any quantitative results for the phase velocity, it can explain qualitatively most of the experimentally observed facts. This helps one to understand the problem physically. Secondly, the problem is treated analytically for quantitative results. In general this problem may be formulated as an eigenvalue problem in the same manner as is done in periodic structure analysis, *viz.* in the case of the determination of propagation constants (eigenvalues) of different modes in helical structure,[4] where the Hertz potential of the helical structure is assumed to be in the form of an infinite Fourier series with unknown coefficients. These coefficients and the possible eigenvalues are determined by applying the proper boundary condition to the Hertz potential. The same technique was tried in the present problem at first. But the complicated nature of the analysis and the difficulty of obtaining a readily computable expression forced the author to abandon that approach. Instead of finding the possible modes (eigenfunctions) of propagation characteristic to the infinite Yagi structure, it is assumed that a particular mode is propagating down the structure with a phase velocity which is unknown. The existence of this mode and the field distribution associated with it have been studied experimentally by Ehrenspeck and Poehler,[1] and by Spector.[2] By the analogy of linear antenna theory a sinusoidal current of axially symmetric distribution, induced by the traveling wave, is assumed in each element. The Hertz potential at any point due to this current distribution is calculated next. The propa-

* Manuscript received by the PGAP, November 14, 1958; revised manuscript received, March 13, 1959. The research reported herein was made possible through support to the Dept. of Elect. Eng., Univ. of Toronto, Can., by the Nat. Res. Council of Canada, under Radio-astronomy Project, Grant No. G 587. The work is in part the subject of a thesis for the Doctor of Philosophy degree at the University of Toronto, submitted in September, 1958.

† Gordon McKay Lab. of Appl. Sci., Harvard Univ., Cambridge, Mass. Formerly with the Dept. of Elect. Eng., Univ. of Toronto, Can.

[1] H. W. Ehrenspeck and H. Poehler, "A Method for Obtaining Maximum Gain from Yagi Antennas," Antenna Lab., Electronics Res. Dir., AFCRC, Bedford, Mass.; July, 1956.

[2] J. O. Spector, "An investigation of periodic rod structures for Yagi aerials," *J. IEE (London)*, vol. 105, pt. B, pp. 38–43; 1958.

[3] D. L. Sengupta, "Traveling wave analysis of certain end-fire antennas," Ph.D. dissertation, Univ. of Toronto, Can.; 1958.

[4] S. Sensiper, "Electromagnetic wave propagation on helical structures." Proc. IRE, vol. 43, pp. 149–161; February, 1955.

gation constant of this mode is derived from the above after applying the proper boundary condition. Although the analysis is similar to the eigenvalue problem referred to previously, the use of an approximate current distribution based on linear antenna theory has simplified the analysis considerably.

Analysis by Transmission Line Analogy

The analogy between plane wave and transmission line propagation[5,6] is often used advantageously for the determination refractive indices and propagation constants of artificial dielectrics consisting of periodic structures. From this analogy the infinite Yagi structure can be represented by a periodically loaded transmission line; the propagation constant in the structure will be the same as that of the loaded line. Fig. 2 represents the loaded line equivalent to the infinite Yagi structure carrying a traveling wave along it. Z_1, Z_3 are the series and shunt impedances respectively offered by each rod to the propagating wave; Z', γ' are the constants of the loaded line as shown in the figure. From the periodically loaded transmission line theory it can be shown[7] that the propagation constant γ' can be expressed as functions of the constants of the unloaded line and the loading elements, as in the following equation:

$$\cosh(\gamma' d) = \left(1 + \frac{Z_1}{Z_3}\right)\cosh \gamma d + \left(\frac{Z}{2Z_3} + \frac{Z_1}{Z} + \frac{Z^2}{2ZZ_3}\right)\sinh \gamma d. \quad (1)$$

It is known[8] that the infinite system does not radiate and that it supports a propagating wave without attenuation. Under these conditions and further assuming the entire system as lossless, the following may be written $\gamma' = j\beta$, $\gamma = jk$ $(k = 2\pi/\lambda)$, $Z_3 = jX_3$, and $Z_1 = jX_1$. After substituting these in (1) the following is obtained:

$$\cosh \beta d = \left(1 + \frac{X_1}{X_3}\right)\cos kd + \left(\frac{Z}{2X_3} - \frac{X_1}{Z} - \frac{X_1^2}{2ZX_3}\right)\sin kd. \quad (2)$$

From the geometry and excitation of the system it may be assumed that X_1 is negligible and hence (2) may be written in the form

$$\cosh \beta d = \cos kd + \frac{Z}{2X}\sin kd, \quad (3)$$

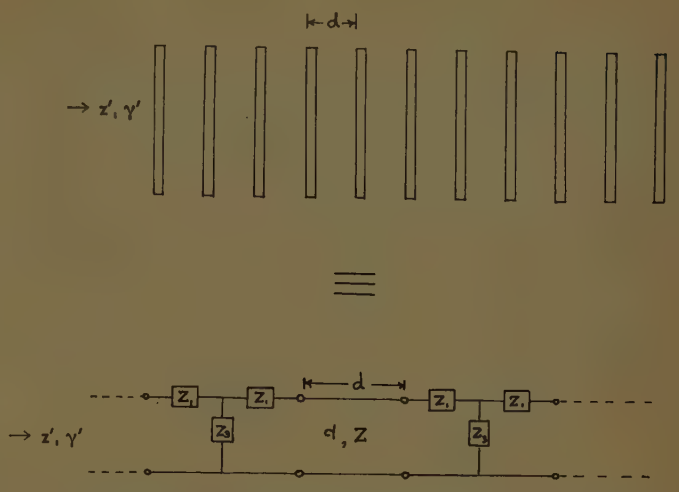

Fig. 2—The infinite Yagi structure and its equivalent periodically loaded line.

where, $X_3 = X$. To a first approximation $\sin kd \approx kd$ and $\cos kd \approx 1 - k^2d^2/2$ and by using the relation $v = \omega/\beta$, the following expression is obtained;

$$\frac{v}{c} = 1 + \frac{z\lambda}{4\pi dX} \quad (4)$$

where,

v is the velocity of propagation in the infinite Yagi,
c is the velocity of propagation in free space.

The following general comments can be made from critical study of (4):

1) The infinite Yagi structure will support a wave propagating without attenuation if the loading is purely reactive.

2) The phase velocity will be slow $(v < c)$ if the loading is capacitive, and fast $(v > c)$ if the loading is inductive. From antenna theory it is known that the rods will be capacitive if their lengths are less than $\lambda/2$. This means that in order to use the infinite Yagi structure as a slow wave structure, the length of each rod should be chosen to be less than $\lambda/2$.

3) The phase velocity decreases as the spacing between the rods is decreased (slow wave case).

4) The phase velocity decreases as the length of each rod $2a$ is increased (for slow wave case). This can be seen from antenna theory[9] where it is known that $|X|$ increases as $2a$ is decreased.

5) The phase velocity increases as the radius R of each rod is decreased. This statement cannot be seen directly from (4) but can be seen by considering the effect of the variation of R on X.[9]

All the above comments are in agreement with experimental results.[1,2]

[5] J. A. Stratton, "Electromagnetic Theory," McGraw-Hill Book Co., Inc., New York, N. Y., pp. 282–284; 1941.
[6] G. G. Macfarlane, "Quasi-stationary field theory and its application to diaphragms and junctions in transmission lines and waveguides," *J. IEE (London)*, vol. 93, pt. 3A, pp. 703–719; 1946.
[7] S. Silver, "Microwave Antenna Theory and Design," McGraw-Hill Book Co., Inc., New York, N. Y., p. 315, 1949.
[8] F. J. Zucker, "The Guiding and Radiation of Surface Waves," *Proc. of the Symp. on Modern Advances in Microwave Techniques*, Polytechn. Inst. of Brooklyn, New York, N. Y., pp. 403–435; 1954.
[9] E. C. Jordan, "Electromagnetic Waves and Radiating Systems," Prentice-Hall Inc., New York, N. Y., p. 364; 1951.

Approximate Expression for Phase Velocity

Let the Yagi structure and its relation to the particular coordinate system be as shown in Fig. 1. It is assumed that a wave with electric vector parallel to the x-direction is traveling along the z-direction. This assumption is reasonable if one considers the nature of excitation used in Yagi structure and the measured field distribution over it.[1] Let the current in the nth rod (Fig. 1) be denoted by $I_n(x')$. In the analysis the primed coordinates will refer to the source points. The Hertz potential at any field point P due to the currents in all the rods is given by

$$\pi_x = \sum_{n=-\infty}^{\infty} \frac{1}{i4\pi\omega\epsilon} \int_{-a}^{a} \frac{I_n(x')e^{-ikr_n}}{r_n}\, dx' \tag{5}$$

where ω is the angular frequency, ϵ is the dielectric constant of free space and

$$r_n^2 = (x - x')^2 + (y - y')^2 + (z - nd)^2,$$
$$n = 0, \pm 1, \pm 2, \pm 3, \cdots. \tag{6}$$

The time dependence is assumed to be of the form $e^{i\omega t}$.

For the present the actual distribution of current $I_n(x')$ in each rod will not be discussed. However, from the nature of excitation and symmetry of the system it may be assumed that the current is directed along the x-direction and its magnitude is of the same value in each rod. The phase of the current in each rod will differ from that of its neighbor by a phase factor due to the finite time taken by the exciting traveling wave to travel from one rod to the other. Assuming propagation without attenuation, the current distribution function may be written as

$$I_n(x') = I(x')e^{-i\beta nd} \tag{7}$$

where β is the propagation constant in the infinite Yagi structure. Eq. (7) may be recognized as the usual Floquet[10] type of phase variation used in periodic structure analysis. This type of phase variation is based on Floquet's Theorem which states that in any medium having a spatial periodicity d, the fields are multiplied by the same complex constant if one moves down the structure by a distance d. This is obvious in the present problem since, if the structure is displaced along the z-axis (Fig. 1) by an amount d, it coincides with itself and the new field can differ from the previous one only by a constant factor.

After substituting (7) into (5), the following is obtained:

$$\pi_x = \sum_{n=-\infty}^{\infty} \frac{1}{i4\pi\omega\epsilon} \int_{-a}^{a} \frac{I(x')e^{-i\beta nd}e^{-ikr_n}}{r_n}\, dx'. \tag{8}$$

The purpose of the analysis is to obtain an expression for the propagation constant β. In order to do this, an expression for the x-component of the electric field E_x at any point P will be derived from (8) and then the proper boundary condition will be applied to this field. The x-component of the electric field E_x may be obtained from (8) by using the following relation:

$$E_x = \frac{d^2\pi_x}{dx^2} + k^2\pi_x. \tag{9}$$

If the rods are assumed to be perfectly conducting, the boundary condition requires

$$E_x = 0, \quad \text{at } -a \le x \le a, \quad \text{and} \quad z = R - nd. \tag{10}$$

The above condition will be applied to (9) for the case of the rod situated at the origin only; this is justified because if in a periodic structure the boundary condition is satisfied at one rod surface, it will certainly be satisfied at the others also.

To obtain the tangential electric field on the surface of the rod situated at the origin, (8) should be rearranged by using the following integral transformation due to Weyrich:[11]

$$\frac{e^{-ik\sqrt{r^2+x^2}}}{\sqrt{r^2+x^2}} = -\frac{i}{2}\int_{-\infty}^{\infty} e^{-i\tau x} H_0^{(2)}(\gamma\sqrt{k^2-\tau^2})\, d\tau \tag{11}$$

where

$$-\pi < \arg\sqrt{k^2-\tau^2} \le 0, \qquad -\pi < \arg k \le 0,$$

and $H_0^{(2)}$ is the usual notation for the zeroth order Hankel function of the second kind. After using (8), (9), and (11), the following equation is obtained for E_x;

$$E_x = -\frac{1}{8\pi\omega\epsilon} \sum_{n=-\infty}^{\infty} e^{-i\beta nd} \int_{-a}^{a} I(x') \int_{-\infty}^{\infty} (k^2 - \alpha^2) \cdot e^{-i\alpha(x-x')} H_0^{(2)}(\rho_n\sqrt{k^2-\alpha^2})\, dx'\, d\alpha'$$
$$\rho_n^2 = (R - nd)^2. \tag{12}$$

The boundary condition (10) is now applied to (12) and the following integral equation of the first kind is obtained:

$$\int_{-a}^{a} I(x')K(x, x')\, dx' = 0 \tag{13}$$

where

$$K(x, x') = \sum_{n=-\infty}^{\infty} e^{-i\beta nd} \int_{-\infty}^{\infty} (k^2 - \alpha^2) \cdot e^{-i\alpha(x-x')} H_0^{(2)}(\rho_n\sqrt{k^2-\alpha^2})\, d\alpha. \tag{14}$$

In (13), $I(x')$ and β are both unknown. In order to obtain an expression for β, a known value for $I(x')$ will be assumed. A convenient and valid approximation of $I(x')$ is the zeroth order current distribution in linear an-

[10] L. Brillouin, "Wave Propagation in Periodic Structures," McGraw-Hill Book Co., Inc., New York, N. Y., p. 173; 1946.

[11] W. Magnus and F. Oberhettinger, "Formulas and Theorems for the Special Functions of Mathematical Physics," Chelsea Publishing Co., New York, N. Y., p. 34; 1949.

tennas for small values of the radius R, which may be written as follows:

$$I(x') = I(0)\frac{\cos kx' - \cos ka}{1 - \cos ka} \tag{15}$$

where $I(0)$ is the current at the central point of the rod. After introducing (15) in (13), the following equation is obtained:

$$\sum_{n=-\infty}^{\infty} e^{-i\beta nd}\int_{-\infty}^{\infty}(k^2-\alpha^2)f(\alpha)H_0^{(2)}(\rho_n\sqrt{k^2-\alpha^2})d\alpha = 0 \tag{16}$$

where

$$f(\alpha) = \frac{1-\cos ka}{I(0)}\cdot\int_{-a}^{a} e^{i\alpha x'}I(x')dx'$$

$$= 2\left[\frac{k}{k^2+\alpha^2}\sin ka\cos\alpha a - \frac{k^2}{(k^2-\alpha^2)\alpha}\cdot\cos ka\sin\alpha a\right]. \tag{17}$$

After substituting the value of $f(\alpha)$ in (16) and performing the integration, the following equation is obtained;

$$\sum_{n=-\infty}^{\infty} e^{-i\beta nd}\left[\sin ka\frac{e^{-ik\sqrt{\rho_n^2+a^2}}}{\sqrt{\rho_n^2+a^2}} - ka\cos ka\frac{e^{-ik\rho_n}}{\rho_n}\right] = 0. \tag{18}$$

By using the relation $e^{nx}/n = -\log(1-e^x)$ and assuming $d \gg a/2$, $a \gg R$, $d \gg R$, the infinite sums in (18) can be summed into closed form[12] and the following result is obtained:

$$\sin ka\frac{e^{-ika}}{a} - \frac{\sin ka}{d}\log(Ae^{i\phi}) - ka\cos ka\frac{e^{-ikR}}{R} + \frac{ka\cos ka}{d}\log(Ae^{i\phi}) = 0 \tag{19}$$

where

$$A = 2\left|\cos kd - \cos\beta d\right| \tag{20}$$

$$\phi = \pi - kd, \tag{21}$$

From (19) and (20) the following expression is obtained for the propagation constant β in the infinite Yagi structure:

$$\log\left\{2\left|\cos kd - \cos\beta d\right|\right\} = kd\left[\frac{\cos ka\left(\frac{\sin ka}{ka}\right) - ka\cos ka\left(\frac{\cos kR}{kR}\right)}{\sin ka - ka\cos ka}\right]. \tag{22}$$

Eq. (22) may be rearranged in the following form:

$$\cos\beta d = \cos kd - \tfrac{1}{2}e^{kdf(a,R)} \tag{23}$$

where

$$f(a, R) = \left[\frac{\cos ka\left(\frac{\sin ka}{ka}\right) - ka\cos ka\left(\frac{\cos kR}{kR}\right)}{\sin ka - ka\cos ka}\right]. \tag{24}$$

The expression for the phase velocity can be obtained from the relation

$$v = \omega/\beta, \tag{25}$$

and it is valid under the following conditions:

$$d \gg R, \qquad a \gg R, \qquad d \gg a/2.$$

It is interesting to compare (23) and (3) obtained by transmission line analogy. Assuming a capacitive reactance (for X) (3) can be written as

$$\cos\beta d = \cos kd - \frac{Z}{2X}\sin kd. \tag{26}$$

Eq. (26) is of a form similar to (23).

Discussion of the Approximate Expression for Phase Velocity

The following remarks may be made from a theoretical study of (23):

1) It is found that as long as $a < \lambda/4$, $v < c$ for all values of d and R. For this restriction on the rod length, this means that the phase velocity along the infinite Yagi structure is slower than the free space velocity, a conclusion arrived at previously from transmission line analogy.

2) Function $f(a, R)$ is a negative valued function for $a < \lambda/4$. As a is decreased continuously from a large value (but less than $\lambda/4$), $|f(a, R)|$ increases continuously, at first very rapidly and then very slowly. This means β approaches k as a is decreased. In other words for small values of a the phase velocity approaches the free space velocity and in that range the effect of slight changes in d and R on the phase velocity becomes very small.

3) It can be shown that as $R \to 0$, $\beta \to k$. This means in the ideal case with infinitely thin rods, phase velocity is equal to free space velocity. As the radii of the rods are increased, phase velocity decreases very rapidly because of the rapid decrease of $|f(a, R)|$.

4) The phase velocity decreases with the decrease of the parameter d, the spacing between the rods.

Comparison Between Theory and Experiment

In this section the dependence of phase velocity on various parameters of the infinite Yagi structure is investigated quantitatively. All the theoretical results are obtained by using (23), (24), and (25). These are compared with existing experimental results in order to judge the accuracy of the approximate expression. All

[12] D. L. Sengupta, *op. cit.*, p. 130.

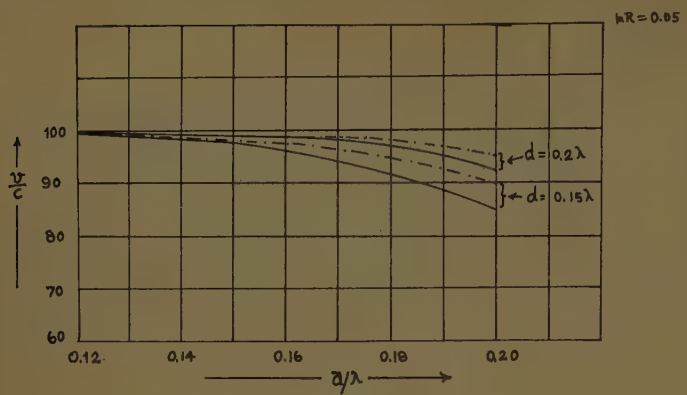

Fig. 3—Relative phase velocity as a function of a/λ with d/λ as parameters and $kR=0.05$; —theoretical, —·—·—experimental.

the experimental results are obtained from the investigations done by Ehrenspeck and Poehler,[1] and Spector.[2]

The authors quoted above have measured the phase velocity of wave propagation along electrically long but finite Yagi structures, whereas the theoretical values of phase velocity are for an infinite Yagi structure. The comparison between the two sets of values are made with the assumption that the phase velocity in a traveling wave structure is independent of the length of the structure.

Before making this comparison a short description will be given of the methods used by the above authors to measure the phase velocity. The method used by Ehrenspeck and Poehler consists in producing a standing wave pattern on the long Yagi structure by reflecting the traveling wave with the help of a large metallic screen placed transversely at the open end of the structure. The traveling wave is launched into the structure by feeding the element at the other end of the structure, as is done commonly in exciting Yagi antennas. Phase velocity is obtained by measuring, in the usual manner, the wavelength on the structure. Spector's method of measurement is similar to the above. For producing standing wave he uses two reflecting screens at the two ends of the structure in the form of a surface wave resonator. The system is excited by means of a circular dielectric filled waveguide in which the dominant H_{11} mode has been launched.

Fig. 3 shows the variation of relative phase velocity as a function of a with d as parameters and for a fixed value of R. Figs. 4 and 5 show the same variation for other values of R. All the three variables a, d and R are expressed in terms of wavelength in order to make them dimensionless quantities so that the results may be general. The dotted curves in Figs. 3 and 4 are the experimental results. From Figs. 3 and 4 it is found that the agreement between theory and experiment is fairly good for $d \geq 0.15\lambda$. With this restriction on d it is found that the maximum deviation of 5 per cent occurs for large values of a. For small values of a the agreement is quite good. The discrepancy for large values of a may

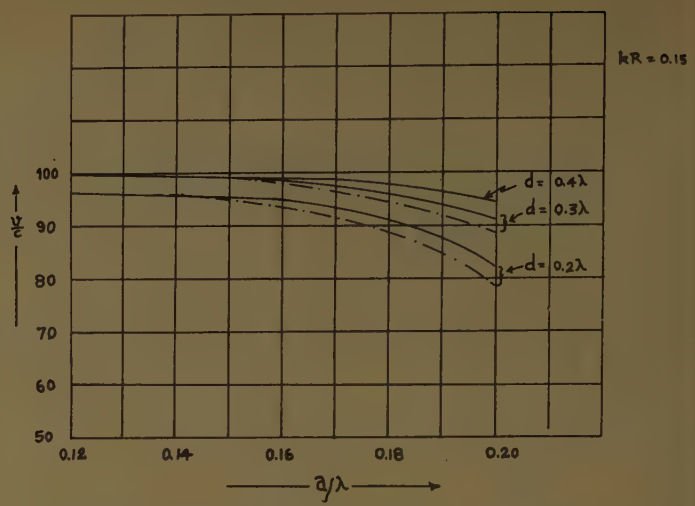

Fig. 4—Relative phase velocity as a function of a/λ with d/λ as parameters and $kR=0.15$; —theoretical, —·—·—experimental.

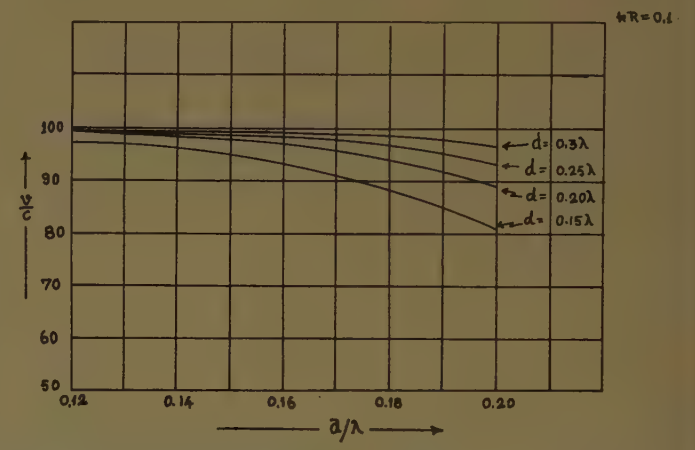

Fig. 5—Relative phase velocity as a function of a/λ with d/λ as parameters and $kR=0.1$. Values shown are theoretical.

be explained if one considers that (23) is obtained by assuming $d \gg a/2$. This condition does not hold for large values of a and small values of d. The discrepancy becomes very pronounced when $d < 0.15\lambda$, for which $a/2$ is of the order of, and even larger than, d.

Fig. 6 shows the theoretical variation of phase velocity as a function of d with a and R as parameters. It is found that the phase velocity increases very rapidly at first with increase of d but the variation becomes very small for larger values of d. This is opposite to the variation of v/c as a function of a (for example, see Fig. 3).

The dependence of v/c on R is not shown separately but it can be seen by comparing Figs. 3–5 where v/c increases continuously as R is decreased. For small values of R, v/c becomes almost independent of d and a, and its value lies very close to unity.

Fig. 7 shows the theoretical variation of v/c as a function of frequency, for fixed values of d, a, and R. It is found that v/c decreases continuously with increase of frequency, the rate of decrease being larger at the higher frequency-end of the curve.

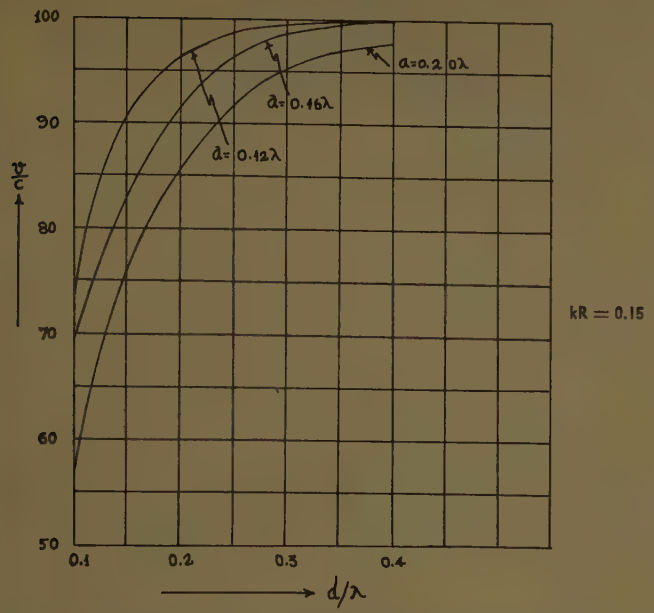

Fig. 6—Theoretical variation of relative phase velocity as a function of d/λ with a/λ as parameters and $kR=0.15$.

Conclusion

From the above investigation it may be said that the physical parameters of a Yagi structure can be chosen theoretically in order to obtain a particular value for the phase velocity of wave propagation along the structure. From the agreement between theory and experiment it may be concluded that the assumption of sinusoidal and axially symmetric current distribution for the induced current in each rod is a fairly good approximation. It may be possible to improve the theory by assuming the first order approximation to the current distribution instead of the zeroth order approximation. However, (23) agrees fairly well with experimental results for those values of the different parameters which are of practical importance. The accuracy of this expression is sufficient for practical design of a long Yagi antenna which consists of a large but finite number of elements. For this reason further investigations on the improvement of the theory have not been carried out. The details of the design of long Yagi antennas using the above results will be reported in a forthcoming paper.

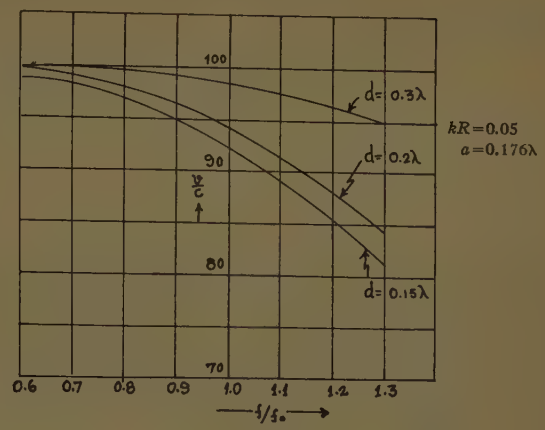

Fig. 7—Theoretical variation of relative phase velocity as a function of frequency with d/λ as parameters. The values of the parameters a, d, and R shown in the figure are at the frequency $f=f_0$.

Acknowledgment

The author wishes to express his thanks to Prof. George Sinclair, for the advice and encouragement received from him at all times, and to Prof. J. L. Yen, for many discussions and helpful suggestions during the course of this work.

Effect of Relatively Strong Fields on the Propagation of EM Waves Through a Hypersonically Produced Plasma*

W. B. SISCO† AND J. M. FISKIN†

Summary—**The simple classical theory employed in the analysis of electromagnetic waves propagating through an ionized gas is not sufficiently general to take into account the variation of the complex conductivity of the plasma with the magnitude of the impressed EM field. Problems of this nature arise when it becomes necessary to transmit radar signals of high energy density through the ionized shock wave produced by a hypersonic vehicle.**

The exact theory of conductivity developed by Margenau[1] is for impressed, relatively high field strengths too difficult to handle from an analysis and computational standpoint. By making two simplifying assumptions in the general velocity distribution function and graphically interpolating between them, two relations, one nearly exact and one employing the simple theory, are obtained for the conductivity. The accuracy of these relations is then examined analytically for a typical case, and graphical comparisons between the methods are made.

Effects of neglecting Coulomb interactions and higher order components in the velocity distribution function are considered briefly. For an example, the complex conductivity of a typical ionized shock wave as a function of field strength and frequency is calculated and plotted.

Introduction

THE propagation of EM waves through a plasma, considered from the standpoint of the simple classical theory, takes into account the behavior of an average individual electron and neglects the overall velocity distribution of the electrons. Also, it is usually assumed that the energy added to the electrons by the incident EM field is small compared to the kinetic energy that they already possess. For some applications it will be necessary to transmit extremely high-energy density microwave radar signals from an aperture type antenna that is adjacent to the plasma. As a consequence, relatively strong EM fields will be incident on the plasma. These high fields will, in general, increase the electron energy considerably and modify the distribution function, which in turn will change the propagation constant of the wave.

The primary purpose of this report is to determine the extent of the effect of relatively high fields on the propagation constant of a plane EM wave normally incident on the gaseous ionized media. These effects are investigated analytically for the exact case and the simple classical one. The effects of neglecting electronic interactions and higher order terms in the expansion of the velocity distribution are also considered briefly. Finally, these results are applied to the problem of propagating an EM wave through the plasma produced by a typical hypersonic vehicle at a fixed altitude and speed.

* Manuscript received by the PGAP, July 30, 1958.

† Douglas Aircraft Co., Long Beach Div., Santa Monica, Calif.

[1] H. Margenau, "Conduction and dispersion of ionized gases," *Phys. Rev.*, vol. 69, pp. 508–513; May 1, 15, 1946.

Approximate Complex Conductivity of an Ionized Gas

The complex conductivity of a gas, together with its permeability and the incident radiation frequency, yields the attenuation and phase constant of a normally incident EM wave. Margenau[1] has developed an exact expression for the complex conductivity but because of its complexity, it is difficult to use in some cases from both the computational and analysis standpoint. Additionally, the particular approximations in his report limiting the field strengths to very low values cannot be employed for this application. However, by using two assumptions, relatively simple expressions for the conductivity can be obtained over a wide range of values for the field strength, frequency, and pressure. Interpolation of the data between these two assumptions will yield complete and reasonably accurate data for a specific case.

Beginning with Margenau's (15) for the spherically symmetric term, f_1, of the velicity distribution function,[1]

$$\log f_0 = -\int_0^{v^2} \frac{m/2d(v^2)}{kT + \dfrac{M\gamma^2\lambda^2}{6(v^2+\omega^2\lambda^2)}}, \qquad (1)$$

two assumptions 1) $v > \omega\lambda$ and 2) $\omega\lambda > v$ for the significant range of energies can be employed to simplify the analysis to a great extent. In (1), m and M are the masses of the electrons and molecules, respectively, T the temperature of the gas, λ the mean free path, ω the radian frequency, v the random velocity of the electrons in the plasma, and γ is equal to eE/m where e is the electronic charge and E is the field strength.

Some additional assumptions that are essential to the analysis are listed below.

3) The gas is considered to be in the ground state.

4) The electrons gain and lose energy through elastic collisions only .

It follows from this that EM fields must necessarily be limited to values below breakdown.

5) The distribution of electrons is homogeneous throughout the gas.

6) A distribution of electrons (n/cc) is maintained in the gas independent of EM fields.

7) The mean free path is considered as a constant independent of energy but not of the gas density.

Case I: $v \gg \omega\lambda$

Eq. (1) reduces to the following expression when the above assumption is employed, and it is also assumed that the kinetic energy added by the EM field is much greater than the thermal energy of the electrons.

$$\log f_0 = -\frac{3m}{M\gamma^2\lambda^2}\int_0^{v^2} v^2 d(v^2). \tag{2}$$

Solving for f_0,

$$f_0 = A_1 \exp\left[-\frac{3mv^4}{2M\gamma^2\lambda^2}\right] \tag{3}$$

where A_1 is a constant of integration and can be determined in the usual manner from the number of electrons per unit volume

$$n = \int_0^{\infty}\int_0^{\pi}\int_0^{2\pi} f_0 v^2 dv \sin\theta d\theta d\phi = \pi A_1\left[\frac{\Gamma(\frac{3}{4})}{(B_1)^{3/4}}\right] \tag{4}$$

and

$$A_1 = \frac{nB_1^{3/4}}{\pi\Gamma(\frac{3}{4})} \tag{5}$$

where

$$B_1 = \frac{3m}{2M\gamma^2\lambda^2}.$$

By definition the current density in a plasma is

$$I = ne\bar{v}_x \tag{6}$$

where $\bar{v}_x$ is the mean drift velocity in the direction of the field, E, and is determined by using the drift velocity term of the general distribution function. Thus,

$$\bar{v}_x = \frac{1}{n}\int_0^{\infty}\int_0^{\pi}\int_0^{2\pi} f(v_x) v_x v^2 dv \sin\theta\, d\theta\, d\phi \tag{7}$$

and

$$f(v_x) = \gamma v_x[f_1(v)\cos\omega t + g_1(v)\sin\omega t]; \tag{8}$$

where

$$g_1 = \frac{\omega\lambda}{v} f_1 \tag{9}$$

and

$$f_1 = -\frac{\lambda}{v^2+\omega^2\lambda^2}\frac{\partial f_0}{\partial v}. \tag{10}$$

Employing the assumption that $v \gg \omega\lambda$ and that $v^2 = 3v_x^2$, the current density is then given by the following expression:

$$I = \frac{4\pi e\gamma}{3}\int_0^{\infty}\left(-\frac{\lambda}{v^2}\cos\omega t - \frac{\omega\lambda^2}{v^3}\sin\omega t\right)\frac{\partial f_0}{\partial v} v^4 dv. \tag{11}$$

After integration and consolidation of terms this reduces to

$$I = \frac{2ne\gamma\lambda B_1^{1/2}}{3\Gamma(\frac{3}{4})}\left[\left(\frac{\pi^2}{B_1}\right)^{1/4}\cos\omega t + 2\Gamma\left(\frac{5}{4}\right)\omega\lambda\sin\omega t\right]. \tag{12}$$

The complex conductivity is obtained by dividing (12) by the field strength E.

From (12) it is noted that the coefficient of the cosine term which is the real part of the complex conductivity is always greater than the coefficient of the imaginary part, the sine term. In fact, the real part of (12) reduces to the expression for the mean drift velocity of electrons under the influence of a dc field obtained by Morse, Allis, and Lamar[2], provided (12) is divided by ne and the rms values of velocity and field strength are used in place of the peak values. This result is to be expected since the assumption of $v \gg \omega\lambda$ explicitly states that many elastic collisions will occur during the period of the incident EM wave resulting in virtually a dc field existing in the plasma.

Case II: $\omega\lambda \gg v$

For this condition (1) reduces to the following:

$$\log f_0 = -\int_0^{v^2}\frac{m/2d(v^2)}{KT + \dfrac{M\gamma^2\lambda^2}{6\omega^2\lambda^2}}. \tag{13}$$

Therefore,

$$f_0 = A_2 \exp\left[-B_2 v^2\right] \tag{14}$$

where

$$B_2 = \frac{m/2}{KT + \dfrac{M\gamma^2}{6\omega^2}},$$

and A_2 is the constant of integration determined by the following relation:

$$n = \int_0^{\infty}\int_0^{\pi}\int_0^{2\pi} f_0 v^2 dv \sin\theta\, d\theta\, d\phi = A_2\left(\frac{\pi}{B_2}\right)^{3/2}.$$

Therefore,

$$A_2 = n\left(\frac{B_2}{\pi}\right)^{3/2}. \tag{15}$$

The current density is then

$$I = ne\bar{v}_x = \frac{ne}{n}\int_0^{\infty}\int_0^{\pi}\int_0^{2\pi} f(v_x) v_x v^2 dv \sin\theta\, d\theta\, d\phi. \tag{16}$$

Consequently,

$$I = \frac{4\pi e\gamma}{3}\int_0^{\infty}(f_1\cos\omega t + g_1\sin\omega t) v^4 dv$$

[2] P. M. Morse, W. P. Allis and E. S. Lamar, "Velocity distribution for elastically colliding electrons," *Phys. Rev.*, vol. 43, pp. 412–419; September 1, 1935.

where $f(v_x)$ is (8), $v^2 = 3v_x^2$ and g_1 and f_1 are

$$g_1 = \frac{\omega\lambda}{v} f_1 \tag{17}$$

and

$$f_1 = -\frac{\lambda}{\omega^2\lambda^2}\frac{\partial f_0}{\partial v}. \tag{18}$$

Then

$$I = \frac{4\pi e\gamma}{3}\int_0^\infty \left[-\frac{\lambda}{\omega^2\lambda^2}\frac{\partial f_0}{\partial v}\cos\omega t - \frac{1}{\omega v}\frac{\partial f_0}{\partial v}\sin\omega t\right] v^4 dv. \tag{19}$$

This becomes, after integration,

$$I = \frac{ne\gamma}{\omega}\left[\frac{8}{3\omega\lambda\sqrt{\pi B_1}}\cos\omega t + \sin\omega t\right], \tag{20}$$

and the complex conductivity is obtained by dividing (20) by the field strength E.

In this case the coefficient of the imaginary term is the dominant term in (20). Margenau's (29)[1] reduces to (20) in this paper if x, x_1 and T are replaced by x', x_1' and T', and x_1' is allowed to approach infinity. In this instance x' and x_1' differ from x and x_1 by replacing T with T' where T' is defined by Margenau's (24). The dominance of the sine term is expected here since the number of oscillations exceeds the number of collisions, resulting in an almost pure electron gas, free of energy-consuming collisions.

Simplified Theory

The preceding development is very nearly exact for the assumptions made. However, from an analytical and computational standpoint the effect of a relatively strong EM field can be more conveniently handled by considering the behavior of an average electron. Employing this classical procedure, the conductivity of a plasma is given by

$$\sigma_r = \frac{ne^2\bar{\nu}}{m(\bar{\nu}^2+\omega^2)} - j\frac{ne^2\omega}{m(\bar{\nu}^2+\omega^2)} \tag{21}$$

where $\bar{\nu}$ is the mean collision frequency. If the random collision frequency defined by v/λ is constant, Everhart and Brown,[3] and Cahn[4] have shown that (21) is the exact expression for the conductivity. In general, for most gases, the collision frequency is not constant but varies with the velocity of the electron. However, it is possible to define a mean collision frequency,

$$\bar{\nu} = \frac{(v^2)^{1/2}}{\lambda} \tag{22}$$

where $(\bar{v}^2)^{1/2}$ is determined from the spherically symmetric term of the distribution function

$$\bar{v}^2 = \frac{1}{n}\int_0^\infty\int_0^\pi\int_0^{2\pi} v^2 f_0(v) v^2 dv \sin\theta\, d\theta\, d\phi \tag{23}$$

and λ is determined from experimental data at the mean velocity $(\bar{v}^2)^{1/2}$. Eq. (21) will then yield reasonably accurate results for all values of E provided that the applicable distribution function is used to determine $(\bar{v}^2)^{1/2}$. The functional dependence of the conductivity on E reduces to the known functional dependence of the collision frequency on E. Thus, any analysis of the propagation constants of an incident wave and a plasma can be easily extended to include the effects of relatively strong EM fields.

Eq. (21) is a good approximation for (20), (12), and Margenau's (29), when these solutions for the current density are divided by E to yield the conductivity. The validity of this approximation can be shown analytically for all three equations. To illustrate the simple method involved, the conductivities determined by (20) and (21) are compared.

For the real part, (21) yields

$$\sigma_{rs} = \frac{ne^2\bar{\nu}}{m(\bar{\nu}^2+\omega^2)}. \tag{24}$$

Employing the distribution given by (14) together with (24),

$$\bar{v}^2 = \frac{4\pi}{n}\int_0^\infty A_2 v^4 \exp\left[-B_2 v^2 dv\right] = \frac{3}{2B_2}. \tag{25}$$

Therefore,

$$(v^2)^{1/2} = \left[\frac{3}{2B_2}\right]^{1/2}.$$

From (22) and the assumption $\omega\lambda \gg v$,

$$\sigma_{rs} = \frac{ne^2}{m\omega^2\lambda}\left(\frac{3}{\pi B_2}\right)^{1/2}. \tag{26}$$

Eq. (20) gives for the real part,

$$\sigma_{re} = \frac{8ne^2}{3m\omega^2\lambda}\left[\frac{1}{\pi B_2}\right]^{1/2} \tag{27}$$

and

$$\frac{\sigma_{rs}}{\sigma_{re}} = \frac{3}{8}\left[\frac{3\pi}{2}\right]^{1/2} \approx 0.82. \tag{28}$$

Repeating the same procedure for the imaginary part from (21),

$$\sigma_{is} = \frac{ne^2\omega}{m(\bar{\nu}^2+\omega^2)} = \frac{ne^2}{m\omega}. \tag{29}$$

[3] E. Everhart and S. C. Brown, "The admittance of high frequency gas discharges," *Phys. Rev.*, vol. 76, pp. 839–842; September 15, 1949.

[4] J. H. Cahn, "Electron velocity distribution in high frequency alternating fields," *Phys. Rev.*, vol. 75, pp. 838–841; March 1, 1959.

For the imaginary part of (20)

$$\sigma_{ie} = \frac{ne^2}{m\omega} \tag{30}$$

and

$$\frac{\sigma_{ie}}{\sigma_{ie}} = 1. \tag{31}$$

Electronic Interactions

The electrostatic coulomb forces between electrons are usually neglected in the development of the velocity distribution functions and consequently in the follow-up derivations of the complex conductivity. Cahn[4,5] has studied these effects in detail for both the dc and high frequency cases, using certain assumptions to simplify the mathematical manipulations. His conclusions as applicable to this analysis may be summarized as follows:

For the dc case which corresponds to Case I ($v \gg \omega\lambda$), and λ assumed constant, electronic interactions may be neglected if the density is on the order of 10^6 to 10^8 electrons/cc or lower. At 10^{12} electrons/cc and above, the distribution function is very nearly Maxwellian and is independent of the EM field. Between these limits the real part of the conductivity can be calculated by employing Cahn's (23) and (17).[5] For the simplified theory, $(\bar{v}^2)^{1/2}$ can be obtained from (23) of Cahn and the previously developed procedure used to determine the complex conductivity.

In the high frequency case, utilizing the assumption that $\omega\lambda \gg v$, the conclusions regarding the upper and lower ranges of the electron densities in the dc case are also valid. For densities between these limits Cahn's last equation,[4] which is practically identical to the simplified expression in the previous section, can be used to determine the complex conductivity, provided $(\bar{v}^2)^{1/2}$ is obtained from his (18).

For conditions such that $\omega\lambda = v$, the exact expression (7) of Cahn can be used, or the results of the two extreme cases can be interpolated to yield reasonably accurate values of the conductivities.

Harmonic Components

The velocity distribution function is usually obtained from an infinite series consisting of Legendre and Fourier terms. Generally it is assumed that the first term of each is adequate for most applications. Margenau and Hartman[6] have extensively examined this assumption, and their results as applicable to this analysis are briefly summarized as follows:

For the condition $\omega\lambda \gg \eta^{1/2}v$, where ω, λ, and v have their usual meaning and η is defined by the relation

$$\eta = \frac{2m}{M},$$

higher order terms may be neglected. Thus the distribution function used for Case II ($\omega\lambda \gg v$) is valid for a fairly wide range of velocities around the mean velocity since η is on the order of 10^{-4}.

With the condition $\omega\lambda \ll \eta^{1/2}v$ which corresponds very closely to Case I ($v \gg \omega\lambda$), the dc case, the distribution reduces to that of Davydov ($T \neq 0$) or that of Druyvesteyn ($T = 0$) which is used in this report.

For the case, $\omega\lambda \approx \eta^{1/2}v$, two additional isotropic terms as specified in Margenau's and Hartman's paper[6] may be of importance.

Application to the Propagation of EM Waves Through a Plasma Produced by Hypersonic Shock Waves

To illustrate the application of the analysis, the complex conductivity of a plasma produced by a shock wave is calculated using the relations developed for Case I and Case II. A typical hypersonic shock wave produces the following electron density, mean free path, and temperature in air:

$$n = 5.2 \times 10^9 \text{ electrons/cc}$$

$$\lambda = 0.15 \text{ cm}$$

$$T = 3000^\circ \text{ K}.$$

Fig. 1 gives the mean random velocity as a function of E with $\omega\lambda$ as a parameter. These velocities are calculated from the applicable distribution function developed for Cases I and II. Fig. 2 compares the real and imaginary components of the conductivity for the simplified theory. In Figs. 3 and 4, the conductivities are calculated from the nearly exact theory for Cases I and II and compared to the simplified theory using the velocities in Fig. 1. In all figures the dotted lines indicate interpolated data between the two assumptions $\omega\lambda \gg v$ and $v \gg \omega\lambda$. The triangular points are obtained from a machine calculation of Margenau's exact theory.[1] Good agreement is obtained for all cases.

In this example, Coulomb interaction and harmonic component effects have not been included. It is noted that for some values of ω and E the plasma may be in a state of breakdown because of the EM field.[7] Here the curves are invalid since the electron density will have increased substantially. Attention is also called to the constant velocity line at one tenth that of light, because above this point relativistic corrections must be included. The extension above the velocity of light is added only to illustrate the fairing of the curves for *Cases I and II.*

[5] J. H. Cahn, "Electronic interaction in electrical discharges in gases," *Phys. Rev.*, vol. 75, pp. 293–300; January 15, 1949.

[6] H. Margenau and L. M. Hartman, "Theory of high frequency gas discharges. II Harmonic components of the distribution function," *Phys. Rev.*, vol. 73, pp. 309–315; February 15, 1948.

[7] L. Gould and L. W. Roberts, "Breakdown of air at microwave frequencies," *J. Appl. Phys.*, vol. 27, pp. 1162–1170; October, 1956.

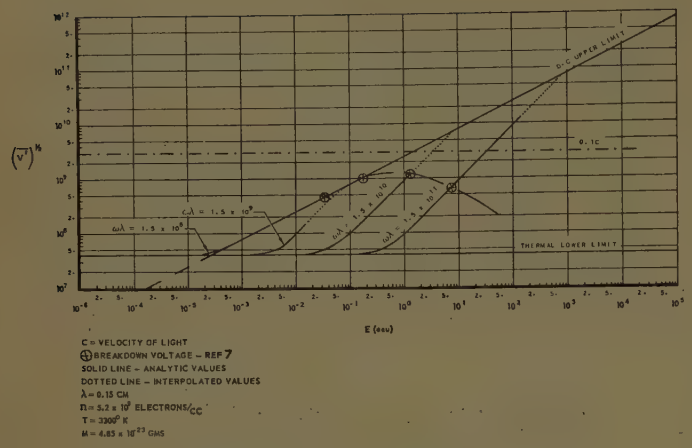

Fig. 1—RMS velocity as a function of field strength.

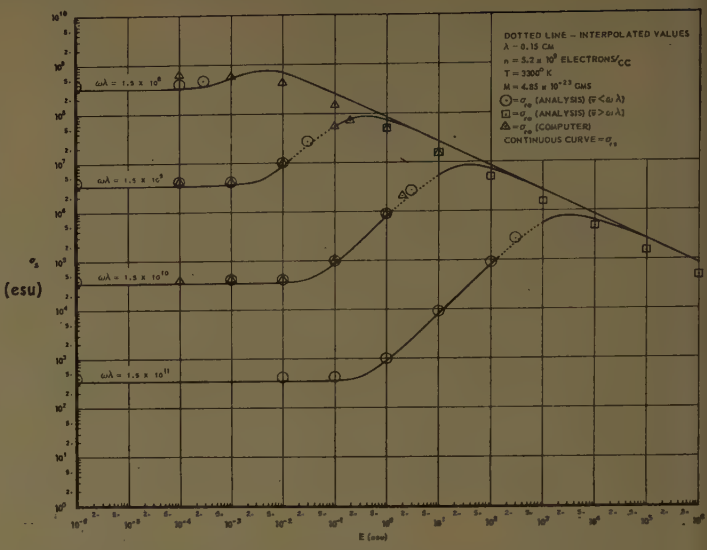

Fig. 3—A graphic comparison of the real part of the complex conductivity as a function of field strength.

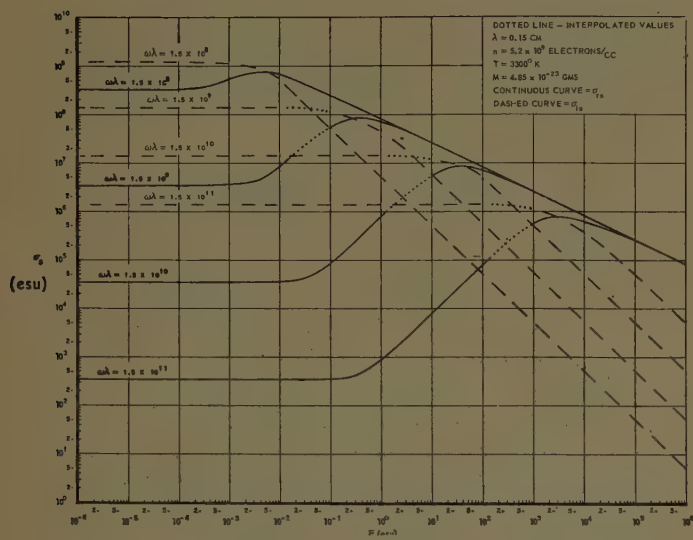

Fig. 2—A comparison of the real and imaginary parts of the complex conductivity as a function of the field strength—calculated from the simple theory.

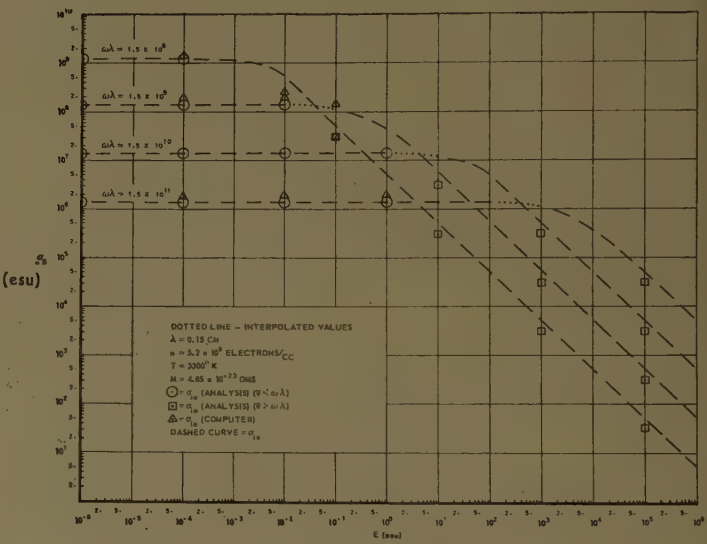

Fig. 4—A graphic comparison of the imaginary part of the complex conductivities as a function of field strength.

Conclusion

Two reasonably accurate methods have been developed for computing the complex conductivity of a hypersonic plasma when excited by relatively strong EM fields. One method utilizes a modification of the simple classical theory which is based on the behavior of an average electron. This permits direct analysis and computation of the effect of relatively strong EM fields on the propagation constant using familiar concepts.

Acknowledgment

The authors wish to acknowledge the helpful suggestions, criticisms, and other assistance of H. H. Peterson, S. J. Press, and C. A. Roberts in the preparation of the material.

Microwave Scattering by Turbulent Air*

CHARLES E. PHILLIPS†

Summary—A system for measuring the power scattered by a region of thermally turbulent air is described, and its performance is analyzed. Also described is the equipment used to generate the turbulent region and the temperature fluctuations therein.

The experimental procedure can be summarized by stating that it consisted in measuring the fluctuations of the null in the interference pattern of an antenna array composed of two antennas excited out of phase, when thermally turbulent air, of known properties, was interposed between the receiving and transmitting systems.

The measured and calculated receiver response due to scattering by the turbulent air is compared, and it is noted that they agree at least within an order of magnitude.

The experiment described shows that a measurement of the angular dependence of the signal scattered by turbulent air is within the possibilities of available techniques, although a more elaborate measuring system and higher microwave power levels would be required.

Introduction

THE work described in this paper was performed in order to find out whether scattering from thermally turbulent air can be detected at microwave frequencies and if so, to make a comparison with theoretical calculations based on: a) the Booker-Gordon scattering cross section,[1] and b) a scattering cross section calculated from an empirically determined temperature correlation function, derived from data presented by Kistler, *et al.*[2]

Great interest exists in the phenomenon of scattering by a region of turbulent air[3] and calculations have been made to estimate the effect of turbulence on the performance of antenna systems.[4,5] A convenient way to verify the calculations previously mentioned is to simulate the turbulent medium in the laboratory.

In essence, the experiment described herein consisted in measuring the level of the fluctuations of the null in the interference pattern of an antenna array, composed of two antennas excited out of phase, when thermally turbulent air was interposed between the receiving and transmitting systems.

It would be desirable to conduct a research program to obtain detailed information about the character (*e.g.*, the frequency spectrum) of the noise signal scattered by a turbulent region, and to measure the angular dependence of the scattered signal. These measurements would undoubtedly dictate modifications of the system described in this paper; however, the present system achieved its primary purpose which was to detect, and measure (at least with some degree of accuracy) the level of the signal scattered by a turbulent region.

Description of the Measuring System

Block Diagram of Transmitting and Receiving Systems

The system used to detect the signal scattered by a turbulent region is outlined in Fig. 1.

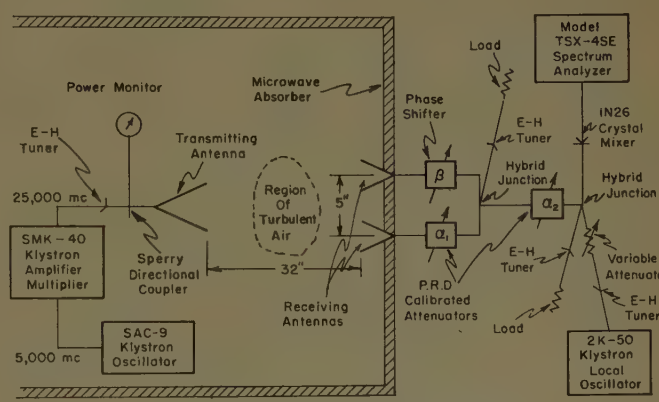

Fig. 1—Diagram of measuring system.

Signal Generator

The selection of the source of microwave power was one of the first considerations. Using the Booker-Gordon scattering cross section[1] for the case of forward scattering, it can be shown that a transmitter figure of merit is proportional to the power output divided by the square of the wavelength. Using the above criterion, together with the fact that it was immediately available, a Sperry type SMK-40 *K*-band ($\lambda = 1.2$ cm) multiplier klystron was selected as the signal generator. A Sperry klystron, SAC-9, was used as a self-excited oscillator (at 5000 mc) to drive the SMK-40. Since ambient temperature fluctuations cause frequency instability of the transmitter signal, the SAC-9 and the SMK-40

* Manuscript received by the PGAP, August 22, 1958. The work reported in this paper constituted the thesis submitted by the author in partial fulfillment for the M.S. degree in the Dept. of Elec. Engrg. of the Ohio State Univ., Columbus. This work was supported and sponsored by Air Res. and Dev. Command, Wright Air Dev. Center, Wright-Patterson AFB, Dayton, Ohio, under Contract AF 33(616)-3353.

† General Dynamics Corp., Convair Div., San Diego, Calif.

[1] H. G. Booker and W. E. Gordon, "Radio scattering in the troposphere," PROC. IRE, vol. 38, 401–412; April, 1950.

[2] A. L. Kistler, V. O'Brian, and S. Corrsin, "Measurements of Turbulence and Temperature Fluctuations Behind a Heated Grid," Dept. of Aeronautics, The Johns Hopkins University, Baltimore, Md. Submitted to NACA in Fulfillment of Contract NAw6321; January, 1955.

[3] "Bombing Antennas," Interim Engrg. Rep. 486–23; May 17, 1954, Antenna Lab., The Ohio State Univ. Res. Foundation, prepared under Contract AF 18(600)-85, Air Res. and Dev. Command, Wright Air Dev. Center, Wright-Patterson Air Force Base, Dayton, Ohio; May 17, 1954.

[4] "Bombing Antennas," Interim Engrg. Rep. 486–42; May 16, 1955, Antenna Lab., The Ohio State University Research Foundation, prepared under Contract AF 18(600)–85, Air Res. and Dev. Command, Wright Air Dev. Center, Wright-Patterson Air Force Base, Dayton, Ohio; May 16, 1959.

[5] W. H. Peake, Rept. 667-3, Antenna Lab., The Ohio State University Research Foundation, to be completed under Contract AF 33(616)-3353, Air Res. and Dev. Command, Wright Air Dev. Center, Wright-Patterson Air Force Base, Dayton, Ohio.

were immersed in a temperature controlled oil tank. See Fig. 2 for a block diagram of the signal generating equipment.

Transmitting and Receiving Antennas

Rectangular horn antennas were used for transmitting and receiving. This type of antenna was chosen because of its adaptability to waveguide feed, the ease with which it can be rigidly supported, and the relatively high gain obtained from a structure of reasonable dimensions. The aperture of the transmitting antenna is 4.58λ by 7.90λ in the E and H planes, respectively. This gives half-power beamwidths of 12.2° in the E plane and 8.5° in the H plane. The aperture of each receiving horn is 3.82λ by 4.41λ in the E and H planes, respectively; giving half-power beamwidths of 14.7° in the E plane and 15.2° in the H plane.

Signal Detector

The detector used consisted of a Model TSX-4SE spectrum analyzer adapted to operate at *K*-band. Measurements indicate a receiver sensitivity of approximately 115 dbw. (Sensitivity in dbw is taken as the amount of signal power (in db below one watt) required to produce in the receiver an rms output equal to the rms noise output.) Important characteristics of the receiver include the following:

IF frequency	20 mc
Bandwidth of IF amplifier	50 kc
Local oscillator sweep frequency	10–20 cps.

This type of receiver was selected because of its adequate sensitivity; it also provides a means for checking the transmitter spectrum.

Function of Components in the Receiving System and Method of Operation

For the description which follows refer to the diagram in Fig. 3.

The signal E_4 is obtained from the *E*-arm of hybrid junction 1; and from the geometrical arrangement of the system it is seen that this signal is given by

$$E_4 = \frac{1}{\sqrt{2}}(E_1 + E_3). \tag{1}$$

To achieve maximum isolation between signals E_1 and E_3, tuning is provided in the *H*-arm of the hybrid junction.

The null in the pattern of the receiving antenna system is obtained by adjusting the phase shift β and attenuation α_1 to give

$$E_1 = -E_3. \tag{2}$$

Actually, coarse tuning for the null is achieved by making the receiving antennas and the paths of signals E_1 and E_2 as nearly equal as possible, while the phase shifter and attenuator provide fine tuning. The attenuation α_1 required to null down to the noise level of the receiver is of the order of 1 db; this indicates that the signals E_1 and E_2 are roughly of the same magnitude. An attenuator (α_2) is provided in the path of signal E_4 in order to calibrate the level of the fluctuations of the null when the amplitude and, or, phase of signals E_1 and E_3 are disturbed from the null condition. This disturbance will occur when a region of turbulent air is placed in front of the receiving antennas, due to the signal scattered by such a region. Furthermore, it is impossible to renull the system due to the random nature of the signal scattered by the turbulent air.

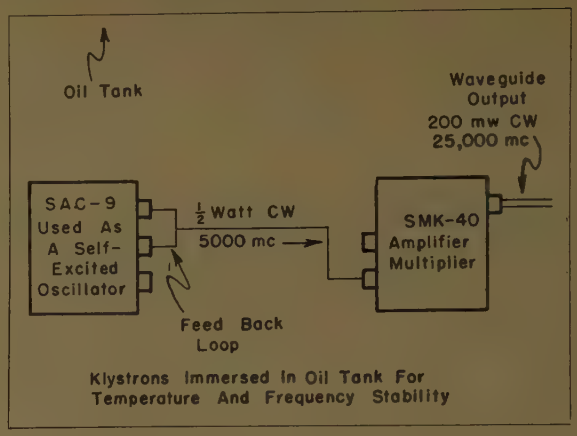

Fig. 2—Signal generating equipment.

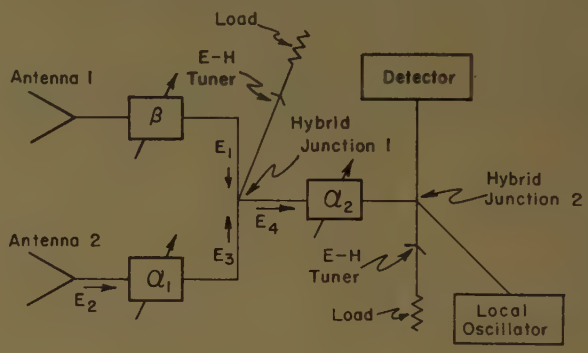

Fig. 3—Receiving system.

The function of hybrid junction 2 is to provide isolation between the local oscillator circuit and the measurement path. This achieves the purpose of providing a constant local oscillator signal level to the mixer when the attenuation α_2 is varied. In this manner the noise level of the receiver is held constant while measurements are taken.

Performance of the System

In order to establish the level of the null in the pattern of the receiving antenna system, the power received by one of these antennas was measured using a Hewlett Packard 430-B power meter. This measurement indicated a power level of 6.5 mw for the signal E_1. Since it was possible to null down to the noise level of the detector, this corresponds to a null level of approximately 93 db. See Appendix I for the reasoning followed to arrive at the above figure for the null level.

As a check on the performance of the system, the power collected by one of the receiving antennas was calculated; this calculation gave a figure of 10 mw. Considering the approximations used in the calculation, this figure compares favorably with the measured value of 6.5 mw. The procedure used in the above mentioned calculation is given in Appendix II.

In order to calibrate the system in terms of a standard scatterer and to further check the receiver noise level, the forward scattered signal from a metallic sphere (of radius equal to 0.125λ) was measured. The maximum signal detected due to the presence of the sphere was 43 db above the receiver noise level. A calculation based on a receiver sensitivity of -115 dbw indicates that the measured signal should be 43.5 db above the receiver noise level. See Appendix III for an outline of the above mentioned calculation.

Generation and Properties of Turbulence

The equipment used to generate the region of thermally turbulent air is shown in Fig. 4. Also shown in the figure is the placement of the turbulent region relative to the transmitting and receiving systems. The centers of the transmitting and receiving antennas and the center of the styrofoam duct lie on a common horizontal plane.

Turbulence in the air flowing through the styrofoam duct is generated by four vertical grids, each consisting of twelve rods ($\frac{1}{4}$ inch in diameter and spaced 0.923 inch apart). Fig. 5 shows two views of the rod arrangement. The temperature fluctuations responsible for the scattering are produced by heating the rods which make up the grids. These rods are copper sheath heaters rated at 500 watts. Therefore, the total power consumed is 24 kw, which produces an average temperature rise in the air stream of 34°C at the air flow velocity employed (16 ft/sec), a velocity which is comparable to that used in experiments on the structure of turbulence described by Kistler, *et al.*[2]

Important properties of the turbulence which are used in the calculation of the signal scattered by the turbulent region include: a) L, the average scale of the temperature fluctuations, and b) $(\Delta T/T)^2$, the mean square fractional deviation from average temperature. By combining the known decay law for velocity fluctuations[6] with a theoretical relation between the velocity and temperature fluctuations,[7] it can be shown that a decay law of the form

$$\overline{\left(\frac{\Delta T}{T}\right)^2} = \frac{(T_0 - T)^2}{T^2} \frac{A}{\left(\frac{X}{M} - B\right)^{3/5}} \qquad (3)$$

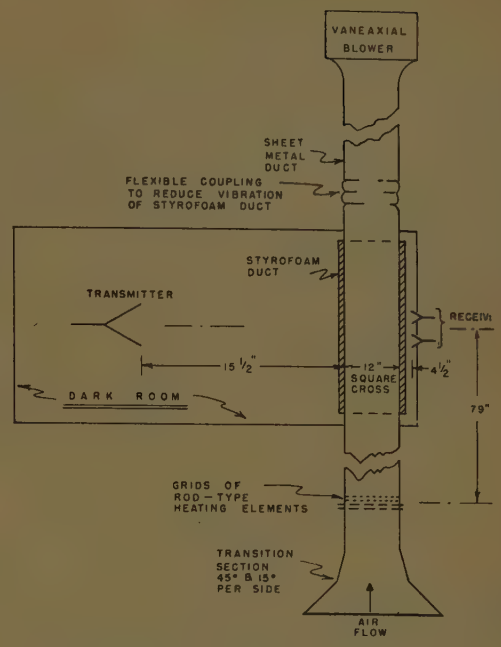

Fig. 4—Equipment used to generate turbulence.

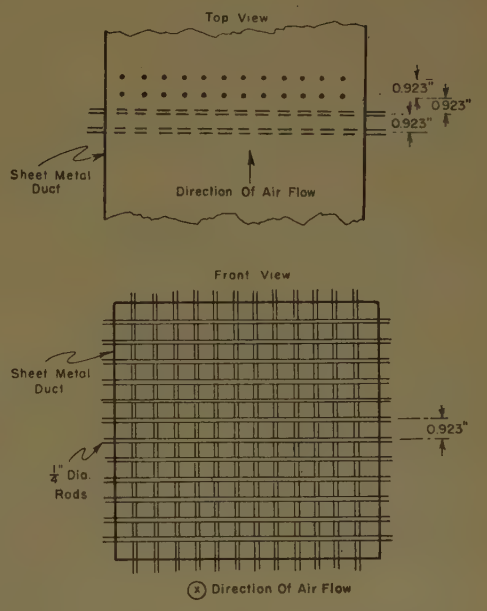

Fig. 5—Top and front views of heating section.

where

M is the separation of grid elements
X is the distance from the grids in the direction of average flow
T is the average temperature
$T_0 - T$ is the average temperature rise

should apply some distance downstream from the grid. This formula is confirmed by the experiments of Kistler *et al.*,[2] from which the constants A and B can be evaluated (for the particular type of grid under consideration) as:

[6] G. K. Batchelor, "The Theory of Homogeneous Turbulence," Cambridge University Press, London, England; 1953.
[7] S. Corrsin, "Decay of isotropic temperature fluctuations in an isotropic turbulence," *J. Aero. Sci.*, vol. 18, pp. 417–423; June, 1951.

$$A \cong 0.0026$$

$$B \cong 9$$

for the range $X/M > 50$. Inspection of the dimensions shown in Figs. 4 and 5 show that for the experiment described in this paper X/M is approximately equal to 86. Use of the data presented by Kistler *et al.*[2] gives $L \cong 1.5\ M$ for $X/M = 86$.

Therefore, for the work described herein,

$$\overline{\left(\frac{\Delta T}{T}\right)^2} \cong 1.92 \times 10^{-4} \frac{(T_0 - T)^2}{T^2} \qquad (5)$$

and

$$L \cong 1.5(0.92'') = 1.38 \text{ inches.} \qquad (6)$$

Results

The experimental procedure consists in nulling the system with the air flowing through the styrofoam duct and the heaters being turned either on or off.

Repeated observations of the null level indicate fluctuations which range from 4 to 8 db above the receiver noise level when the heaters are turned on, whereas when the heaters are turned off it is possible to null quite close to the receiver noise level.

The 4 db spread in the measurements can be attributed to the difficulty of accurately calibrating a signal so close to the noise level of the detector; other factors which contribute to the experimental error are the small vibrations of the styrofoam duct due to the passage of the air stream, and the small difference in level between the unknown signal and the null of the system.

A calculation based on the Booker-Gordon scattering cross section[1] indicates that the receiver response due to the scattering by the thermally turbulent air should be approximately 4.3 db above the receiver noise level. This calculation is carried out in Appendix IV. A similar calculation based on an empirical temperature correlation, derived from data presented by Kistler *et al.*,[2] indicates that the receiver response should be approximately 12.4 db above the receiver noise level. Appendix V contains this last calculation.

Because of the particular geometry of the experiment, imposed by the available transmitter power and small wind tunnel cross section, the effective scattering volume was essentially bounded by the beamwidth of the scattered radiation if the Booker-Gordon scattering cross section[1] were appropriate. Consequently, what was measured was the product of the forward scattering cross section and the solid angle subtended by the beamwidth of the scattered radiation. If, however, the forward scattering cross section and beamwidth are separately calculated from the empirical temperature correlation function, a different effective scattering volume and over-all scattered power are obtained.

The theoretical and experimental results are shown in Table I and in the power level diagram of Fig. 6. The terms given in Table I have the following meaning:

TABLE I

Comparison of Forward Scattering Cross Section, Scattering Angle, Effective Scattering Volume, and Received Power

	Booker-Gordon	Empirical	Experimental
σ_f	4.35×10^{-9}/cm	3.6×10^{-9}/cm	
θ_s	3.12°	8.8°	
V_{eff}	49.3 cm³	386 cm³	
Received Power	8.5×10^{-12} watts	55×10^{-12} watts	8.0×10^{-12} watts 20.1×10^{-12} watts

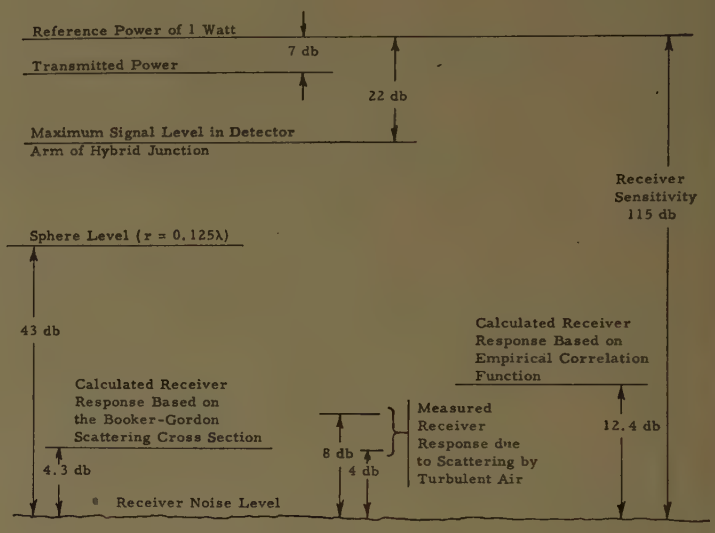

Fig. 6—Power level diagram.

- σ_f is the power scattered in the forward direction
  1) per unit solid angle
  2) per unit incident power density
  3) per unit element of volume
- θ_s is the beamwidth of the scattered radiation (the scattering angle)
- V_{eff} is the volume of turbulence whose scattering contributes to the receiver response
- P_r is the power arriving at the detector, due to scattering by the turbulent region.

Conclusions

Examination of the measured and calculated receiver response shows that the Booker-Gordon scattering cross section[1] gave an adequate indication of the over-all power scattered by the turbulent region. Reasonable agreement was also obtained through use of the scattering cross section and half-power beamwidth of the scattered radiation calculated from the empirical correlation function.

It is obvious from the results that, in order to measure the angular dependence of the signal scattered by a turbulent region using the system described in this paper, it would be necessary to greatly increase the transmitted power in order to operate sufficiently above the receiver noise level. This would not necessarily in-

crease the difficulty of the "nulling" procedure since the receiving antennas would then be located at an angle to the main beam from the transmitter, and hence the power level in each antenna is reduced. The experiment described has shown that such a measurement is within the possibilities of available techniques although a somewhat more elaborate mechanical structure and higher microwave power levels would be required.

Appendix I

Determination of System Null Level

The maximum power level of the signal E_4 is obtained when,

$$|E_4| = \frac{1}{\sqrt{2}}(|E_1| + |E_3|). \tag{7}$$

Since the attenuation α_1 is adjusted to give $|E_3| = |E_1|$, this gives a maximum power level for E_4 equal to two times the power level of E_1, or 13 mw. This is a power level approximately 96 db above the receiver sensitivity; however, to obtain the null level 3 db should be subtracted from this figure due to the equal division of power in the detector and load arms of hybrid junction 2.

This gives 93 db for the null level when the system is nulled to the noise level of the receiver.

Appendix II

Calculation of Power Collected by One Receiving Antenna

To calculate the power collected by one of the receiving antennas the Friis transmission formula[8] is used as follows:

$$\frac{P_r}{P_t} = \frac{A_{emr}A_{emt}}{\lambda^2 r^2} \tag{8}$$

where

P_r is the received power
P_t is the transmitted power
A_{emr} is the maximum effective aperture of the receiver
A_{emt} is the maximum effective aperture of the transmitter
λ is the wavelength
r is the distance between receiver and transmitter.

The maximum effective aperture of the transmitting and receiving antennas can be obtained from:[9]

$$A_{em} = \frac{\lambda^2 D}{4\pi} \tag{9}$$

where D is the directivity of the antenna. The directivity can be estimated using the approximate formula[9]

$$D = \frac{41{,}253}{\phi^\circ\,\theta^\circ} \tag{10}$$

where ϕ° and θ° are the half-power beamwidths in degrees. Use of (9) and (10) in (8) yields:

$$\frac{P_r}{P_t} = \left(\frac{41.253\lambda}{4\pi r}\right)^2 \frac{1}{\phi_r^\circ\theta_r^\circ\phi_t^\circ\theta_t^\circ}. \tag{11}$$

Substitution of the appropriate numerical values in (11) gives a received power of 10 mw. It should be noted that in the calculation P_t was taken as half the transmitted power because the receiving horns were located approximately at the half-power points of the transmitting antenna pattern.

Appendix III

Sphere Calibration

The maximum signal detected due to the forward scattering from the calibrating sphere can be calculated with the aid of the radar range equation and the dimensions shown in Fig. 7.

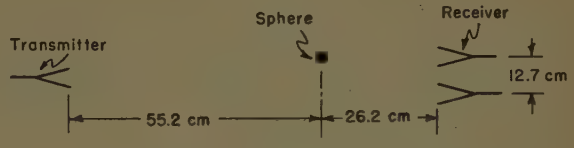

Fig. 7—The relative location of the calibrating sphere.

The radar range equation can be written as follows:

$$P_r = \left(\frac{G_t P_t}{4\pi R_1^2}\right)\left(\frac{\sigma_f}{4\pi R_2^2}\right)\left(\frac{\lambda^2 G_r}{4\pi}\right) \tag{12}$$

where G_t and G_r are the gains of the transmitting and receiving antennas, respectively, R_1 and R_2 are the distances from the scatterer to the transmitting and receiving antennas, respectively, and σ_f is the target echo area when scattering in the forward direction.

For a metallic sphere of radius equal to 0.125λ, σ_f was calculated to be equal to $0.0352\lambda^2$. The procedure for this type of calculation is given.[10]

Noting that when the sphere is in front of one of the receiving horns it is situated approximately at the half-power point of the transmitting antenna pattern, the value of P_t to use in (12) was taken as half the transmitted power. Insertion of numerical values in (12) yields a value of -68.5 dbw for P_r. However, to obtain the power level of the signal arriving at the detector, 3 db should be subtracted from the above level of P_r. This is due to the equal power division in the hybrid junction. Therefore, P_r (at the detector) is -71.5 dbw, or 43.5 db above the receiver noise level.

[8] H. T. Friis, "A note on a simple transmission formula," Proc. IRE, vol. 34, pp. 254–265; May, 1946.
[9] J. D. Kraus, "Antennas," McGraw-Hill Book Co., Inc., New York, N. Y.; 1950.
[10] Ninth Quarterly Prog. Rep. 302–29, Antenna Lab., The Ohio State Univ. Res. Foundation, prepared under Contract W 36-039 sc33634 with U. S. Army, Evans Signal Lab., Belmar, N. J.; May 1, 1949.

Appendix IV

Approximate Calculation of Receiver Response Due to Signal Scattered by Turbulent Air

Assuming far field conditions to exist, the ratio of the power collected by one of the receiving horns, due to scattering by the turbulent region, to the power radiated by the transmitter is given by[1]

$$\frac{P}{P_t} = \frac{A_{et}A_{er}}{\lambda^2}\int \frac{\sigma}{R_0^2R^2}\,dV \tag{13}$$

where A_{er} and A_{et} are the effective apertures of the receiver and transmitter, respectively, λ is the wavelength, σ is the scattering cross section, dV is an element of volume common to the transmitter and receiver beams, and R_0 and R are the distances from the element of volume to the transmitter and receiver, respectively.

Evaluation of the integral (13) can be simplified if σ is taken as constant throughout the scattering volume. For the case of forward scattering σ would then be given by[1]

$$\sigma_f = \frac{1}{\lambda}\overline{\left(\frac{\Delta\epsilon}{\epsilon}\right)^2}\left(\frac{2\pi L}{\lambda}\right)^3 \tag{14}$$

where L is the average scale of the temperature fluctuations. $\overline{(\Delta\epsilon/\epsilon)^2}$ is the mean square fractional deviation from average dielectric constant.

The geometry used in the evaluation of (13) is shown in Figs. 8 and 9.

An expression for the element of volume dV is arrived at by evaluating the turbulent region whose scattering contributes to the receiver response. For the Booker-Gordon scattering cross section, the angle of the scattered beam is given by:[1]

$$\frac{4\pi L}{\lambda}\sin\theta_s/2 = 1. \tag{15}$$

Substitution of numerical values in (15) gives,

$$\frac{\theta_s}{2} = 1.56°.$$

At this point, inspection of Fig. 9 shows that the effective scattering volume is essentially bounded by the beamwidth of the scattered radiation. Therefore, the element of volume dV may be approximated by the expression

$$dV = \pi r^2 dR, \tag{16}$$

where r is the radius of the circular cross section of the effective scattering volume; and its value is calculated using the semi-angle of the scattered beam. To simplify the evaluation of (13) r was taken as constant and equal to its average value of

$$r = \left[\frac{(41.4 + 11.0)}{2} \times \tan\frac{\theta_s}{2}\right]\text{cm}.$$

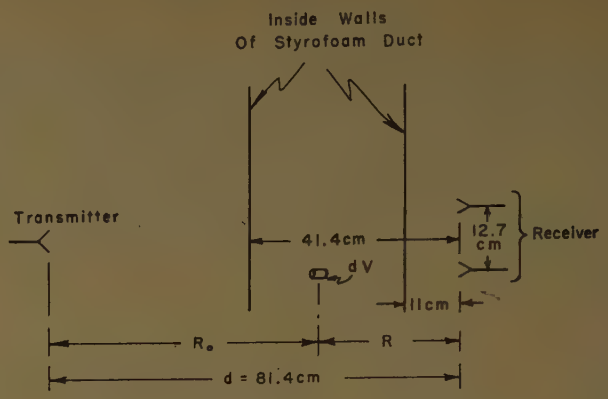

Fig. 8—Dimensions used in evaluating (13).

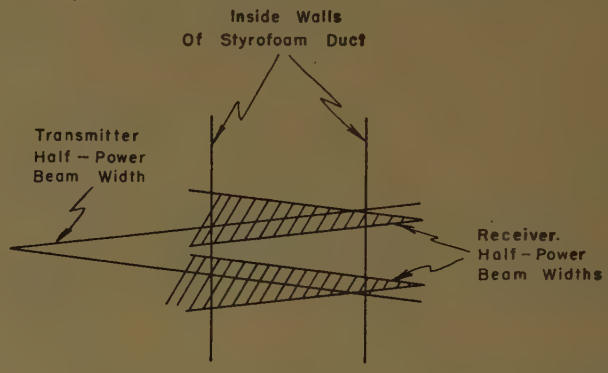

Fig. 9—Transmitter and receiver half-power beam widths.

It should be noted that since θ_s is a small angle, $\tan\theta_s/2 \cong \theta_s/2$, and therefore the effective scattering volume is proportional to θ_s^2. Use of numerical values gives $dV = 1.62\,dR$.

Therefore,

$$\int \frac{dV}{R^2R_0^2} = 1.62\int_{11}^{41.4} \frac{dR}{(81.4 - R)^2R^2}$$
$$= 3.04 \times 10^{-5}/\text{cm}. \tag{17}$$

Now,

$$\overline{\left(\frac{\Delta\epsilon}{\epsilon}\right)^2} = 34.4 \times 10^{-8}\overline{\left(\frac{\Delta T}{T}\right)^2}$$
$$= 66 \times 10^{-12}\frac{(T_0 - T)^2}{T^2}. \tag{18}$$

Substitution of numerical values in (13) yields,

$$\frac{P}{P_t} = 8.5 \times 10^{-11}. \tag{19}$$

Inspection of Fig. 9 shows that the effective scattering volume is located approximately at the half-power points of the transmitting antenna beam, therefore the value of P_t is taken as half the transmitted power. This gives a value of 8.50×10^{-12} watts for the power collected by one of the horns. Since both receiving horns contribute to the receiver response, the power collected by one horn is doubled. The reason for adding power

instead of signal amplitude is that each receiving antenna "sees" a different section of the turbulent region, and the scattering by a turbulent region is a random phenomenon.

Finally, to obtain the power level of the signal arriving at the detector, the value of 17×10^{-12} watts is halved due to the equal power division in the hybrid junction. This gives 8.5×10^{-12} watts for the power level of the signal arriving at the detector, which corresponds to 4.3 db above the receiver noise level.

Appendix V

Calculation of Forward Scattering Cross Section, Half-Power Beamwidth, Effective Volume, and Received Power from Empirical Temperature Correlation Function

The scattering cross section of the turbulent medium is given by[11]

$$\sigma = \frac{4\pi^3}{\lambda^4 q}\overline{\left(\frac{\Delta\epsilon}{\epsilon}\right)^2}\int_0^\infty R\sin(qR)C(R)dR \qquad (20)$$

where $q=4\pi/\lambda \sin(\theta/2)$ and θ is the scattering angle, $C(R)$ is the temperature correlation function, and R is a space interval.

For the experimental conditions described in this work, an empirical relationship for the temperature correlation may be obtained by using the data given by Kistler *et al.*[2] This relationship is of the form:

$$C(R) = 0.45e^{-0.134R} + 0.55e^{-0.826R}. \qquad (21)$$

[11] A. D. Wheelon, "Note on scatter propagation with a modified exponential correlation, Proc. IRE, vol. 43, 1381–1390; October, 1955.

In (21) R is measured in centimeters.

Substitution of (21) into (20), integration, and use of the appropriate numerical values yield:

$$\sigma = \frac{1}{\lambda^4}\overline{\left(\frac{\Delta\epsilon}{\epsilon}\right)^2}\,[2.76e^{-12q^2} + 0.22e^{-195q^2}]. \qquad (22)$$

To evaluate the forward scattering cross section q is set equal to zero, giving,

$$\sigma_f = 2.98\frac{1}{\lambda^4}\overline{\left(\frac{\Delta\epsilon}{\epsilon}\right)^2}. \qquad (23)$$

Eq. (22) may be used to find the half-power beamwidth of the scattered radiation; the numerical work indicates that this beamwidth is equal to 8.8°.

The element of effective scattering volume may be calculated as outlined in Appendix IV, in this case using $\theta_s=8.8°$. The result is

$$dV = 12.7\,dR \qquad (24)$$

A calculation similar to that given in Appendix IV, but based on the forward scattering cross section and half-power beamwidth of the scattered radiation as evaluated from the empirical correlation function, gives a value of 55×10^{-12} watts for the power level of the scattered signal arriving at the detector. This corresponds to a power level 12.4 db above the receiver noise level.

Acknowledgment

The author is indebted to Prof. T. E. Tice and W. Peake for their guidance and aid in the pursuance of this work. It is also a pleasure to acknowledge many helpful discussions with J. N. Hines.

Correction

The following correction has been brought to the attention of the editor. In "Radiation from Ring Sources in the Presence of a Semi-Infinite Cone," by Leopold B. Felsen, which appeared in these Transactions, Vol. AP-7, No. 2, pp. 168–180, April, 1959, on page 175, lines 2–7, counted from the bottom of the first column, should read:

It is noted that to $0(1/\sqrt{kr'})$ the functional form of the diffracted wave as a function of θ, θ' in (24), contributed by a typical term due to $\bar{G}_\theta{}'^\infty$ in (21a), is independent of the geometric-optical domain, *i.e.*, the same function applies for $|\theta-\phi|<\pi$ and $|\theta-\phi|>\pi$, where ϕ denotes the location of the source in the infinitely extended θ-transmission line. The same comment applies to the diffracted wave contribution arising from I_1 in (20a) when one inserts into the integrand the $(\bar{G}_\theta{}'-\bar{G}_\theta{}'^\infty)$-term in (21), as shown in Appendix II. The diffracted wave contribution from I_2 in (20b) has an angular dependence given by $(I_2)_0$ which, as noted from an examination of (11a) with f replaced by $(\bar{G}_\theta{}'-\bar{G}_\theta{}')$ (see (17)–(17c)), also has the same functional form for all values of $0\leq(\theta,\theta')\leq\theta_0$. Thus, the total diffracted wave function obeys this property to $0(1/\sqrt{kr'})$ and can therefore be evaluated from the alternative closed form expression $A_0(\theta,\theta')$, for which an integral representation valid when $(\theta+\theta')<(2\theta_0-\pi)$ is given in (9a).

Influence of an Atmospheric Duct on Microwave Fading*

F. IKEGAMI†

Summary—**The results of continuous observation of a duct carried out utilizing a tower 312 meters high are presented together with those of measurements of microwave fading conducted simultaneously.**

The variation of duct height with time, as well as the influence of the duct on fading for a horizontal and an oblique propagation path, are investigated in detail.

A ray-theoretical analysis is given, indicating that fading may be attributed to the divergence or the convergence of radio waves and to the interference of two or more rays, caused by existence of a duct, or, more generally, of nonlinear *M*-profile.

A comparison of calculation with experimental results shows that many of the characteristics of microwave fading are well explained by means of this interpretation.

Introduction

ALTHOUGH general characteristics of microwave fading have been clarified by many investigations carried out in the past several years, its exact mechanism still remains unsolved chiefly because of the lack of knowledge pertaining to the nature of atmospheric ducts.

Towards a solution of this question, continuous measurement of *M*-profile together with a microwave propagation experiment was made by utilizing a broadcasting antenna tower. Use of a tower was considered to be preferable to the conventional way of observation by means of a captive balloon or aircraft for measuring fine variations in height and structure of duct with time.

This paper describes the experimental relationship between fading and duct, especially the influence of the duct on fading for horizontal and oblique propagation paths. A ray-theoretical interpretation of a fading mechanism is also given for a better understanding of the experimental results.

Experimental Investigation

General Description of the Experiment

Observation of the Duct in the Lower Atmosphere: Continuous and precise measurement of the variation of a duct with time, essential to the analysis of relation between fading and the duct, was performed by utilizing the 312 meter-high broadcasting antenna tower at Kawaguchi Broadcasting Station, NHK.

The air temperature and humidity were measured by means of dry and wet bulb mercurial thermometers with very thin carbon filaments sealed in, the resistance being recorded continuously at the bottom of the tower.

Twelve sets of dry and wet bulb electrical thermometers mounted in a shelter with forced ventilation were installed on the tower at the heights of 13, 33, 54, 74 94, 123, 152, 181, 210, 239, 269, and 296 meters.

Over-all accuracy of the measurement of temperature, estimated to be within $\pm 0.1°C$, yields the error not exceeding 1 in NU. Very thin and weak ducts may, therefore, not be measured because of restrictions of the observational error and the spacing of equipment installation. The obtained data, however, were all available for the analysis of fading as far as the mean structure of the atmosphere was concerned.

Wave Propagation Test: Two paths of propagation were chosen so that radio data could be put into analysis together with results of the observation of the duct. Transmitters at the frequencies of 3982 mc and 4020 mc were installed at heights of 49 and 223 meters, respectively, on the tower where the meteorological equipment was installed. Receivers were located at the side of Mt. Tsukuba, 245 meters above sea level, the distance between the terminals being 54.8 km. The higher propagation path was nearly parallel to the earth surface and the lower path was oblique.

Experimental Results

Simultaneous measurements of the duct and fading were carried out from November 1–15, 1954, and data available for analysis were obtained for nine days from November 3–11.

Severe fading was observed almost every night during the test period corresponding to remarkable diurnal variations in the structure of the lower atmosphere. Ducts were formed in a temperature inversion layer when it was accompanied with a distinguished lapse rate of humidity. Appreciable correlation is seen in the obtained data between fading and the duct as well as between fading and the temperature inversion layer.

For further analysis, detailed observations were made of the variation of the duct with time, in particular, of the transitions that an initially formed surface duct undergoes when it is modified into an elevated duct, and that an elevated duct appearing in the higher atmosphere undergoes when it comes down near to the ground surface and vanishes after sunrise. Fig. 1 shows a typical example of the variation in structure of the lower atmosphere observed every ten minutes in comparison with simultaneous records of fading on the two propagation paths.

Relation Between Fading and Duct

Utilizing the results mentioned above, relations between fading and duct are analysed.

Mean received power on the two propagation paths varied almost independently and no significant corre-

* Manuscript received by the PGAP, October 13, 1958.

† Elec. Commun. Lab., Nippon Telegraph and Telephone Corp., Tokyo, Japan.

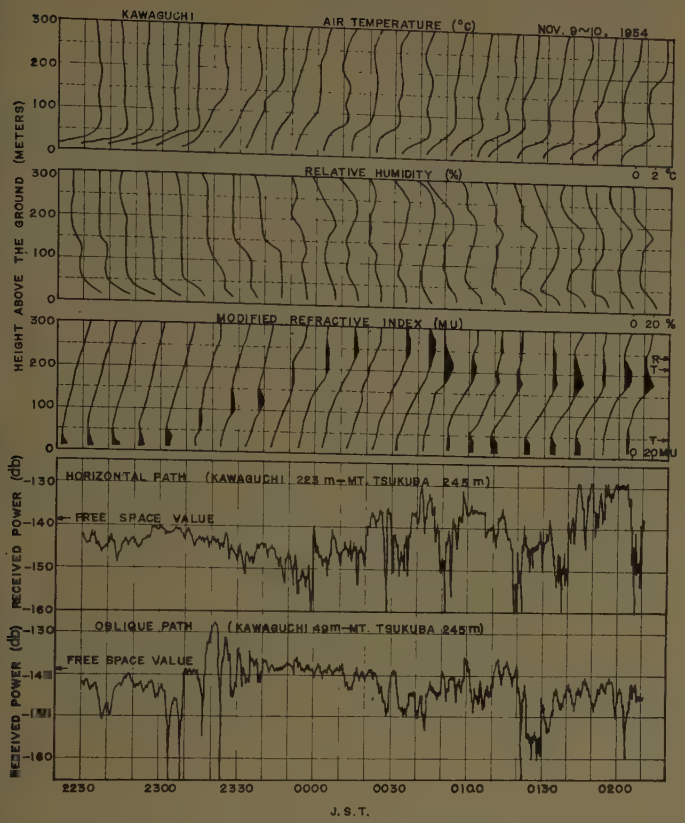

Fig. 1—Fading records in comparison with simultaneous meteorological observations in the lower atmosphere.

lation can be seen between them. However, when they are plotted against duct height, a remarkable property is found as shown in Fig. 2. In this figure, a single duct is represented by a circle and two or more ducts existing simultaneously are represented by dots, a larger dot indicating the stronger duct and a smaller one the weaker. Dashed lines in the figure, corresponding to the range of dispersion of circles, give tendency of the influence of duct on the mean received power.

On the oblique path, a considerable decrease in received power occurs only when a duct exists near the height of the lower terminal. No significant effect appears to be caused by ducts higher than 100 meters above the ground. On the contrary, large variation in received power occurs on the horizontal path, if a duct exists near the height of the propagation path, with only one exceptional case. It should be noted that the received power has a tendency to decrease on the oblique path while it is apt to increase on the horizontal path.

Relations between the maximum fading range for every 5 minutes and the duct height are shown in Fig. 3 for the two paths. Meanings of the points and the dashed lines in the figure are the same as in the previous case. Large fading range occurs if the duct is near the height of the horizontal path, or if it is near the height of the lower terminal of the oblique path.

Although a small number of cases of single duct encountered does not confirm the effect of duct height on

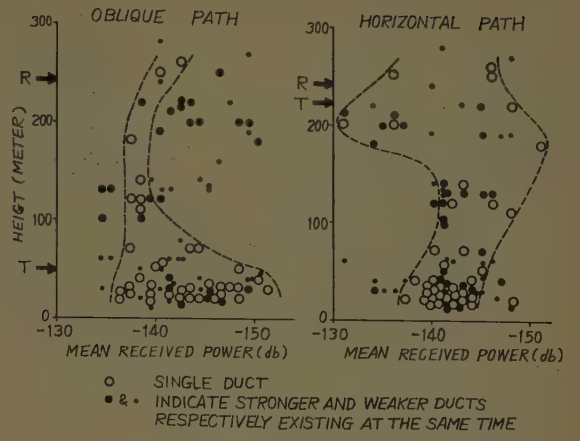

Fig. 2—Comparison of mean received power with duct height.

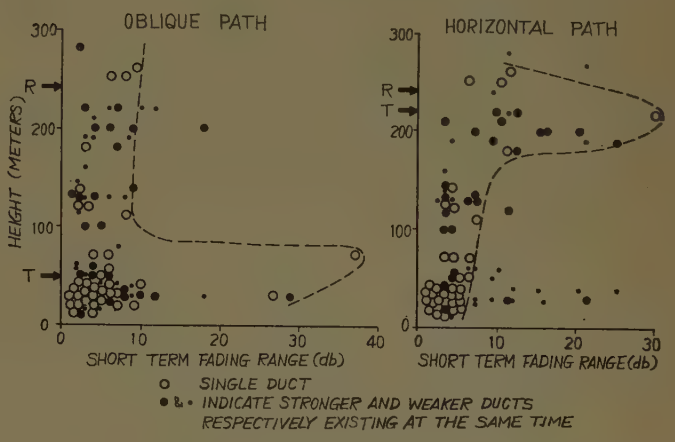

Fig. 3—Comparison of short term fading range with duct height.

fading completely, it might be concluded that, on the horizontal path, fading is caused mainly by a duct formed near the terminal heights, while, on the oblique path, by a duct formed near the lower terminal height.

Ray-Theoretical Interpretation of Fading

Interference and Attenuation Regions Caused by a Duct

It is known that, if the transmitter is situated in a duct, interference and blind regions extend near and within the duct.[1–3] In this section it will be shown, by means of a ray-theoretical treatment, that both interference and attenuation regions exist even if the transmitter is not situated in a duct layer.[4]

The beam of rays emitted at angles between θ_a and θ_c, as shown in Fig. 4, will interfere with that emitted at

[1] D. R. Hartree, J. G. L. Michel and P. Nicolson, "Practical Methods for the Solution of the Equations of Tropospheric Refraction," Meteorological Factors in Radio-wave Propagation, The Physical Society and the Royal Meteorological Society, London, pp. 127–168; 1946.

[2] C. R. Burrows, "Radio Wave Propagation," Consolidated Summary Tech. Rep. of the Committee on Propagation of the Nat. Defence Committee, New York, N. Y.; 1949.

[3] S. Matsuo, S. Ugai, K. Kakita, F. Ikegami and Y. Kono, "Fading of microwaves," *Elec. Commun. Lab. Tech. J.*, vol. 2, pp. 80–171; April, 1953.

[4] After submission of this paper, similar results were shown by M. S. Wong, "Refraction anomalies in airborne propagation," Proc. IRE, vol. 46, pp. 1628–1638; September, 1958.

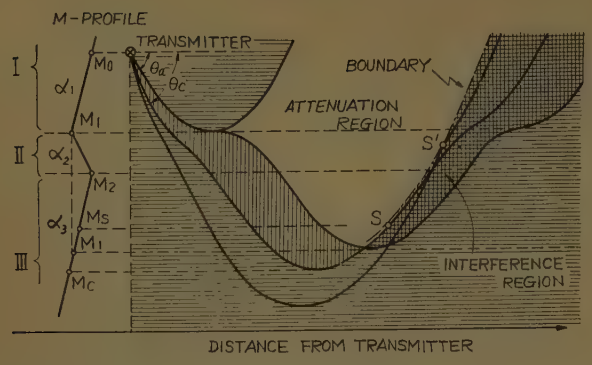

Fig. 4—Interference and attenuation regions in the case of a transmitter situated above an elevated duct. α denotes gradient of M-profile.

angles larger than θ_c, the angle corresponding to the ray whose horizontal distance is minimum at a given height. The region of interference will be bounded from that of attenuation by the envelope of the rays radiated at angles larger than θ_a. The position of an arbitrary point S on the envelope can be found by solving one of the following equations corresponding to the medium in which the point in consideration lies (Fig. 4).

$$\left.\begin{aligned}
&-\frac{1}{\alpha_1}\frac{1}{\sqrt{M_0-M_c}}+2\left(\frac{1}{\alpha_1}+\frac{1}{\alpha_2}\right)\frac{1}{\sqrt{M_1-M_c}}-2\left(\frac{1}{\alpha_2}+\frac{1}{\alpha_3}\right)\frac{1}{\sqrt{M_2-M_c}}-\frac{1}{\alpha_1}\frac{1}{\sqrt{M_s-M_c}}=0 \text{ (Medium I)}\\
&-\frac{1}{\alpha_1}\frac{1}{\sqrt{M_0-M_c}}+\left(\frac{1}{\alpha_1}+\frac{1}{\alpha_2}\right)\frac{1}{\sqrt{M_1-M_c}}-2\left(\frac{1}{\alpha_2}+\frac{1}{\alpha_3}\right)\frac{1}{\sqrt{M_2-M_c}}+\frac{1}{\alpha_2}\frac{1}{\sqrt{M_s-M_c}}=0 \text{ (Medium II)}\\
&-\frac{1}{\alpha_1}\frac{1}{\sqrt{M_0-M_c}}+\left(\frac{1}{\alpha_1}+\frac{1}{\alpha_2}\right)\frac{1}{\sqrt{M_1-M_c}}-\left(\frac{1}{\alpha_2}+\frac{1}{\alpha_3}\right)\frac{1}{\sqrt{M_2-M_c}}-\frac{1}{\alpha_3}\frac{1}{\sqrt{M_s-M_c}}=0 \text{ (Medium III)}
\end{aligned}\right\}. \quad (1)$$

Solving one of these equations, M_c, the value of M at the turning point C, is obtained and from that the initial angle θ_c, corresponding to a given value of M_s. Thus, the point S is determined for any value of M_s, and the locus of S gives the envelope required. Other boundaries of the regions can readily be found for both cases of the transmitter located in and above an elevated duct (Fig. 7).

Fading is considered to be caused by the movement of interference and attenuation regions that arises from the variations in height and structure of the duct.

Results of calculation show that the widths of these regions increase with distance and decrease with increasing angle of inclination of the propagation path. It is also shown that fading is caused by a duct appearing near or below the height of the lower terminal point.

Convergence and Divergence of Radio Waves

It is frequently observed that the median level of received power deviates more or less from the free space value. This phenomenon may be attributed to the convergence or divergence effect of the wave propagated through an inhomogeneous medium analogous to an optical convex or concave lens.

Although an air mass in the shape of an optical lens might possibly exist in the actual atmosphere, divergence or convergence can occur, it will be shown, even in a stratified medium.

The divergence or convergence effect may be expressed in terms of the energy density at the receiving point compared with that in the homogeneous medium of the wave bundle emitted from the transmitter into a unit solid angle. In the case of a linear M-profile it is easily verified by ray geometrical calculations that the spread of the wave bundle is approximately equal to that expected in the homogeneous atmosphere.

In what follows, multi-linear M-profiles will be considered, assuming that the atmosphere is uniform horizontally. Then, only the vertical cross section of wave bundle must be considered.

Let the spread of wave bundle in a homogeneous medium be denoted by dl_{hom}, and that in an inhomogeneous medium by dl. Then the received power relative to free space is given by the following equation:

$$\frac{p_r}{p_{r0}}=\left|\frac{dl_{\text{hom}}}{dl}\right|=x\Big/\left|\sum_i x_i'\frac{\theta_0\theta}{\theta_{i-1}\theta_i}-\sum_j x_j'\frac{\theta_0\theta}{\theta_{j-1}\theta_j}\pm x'\frac{\theta_0}{\theta_n}\right|. \quad (2)$$

Symbols used in this equation have the meanings as shown in Fig. 5 and summations $\sum_i$ and $\sum_j$ cover all downcoming and upgoing rays, respectively. Of the last term in the denominator, the positive sign is to be taken if the ray at the receiver is downcoming and the negative sign if it is upgoing. Eq. (2) is the fundamental equation which gives the received power in an atmosphere of multi-linear M-profile.

Radio waves are convergent or divergent according to the value determined by the above equation being larger or smaller than unity. This implies that the convergence or the divergence of waves arises from the curvature of M-profile, depending upon the shape of M-profile and upon the condition of propagation path.

In the particular case that the denominator of (2) tends to zero, p_r/p_{r0} takes an anomalously large value. This condition is satisfied at the point on the path of ray where the angle of ray is given by

$$\theta_\infty=\frac{\mp x'}{\sum_i x_i'\frac{\theta_0\theta_n}{\theta_{i-1}\theta_i}-\sum_j x_j'\frac{\theta_0\theta_n}{\theta_{j-1}\theta_j}}\cdot\theta_0. \quad (3)$$

It is obvious that in order to make the denominator of (2) vanish, it will have to include terms of opposite signs, all quantities involved being positive. That is,

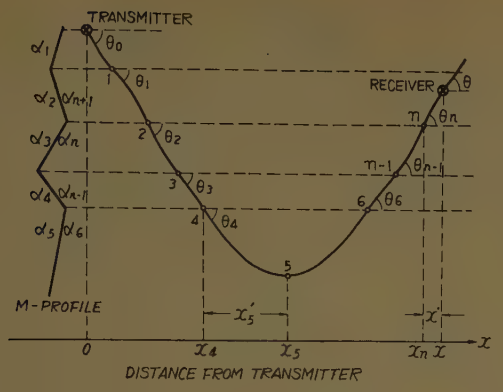

Fig. 5—Geometry of a ray propagated through a multi-linear M-profile. α denotes gradient of M-profile.

for the existence of the angle θ_∞, or in other words, for an extreme increase of received power, the path of ray should have a turning point.

In the simplest case of a bi-linear M-profile, convergence occurs in a substandard layer while divergence takes place in a super-standard or a duct layer.

If the transmitter is located above an elevated duct, the question is not simple. Fig. 6 shows an example of the spacial distribution of received power calculated by (2) at each point on each of the rays for various initial angles.

Eqs. (1) and (3) show that the waves converge infinitely on the boundary of the attenuation and interference regions. Below this boundary there is an interference region in which received power is composed of two groups of rays. One is the assembly of rays whose initial angle is smaller than θ_c, while the other is that of rays whose initial angle is larger than θ_c. The received power of the former is quickly attenuated as the receiving point in question departs further from the boundary, and attains zero at the lower end of the interference region. On the other hand, the received power of the latter is attenuated rapidly at first and then rather slowly until it approaches the free space value. Fig. 6 illustrates the drawing of equi-field-strength contours for the latter group of rays that are larger in magnitude than those of the former. Numerical values indicated on the contours represent the field strength in db relative to free space value.

Comparison with Experimental Results

Attenuation and Interference Regions: To check what has been stated of the attenuation and interference due to a duct, this section makes a comparison with the experimental results obtained during the period from 23^h00^m to 24^h00^m, November 9, 1954.

Corresponding to the monotonous increase of duct height, fading on the two paths shows very remarkable variations, as seen in Fig. 1. At first a low surface duct is formed when fading of attenuation type appears on the oblique path, while no significant fading is seen on the horizontal path. As the duct approaches the lower terminal height of the oblique path, a distinguished

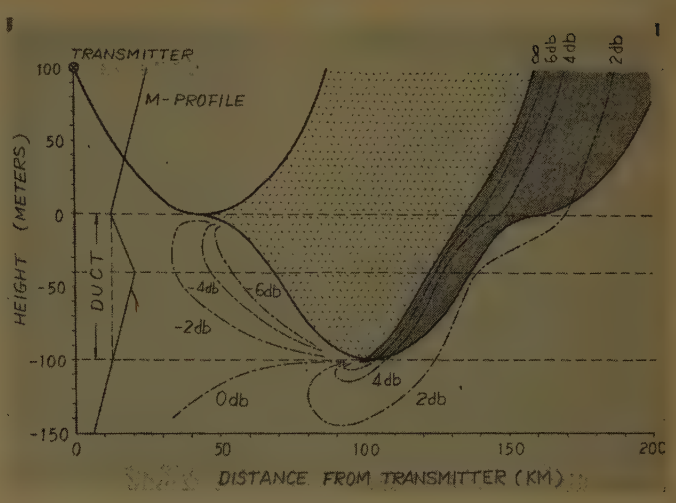

Fig. 6—Calculated spacial distribution of received power in the neighborhood of an elevated duct.

fading of interference type appears on the oblique path, and the magnitude of fading decreases in accordance with the ascent of duct, a stable state being attained and lasting after 23^h40^m. As the duct ascends, however, the received power decreases on the horizontal path until the maximum attenuation occurs just before 24^h00^m.

At 24^h00^m, when the duct reaches the height of the horizontal path, the received power suddenly increases and shows distinct fading of interference type which continues for a few hours as long as the duct stays at this height. The different features of fading observed on these two paths can be explained as follows.

Attenuation and interference regions for every 10 minutes are drawn in Fig. 7 for the observed M-profiles. Heights of the lower and higher transmitters and of the receiver are indicated by crossed circles in the figure. At 23^h00^m and 23^h10^m, a low duct near the ground surface produces only an attenuation region, the oblique path suffering from the fading of attenuation type. At 23^h20^m and 23^h30^m, an interference region is formed near the lower terminal height of the oblique path, while the horizontal path is almost free from both attenuation and interference regions. At 23^h40^m, the interference region ascends way above the lower transmitter height, as the duct ascends, and no effect occurs on the oblique path any more. At 23^h50^m, the duct is elevated higher, and the higher transmitter comes in an attenuation region, the fading of attenuation type being apparent on the horizontal path. At 24^h00^m, the interference region reaches the height of the horizontal path, and fading of the interference type is caused on this path.

At times, however, a discrepancy happens to arise between theory and measurements. This might be attributed to the nonuniformity of M-profile which is quite plausible if the whole propagation path is considered.

Divergence and Convergence Effect: Comparison of the theoretical prediction on the divergence and convergence effect with observed results encounters a difficulty because of the nonuniformity of M-profile over the path

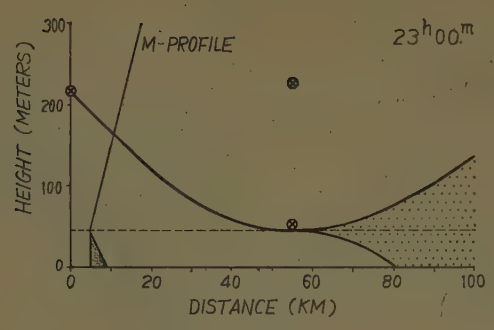

(a)

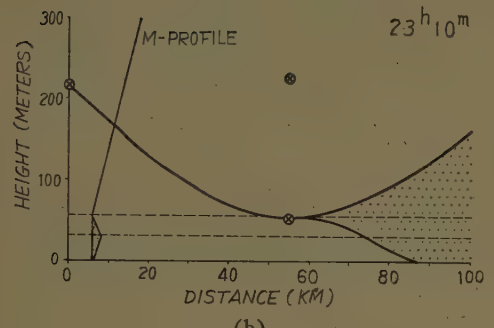

(b)

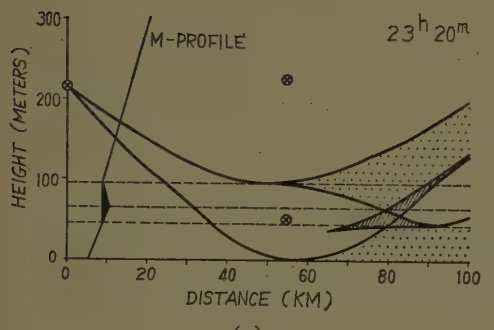

(c)

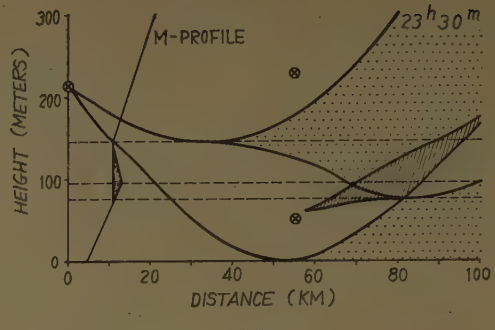

(d)

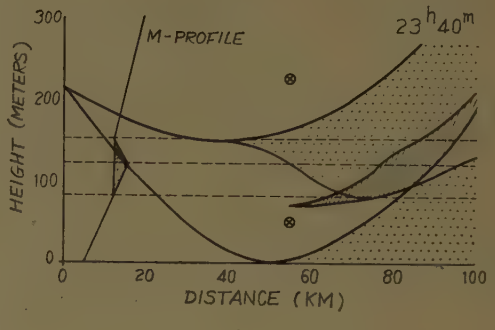

(e)

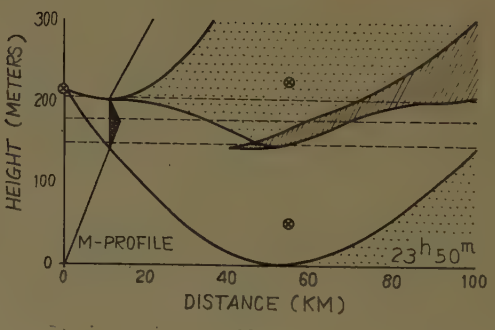

(f)

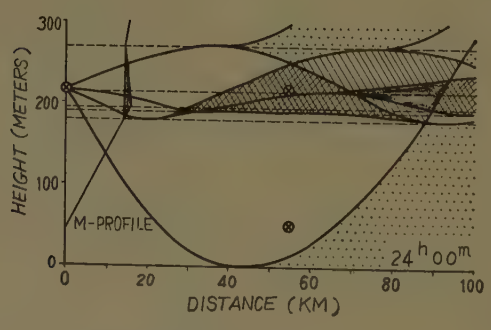

(g)

Fig. 7 (a)–(g)—Attenuation and interference regions calculated for *M*-profiles observed at Kawaguchi between 23h00m and 24h00m, November 9, 1954.

in the actual atmosphere. Qualitative characteristics only will be examined of the spacial distribution of received power on the oblique path.

A typical example of the calculated distribution is shown in Fig. 6 for the case of an elevated duct formed near the lower terminal height of an oblique path. This may give general characteristics to the effect in consideration. The spacial distribution of the received power would, more or less, be modified by variation in duct height. However, since the ascent of duct is thought to be equivalent to lowering the lower terminal height, the variation in received power caused by an ascent of duct may be treated as a function of elevation, the duct height being kept fixed. This will be referred to as antenna height pattern.

Antenna height patterns obtained from Fig. 6 for various distances are shown in Fig. 8. Full line indicates the magnitude of the stronger ray in the interference region, and the hatched parts represent amplitudes of the variation caused by two-ray interference.

Record of fading taken between 23^h00^m and 24^h00^m, November 9, shows a variation of received power caused by ascent of an elevated duct, giving an antenna height pattern in the sense of equivalence. This record is redrawn in Fig. 9 with the absissa and the ordinate interchanged. Comparing this curve with height patterns shown in Fig. 8, it is found that features of variation are quite similar except that the received power is not zero in the blind region for the actual case.

Thus, it is seen that the concept of divergence and convergence can account, qualitatively at least, for the spacial distribution of received power near the interference region.

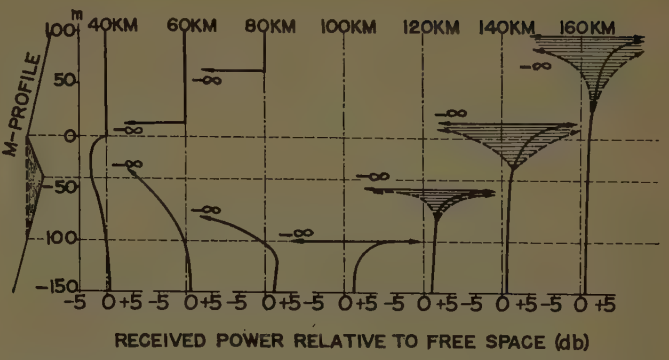

Fig. 8—Antenna height patterns at various distances, obtained from the spacial distribution illustrated in Fig. 6.

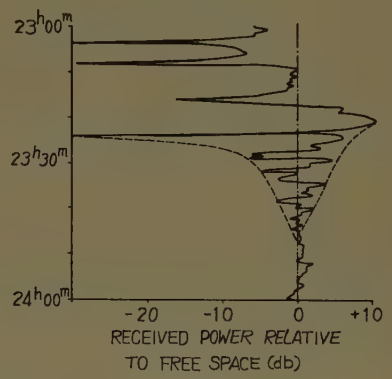

Fig. 9—Variation of received power with monotonous ascent of a duct. _____simulated antenna height pattern.

Conclusion

Relations between fading and duct are discussed on the basis of radio and meteorological experiments carried out utilizing a high tower. Continuous observation of duct made it possible to analyse its effect on the variation of received power recorded simultaneously.

Results of a ray-theoretical analysis indicate that fading is caused by the convergence or the divergence of radio waves and by the interference between converged and diverged waves, and it was also found that fading occurs when a duct is formed near or below the height of the lower terminal of the propagation path.

Comparison with experimental results shows that the ray-theoretical treatment is available for understanding the significant characteristics of microwave fading within line-of-sight.

Acknowledgment

The author is indebted to H. Yokoyama and S. Ugai for their guidance in general planning, to O. Tukizi for his instructive advice in analysis, and to M. Haga, T. Fukuda, and H. Yoshida for their valuable contributions in conducting the observations and in dealing with the obtained data.

He also wishes to thank R. Imaeda, Chief of Kawaguchi Broadcasting Station, NHK, for his cooperation in the performance of the experiment.

Comparison of Computed with Observed Atmospheric Refraction*

W. L. ANDERSON†, N. J. BEYERS‡, AND B. M. FANNIN§

Summary—Ray tracing methods have been applied in the computation of atmospheric refraction for a path at White Sands Missile Range, N. Mex., with a range of about 48 miles and an elevation angle of 14.5 milliradians. The atmosphere was assumed to be horizontally stratified. Refractive index profiles were derived from meteorological data obtained from surface observations, wiresondes, radiosondes, and airborne refractometer soundings. The profiles were classified "A", "B," or "C," in descending order of reliability, prior to radar refraction computations. The classification system considered the variety of data available, the time lag between radar and weather observations, and the proximity of the sounding to the propagation path. A good correlation between observed and computed angles resulted and the correlation was directly related to the classification.

Radar observations were made in the *X*-band and instrumental precision maintained to within 0.25 milliradian. Total bending ranged between 0.56 and 2.23 milliradians, with standard deviation 0.38 milliradian.

The rms deviation of computed from observed angles ranges from 0.19 to 0.41 milliradian for Class A and Class C data, respectively. The correlation coefficient ranges from 0.81 to 0.13. It is concluded that within the limits of this experiment: a) ray tracing methods are justified, b) horizontal stratification may be assumed and c) the accuracy of bending predictions is increased by improving the meteorological data.

Introduction

In the past, estimates of the accuracy with which atmospheric refraction can be computed have emphasized the limitations imposed by the following factors:[1,2]

1) Uncertainties in meteorological measurements.
2) Uncertainties in refractive index calculations.
3) The assumption of a horizontally stratified atmosphere.
4) Approximations associated with ray-tracing.

The work to be described shows that, on the average and under the particular experimental conditions of this case, the first factor mentioned above contributes the greatest error to the computations. Previous work on the general problem of predicting refraction has been based largely upon radiosonde data. It is shown here that if radiosonde is supplemented with other data, such as surface readings taken at the radar site, wiresonde, and airborne refractometer readings, the prediction accuracy is much improved.

* Manuscript received by the PGAP, November 24, 1958. This work was performed under Contract No. DA 29-040-ORD-1238.

† Elect. Engrg. Dept., Univ. of New Mexico, Albuquerque, N. Mex.

‡ Missile Geophys. Div., U. S. Army Signal Missile Support Agency, White Sands Missile Range, N. Mex.

§ Elec. Engrg. Dept., Univ. of Texas, Austin, Tex.

[1] M. Schulkin, "Average radio-ray refraction in the lower atmosphere," PROC. IRE, vol. 40, pp. 554–561; May, 1952.

[2] L. J. Anderson, L. G. Trolese, and J. B. Smyth, "Comparison of measured and computed refractive bending in the troposphere," paper presented at URSI Twelfth General Assembly, Boulder, Colo.; 1957.

Radar and Terrain

The experimental work upon which the calculations are based was performed over the period November 1, 1957, through March 25, 1958, at the White Sands Missile Range, N. Mex. A standard Nike-Hercules missile tracking radar (*X*-band) was used and instrumental precision was maintained to within 0.25 milliradian. A beacon target equipped with a horn antenna was fixed on a peak in the Sacramento Mountains and radar elevation angles to the beacon were recorded photographically every one-tenth second for about 30 seconds. An average was taken of the readings thus obtained.

Fig. 1 shows the topography involved. The scale representing altitude has been multiplied by a factor of about 7.5. Target elevation is 5285 feet above that of the transmitter, and the slant range is 256,404 feet. The terrain between transmitter and target consists of relatively flat desert valley.

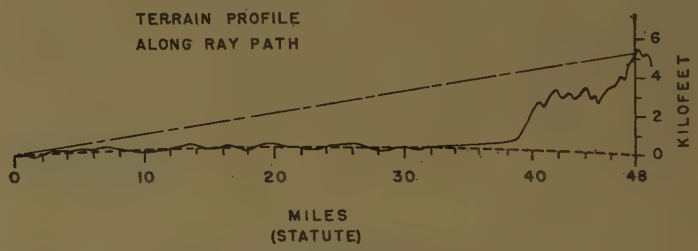

Fig. 1—Profile of desert terrain between transmitter and target. Vertical scale is expanded by a factor of 7.5.

Meteorological Data

Table I gives a breakdown of the types of meteorological information used in preparing the refractive index profiles with the number of classifications into Class A (most reliable), Class B (average reliability) and Class C (least reliable).

TABLE I

	R.S. only	W.S. only	S.O. only	R.S.-W.S.	W.S. S.O.	R.S. S.O.	R.S. A.R.	R.S.-W.S. -S.O.	R.S.-S.O. -A.R.
Class A	—	—	—	7	1	1	—	4	2
Class B	5	2	4	1	1	23	7	1	—
Class C	10	—	—	—	—	—	—	—	—

The abbreviation "R.S." is used for radiosonde, "W.S." for wiresonde, "S.O." for surface observation, and "A.R." for airborne refractometer. The assessment of reliability in each case was made before the bending calculations were performed. The requirements placed upon each category were as follows:

Class A:
1) At least two observational methods used.
2) Close agreement between observations made by different methods.
3) All data obtained within two hours of radar observation.
4) Stable synoptic situation.
5) Soundings made within five miles of propagation path.

Class B:
1) One sounding available.
2) Data within two hours of radar observation.
3) Stable synoptic situation.
4) Soundings within five miles of propagation path.
5) Supplementary data more than two hours old may be used.

(It will be noted from Table I that four cases were assigned Class B when only surface observations were available. Exceptional profile persistence permitted this relatively high classification.)

Class C:
1) Made up of radiosonde profiles which did not qualify for Class A or B. Still considered to be a fair representation of existing conditions.

Most radiosonde and all wiresonde soundings were taken about $2\frac{1}{2}$ miles from the radar site and $1\frac{1}{2}$ miles from the ray path. In a few cases, surface observations were taken here, also, but the majority of these were at the radar site. A small fraction of the radiosonde data consisted of soundings taken at Holloman Air Force Base, which is located about 15 miles from the target and 11 miles from the ray path. The few refractometer flights consisted of spiral ascents near Holloman or gradual ascents from transmitter to target, roughly coinciding with the ray path. These latter were too few to be of much statistical significance here; in fact, only one Class A profile was partially based on soundings obtained in this manner.

Ray Tracing Procedure

The bending to be expected in the case of a linear refractive index profile can be calculated analytically to any desired degree of precision. It is therefore convenient for computational purposes to compare the particular profile being considered with a linear "reference profile." In each case the reference profile is chosen so that its slope compares fairly closely with the average slope of the actual profile. The quantity $\Delta\alpha_0$ is then defined:

$$\Delta\alpha_0 = \alpha_0 - \alpha_0' \tag{1}$$

where α_0' is the computed elevation angle for the linear reference profile, and α_0 is the (yet to be determined) elevation angle for the actual profile. With proper choice of the reference profile, the magnitude of $\Delta\alpha_0$ can usually be made to fall within 1 or 2 per cent of α_0.

The convenience of dealing with the small quantity $\Delta\alpha_0$ lies in the fact that it permits a considerable simplification in the ray-bending computations. To begin with, the ray path is considered to be described by the familiar relationship for refraction in a spherically symmetric atmosphere:

$$nr \cos\alpha = n_0 r_0 \cos\alpha_0. \tag{2}$$

For given transmitter and target heights (r_0 and r_1, respectively) and taking θ_0 as the angle between them, measured at the earth's center, it follows that:

$$r_0\theta_0 = \int_{r_0}^{r_1} \frac{r_0}{r}\left[\left(\frac{nr}{n_0 r_0}\right)^2 \sec^2\alpha_0 - 1\right]^{-1/2} dr. \tag{3}$$

In this expression n is, thus far, an arbitrary function of r. This integral can be equated to one that is identical except that n is specified. The specified n we refer to as n', and as mentioned previously, allow it to be of the simple linear form:

$$n' = n_0' - B(r - r_0) \tag{4}$$

where B is a suitably chosen constant. By subtracting the integral with primed quantities from the other, and taking the quantities $(n-n_0)$, $(n'-n_0')$, $(r-r_0)$, and $\Delta\alpha_0$ to be quite small, the following approximate expression is developed:[3]

$$\Delta\alpha_0 = \cot\alpha_0'\left[(n_0 - n_0') - \frac{1}{Z_1}\int_0^{Z_1}(n - n')dZ\right] \tag{5}$$

where

$$Z = \left\{1 - \sin\alpha_0'\left[\left(\frac{r}{r_0}\right)^2 - \cos^2\alpha_0'\right]^{-1/2}\right\}.$$

The integral in (5) can be evaluated conveniently by graphical means. If $n(r)$, the actual profile, has been plotted on graph paper, then the reference profile, *i.e.*, the straight line representing $n'(r)$, can be drawn on the same paper. The figures for $(n-n')$ are read from the graph for various values of r, and replotted as a function of z on another graph. A simple area measurement then gives the value of the integral. Any desired degree of precision can be attained in this graphical integration by sufficiently expanding the scales. In view of the meteorological uncertainties, however, it is believed adequate if $\Delta\alpha_0$ is determined with a precision of a few per cent.

Comparison, Observed with Computed Angles

A total of 69 profiles was evaluated by the preceding method, and angles were compared with those observed. Fig. 2 is a scatter diagram for the results. The radar precision is within plus or minus one-fourth milliradian; consequently points within the area between the upper and lower 45° lines are considered to be in good agree-

[3] B. M. Fannin and K. H. Jehn, "A study of radar elevation-angle errors due to atmospheric refraction," IRE Trans. on Antennas and Propagation, vol. AP-5, pp. 71–77; January, 1957.

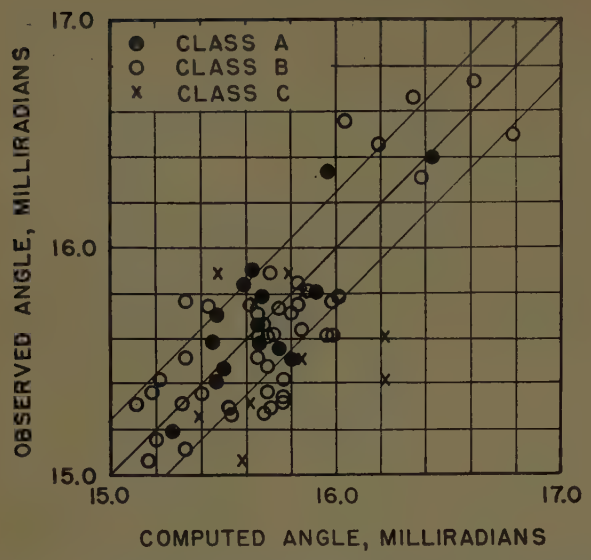

Fig. 2—Scatter diagram for comparison of computed with observed elevation angles. The geometric angle is 14.497 milliradians.

ment. Since the geometric angle is 14.497 milliradians, the observed bending ranges from 0.56 to 2.23 milliradians. The mean bending is 1.16 milliradians, and the standard deviation is 0.38 milliradian.

Table II gives mean and rms deviation of computed from observed angles for the three classes of data, and for all data. Also given are the correlation coefficients. Since these test linearity only, their values for different classes of data should not be considered to be an especially good criterion of comparison. They should here be interpreted in a qualitative rather than a quantitative sense.

TABLE II

(e = |computed angle minus observed angle|)

	$\bar{e}$	$\sqrt{\bar{e}^2}$	ρ
Class A	0.152 mr	0.187 mr	0.81
Class B	0.205 mr	0.248 mr	0.81
Class C	0.340 mr	0.412 mr	0.13
All data	0.213 mr	0.268 mr	0.74

In the Class C category, it may be noted that $\sqrt{\bar{e}^2}$ does not differ greatly from the standard deviation previously mentioned. From the view point of rms error, then, the use of a mean elevation angle may be no more inaccurate than predictions based on Class C data.

The Class B predictions are a great deal better than those of Class C. Since nearly two-thirds of all cases fell in this category, the results furnish strong evidence that significant corrections to the observed angles can be predicted routinely on the basis of simple meteorological information.

Slightly greater pains in taking weather data result in the Class A cases, and here a further improvement is gained. In consideration of the stated limits as to radar precision and the uncertainties in the meteorological data, it is believed that the Class A results are nearly as good as can be expected.

A limiting factor in the reduction of radar refraction errors may be the scintillation effect, caused by irregular inhomogeneities in the atmosphere. There is some uncertainty as to the extent of the effect in this case. It was observed that if two or three readings were taken in succession at intervals of a few seconds, differences of up to 0.2 milliradian might occasionally occur between readings. However, when a large number of readings were made over a time interval (*e.g.*, readings every one-tenth second for thirty seconds) the distribution almost invariably appeared to be normal about some mean value. The "spread" of the distribution varied considerably from day to day; thus it might be supposed that atmospheric conditions caused the variability in readings. It is believed, however, that instrumental effects—for example, wind pressures on the radar dish—might also have had a bearing on the matter. Since deviations were within the limits of radar precision, the uncertainty probably cannot be resolved without further study.

Conclusions

A comparison of Class A, B, and C results shows that the ability to predict ray bending improves directly with reliability of meteorological information. The Class A and B results show that, within the limits stated as to radar accuracy and the uncertainties in atmospheric information, the following conclusions can be reached:

1) Ray tracing techniques and associated approximations are justified.
2) The assumption of horizontal stratification is justified.
3) The errors arising from sources other than meteorological are not so great as to preclude the necessity for detailed, accurate meteorological information.

It is expected in the future that a helicopter-mounted refractometer will give more detailed information on the tropospheric structure, and that the use of better radar equipment will improve the accuracy of angle and range observations. It is hoped that an exploration can thereby be made of the ultimate limits within which ray-bending can be predicted in this locality.

Diffraction Theory of Tropospheric Propagation Near and Beyond the Radio Horizon*

Part I—Theory

O. TUKIZI†

Summary—By means of the earth-flattening approximation, the problem of radio diffraction by the earth is treated as that of refraction in an atmosphere with a linear profile of modified index. Use is made of the saddle point method, whose special case, known as the method of stationary phase, proves useful for analysis of the normal propagation within the horizon.

It is found that the classical diffraction theory is as valid at ranges beyond the horizon as in its neighborhood, if account is taken of the contribution of other terms than the first of the residue series, and that exclusive use of the saddle point method makes it possible to deal systematically with the tropospheric propagation for all regions within, near, and beyond the horizon.

Theoretical derivations are presented in Part I. Part II gives a comparison of the theory with experiments, showing a fairly good agreement between them.

I. Introduction

IT is well-known that the diffraction theory due to Watson[1] and to van der Pol and Bremmer[2] does not succeed in explaining the fact that the field strength well beyond the horizon decreases with distance at a considerably slow rate. An account for this phenomenon was given by Booker and Gordon[3] and their theory of tropospheric scattering now seems to prevail.

The aim of this paper is to present, nevertheless, an alternative theory which is essentially a modification of the classical diffraction theory. The formal difference lies in the fact that the present theory replaces the procedure of contour transformation by the one that utilizes the saddle point method to take into account the contribution of *all* terms of the residue series.

It can be shown that the residue series is not of very rapid convergence unless the transmitting and receiving antennas are both on the surface of the earth. If either or both of them are elevated and at a sufficiently large distance from each other, the sum of all but the first term of the series takes on a value not negligible in comparison with the first term.

Carroll and Ring[4] appear to have noticed the fact. They show by numerical calculation that, for some types of stratified atmosphere, there exist the modes which contribute most to the field strength given by the residue series. It should be emphasized, however, that this is also the case for a homogeneous atmosphere, *i.e.*, for an atmosphere with a linear profile of the modified index of refraction.

In the sections that follow, starting from the wave equation based on the flat-earth treatment,[5] we shall obtain three significant wave functions. The first, formulated in Section III, is of exactly the same form as the first term of the residue series, giving the field strength at ranges near the horizon. The others, expressed in Section IV in terms of infinite series, will be summed up in Section V to give the field strength beyond the horizon in a simpler form.

Here, by the terms "near" and "beyond" the horizon, are meant those regions which are customarily referred to as "diffraction" and "scatter" regions, respectively. Use of these terms will be avoided in the present paper, since it is aimed at showing that the diffraction by the earth accounts for the field strength at ranges beyond the horizon as well as in its neighborhood.

II. Mathematical Formulation

Consider a flat earth and introduce the rectangular coordinate system 0-xyz whose xy-plane coincides with the surface of the earth. Let $(0, 0, z_1)$ and (x, y, z) be coordinates of the source and the field point, respectively, and $r(=\sqrt{x^2+y^2})$ the plan distance between them.

If ψ is the z-component of Hertz vector whose x- and y-components are zero, the wave equation is written

$$\Delta\psi + k^2N^2(z)\psi = 0, \tag{1}$$

where k is the propagation factor for free space and $N(z)$ is the modified index of refraction assumed to be a function of the altitude above the surface z alone.

We shall use the MKS unit system and suppress the time factor $\exp(-i\omega t)$.

The matter with which we are concerned is to find a solution of (1) which satisfies the appropriate boundary conditions. It is given by[6]

* Manuscript received by the PGAP, September 12, 1958.

† Electrical Commun. Lab., Musasino-si, Tokyo, Japan.

[1] G. N. Watson, "The diffraction of electrical waves by the earth," *Proc. Roy. Soc., London*, vol. A95, pp. 83–99; October, 1918; vol. A95, pp. 546–563; July, 1919.

[2] B. van der Pol and H. Bremmer, "The diffraction of electromagnetic waves from an electric point source round a finitely conducting sphere," *Phil. Mag.*, vol. 24, pp. 141–176; July, 1937; pp. 825–864; Suppl., November, 1937; vol. 25, pp. 817–834; Suppl., June, 1938; vol. 27, pp. 261–275; March, 1939.

[3] H. G. Booker and W. E. Gordon, "A theory of radio scattering in the troposphere," Proc. IRE, vol. 38, pp. 401–412; April, 1950.

[4] T. J. Carroll and R. M. Ring, "Propagation of short radio waves in a normally stratified atmosphere," Proc. IRE, vol. 43, pp. 1384–1390; October, 1955. See also, "Propagation des micro-ondes dans la zone d'ombre à travers une couche d'air dont l'indice décroit de façon monotone," *Onde élect.*, vol. 37, pp. 471–479; May, 1957.

[5] M. H. L. Pryce, "The diffraction of radio waves by the curvature of the earth," *Advances in Physics*, vol. 2, pp. 67–95; January, 1953. See also C. L. Pekeris, "Accuracy of the earth-flattening approximation in the theory of microwave propagation," *Phys. Rev.*, vol. 70, pp. 518–522; October, 1946.

[6] J. E. Freehafer, "Physical Optics," in D. E. Kerr, ed., "Propagation of Short Radio Waves," M.I.T. Rad. Lab. Ser., McGraw-Hill Book Co., Inc., New York, N. Y., vol. 13, pp. 58–112; 1951.

$$\psi = \int_0^\infty \lambda J_0(\lambda r) u(z, \lambda) d\lambda. \tag{2}$$

where

$$\left.\begin{aligned} u &= \frac{2}{W}\left[\frac{u_2'(0)+pu_2(0)}{u_1'(0)+pu_1(0)} - \frac{u_2(z)}{u_1(z)}\right] u_1(z_1)u_1(z), \quad (z_1 > z) \\ &= \frac{2}{W}\left[\frac{u_2'(0)+pu_2(0)}{u_1'(0)+pu_1(0)} - \frac{u_2(z_1)}{u_1(z_1)}\right] u_1(z_1)u_1(z), \quad (z_1 \leqq z) \end{aligned}\right\}. \tag{3}$$

The symbols used in (3) have the following meanings:

u, u_1 and u_2 are all solutions of the equation

$$\frac{d^2u}{dz^2} + (k^2N^2 - \lambda^2)u = 0, \tag{4}$$

$u_1(z)$ and $u_2(z)$ being, however, those solutions of (4) which for large z represent waves traveling in the direction of increasing and decreasing z, respectively.

W is the Wronskian of $u_1(z)$ and $u_2(z)$ and is independent of z.

$p(\lambda^2)$ is a function of λ that depends on polarization;

$$\left.\begin{aligned} p(\lambda^2) &= i(k_0/k_1)^2\sqrt{k_1^2 - \lambda^2}, \\ &\qquad \text{for vertical polarization} \\ &= i\sqrt{k_1^2 - \lambda^2} \quad \text{for horizontal polarization} \end{aligned}\right\}, \tag{5}$$

where k_0 is the propagation factor of the atmosphere at the surface and k_1 is the propagation factor of the earth.

In the following discussions, we shall confine ourselves to a homogeneous atmosphere and write

$$N(z) = n_0(1 + \gamma z), \tag{6}$$

where n_0 is the true index of refraction at the surface and γ is the gradient with respect to height of the modified index divided by n_0.

Upon introducing the parameter ζ, related to λ by

$$\zeta = (\lambda^2 - k_0^2)/2k_0^2, \qquad (k_0 = kn_0), \tag{7}$$

we change the variable by the relation

$$\left.\begin{aligned} s &= \beta^{-1}(\gamma z - \zeta) \\ \beta &= (\gamma/\sqrt{2}k_0)^{2/3} \end{aligned}\right\}. \tag{8}$$

The solution of (4) is then readily seen to be expressed in terms of cylinder functions of order one-third.

We shall choose Hankel functions for basic independent solutions and make use of the modified Hankel functions of order one-third, defined by[7]

$$\left.\begin{aligned} h_1(s) &= \left(\frac{2}{3}s^{3/2}\right)^{1/3} H_{1/3}^{(1)}\left(\frac{2}{3}s^{3/2}\right) \\ h_2(s) &= \left(\frac{2}{3}s^{3/2}\right)^{1/3} H_{1/3}^{(2)}\left(\frac{2}{3}s^{3/2}\right) \end{aligned}\right\}. \tag{9}$$

If we take into account that asymptotic expansions of $h_j(s)$ as $z \to \pm\infty$ $(s \to \pm\infty)$ are given by

$$\left.\begin{aligned} h_1(s) &\sim \alpha s^{-1/4} e^{-(2\pi/3)i} \exp\left(i\frac{2}{3}s^{3/2} + i\frac{\pi}{4}\right)[1 + O(s^{-3/2})], \quad \left(-\frac{2\pi}{3} < \arg s < \frac{4\pi}{3}\right) \\ &\sim \alpha s^{-1/4} e^{-(2\pi/3)i} \cdot 2\cos\left(\frac{2}{3}s^{3/2} + \frac{\pi}{4}\right)[1 + O(s^{-3/2})], \quad \left(-\frac{4\pi}{3} < \arg s < 0\right) \\ h_2(s) &\sim \alpha s^{-1/4} e^{(2\pi/3)i} \exp\left(-i\frac{2}{3}s^{3/2} - i\frac{\pi}{4}\right)[1 + O(s^{-3/2})], \quad \left(-\frac{4\pi}{3} < \arg s < \frac{2\pi}{3}\right) \\ &\sim \alpha s^{-1/4} e^{(2\pi/3)i} \cdot 2\cos\left(\frac{2}{3}s^{3/2} + \frac{\pi}{4}\right)[1 + O(s^{-3/2})], \quad \left(0 < \arg s < \frac{4\pi}{3}\right) \end{aligned}\right\}, \tag{10}$$

where

$$\alpha = (2/\pi)^{1/2}(3/2)^{1/6},$$

we are led to choosing for solutions of (4) the functions

$$u_1(z) = e^{(2\pi/3)i}h_1(s), \qquad u_2(z) = e^{-(2\pi/3)i}h_2(s), \tag{11}$$

which, in conjunction with the time factor $\exp(-i\omega t)$, represent waves traveling in the direction of increasing and decreasing z respectively.

The Wronskian of $u_1(z)$ and $u_2(z)$ then becomes

$$\begin{aligned} W &= \beta^{-1}\gamma W[h_1(s), h_2(s)], \\ &= -i\frac{4}{\pi}\left(\frac{3}{2}\right)^{1/3}\beta^{-1}\gamma = -i2\alpha^2\beta^{-1}\gamma. \end{aligned} \tag{12}$$

In what follows, we shall assume that the height of transmitter is greater than that of receiver, *i.e.*, $z_1 > z$. Then there arises no loss of generality because if $z_1 \leqq z$, it is only necessary to interchange z_1 and z in the end result, as (3) indicates.

Now, we rewrite the first equation of (3) as

$$u = \frac{2}{W}\left[\frac{u_2'(0) - u_1'(0) + pu_2(0) - pu_1(0)}{u_1'(0) + pu_1(0)} - \frac{u_2(z) - u_1(z)}{u_1(z)}\right] u_1(z_1)u_1(z), \tag{13}$$

[7] "Tables of the modified Hankel functions of order one-third and of their derivatives," *Ann. Harvard Univ. Computation Lab.*, vol. 2, pp. xviii–xxix; 1945.

and make use of the relation[7]

$$e^{(\pi/3)i}h_1(s) + h_2(s) = -e^{-(\pi/3)i}h_1(se^{-(2\pi/3)i}). \quad (14)$$

Then, (13) reduces to

$$\left.\begin{aligned} u &= v_s(s) + v_p(s) \\ v_s(s) &= \frac{2}{W}e^{(2\pi/3)i}\frac{\left[\frac{d}{ds}h_1(se^{-(2\pi/3)i})\right]_{s=s_g} + \tau(s_g)h_1(s_ge^{-(2\pi/3)i})}{\left[\frac{d}{ds}h_1(s)\right]_{s=s_g} + \tau(s_g)h_1(s_g)}h_1(s_1)h_1(s) \\ v_p(s) &= -\frac{2}{W}e^{(2\pi/3)i}h_1(s_1)h_1(se^{-(2\pi/3)i}) \end{aligned}\right\} \quad (15)$$

where s_1, s and s_g denote values of s corresponding respectively to $z=z_1$, z and 0, and $\tau(s_g)$ is related to $p(\lambda^2)$, *qua* function of s_g, by

$$\tau(s_g) = \beta\gamma^{-1}p(s_g). \quad (16)$$

It is convenient for our present purpose to transform the integral expression (2) into one that involves $H_0^{(1)}(\lambda r)$ instead of $J_0(\lambda r)$. This is done by means of Freehafer's procedure,[6] giving

$$\psi = \frac{1}{2}\int_L \lambda H_0^{(1)}(\lambda r)u(z,\lambda)d\lambda, \quad (17)$$

where the path of integration L extends from $+i\infty$ to 0 along the positive imaginary axis and then to $+\infty$ along the positive real axis.

We change by (7) the variable of integration from λ to ζ and take into account that k_0r is very large compared with unity. Then, on assuming that $|\zeta/2|^2 \ll 1$, the integral can be approximated to

$$\psi = \frac{1}{2}k_0^2H_0^{(1)}(k_0r)\int_{-\infty}^{\infty}u(z,\zeta)\exp(ik_0r\cdot\zeta)d\zeta. \quad (18)$$

The assumption does not cause a large error, since the contribution to the integral, as will be seen later, comes most from ζ that satisfies the condition just introduced.

The next step is to apply the saddle point method[8,9] to evaluating the integral (18). We put

$$\left.\begin{aligned} u(z,\zeta) &= A(\zeta)\exp[-if(\zeta)] \\ k_0F(\zeta) &\equiv -if(\zeta) + ik_0r\cdot\zeta \end{aligned}\right\}, \quad (19)$$

and seek the roots ζ_{0j} of the equation

$$k_0F'(\zeta) = -if'(\zeta) + ik_0r \equiv 0, \quad (20)$$

where the prime denotes differentiation with respect to ζ.

Upon appropriately deforming the contour of integration and using values of the saddle points, *i.e.*, the roots of (20), we have ultimately

$$\psi = \left(\frac{\pi}{2}\right)^{1/2}k_0^2H_0^{(1)}(k_0r)\sum_j A(\zeta_{0j})e^{i\theta_2}|f''(\zeta_{0j})|^{-1/2} \cdot\exp\{k_0F(\zeta_{0j})\}, \quad (21)$$

where

$$\theta_2 = \frac{\pi}{2} - \frac{1}{2}\arg F''(\zeta_{0j}). \quad (22)$$

The summation must cover all possible values of the saddle points ζ_{0j}, since there exist possibly more than one saddle point which satisfies (20).

III. Wave Function for Ranges Near the Horizon

In this section we shall obtain the wave function valid at ranges near the horizon.

Consider the term $v_s(s)$ on the right of the first equation of (15). If we put, for brevity,

$$\left.\begin{aligned} w(s_g) &= h_1'(s_g) + \tau(s_g)h_1(s_g) \\ w(s_ge^{-(2\pi/3)i}) &= e^{-(2\pi/3)i}h_1'(s_ge^{-(2\pi/3)i}) \\ &\quad + \tau(s_g)h_1(s_ge^{-(2\pi/3)i}) \end{aligned}\right\}, \quad (23)$$

the wave function, which corresponds to $v_s(s)$ and is denoted by ψ_s, is written, by (15) and (18),

$$\psi_s = \frac{k_0^2}{W}e^{(2\pi/3)i}H_0^{(1)}(k_0r) \cdot\int_{-\infty}^{\infty}\frac{w(s_ge^{-(2\pi/3)i})}{w(s_g)}h_1(s_1)h_1(s)e^{ik_0r\cdot\zeta}d\zeta. \quad (24)$$

The next step is to decompose the integrand into two factors $A(\zeta)$ and $\exp[-if(\zeta)]$, as given by the first equation of (19), and to construct therefrom the saddle point equation (20).

The saddle points with which we are concerned, as will be seen immediately, have values which closely approximate the zeros of the modified Hankel function $h_1(z)$. Hence, we have to consider the saddle points by groups in connection with the four functions involved in the integrand. Let us consider first the ones lying in the neighborhood of zeros of the function $w(s_g)$.

It is known that modified Hankel function $h_1(s)$ has an infinite number of zeros which, denoted by $s_0^{(n)}$, are given approximately by

[8] R. Courant and D. Hilbert, "Methoden der mathematischen Physik," 2nd ed., Springer, Berlin, Ger., vol. 1, p. 455 *et seq.*; 1931.
[9] H. Jeffreys and B. S. Jeffreys, "Methods of Mathematical Physics," 3rd ed., Cambridge Univ. Press, Cambridge, Eng., pp. 503–507; 1956.

$$s_0^{(n)} = |s_0^{(n)}| e^{-(2\pi/3)i},$$

$$|s_0^{(n)}| \simeq \left[\frac{3}{2}\left(n+\frac{3}{4}\right)\pi\right]^{2/3}, \quad (n = 0, 1, 2, \cdots). \quad (25)$$

If we confine ourselves to a small domain of s centered at one of these zeros, we see from (10) that $h_1(s)$ varies most rapidly in the vicinity of that point, the rate of change decreasing with increasing separation. This is the case also for the function $w(s_g)$, and hence, we may reasonably assume that the three other functions can be regarded nearly constant for a small variation of s within the domain in consideration.

Therefore, we put

$$\left.\begin{aligned} A(\zeta) &= \frac{2}{W} e^{(2\pi/3)i} h_1(s_1) h_1(s) w(s_g e^{-(2\pi/3)i}) \\ -if(\zeta) &= -\log w(s_g) \end{aligned}\right\}, \quad (26)$$

and make use of (8), giving the saddle point equation

$$w'(s_g)/w(s_g) = i\beta k_0 r. \quad (27)$$

Noting that $h_j(s)$ is an analytic function of s and that the right-hand side of (27) attains a large value at ranges beyond the horizon, we expect that the roots of this equation have values which closely approximate the zeros of the denominator $w(s_g)$ on the left.

It can be shown that zeros of $w(s_g)$ are approximately equal to those of $h_1(s)$. Therefore, expansion of $w(s_g)$ about the zeros $s_0^{(n)}$ leads to

$$s_g^{(n)} = s_0^{(n)} + i\frac{1}{\beta k_0 r}, \quad (28)$$

giving the roots of (27) that correspond to the $(n+1)$th zero $s_0^{(n)}$.

Since the zeros $s_0^{(n)}$ lie, in the s_g-plane, on the ray arg $s_0^{(n)} = -2\pi/3$, the saddle points $s_g^{(n)}$ given by (28) also lie on a semi-infinite straight line parallel to the ray. Therefore, together with the requirement that the path of integration goes from $-\infty$ to $+\infty$ along the real axis, the properties of $h_1(s_g)$ near zeros suggest that the contour of the steepest descent be so chosen as to pass the point $s_g^{(0)}(n=0)$ in the direction perpendicular to the semi-infinite line, as indicated by Γ_1 in Fig. 1. It is obvious that the contour makes, in the ζ-plane, an angle $\theta_2 = \pi/6$ with the real axis.

Thus, on using the value of the first saddle point $s_g^{(0)}$, the wave function, denoted by ψ_{s_1}, can be written by (21),

$$\psi_{s_1} = \frac{2}{W} e^{(5\pi/6)i}\left(\frac{\pi}{2}\right)^{1/2} k_0^2 H_0^{(1)}(k_0 r)\,|f''(\zeta^{(0)})|^{-1/2} \cdot \frac{w(s_g^{(0)} e^{-(2\pi/3)i})}{w(s_g^{(0)})} h_1(t_1^{(0)}) h_1(t^{(0)}) \exp\left[-i\beta k_0 r \cdot s_g^{(0)}\right]. \quad (29)$$

Here, we have replaced ζ by s_g in virtue of (8) and have introduced for brevity the symbols

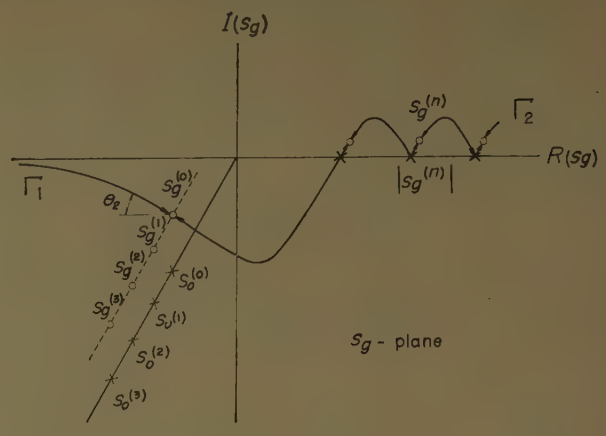

Fig. 1—Contours of integration Γ_1 for the integral ψ_{s_1} and Γ_2 for ψ_{s_2}. Arrows indicate the senses of increasing $R\{F(\zeta)\}$.

$$\left.\begin{aligned} t_1^{(0)} &= s_g^{(0)} + s_m + s_l \\ t^{(0)} &= s_g^{(0)} + s_l \end{aligned}\right\}, \quad (30)$$

$$\left.\begin{aligned} s_m &= \beta^{-1}\gamma(z_1 - z) = s_1 - s \\ s_l &= \beta^{-1}\gamma z = s - s_g \end{aligned}\right\}. \quad (31)$$

It is to be noted that, in deriving (29), the saddle point $s_g^{(0)}$ alone has been taken into account. The role of other saddle points lying on the continued part of the contour Γ_1 will be discussed in the next section.

Now, by (26) and (27),

$$f''(\zeta) = i\beta^{-2}[w(s_g)]^{-2}[w'^2(s_g) - w'(s_g)w(s_g)], \quad (32)$$

so that the relations

$$\left.\begin{aligned} w(s_g^{(0)}) &= h_1'(s_g^{(0)}) + \tau(s_g^{(0)}) h_1(s_g^{(0)})) \simeq 0 \\ w'(s_g^{(0)}) &\simeq h_1''(s_g^{(0)}) + \tau(s_g^{(0)}) h_1'(s_g^{(0)}) \\ &= \{\tau(s_g^{(0)}) + s_g^{(0)}/\tau(s_g^{(0)})\} h_1'(s_g^{(0)}) \end{aligned}\right\}, \quad (33)$$

yield

$$|f''(\zeta^{(0)})|^{-1/2}/w(s_g^{(0)}) = \beta/\tau(s_g^{(0)})[1 + s_g^{(0)}\{\tau(s_g^{(0)})\}^{-2}] h_1'(s_g^{(0)}). \quad (34)$$

The last equation in (33) is a direct consequence of the fact that $h_1(s_g^{(0)})$ satisfies a differential equation.

By (14), the second equation of (23) can be written

$$w(s_g e^{-(2\pi/3)}) = -e^{(2\pi/3)i} w(s_g) - e^{(\pi/3)i}[h_2'(s_g) + \tau(s_g) h_2(s_g)]. \quad (35)$$

Hence, use of the Wronskian of $h_1(s_g^{(0)})$ and $h_2(s_g^{(0)})$, expressed by (12) and (33) as

$$\begin{aligned} \beta\gamma^{-1} W &= h_1(s_g^{(0)}) h_2'(s_g^{(0)}) - h_1'(s_g^{(0)}) h_2(s_g^{(0)}) \\ &= -\{h_1'(s_g^{(0)})/\tau(s_g^{(0)})\} \cdot [h_2'(s_g^{(0)}) + \tau(s_g^{(0)}) h_2(s_g^{(0)})], \end{aligned} \quad (36)$$

leads readily to

$$w(s_g^{(0)} e^{-(2\pi/3)i}) = e^{(\pi/3)i}\beta\gamma^{-1} W \tau(s_g^{(0)})/h_1'(s_g^{(0)}). \quad (37)$$

Substitution of (34) and (37) into (29) gives ultimately

$$\psi_{s_1} = e^{(7\pi/6)i}(2k_0{}^2\gamma)^{1/3}\left(\frac{\pi}{2}\right)^{1/2} H_0{}^{(1)}(k_0 r) \cdot \frac{h_1(t_1{}^{(0)})h_1(t^{(0)})}{[1 + s_g{}^{(0)}\{\tau(s_g{}^{(0)})\}^{-2}]h_1{}'^2(s_g{}^{(0)})} e^{-i\beta k_0 r \cdot s_g{}^{(0)}}, \quad (38)$$

where $t_1{}^{(0)}$ and $t^{(0)}$, as defined by (30), are functions of altitudes of the transmitting and receiving antennas, respectively.

We see that (38) is identical with the first term of the residue series in classical diffraction theory. It should be noted that only its first term, in a very good approximation, gives the field strength at ranges near the horizon, the sum of the succeeding terms making little contribution to it in practical application.

It is obvious that (38), owing to the factor $\exp[-i\beta k_0 r \cdot S_g{}^{(0)}]$, represents the field strength which decreases exponentially with distance. This nature of exponential decay arises from the fact that the first term of the saddle point (28) has an imaginary part of appreciable magnitude. Hence, if any nearly real saddle point (with negligibly small imaginary part) exists, it will give rise to the field strength which decreases with distance at a considerably smaller rate. We shall see later that this is certainly enough to explain the strong field strength at ranges beyond the horizon.

IV. Wave Functions for Ranges Beyond the Horizon

We shall, in this section, be concerned with the saddle points whose imaginary part is very small compared with the real part.

Inspection of (24) suggests that it is important in this case to consider the function $w(s_g e^{-(2\pi/3)i})$ in the neighborhood of its zeros. Although $h_1(s_1)$ and $h_1(s)$ in (24) yield complex saddle points of the same form as in the preceding section, their contribution can be neglected because the associated wave functions give values of field strength negligibly small in comparison with that given by (38), as is obvious from the form of (24).

Upon putting

$$\left.\begin{aligned} A(\zeta) &= \frac{2}{W} e^{(2\pi/3)i} h_1(s_1)h_1(s)/w(s_g) \\ -if(\zeta) &= \log w(s_g e^{-(2\pi/3)i}) \end{aligned}\right\}, \quad (39)$$

we have the saddle point equation

$$e^{-(2\pi/3)i} w'(s_g e^{-(2\pi/3)i})/w(s_g e^{-(2\pi/3)i}) = i\beta k_0 r. \quad (40)$$

In the same manner as in the preceding section, it can be shown that zeros of $w(s_g e^{-(2\pi/3)i})$, in a first approximation, are equal to those of $h_1(s_g e^{-(2\pi/3)i})$. Hence, expansion of $w(s_g e^{-(2\pi/3)i})$ about $|s_0{}^{(n)}|e^{-(2\pi/3)i}$ yields at once the saddle points

$$s_g{}^{(n)} \doteq |s_0{}^{(n)}| + \frac{1}{\beta k_0 r} e^{(\pi/6)i}, \quad (41)$$

where $|s_0{}^{(n)}|$ represents the infinite number of real values given by the second formula in (25).

From (39) and (40), it follows that

$$|f''(\zeta^{(n)})|^{-1/2} w(s_g{}^{(n)} e^{-(2\pi/3)i}) \simeq e^{-(7\pi/6)i}\beta(\beta k_0 r)^{-2} w'(s_g{}^{(n)} e^{-(2\pi/3)i}), \quad (42)$$

whence, by (21),

$$\psi_{s_2} = \frac{2}{W}\left(\frac{\pi}{2}\right)^{1/2} H_0{}^{(1)}(k_0 r) e^{-(1\pi/3)i}(\beta r^2)^{-1} \exp[i\beta k_0 r \cdot s_l] \cdot \sum_{n=0}^{\infty} \frac{w'(s_g{}^{(n)} e^{-(2\pi/3)i})}{w(s_g{}^{(n)})} h_1(t^{(n)} + s_m)h_1(t^{(n)}) \cdot \exp[-i\beta k_0 r \cdot t^{(n)}], \quad (43)$$

where ψ_{s_2} denotes the wave function related to $v_s(s)$ in (15) and associated with the saddle points $s_g{}^{(n)}$ given by (41). Also, $t^{(n)}$ stands for

$$t^{(n)} = s_g{}^{(n)} + s_l. \quad (44)$$

The path of integration is so chosen that, as indicated by Γ_2 in Fig. 1, it is a continuation of Γ_1 and goes to $+\infty$ along the real axis on the right half of the s_g-plane passing all zeros $|s_0{}^{(n)}|$ and relevant saddle points $s_g{}^{(n)}$, the latter at an angle $\theta_2 = -\pi/6$ in the ζ-plane.

Saddle points of nearly real values can also be derived from the expression for $v_p(s)$ in (15). Denoting by ψ_p the wave function that corresponds to $v_p(s)$, we obtain from (15) and (18)

$$\psi_p = -\frac{k_0{}^2}{W} e^{(2\pi/3)i} H_0{}^{(1)}(k_0 r) \cdot \int_{-\infty}^{\infty} h_1(s_1)h_1(se^{-(2\pi/3)i}) e^{ik_0 r \cdot \zeta} d\zeta, \quad (45)$$

where integration is, as in the case of (24), performed almost along the real axis in the ζ-plane.

The same procedure as before leads readily to

$$\psi_p = -\frac{2}{W}\left(\frac{\pi}{2}\right)^{1/2} H_0{}^{(1)}(k_0 r) e^{-(\pi/3)i}(\beta r^2)^{-1} \exp[i\beta k_0 r \cdot s_l] \cdot \sum_{n=0}^{\infty} h_1(s^{(n)} + s_m)h_1{}'(s^{(n)} e^{-(2\pi/3)i}) \exp[-i\beta k_0 r \cdot s^{(n)}], \quad (46)$$

where $s^{(n)}$ are values of the saddle points given by

$$s^{(n)} = |s_0{}^{(n)}| + \frac{1}{\beta k_0 r} e^{(\pi/6)i}. \quad (47)$$

The path of integration, Γ_2, is chosen as shown in Fig. 2.

Comparison of (43) with (46) shows that they have resembled forms and comparable magnitudes. In addition, as is obvious from (15), we shall ultimately be interested in the difference of the series involved in these two equations. Therefore, it is convenient as the next step to formulate the difference in a form suitable for evaluation.

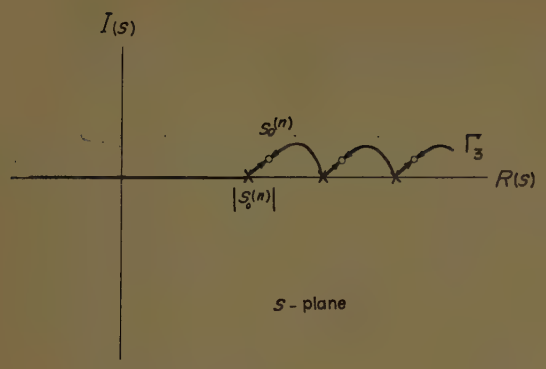

Fig. 2—Contour of integration Γ_3 for the integral ψ_p. Arrows indicate the senses of increasing $R\{F(\zeta)\}$.

On making use of the relation (23) and taking into account that $s_g^{(n)}$ have values very near to zeros of $w(s_g e^{-(2\pi/3)i})$, we obtain

$$\frac{w'(s_g^{(n)}e^{-(2\pi/3)i})}{w(s_g^{(n)})} = \frac{\tau(s_g^{(n)})}{\dfrac{h_1'(s_g^{(n)})}{h_1(s_g^{(n)})} + \tau(s_g^{(n)})} \frac{h_1'(s_g^{(n)}e^{-(2\pi/3)i})}{h_1(s_g^{(n)})}$$

$$= (1 + is_g^{(n)1/2}/\tau)^{-1} h_1'(s_g^{(n)}e^{-(2\pi/3)i})/h_1(s_g^{(n)}). \quad (48)$$

Here we have used asymptotic expansions of the modified Hankel functions and regarded τ, which stands for $\tau(s_g^{(n)})$, as independent of $s_g^{(n)}$ approximately.

Making use of (44), we write

$$\left.\begin{aligned} &h_1(t^{(n)} + s_m)h_1(t^{(n)})e^{-i\beta k_0 r\cdot t^{(n)}} \\ &\quad = h_1(s_g^{(n)} + s_m)h_1(s_g^{(n)})e^{-i\beta k_0 r\cdot s_g^{(n)}}\cdot L(s_g^{(n)}) \\ &L(s_g^{(n)}) = \frac{h_1(s_g^{(n)} + s_m + s_l)}{h_1(s_g^{(n)} + s_m)} \frac{h_1(s_g^{(n)} + s_l)}{h_1(s_g^{(n)})} e^{-i\beta k_0 r\cdot s_l} \end{aligned}\right\}, \quad (49)$$

and put

$$L(s_g^{(n)})(1 + is_g^{(n)1/2}/\tau)^{-1} \equiv 1 + M(s_g^{(n)}). \quad (50)$$

Then, it follows from (43) that

$$\psi_{s_2} = \frac{2}{W}\left(\frac{\pi}{2}\right)^{1/2} H_0^{(1)}(k_0 r) - \frac{\pi}{3} i(\beta r^2)^{-1} \exp[i\beta k_0 r\cdot s_l]$$
$$\cdot \sum_{n=0}^{\infty} [1 + M(s_g^{(n)})]h_1(s_g^{(n)} + s_m)h_1'(s_g^{(n)}e^{-(2\pi/3)i})$$
$$\cdot \exp[-i\beta k_0 r\cdot s_g^{(n)}]. \quad (51)$$

If we write $s^{(n)}$ for $s_g^{(n)}$, noting that the right-hand side of (41) is identical with that of (47), we obtain from (15), (46), and (51)

$$\psi_b = \psi_{s_2} + \psi_p$$
$$= \frac{2}{W}\left(\frac{\pi}{2}\right)^{1/2} H_0^{(1)}(k_0 r)e^{-(\pi/3)i}(\beta r^2)^{-1} \exp[i\beta k_0 r\cdot s_l]$$
$$\cdot \sum_{n=0}^{\infty} M(s^{(n)})h_1(s^{(n)} + s_m)h_1'(s^{(n)}e^{-(2\pi/3)i})$$
$$\cdot \exp[-i\beta k_0 r\cdot s^{(n)}]. \quad (52)$$

This is the expression for ψ_b, which represents the sum of the wave functions ψ_p and ψ_{s_2}, both associated with nearly real saddle points. Eq. (52) gives practically the wave function valid at ranges beyond the radio horizon.

It should be noted that these component functions have been derived from $v_p(s)$ and $v_s(s)$ in (15) which give, respectively, the direct and reflected waves in the case of propagation in the illuminated zone.

V. Summing the Infinite Series

The series involved in the expression for ψ_b is of very slow convergence, since the saddle points $s^{(n)}$ appearing in the exponent have the imaginary part of small magnitudes, as obvious from (47) and (25). To sum up the infinite series, we shall first transform it into an infinite integral and then make its approximate evaluation again by use of the saddle point method.

Following a procedure due to Watson,[1] the series on the right of (52) is transformed into the complex integral

$$\sum = -\frac{1}{2\pi i}$$
$$\cdot \int_L \frac{1}{\operatorname{tg}\nu\pi} M(s_\nu)h_1(s_\nu + s_m)h_1'(s_\nu e^{-(2\pi/3)i})e^{-iRs_\nu}d\nu, \quad (53)$$

where R stands for $\beta k_0 r$ for brevity. The contour L is so chosen that, as shown in Fig. 3, it starts at $\infty - i\epsilon$ in the ν-plane, goes below the real axis to $\nu = -\frac{1}{2}$, and then above the real axis to $\infty + i\epsilon$. It is evident that the integral is equivalent to the series now in consideration since $h_1(s_\nu)$, accordingly $M(s_\nu)$ too, are analytic functions of ν, the only singularities of the integrand being poles at those values of ν inside L for which $\operatorname{tg}\nu\pi \times 0$.

Since, by (25) and (47),

$$s_\nu = \left[\frac{3}{2}\left(\nu + \frac{3}{4}\right)\pi\right]^{2/3} + \frac{1}{R}e^{(\pi/6)i}, \quad (54)$$

(53) reduces, after a change of variables, to

$$\sum = \frac{i}{2\pi}\int_L \operatorname{ctg}\nu\pi$$
$$\cdot \left(s_\nu - \frac{1}{R}e^{(\pi/6)i}\right)^{1/2} M(s_\nu)h_1(s_\nu + s_m)h_1'(s_\nu e^{-(2\pi/3)i})$$
$$\cdot e^{-iRs_\nu}ds_\nu, \quad (55)$$

where $\nu\pi$ is the quantity expressible in terms of s_ν and L is the contour in the s_ν-plane as shown in Fig. 3.

The next step is to apply the saddle point method to evaluating the integral (55), in which most significant is the function $M(s_\nu)$ which, by (50), characterizes the sum of the wave functions ψ_{s_2} and ψ_p.

We put

$$k_0 F(s_\nu) = \log M(s_\nu) - iRs_\nu, \quad (56)$$

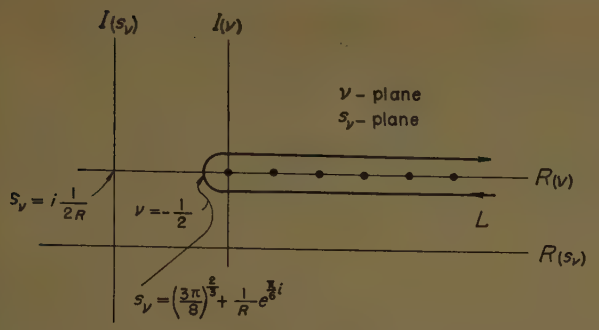

Fig. 3—Contour of integration for summing the infinite series.

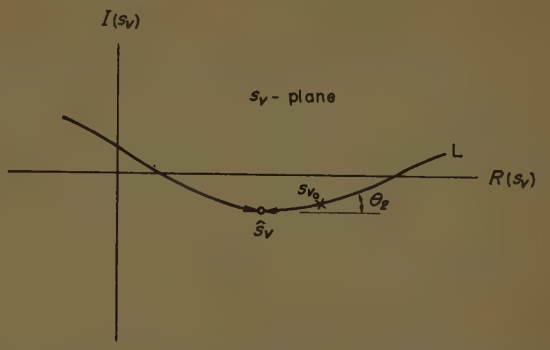

Fig. 4—Contour of integration L in the vicinity of the saddle point $\hat{s}_\nu$. Arrows indicate the senses of increasing $R\{F(s_\nu)\}$.

and construct the saddle point equation

$$M'(s_\nu)/M(s_\nu) = iR. \tag{57}$$

To obtain the saddle points, *i.e.*, the roots of this equation, we first apply (10) to (49) and expand the exponent in powers of s_ν. Then, assuming that $1 \gg s_l/|s_\nu|$, we obtain by (50)

$$M(s_\nu) = (1 + is_\nu^{1/2}/\tau)^{-1} \exp\left[is_l\left\{(s_\nu + s_m)^{1/2} + s_\nu^{1/2} - R\right\}\right.$$
$$\left. - \frac{s_l}{4}\left\{(s_\nu + s_m)^{-1} + s_\nu^{-1}\right\} + O(s_\nu^{-3/2})\right] - 1. \tag{58}$$

The saddle points, which are reasonably expected to have values near the zeros of $M(s_\nu)$, are given by

$$\hat{s}_\nu = \frac{(R^2 - s_m)^2}{4R^2} - \left(\frac{s_l}{2} + i\frac{2}{R}\right), \tag{59}$$

provided that

$$\left.\begin{aligned} |\tau| &\gg (R^2 + s_m)/2R^2 s_l \\ \left(1 - \frac{s_m}{R^2}\right)^2 &\gg (4/5R)^2 \end{aligned}\right\}. \tag{60}$$

The first of these conditions is an assumption that is plausible while the second is a direct consequence of neglecting the terms higher than the first in asymptotic expansions of the modified Hankel functions.

It is evident from (59) that the path of integration L makes, with the real axis, an angle

$$\theta_2 \doteq -\operatorname{arctg}(2/Rs_l) \simeq -\pi, \tag{61}$$

in the vicinity of the saddle point $\hat{s}_\nu$, as shown in Fig. 4.

From (21), (55), (58), and (61), it follows that

$$\sum = (2\pi)^{-1/2} \operatorname{tg}\left[\frac{2}{3}\left(\hat{s}_\nu - \frac{1}{R}e^{(\pi/6)i}\right)^{3/2} - \frac{\pi}{4}\right]$$
$$\cdot\left(\hat{s}_\nu - \frac{1}{R}e^{(\pi/6)i}\right)^{1/2}$$
$$\cdot R^{-2} M'(\hat{s}_\nu) h_1(\hat{s}_\nu + s_m) h_1'(\hat{s}_\nu e^{-(2\pi/3)i}) e^{-iR\hat{s}_\nu}, \tag{62}$$

whence, by (52),

$$r\psi_b e^{-ik_0 r} = e^{-(\pi/12)i}(2\sqrt{\pi}\alpha^2)^{-1}$$
$$\cdot \operatorname{tg}\left[\frac{2}{3}\left(\hat{s}_\nu - \frac{1}{R}e^{(\pi/6)i}\right)^{3/2} - \frac{\pi}{4}\right]\left(\hat{s}_\nu - \frac{1}{R}e^{(\pi/6)i}\right)^{1/2}$$
$$\cdot R^{-7/2} M'(\hat{s}_\nu) h_1(\hat{s}_\nu + s_m) h_1'(\hat{s}_\nu e^{-(2\pi/3)i}) e^{-iR(\hat{s}_\nu - s_l)}, \tag{63}$$

where the relation (12) and the asymptotic expansion of $H_0^{(1)}(k_0 r)$ have been used.

Now we take into account that, by (49) and (50),

$$M(\hat{s}_\nu) \simeq (1 + i\hat{s}_\nu^{1/2}/\tau)^{-1} L(\hat{s}_\nu)$$
$$\simeq i\frac{s_l}{2}(1 + i\hat{s}_\nu^{1/2}/\tau)^{-1}\hat{s}_\nu^{-1/2}\left[1 + \left(\frac{\hat{s}_\nu}{\hat{s}_\nu + s_m}\right)^{1/2}\right], \tag{64}$$

and make use of asymptotic expansions of the modified Hankel functions. Eq. (53) then reduces to

$$r\psi_b e^{-ik_0 r + i(4\pi/3)} = \frac{1}{4\sqrt{\pi}} s_l R^{-7/2}\left(\frac{\hat{s}_\nu}{\hat{s}_\nu + s_m}\right)^{1/4}$$
$$\cdot\left[1 + \left(\frac{\hat{s}_\nu}{\hat{s}_\nu + s_m}\right)^{1/2}\right]\sigma(\hat{s}_\nu) F(\hat{s}_\nu), \tag{65}$$

where

$$\left.\begin{aligned} \sigma(\hat{s}_\nu) &= \left\{1 - \exp i\left(\frac{\pi}{2} - \frac{4}{3}\hat{s}_\nu^{3/2}\right)\right\} \\ &\quad \cdot \operatorname{tg}\left[\frac{2}{3}\hat{s}_\nu^{3/2}\left(1 - \frac{1}{\hat{s}_\nu R}e^{(\pi/6)i}\right)^{3/2} - \frac{\pi}{4}\right] \\ F(\hat{s}_\nu) &= \left(1 - \frac{1}{\hat{s}_\nu R}e^{(\pi/6)i}\right)^{1/2}(1 + i\hat{s}_\nu^{1/2}/\tau)^{-1} \\ &\quad \cdot \exp i\left[\frac{2}{3}(\hat{s}_\nu + s_m)^{3/2} + \frac{2}{3}\hat{s}_\nu^{3/2} - R(\hat{s}_\nu - s_l)\right] \end{aligned}\right\}. \tag{66}$$

Eq. (65), together with (66), is the expression for the field strength relative to free space at ranges beyond the radio horizon.

Diffraction Theory of Tropospheric Propagation Near and Beyond the Radio Horizon*

Part II—Comparison with Experiments

O. TUKIZI†

I. Introduction

In the companion paper, Part I, theoretical derivations of two wave functions are given. One is identical in form with the first term of the residue series in classical diffraction theory so that it gives, as it should, the field strength which decreases exponentially with distance at ranges near the horizon. The other, it will be shown, manifests a remarkable feature of oscillation in time and distance, whereas its mean value decreases steadily with distance, in the region beyond the horizon, at a considerably slower rate than the former.

In the sections that follow, comparison of theory with experiments will be made of the variation of field strength with distance, its dependence on frequency, and characteristics of fading and height gain, to show that the theory can fairly account for experimental facts.

Discussions will be concerned, however, solely with expressions for ranges beyond the horizon, because the formula, valid at ranges near the horizon, is found identical with the result of Watson, van der Pol and Bremmer and others, which is well-known to be in good accord with experiments.

II. Summary of Theoretical Results

Theoretical results obtained in Part I can be rewritten in forms suitable for numerical computation as follows:

$$E_n = r\left|\psi_{s_1}\right| = \frac{1}{2\sqrt{2}} A(r) \exp\left\{1 + \phi(r)\right\}, \tag{1}$$

where

$$\left.\begin{aligned} A(r) &= (\beta k_0 r)^{1/2} \left|\bar{s}_0 + s_m + s_l + i\frac{1}{\beta k_0 r}\right|^{-1/4} \left|\bar{s}_0 + s_l + i\frac{1}{\beta k_0 r}\right|^{-1/4} \left|\bar{s}_0 + i\frac{1}{\beta k_0 r}\right|^{-1/2} \\ \phi(r) &= -\frac{2}{3} I\left\{\left(\bar{s}_0 + s_m + s_l + i\frac{1}{\beta k_0 r}\right)^{3/2} + \left(\bar{s}_0 + s_l + i\frac{1}{\beta k_0 r}\right)^{3/2} - \frac{3}{2}\beta k_0 r \cdot \bar{s}_0\right\} \end{aligned}\right\}, \tag{2}$$

and

$$E_b = r\left|\psi_b\right| = \frac{1}{\pi}\frac{z}{\gamma^2}\lambda^{1/2} r^{-7/2} \frac{\left(1 - \frac{2}{\gamma}\frac{z_1 - z}{r^2}\right)^{1/2}}{\left(1 + \frac{2}{\gamma}\frac{z_1 - z}{r^2}\right)^{3/2}} \left|\sigma(r)\right| \left|F(r)\right|, \qquad (z_1 \geqq z), \tag{3}$$

where

$$\left.\begin{aligned} \left|F(r)\right| &\simeq 1 \\ \left|\sigma(r)\right| &\simeq \left[1 - \operatorname{sech}\left(2 - \frac{4}{\gamma}\frac{z_1 - z}{r^2}\right) \sin\left\{\frac{\gamma^2 k_0 r^3}{12}\left(1 - \frac{2}{\gamma}\frac{z_1 - z}{r^2}\right)^3\right\}\right] \\ &\quad \cdot \left[1 + \operatorname{sech}\left(2 - \frac{4}{\gamma}\frac{z_1 - z}{r^2}\right) \sin\left\{\frac{\gamma^2 k_0 r^3}{12}\left(1 - \frac{2}{\gamma}\frac{z_1 - z}{r^2}\right)^3\right\}\right] \end{aligned}\right\}. \tag{4}$$

The symbols used in these expressions have the following meanings:

E_n, E_b: field strength relative to free space at ranges "near" and "beyond" the radio horizon, respectively.

k_0: propagation factor of the atmosphere at the surface of the earth.

r: plan distance between the transmitter and the receiver.

λ: wavelength.

γ: gradient with respect to height, approximately, of the modified index of refraction.

* Manuscript received by the PGAP, September 12, 1958.

† Electrical Commun. Lab., Musasino-si, Tokyo, Japan.

$\bar{s}_0$ denotes the first zero of the modified Hankel function $h_1(s)$ whose numerical value is

$$\bar{s}_0 = -1.1691 - i2.0249. \tag{5}$$

s_m and s_l are related to the heights z_1 and z ($z_1 \geqq z$) of the transmitting and receiving antennas, by

$$\left.\begin{aligned} s_m &= \gamma(z_1 - z)/\beta \\ s_l &= \gamma z/\beta \end{aligned}\right\}, \tag{6}$$

where

$$\beta = (\gamma/\sqrt{2}k_0)^{2/3}. \tag{7}$$

The symbol I in the expression for $\phi(r)$ means "the imaginary part of."

In deriving (1), we have used asymptotic expansions of $H_0^{(1)}(k_0 r)$ and of modified Hankel functions. Also we have confined ourselves, for simplicity, to the case of horizontal polarization, whereas the field strength beyond the horizon is almost independent of polarization.

Furthermore, (2) and (3) must be subject to the conditions

$$\{(\beta k_0 r)^2 - s_m\}^2 \gg 2s_l(\beta k_0 r)^2, \tag{8}$$

$$1 \gg 2(z_1 - z)/\gamma r^2, \tag{9}$$

which have been assumed for the sake of simplicity.

It can readily be shown that $|\sigma(r)|$ is an oscillating function of distance such that

$$\left.\begin{aligned} |\sigma(r)| &= 1, \\ &\text{if } \frac{\gamma^2 k_0 r^3}{12}\left(1 - \frac{2}{\gamma}\frac{z_1 - z}{r^2}\right)^3 = m\pi, \qquad (m = 0, 1, 2, \cdots) \\ |\sigma(r)| &= \left[1 + \operatorname{sech}\left(2 - \frac{4}{\gamma}\frac{z_1 - z}{r^2}\right)\right]\left[1 - \operatorname{sech}\left(2 - \frac{4}{\gamma}\frac{z_1 - z}{r^2}\right)\right]^{-1/2} \\ &\text{max., if } \frac{\gamma^2 k_0 r^3}{12}\left(1 - \frac{2}{\gamma}\frac{z_1 - z}{r^2}\right)^3 = 2\left(m + \frac{3}{4}\right)\pi \\ |\sigma(r)| &= \left[1 - \operatorname{sech}\left(2 - \frac{4}{\gamma}\frac{z_1 - z}{r^2}\right)\right]\left[1 + \operatorname{sech}\left(2 - \frac{4}{\gamma}\frac{z_1 - z}{r^2}\right)\right]^{-1/2} \\ &\text{min., if } \frac{\gamma^2 k_0 r^3}{12}\left(1 - \frac{2}{\gamma}\frac{z_1 - z}{r^2}\right)^3 = 2\left(m + \frac{1}{4}\right)\pi \end{aligned}\right\}. \tag{10}$$

Therefore, if $|\sigma(r)|$ is put equal to unity, (3) gives the mean field strength relative to free space at ranges beyond the horizon. It is a function of wavelength λ, altitudes of transmitting and receiving antennas z_1 and z, distance r and gradient γ of the modified index of refraction. But practically, it is almost independent of z_1 ($\geqq z$) unless the difference of antenna elevations is very large.

III. Decrease of Mean Field Strength with Distance

Figs. 1–3 show theoretical curves in comparison with median levels of the received field strength as a function of distance. Experimental results which Megaw[1] obtained in the North Sea using the frequency of 3000 mc have been reproduced in Fig. 1. Fig. 2 shows the measurement by Ames, Newman, and Rogers[2] carried out at 220 mc in the Northern Atlantic, and Fig. 3 the measurement at 400 mc reported by Chisholm, Morrow, Roche and Teachman.[3]

The curve extending from 70 to 600 km in Fig. 1 is the theoretical one[4] based on (3) assigning to γ the value of $2.49 \cdot 10^{-8}\,\mathrm{m}^{-1}$. The agreement with experiments appears satisfactory except in the "hump" region centered at about 300 km. Theoretical curves are also drawn in Figs. 2 and 3 by use of the value of γ indicated, showing fairly good agreements with measurements. The straight line ranging from 50 to 150 km in Fig. 2 has been drawn to show that (1) is valid in the region near the horizon.

In drawing the theoretical curves in Fig. 3, heights of transmitting and receiving antennas have arbitrarily been chosen as indicated in the illustration, since they are not found in the original paper by Chisholm and his collaborators. It will be of interest to note that the over-water data again manifest the "hump" at ranges between 300 and 450 km as occasionally as in Megaw's experiment (Fig. 1).

Mention should be made at this point of the fact that, in all three cases referred to, the gradient of refractive index takes on values much smaller than that for the

[1] E. C. S. Megaw, "The scattering of electromagnetic waves by atmospheric turbulence," *Nature*, vol. 166, pp. 1100–1104; December 30, 1950. See also "Waves and fluctuations," *Proc. IEE*, pt. III, vol. 100, pp. 1–8; January, 1953.

[2] L. A. Ames, P. Newman and T. F. Rogers, "VHF tropospheric overwater measurements far beyond the radio horizon," Proc. IRE, vol. 43, pp. 1369–1373; October, 1955.

[3] J. H. Chisholm, W. E. Morrow, J. F. Roche and A. E. Teachman, "Tropospheric path loss measurements at 400 mc/s over distances 25–830 miles," 1957 WESCON Convention Record, pt. 1, p. 115. Just after the submission of his manuscript, the author received H. E. Dinger, W. E. Garner, D. H. Hamilton, Jr. and A. E. Teachman, "Investigation of long-distance over-water tropospheric propagation at 400 mc," Proc. IRE, vol. 46, pp. 1401–1410; July, 1958. Their results of measurements (Fig. 7 on p. 1405) appear identical with those reproduced in Fig. 3 of the present paper.

[4] The author is indebted to M. A. Johnson, Admiralty Signal and Radar Establishment, Portsmouth, Eng. for his kind information on experimental data including the heights of transmitting and receiving antennas.

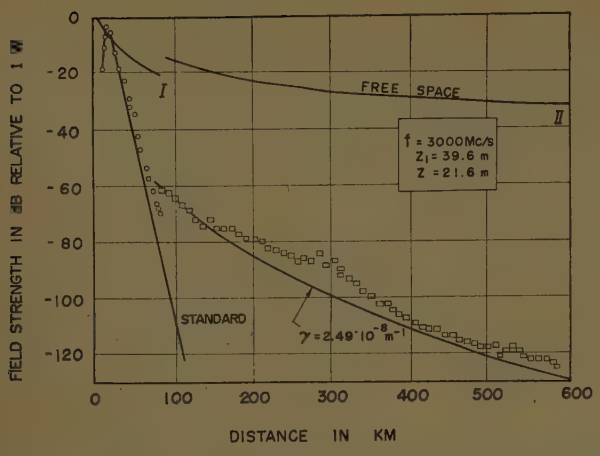

Fig. 1—Variation of mean field strength with distance (Megaw[1]). The break at 80 km is due to an experimental change.

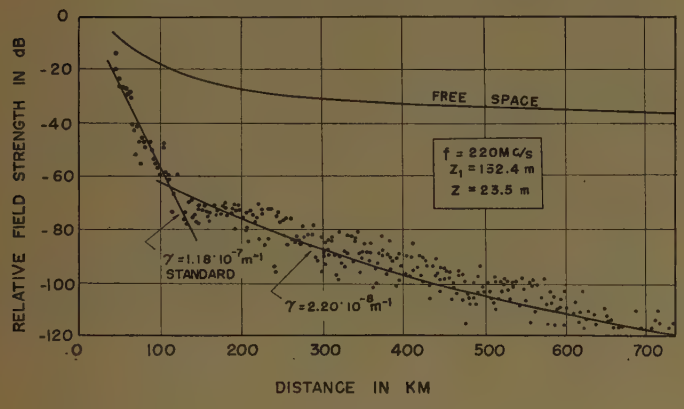

Fig. 2—Variation of mean field strength with distance (Ames, Newman and Rogers[2]).

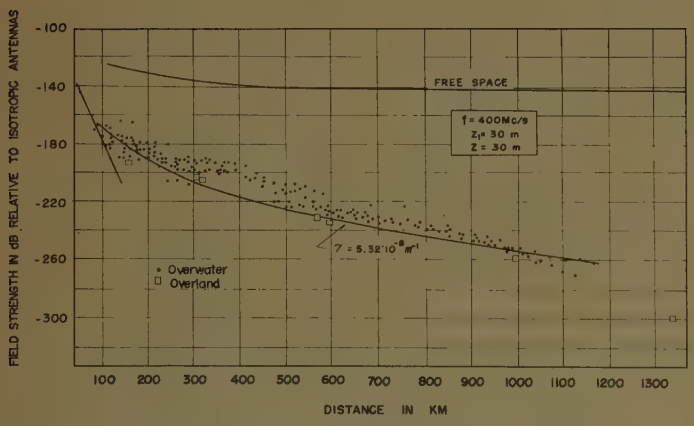

Fig. 3—Variation of mean field strength with distance (Chisholm, Morrow, Roche and Teachman[3]).

standard atmosphere ($\gamma_0 = 1.18 \cdot 10^{-7}$ m^{-1}). This trend, conspicuous for the propagation over the sea rather than over the land, can be explained as follows.

The mode of diffraction by the curvature of a smooth earth implies that radio waves are propagated along the earth's surface, the path being as illustrated schematically in Fig. 4. Elevations of the transmitter T and the receiver R are denoted by z_1 and z_2, and their radio horizons by H_1 and H_2, respectively. The gradients γ_0; $(i=1, 2)$ of refractive index which are effective for propagation within the regions TH_1 and RH_2 will be some mean values taken over height intervals from $z=0$ to z_1 and to z_2; in the region H_1H_2, the gradient γ' of refractive index near the surface of the earth plays an important role.

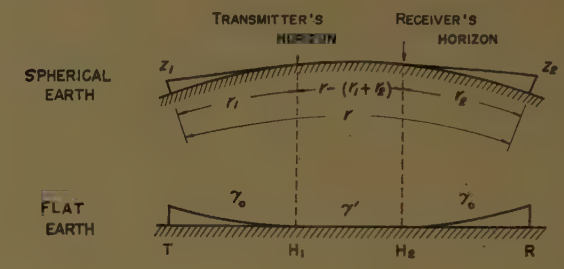

Fig. 4—Illustrating the contribution of γ' near the surface of the earth.

Now it is legitimate to assume that the contribution of γ' to propagation is proportional to the distance between H_1 and H_2. Then, the effective gradient of refractive index which will be denoted by $\gamma(z, r)$ can be written

$$\gamma(z, r) = \gamma' + (\gamma_0 - \gamma')(r_1^2 + r_2^2)/r,$$
$$r_i = (2z_i/\gamma_0)^{1/2}, \qquad (i = (1, 2), \qquad (11)$$

where r_i represents distances of radio horizons from both terminals and γ_0 the standard gradient substituted, for simplicity, for the mean values within these regions. Eq. (11) shows that, at ranges beyond the horizon where $r \gg r_1 + r_2$, the effective gradient $\gamma(z, r)$ has a considerably small value compared with γ_0 if γ' is appreciably small, which is usually the case in an atmosphere of super-standard type.

In this case of such an atmosphere, the present theory is, of course, not strictly valid, because it is based on the assumption of a linear M-profile. But, if the actual M-profile is not much deformed from a linear one, it will be permissible, to a first approximation, to take an appropriate mean value of $\gamma(z, r)$ which may be regarded as representative of the values at points around the path of propagation.

Values of γ' estimated from (11) for three examples given above are found to be all of the order of 10^{-8} m^{-1}. While little is known of the gradient γ' of refractive index near the earth's surface, it appears certain: 1) that the modified-index profile over sea water takes in large probability a form of super-standard type[5] where

[5] "Report of Factual Data from the Canterbury Project, A Radio-Meteorological Investigation in the South Island of New Zealand," Dept. Sci. Indust. Res., New Zealand, vols. I, II and III; 1951.

$\gamma' < 0$, and 2) that, also of the atmosphere over the land, values of γ' are very often smaller than the standard value γ_0 if an atmosphere below the heights of several ten meters is concerned. In other words, it will be legitimate to assume that $\gamma' < \gamma_0$, and accordingly, the average gradient γ is smaller in general than the standard value.

Also, the average gradient of refractive index is presumably smaller over the water than over the land, and this, together with (3), implies that overwater propagation usually gives a higher field-strength level compared with the propagation over the land. It appears that, though not yet corroborated, this is in a qualitative agreement with exerimental trends well known.

IV. Interference Pattern

Let us consider next the expression for $|\sigma(r)|$ which is an oscillating function of r as already mentioned. Because (3) involves, on the right, the term $|\sigma(r)|$, the field strength at ranges beyond the horizon is oscillatory in distance, even when the atmospheric condition, and hence γ, is constant throughout the space of propagation. Its period is a function of frequency, antenna heights and gradient of refractive index as in the case of the propagation within the horizon.

This property is a direct consequence of the fact that, at ranges beyond the horizon, there exist two wave functions of comparable magnitudes, as shown in Part I, corresponding respectively to the direct and reflected waves in the illuminated zone. It is of interest to note that the field strength beyond the horizon is characterized by such a property of interference contrasted to the well-known nature of the exponential decay at ranges near the horizon.

In Fig. 5 are reproduced records of the field-strength variation with distance observed by Ames, Newman and Rogers[2] in an aircraft flying through the regions within, near, and beyond the radio horizon in the direction of leaving the transmitting site. In each section of chart, the relative amplitude and time scale are reported to be the same; each large vertical division represents a field-strength variation of about 3 db and the total time in each case is about 2 to 3 minutes.

Fig. 5(a) is a portion of the chart representative of the field-strength variation within the horizon in which the large lobe structure is readily apparent with the usual scintillation type of fading superimposed upon it. Fig. 5(b) is a sample of the field strength near the horizon, showing the remarkable feature of exponential decay with the fading essentially disappeared. It demonstrates that the field strength in this region can be expressed by a single wave function, as shown in Part I. Fig. 5(c), recorded on a flight through the region beyond the horizon, manifests the field-strength variation of entirely different type. It is characterized by the intense variations which take place at a much faster rate compared with the interference pattern on the record [Fig. 5(a)].

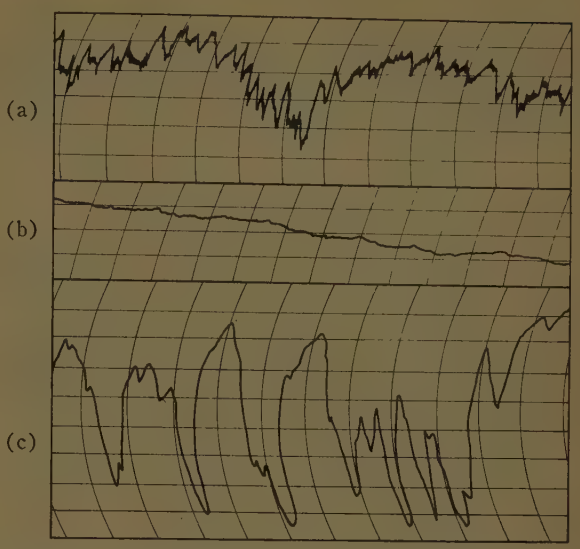

Fig. 5—Observed field-strength variation with distance at ranges (a) within, (b) near, and (c) beyond the horizon (Ames, Newman and Rogers[2]).

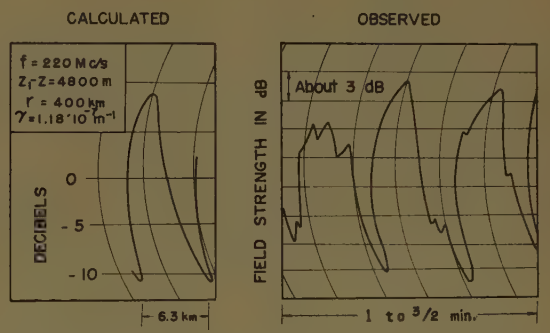

Fig. 6—Interference pattern at ranges beyond the horizon. Left, calculated $|\sigma(r)|$; right, portion of Fig. 5(c) reproduced for comparison.

To show what the theory predicts of this feature, the field-strength variation with distance calculated from (4) is drawn on the left of Fig. 6, the illustration to the right being a portion of Fig. 5(c) reproduced for comparison. On calculation, numerical values other than that of frequency have arbitrarily been chosen as indicated in the illustration, since they are not specified in the original paper by Ames and his collaborators. Also, the gradient of refractive index has been assumed constant of distance and time during one cycle of the oscillation of $|\sigma(r)|$. Fig. 6 shows that the theoretical interference pattern, its shape at least, is in a fair agreement with the observed one.

Of actual atmosphere, however, γ varies more or less with distance and time, the variation being superimposed upon that of $|\sigma(r)|$. The interference pattern on actual records will, therefore, be of less regular shape and shorter period compared with the calculated curve

and this accounts plausibly for the distortion apparent in the observed pattern of Fig. 5(c), particularly in its right-half portion where the lobe structure is considerably deformed from the theoretical curve.

V. Frequency Dependence and Rate of Fading

Eq. (3) states that the field strength relative to free space is proportional to the square root of wavelength. The relation appears to hold good as seen in Fig. 7, in which values of the observed field strength are plotted against wavelength to compare with the theoretical straight line drawn according to (3) with the value of γ of $7.73 \cdot 10^{-8}$ m^{-1}. The points of observation are the median values based on data of a short-term measurement conducted by the Electrical Communication Laboratory[6] on the path between Tokyo and the Isle of Hatizyo.

Next we shall consider the rate of change of the field strength at ranges beyond the horizon. Although the field strength relative to free space is inversely proportional to γ^4, as (3) shows, we confine ourselves for a while to its variation due to the time-change of the term $|\sigma(r)|$. This approximation is justified if the variation of γ^2 with time is sufficiently small compared with that of $|\sigma(r)|$, as will later be found to be the case.

From (10), the rate of fading, which is defined by the number of times that the decreasing field strength crosses the mean level, can be written

$$\frac{\partial m}{\partial t} = \frac{fr^3}{6c}\left(1 - \frac{2}{\gamma}\,\frac{z_1 - z}{r^2}\right)^2\left(1 + \frac{1}{\gamma}\,\frac{z_1 - z}{r^2}\right)\frac{\partial}{\partial t}\gamma^2, \quad (12)$$

where f denotes the frequency and c the light velocity *in vacuo*. The rate of fading is found to be proportional to frequency, cube of distance and rate of change of γ^2, if the difference of heights of transmitting and receiving antennas is small at a sufficiently large distance. It is well-known that the rate of fading is likely to increase as the interterminal distance is increased and to have a characteristic of diurnal variation, although their quantitative relations have not yet been established.

Fig. 8 shows a relation between frequency and rate of fading based on data of the experiment stated in the preceding section. The straight line is the theoretical one calculated from (12) while the points of observation have been taken from the chart on which the received field strength was recorded at a rapid speed of 240 mm/min. The rate of fading appears to be proportional to frequency though there remains a slight uncertainty that arises from lack of measurements in the frequency range between 250 and 900 mc.

The rate of change, $\partial\gamma^2/\partial t$, appropriate to this case is estimated to be of $5.05 \cdot 10^{-7}$ m^{-2} sec^{-1}, corresponding

[6] H. Fujimura, "Field strength and fading period of TV waves observed on an overwater beyond-the-horizon path," Electrical Commun. Lab., Japan, Rept. No. 1047; August, 1957 (in Japanese).

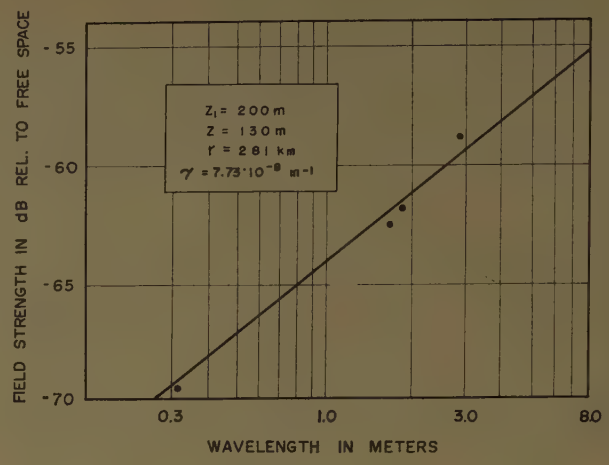

Fig. 7—Dependence of field strength on wavelength. Straight line shows the theoretical relation (3).

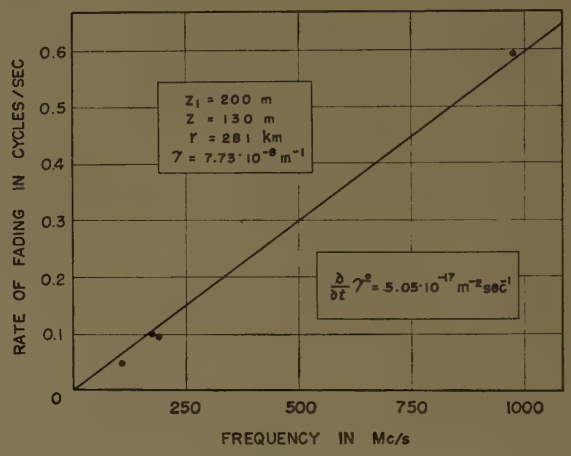

Fig. 8—Dependence of fading rate on frequency. Straight line shows the theoretical relation (12).

to the relative rate $(\partial\gamma/\partial t)/\gamma$ of about 4 per cent per second. These values, not yet found experimentally, are plausible in the order of magnitude at least. Also, the variation in the mean level of field strength is seen to be of negligible order of magnitude compared with the rate of change in γ just derived, and this justifies the approximation which we have made at the beginning of this section.

VI. Height Gain

We shall next consider the mean level of field strength as a function of the height of receiving antenna, keeping frequency, height of transmitting antenna, and interterminal distance fixed.

Eq. (3) shows that the field strength is proportional to the height of observation z, provided that the difference of antenna elevations $z_1 - z$ is not so large. It should be noted, however, that this is the case only for the receiver height smaller than the fixed height of transmitter, the field strength being constant at and above that

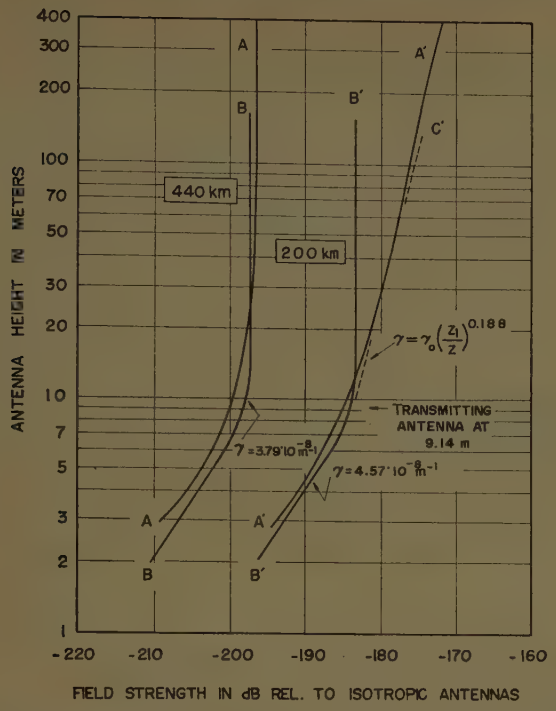

Fig. 9—Height-gain curves at 100 mc. for distances of 440 and 200 km. A, A′: empirical curves by the F.C.C. B, B′: theoretical curves with values of $\gamma=3.79\cdot10^{-8}$ m^{-1} and $4.57\cdot10^{-8}$ m^{-1}, respectively. C′: with γ assumed to decrease with height as $z^{-0.188}$

level. It is so because (3) has been derived for z not larger than z_1 so that, if $z_1<z$, it should be used with z and z_1 interchanged.

Fig. 9 gives for comparison with the theoretical prediction the "empirical height-gain curves," presented by the Federal Communications Commission[7] to the Plenary Assembly of the CCIR, held in London in 1953. Curves A and A′, deduced from a large number of overland propagation measurements which cover frequencies of 90 to 110 mc and distances up to 1011 km, are given as of the empirical height gain for the frequency of 100 mc and for the distances of 440 and 200 km, respectively.

[7] Federal Communications Commission, "Document 201," 7th Plenary Assembly, CCIR, London, Eng.: September, 1953.

Curves B and B′ are the theoretical curves drawn on the basis of (3) with values of γ of $3.79\cdot10^{-8}$ m^{-1} and $4.57\cdot10^{-8}$ m^{-1} respectively. The field strength relative to the strength of radiation is taken as abscissa, by virtue of the relation

$$(E_r/E_t)_{\text{free space}}=\lambda/4\pi r, \qquad (13)$$

which gives the relative field strength in free space for isotropic antennas.

Theoretical prediction appears to be in good accord with experiment on the 440-km path while, on the 200-km path, the observed field strength increases monotonously with height at elevations greater than that of the transmitting antenna (9.14 m). The discrepancy may be accounted for by the possibility that the gradient of refractive index decreases with height instead of being constant, *i.e.*, the profile of the modified index is concave upward in a certain height interval above the transmitter's level. The dotted curve C′ in Fig. 9 shows how the height-gain curve is modified if γ decreases with height, for example, as

$$\gamma=\gamma_0(z_1/z)^{0.188}. \qquad (14)$$

The gradient of γ with respect to height is often observed to be negative, in particular, over the land, so that the value of the exponent of 0.188 may be of very plausible order of magnitude for an actual atmosphere.

Eq. (3) is not strictly valid if γ depends on height, since the theory is based on the assumption of a linear profile of modified index. In a sense of approximation, however, it will be permissible to introduce the gradient $\gamma(z)$ as a slowly-varying function of z if the rate of decrease of $\gamma(z)$ is so small that the profile in question does not appreciably deviate from a linear one.

Acknowledgment

The author wishes to express his indebtedness to Prof. K. Maeda who read the manuscript and gave helpful comments and suggestions. Thanks are also due Dr. F. Ikegami, H. Fujimura, T. Nomura, S. Ugai and Dr. T. Fukami for their valuable discussions and comments.

communications

A Note on Surface Waves Along Corrugated Structures*

L. O. GOLDSTONE† AND A. A. OLINER†

THE recent paper by Hougardy and Hansen,[1] which is concerned with an obliquely propagating surface wave guided by a plane corrugated surface, has prompted the writing of this note in which we would like first to present an alternative approach to the solution of problems of this type and second to point out a certain general property of uniform structures, such as that analyzed by Hougardy and Hansen.

Although this alternative approach is not new, the extent of its applicability is not generally appreciated. This approach is based on a microwave network representation of the structure and employs the transverse resonance method for the determination of the propagation characteristics of the structure. The use of microwave network methods exploits the decomposition of an over-all problem into two essentially independent parts. One of these parts consists of obtaining the transverse network representation of the structure, for which the solution of a discontinuity problem is usually required. However, in many cases the solution of the relevant discontinuity problem is already known, and the network representation can be obtained immediately with very little effort. Such is the case for the corrugated structure under consideration.[1] The second part consists of the application of the transverse resonance procedure to determine the propagation characteristics. This second part is a relatively simple network calculation and involves no field considerations. It should be recognized, of course, that this procedure does not yield the detailed microscopic nature of the fields in the vicinity of the edges of the corrugations, but it does solve for all of the macroscopic properties, such as the propagation characteristics and the fields not near to the corrugation edges. For many applications, only these macroscopic quantities are of practical interest. In contrast, the field approach taken by Hougardy and Hansen, while being far more involved, does yield the complete solution, including the field everywhere.

The general property of uniform structures referred to above is that, in all such structures, the propagation characteristics for oblique propagation can be obtained directly from the special two-dimensional case of perpendicular propagation by a simple wavenumber transformation. This property may be exploited in either of two ways. Either the constituent portions of the network representation for the two-dimensional case may be appropriately modified to yield the results for oblique propagation directly, or the problem may be solved completely for the two-dimensional case, and these results can then be modified by the simple transformation referred to above.

We have utilized this point of view in the analyses of a number of leaky wave antennas,[2] and have presented

* Manuscript received by the PGAP, December 12, 1958.
† Polytechnic Inst. of Brooklyn, Brooklyn, N. Y.

[1] R. W. Hougardy and R. C. Hansen, "Scanning surface wave antennas—Oblique surface waves over a corrugated conductor," IRE TRANS. ON ANTENNAS AND PROPAGATION, vol. AP-6, pp. 370–376; October, 1958.

[2] L. O. Goldstone and A. A. Oliner, "Leaky Wave Antennas. I: Rectangular Waveguides," Rep. R-606-57, PIB-534, Microwave Res. Inst.; Polytech. Inst. of Brooklyn; August, 1957.

the rigorous justification for this transformation in that context. The application of this transformation to the determination of equivalent circuits for certain discontinuities subject to obliquely incident waves has also been described in detail.[3]

Hougardy and Hansen consider the problem of propagation at an oblique angle along a corrugated surface of the type shown in Fig. 1. In the discussion below we shall employ the same notation as that used in their paper. As these authors point out, the case of propagation normal to the corrugations has been treated by various individuals, including Hurd[4] who obtained a rigorous solution and whose development they parallel. It might also be added that it was recognized prior to Hurd's paper that a rigorous solution for the propagation characteristics could be obtained via the transverse resonance technique.[5]

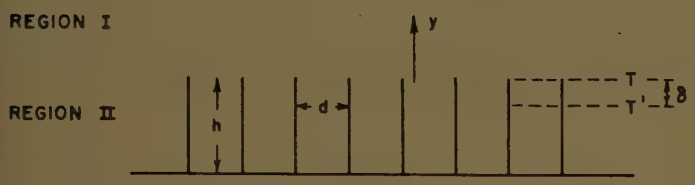

Fig. 1—Infinite corrugated plane surface.

We illustrate the two principles discussed above by applying them separately below. First, the simplicity and directness of the transverse resonance approach is illustrated by its application to the case considered by Hurd,[4] that of propagation normal to the corrugations. The simple wavenumber transformation necessary to obtain the result for oblique incidence is then indicated.

The infinite corrugated plane surface of Fig. 1, when viewed in the transverse (y) direction, is seen to correspond directly to the transverse equivalent network of Fig. 2(a). The upper and lower transmission lines correspond to regions I and II, respectively. Since a particularly simple representation for the junction discontinuity between these two lines is available,[6] the transverse network can be reduced to the simplified form shown in Fig. 2(b), in which the transmission lines meet at a displaced reference plane T' rather than at the physical junction plane T. The wavenumber k for the lower transmission line corresponds to the fact that the TEM mode is the only mode propagating in the region of the plates.

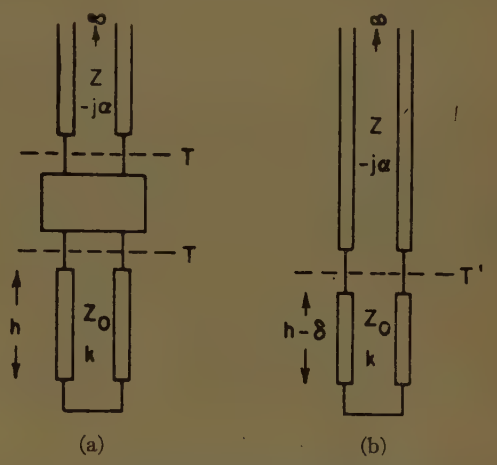

Fig. 2—Transverse equivalent networks for corrugated plane surface.

Application of the resonance relation

$$\overleftarrow{Z}(T') + \overrightarrow{Z}(T') = 0, \tag{1}$$

where the impedances are taken looking in opposite directions from the reference plane T', which is displaced a distance δ from T, immediately yields

$$jZ_0 \tan k(h - \delta) + Z = 0. \tag{2}$$

The input impedance Z of the upper line, of infinite length, is its characteristic impedance which takes the form

$$Z = \frac{\kappa}{\omega\epsilon}, \tag{3}$$

since the mode under consideration is an E (or TM) mode. Satisfaction of (2) to yield a modal solution then requires that the upper transmission line be below cutoff, so that

$$Z = \frac{-j\alpha}{\omega\epsilon}, \tag{4}$$

in agreement with the well-known physical properties of region I. Writing the characteristic impedance Z_0 of the TEM mode as $k/\omega\epsilon$, (2) becomes

$$\tan k(h - \delta) = \frac{\alpha}{k}. \tag{5}$$

However, since α is related to the propagation wavenumber β_0 of the surface wave by

$$\left(\frac{\alpha}{k}\right)^2 = \left(\frac{\beta_0}{k}\right)^2 - 1, \tag{6}$$

[3] H. M. Altschuler and L. O. Goldstone, "On network representations of certain obstacles in waveguide regions," IRE TRANS. ON MICROWAVE THEORY AND TECHNIQUES, vol. 7, pp. 213–221; April, 1959.

[4] R. A. Hurd, "The propagation of an electromagnetic wave along an infinite corrugated surface," *Can. J. Phys.*, vol. 32, pp. 727–734; December, 1954.

[5] See remarks by A. A. Oliner in "Round Table Discussion on Mode and Field Problems in Non-Conventional Waveguides," Prod. Symp. on Modern Advances in Microwave Techniques, Polytech. Inst. of Brooklyn, N. Y., p. 489; November, 1954.

[6] N. Marcuvitz, "Waveguide Handbook," Rad. Lab. Series, vol. 10, McGraw-Hill Book Co., Inc., New York, N. Y., sect. 5.22; 1951.

(5) becomes

$$\cos k(h-\delta) = \frac{k}{\beta_0}, \tag{7}$$

or

$$kh = \cos^{-1}\frac{k}{k_0} + k\delta. \tag{8}$$

The value of the reference plane shift δ is given explicitly as (3a) in Marcuvitz.[7] When the appropriate change in notation are made; *i.e.*,

$$d = \delta$$
$$k \sin\theta = \beta_0, \tag{9}$$

and when it is recognized that [see (5) of Hurd[4]]

$$\beta_n = \beta_0 + 2\pi n d/d, \qquad n = 0, \pm 1, \pm 2, \cdots, \tag{10}$$

the substitution of the resulting expression for δ into (8) yields exactly the rigorous result (28) of Hurd's paper.

The solution for the case of propagation at an oblique angle (the problem considered by Hougardy and Hansen) becomes only a simple extension of the perpendicular propagation case if the proper viewpoint is taken. If τ represents the wavenumber characterizing the variation along the corrugations, then the solution for oblique propagation is obtainable from that for perpendicular propagation by the replacement of wavenumber k by wavenumber $\sqrt{k^2-\tau^2}=\gamma_0$, wherever the former appears. Comparison between Hurd's result (28) and result (22) of Hougardy and Hansen indicates that they differ indeed only in the replacement of k by γ_0. (An evident typographical error appears in (22); symbol n should be π.) The justification for this wavenumber transformation follows from the recognition that the surface wave mode associated with oblique propagation is best characterized as an H-type mode; *i.e.*, in terms of the absence of a component of electric field along the corrugations. The validity of this wavenumber transformation in general terms has been previously given.[2]

[7] *Ibid.*, p. 289.

Comments on "Scanning Surface Wave Antennas—Oblique Surface Waves Over a Corrugated Conductor"*

R. E. Collin†

In a recent paper above,[1] the solution for a surface wave propagating obliquely across a corrugated plane was given. This solution may be obtained at once from the special case treated by Hurd.[2] Let $g(x, y, k^2)$ be the scalar function giving rise to the fields for a surface wave propagating normally across the corrugations. The solution for a surface wave propagating obliquely across the corrugations is then

$$f(x, y, z, k^2) = e^{-j\tau z} g(x, y, k^2 - \tau^2). \tag{1}$$

The notation used here is the same as that in the paper by Hougardy and Hansen.[1] The argument leading to (1) is the same as that used to obtain the solution for an E plane bifurcated rectangular guide from the solution for a bifurcated parallel plate transmission line.[3]

Finally it should be noted that the solution given by Hurd is readily obtained from the classical solution to the parallel plate problem as given by Carlson and Heins.[4] By considering a single mode propagating from the parallel plate region into the free space region, one finds that the reflection coefficient R at the interface is given by

$$R = -\frac{\gamma_0 + j\alpha_0}{\gamma_0 - j\alpha_0} e^{j\phi} \tag{2a}$$

where

$$\phi = \frac{2\gamma_0 d \ln 2}{\pi} + 2\sum_{n=1}^{\infty}\left\{\sin^{-1}\frac{\gamma_0 d}{n\pi} - \sin^{-1}\frac{\gamma_0}{\beta_n} - \sin^{-1}\frac{\gamma_0}{\beta_{-n}}\right\}. \tag{2b}$$

* Manuscript received by the PGAP, October 27, 1958.
† Elec. Engrg. Dept., Case Inst. Tech., Cleveland, Ohio.
[1] R. W. Hougardy and R. C. Hansen, "Scanning surface wave antennas—Oblique surface waves over a corrugated conductor," IRE Trans. on Antennas and Propagation, vol. AP-6, pp. 370–376; October, 1958.
[2] R. A. Hurd, "The propagation of an electromagnetic wave along an infinite corrugated surface," *Can. J. Phys.*, vol. 32, pp. 727–734; December, 1954.
[3] N. Marcuvitz, "Waveguide Handbook," McGraw-Hill Book Co., Inc., sect. 3.5; 1951.
[4] This solution is given in Hurd, *op. cit.*, sect. 5.22.

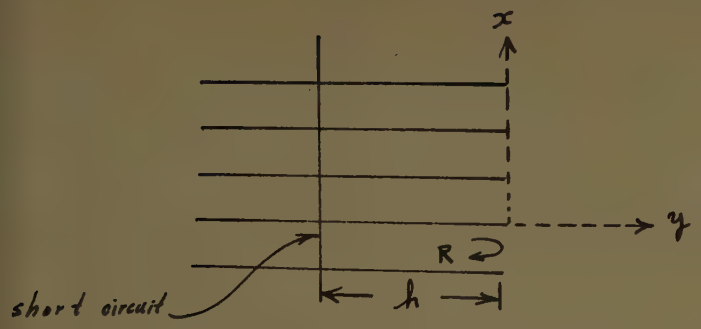

Fig. 1.

With reference to Fig. 1, it is apparent that when all evanescent modes excited at the interface are negligible at a distance h away, a short circuit may be placed at the point where the effective reflection coefficient $R' = e^{-2j\gamma_0 h} R$ equals minus one. Since the parallel plate medium is terminated in a pure capacitive susceptance, $|R| = 1$ and, hence, the short circuit position is given by the condition $< R' = \pi$. Substitution from (2a) and (2b) now yields the eigenvalue (23) given by Hougardy and Hansen.

Authors' Comments[5]

Dr. Collin is certainly correct in that our eigenvalue (23) could be obtained by a direct generalization of Hurd's work. However, to show that a solution can be found, one must first write a Maxwellian solution and then reduce this to the scalar problem. It is often easy to see, *ex post facto* how many steps in solving a problem can be omitted; in this case, we believe both the physical and mathematical understanding of the problem benefits from inclusion of the actual steps.

[5] Received by the PGAP, December 2, 1958.

The Filling in of an Antenna Null by Off-Path Scattering on a Tropospheric Scatter Circuit*

HAROLD STARAS†

Summary—**The concept and characteristics of Antenna-to-Medium Coupling loss have already been discussed in the literature in some detail. These earlier analyses show that the coupling loss is not significant unless the beamwidth of the antenna becomes equal to or less than the angular width of the scatter volume as seen from the antenna. An inverse phenomenon occurs if one tries to design an antenna null to protect a given location beyond the horizon; namely, if the width of the null is narrower than the angular width of the scatter volume, the null can be filled in by off-path scattering and the desired protection might not be achieved. This paper outlines the analysis used in evaluating the "filling in" of the antenna null by off-path scattering and presents curves which should prove useful in obtaining quantitative estimates.**

An examination of the interrelation between the scattering process and the free-space antenna pattern reveals that the scattering process averages the free-space antenna pattern, the averaging interval being of the order of several degrees. Thus a qualitative conclusion can be drawn that if it is desired to protect an installation with a 40 db null, this null must be maintained over at least several degrees in order to be effective. A cosine squared pattern is not satisfactory.

WITH the advent of high power transmitters in almost all parts of the radio frequency spectrum and with the installation of many different types of radio circuits all over the world, the problem of mutual interference is becoming very severe. Both theory and experience indicate that the radio signals many hundreds of miles away from a high power transmitter may be quite strong. An obvious method for reducing the interference at a particular installation from a high power transmitter over the horizon is to introduce a deep null in the transmitter's antenna pattern. It is the purpose of this paper to evaluate the effect of off-path tropospheric scattering on the free-space antenna null.

According to scatter theory, the received signal over the horizon is the sum of the scattered signals from all the elemental parts of the scatter volume. The contribution of each of the elemental parts of the scatter volume is determined by the product of the free-space antenna patterns and the scatter cross-section polar pattern. We begin our analysis with the same formulation used by the author in a previous paper.[1]

$$\langle P_s \rangle \sim \int_{H_0}^{\infty} \int_{-\infty}^{\infty} \frac{(h - H_0)(\vec{f_0} \cdot \vec{f})^2}{(x^2 + r^2 h^2)^2 (h - H_0/2)^2} \, d \times dh. \quad (1)$$

* Manuscript received by the PGAP, March 19, 1959.
† RCA Labs., Princeton, N. J.

[1] H. Staras, "Antenna-to-medium coupling loss," IRE TRANS. ON ANTENNAS AND PROPAGATION," vol. AP-5, pp. 228–231; April, 1957.

Where $\langle P_s \rangle$ is the average received scattered power measured relative to free space, $\sim$ means proportional to, $(\vec{f_0} \cdot \vec{f})^2$ represents the free-space antenna power patterns and r is the anisotropy parameter defined by

$$r = \frac{\text{scale of turbulence in the vertical dimension}}{\text{scale of turbulence in the horizontal dimension}} .$$

The other variables x, h, and H_0 refer to the coordinate system used and are best defined through Fig. 1, where a is the radius of a 4/3 earth and d is the distance between transmitter and receiver.

As previously pointed out[1] the integrand in (1) above is a non-negative real function and precise knowledge of the free-space antenna pattern or the scatter cross-section polar pattern is not essential in order to evaluate the magnitude of the scattered signal. With this philosophy in mind, we assume that the antenna patterns are broad in the vertical dimension and that in the horizontal dimension, the antenna pattern can be represented by the sketch in Fig. 2 in the vicinity of the null. In the sketch, the angle "0" represents the direction between the transmitter and the receiver, the angle ϕ represents the one-sided width of the depth of the null, while the angle ψ is a measure of the rate at which the antenna pattern rises from the null to the reference level. The reference level can be either the maximum of the antenna pattern or just a local maximum which is flat over a large angle (10°, say). With this assumption about the shape of the antenna pattern, it is not necessary that the antenna null pattern be symmetrical about zero.

With the above assumptions, the integral in (1) reduces to

$$\langle P_s \rangle \sim \int_0^D \frac{\epsilon dx}{(x^2 + H^2)^2} + \int_D^{D+(1-\epsilon)/b} \frac{(\epsilon - bD) + bx}{(x^2 + H^2)^2} dx + \int_{D+(1-\epsilon)/b}^{\infty} \frac{dx}{(x^2 + H^2)^2} . \quad (2)$$

In the above $D = d/2\phi$, $b = (d/2\psi)^{-1}$ and H is the parameter rh evaluated at the center of the scatter volume. It is straightforward, albeit tedious, to evaluate (2). The result, normalized to unity for an isotropic antenna, is given by

$$\langle P_s \rangle = \frac{2}{\pi}\left\{-\frac{p}{q}\left[\tan^{-1}(p+q) - \tan^{-1} p\right] + \pi/2 - \tan^{-1}(p+q)\right\} + \frac{2}{\pi}\epsilon\left[\tan^{-1}(p+q) + \frac{p+q}{1+(p+q)^2}\right] \quad (3)$$

where

$$p = \frac{D}{H} = \frac{\phi}{0.6r\theta_0} \cong 5\frac{\phi}{\theta_0}$$

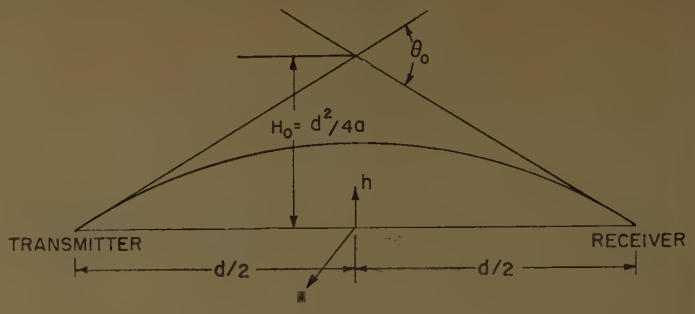

Fig. 1—Geometry of a tropospheric scatter circuit.

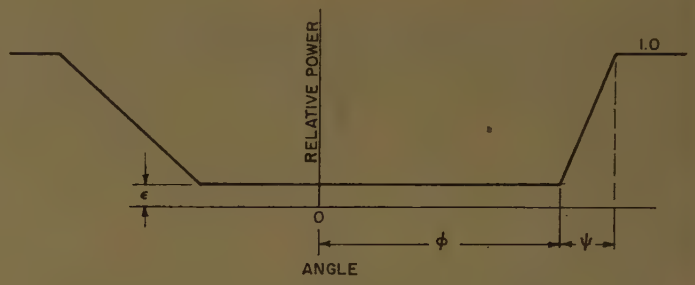

Fig. 2—Free-space antenna power pattern in vicinity of null.

and

$$q = \frac{1}{bH} = \frac{\psi}{0.6r\theta_0} \cong 5\frac{\psi}{\theta_0} .$$

The parameters p and q are normalized measures of the antenna pattern, p measures the one-sided width of the antenna null while q is a reciprocal measure of the rate at which the antenna pattern rises from the null to the reference level. In the expressions for p and q occur the anisotropy parameter associated with tropospheric scattering. For a more detailed discussion of this parameter, the reader is referred to earlier work of the author.[1,2] For the purposes of this paper it was assumed that the anisotropy parameter, $r \cong \frac{1}{3}$.

It is to be noted that the coefficient of ϵ on the right hand side of (3) is asymptotically unity for $(p+q) > 1$ and approaches zero linearly for $(p+q)$ approaching zero. Therefore, the second term in the right hand side of (3) is at most ϵ which, in turn, is much less than unity. The first term on the right hand side of (3) is plotted in Fig. 3. For completeness sake, it is mentioned that for $q = 0$ (*i.e.*, a square shaped null), the first term in (3) becomes

$$1 - 2/\pi(\tan^{-1} p + p/1 + p^2)$$

while for p greater than about 5 and $q \neq 0$, a useful asymptotic expression is

$$\frac{2}{\pi q}\left\{\frac{1}{3}\left[\frac{1}{p^2} - \frac{1}{(p+q)^2}\right] - \frac{1}{5}\left[\frac{1}{p^4} - \frac{1}{(p+q)^4}\right] + \cdots\right\} .$$

[2] H. Staras, "Forward scattering of radio waves by anisotropic turbulence," PROC. IRE, vol. 43, pp. 1364–1380; October, 1955.

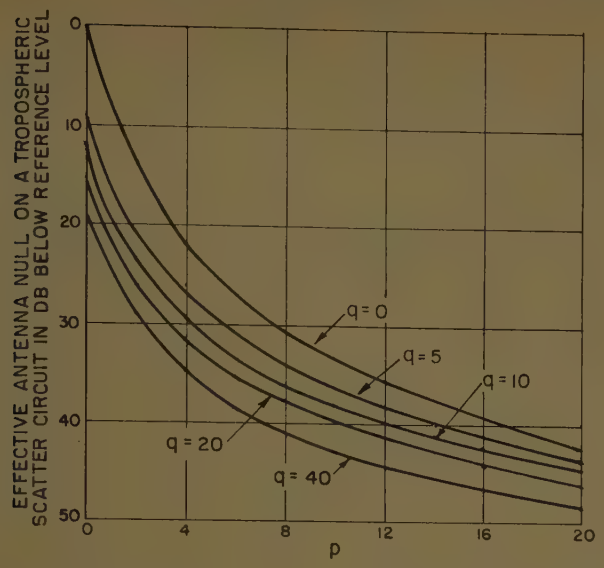

Fig. 3—Effective antenna null on a tropospheric scatter circuit.

From the curves, one general conclusion can immediately be drawn. A cosine pattern (which, when measured in db, rises very rapidly from a point null; *i.e.*, $p=0$) will not provide significant protection to a receiver installation even if the receiver is in the free space null of the transmitter antenna pattern. The following example should explain the use of Fig. 3. Consider an antenna null 40 db below the reference level which is 5° wide and which rises from the null to the reference level in 5°. Let us evaluate the effective antenna pattern at a receiver 200 miles away (*i.e.*, $\theta_0=2°$) located 1° from one end of the null and therefore 4° from the other end of the null. Assuming the anisotropy parameter $r=\frac{1}{3}$, $q=12.5$ while $p=2.5$ to one edge of the null and $p=10$ to the other edge of the null. From Fig. 3, we estimate that at the receiver the null is filled in to -25 db of the reference level due to the nearer edge of the null and to -39 db due to the other edge. Averaging these in power units yields 1.64×10^{-3} in relative power units. We next add 10^{-4} relative power units because of the free-space antenna pattern to obtain a resulting signal of 1.74×10^{-3} relative power units or only -27.6 db down. Thus the antenna null as measured at the receiver has been filled in by 12.4 db. It should be noted that if tropospheric scattering were isotropic, the filling in of the antenna null would be more pronounced because the parameters p and q would be reduced to $\frac{1}{3}$ their values assumed in this example.

An Investigation of the Complex Mutual Impedance between Short Helical Array Elements*

A. R. STRATOTI† AND E. J. WILKINSON†

IN electronically scanned arrays it is necessary to know the complex mutual impedance between array elements in order to compute the variation of array element terminal impedance with scanning angle. The short helix with its elliptically polarized radiation pattern is ideally suited for use as an array element in the UHF range when wide angle scanning is employed. It is the purpose of this paper to present the results of a series of measurements of the magnitude and phase angle of the mutual impedance between two turn helical elements as a function of array spacing. Specifically, the results show: 1) The coupling between helices is considerably smaller than between dipoles having the same center-to-center spacing (Fig. 1).[1] 2) The coupling can be reduced even further with only a negligible change in efficiency by inserting a resistor in series with the helix a quarter wavelength back from the open end (Fig. 1). This reduction in mutual results in a significant improvement in the axial ratio over the main beam of the helix when in an array environment. There is little or no change in the characteristics of the helix by itself. 3) The mutual impedance between a pair of helices surrounded by other helices forming an array is significantly different than for the same pair with all other helices in the array removed (Fig. 2). This is especially true when a helix is interposed between the coupled pair as in the case when mutual impedance between the

* Manuscript received by the PGAP, September 19, 1958; revised manuscript received, March 11, 1959.
† Sylvania Elec. Prods., Inc., Waltham, Mass.

[1] Figs. 1–4 were taken from the Master's thesis of the same title, by A. R. Stratoti at Northeastern University, Boston, Mass., January, 1958.

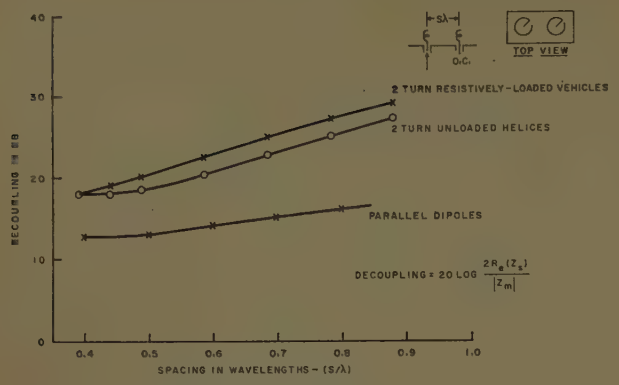

Fig. 1—Comparison of decoupling between helices and dipoles.

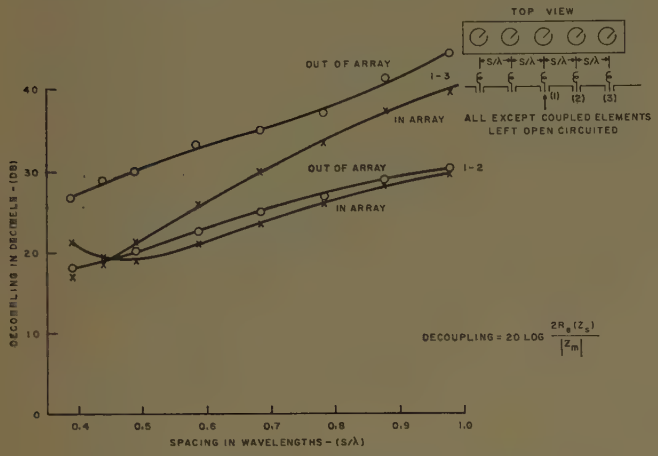

Fig. 2—Effect of array environment on decoupling between two-turn resistively loaded helices

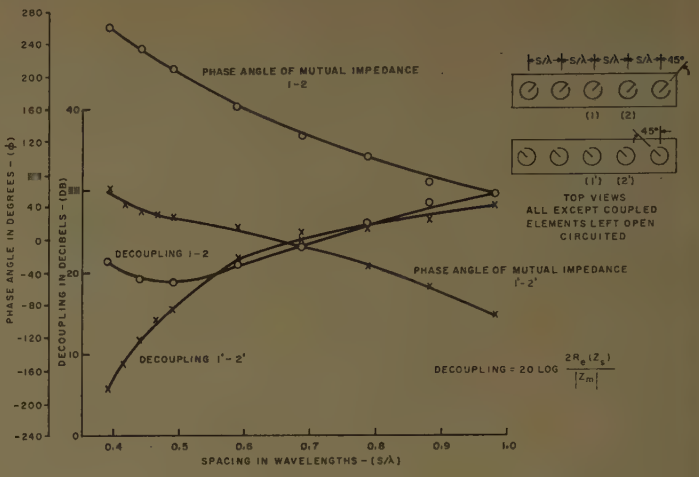

Fig. 3—Effect of rotational orientation on decoupling between two-turn resistively loaded helices in array environment.

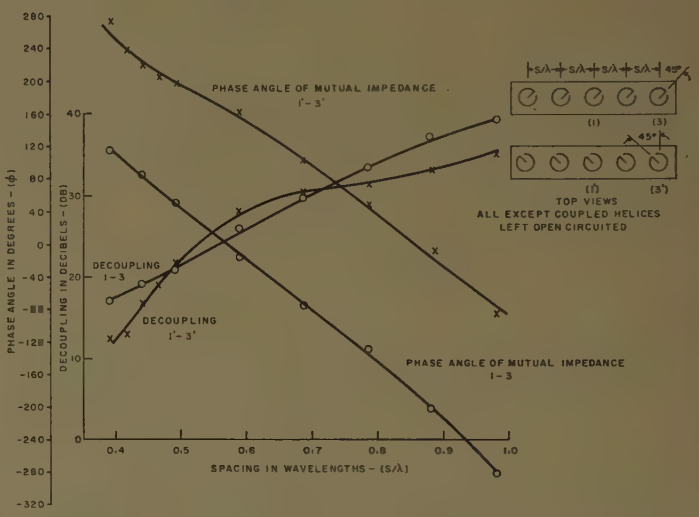

Fig. 4—Effect of rotational orientation on decoupling between two-turn resistively loaded helices in array environment.

n and $n+2$ elements in the array is desired, with the magnitude of the mutual between such nonadjacent elements actually approaching and even exceeding the mutual between adjacent elements for close array spacing. 4) A 90° rotation of the coupled helices about their axes results in an approximate 180° shift of the phase angle of the mutual impedance, much the same as for a similar rotation of collinear dipoles into side-by-side dipoles (Figs. 3 and 4). This dependence of the phase of the coupled signal on rotational orientation can result in widely different element patterns in the principal planes of a two dimensional array when the magnitude of the mutual is large as it is for close spacings. Alternatively, it can be used to broaden the element pattern in the plane of a one dimensional array when unusually wide angle scanning is employed.

The method used to obtain the complex mutual is also of interest, since it overcomes to a large extent the limitation of the open-circuit short-circuit method in regard to poor accuracy for small values of mutual. The method was first used by Moritz[2] and involves measuring the terminal impedance of the driven element and the ratio of the terminal voltage of the driven element to the open-circuit voltage of the coupled element, both quantities being easy to measure even for relatively small values of mutual. The paper describes the techniques and equipment used in making the above measurements.

[2] R. W. P. King, "Theory of Linear Antennas," Harvard University Press, Cambridge, Mass., p. 349; 1956.

Gains of Finite-Size Corner-Reflector Antennas*

E. F. HARRIS†

I WOULD like to point out an exception to the statement by H. C. Cottony and A. C. Wilson[1] in the first paragraph of their paper referring to the fact that there is no record of experimental measurement on corner-reflector antennas having values of aperture angle other than those obtained by dividing 180° by an integer.

Several years ago I performed a large number of experimental measured patterns on the corner-reflector configuration using reflector sheets 4 by 6 wavelengths,[2] which were practically the same as those described by Cottony and Wilson where they used reflectors 5 by 5 wavelengths. Previously,[2] I had shown data for various corner-angles including 40° and 120°, which, of course, are not the case of 180° divided by an integer. Due to the limited space available for publication in the IRE, much of the experimental data was not published, since my work[3] consisted of measurements every 10° in angle from 10° through 270° and *E*-plane and *H*-plane patterns from 1/10 through 3 wavelengths.

As an example, Cottony and Wilson mentioned data[4] that cannot be traced beyond 2.5 wavelengths on a 70° aperture; however, my work clearly showed this data out to 3 wavelengths.

I find this recent paper most informative and certainly feel that it adds to the fund of information available on corner-reflectors. However, I am quite disappointed that these authors failed to notice my previous work in this field.

* Manuscript received by the PGAP, October 27, 1958.
† Mark Products Co., Morton Grove, Ill.
[1] "Gains of finite-size corner-reflector antennas," IRE TRANS. ON ANTENNAS AND PROPAGATION, vol. AP-6, pp. 366–369; October, 1958.
[2] "An experimental investigation of the corner-reflector antenna," PROC. IRE, vol. 41, pp. 645–651; May, 1953.
[3] E. F. Harris, "An experimental investigation of the corner-reflector antenna," Master's thesis, Tech. Inst., Northwestern University, Evanston, Ill.; June, 1952.
[4] Cottony and Wilson, *op. cit.*, p. 367.

A Method to Achieve a Collimated Circularly Polarized Beam*

C. L. GRAY† AND J. C. HUBER, JR.†

A LENS is described which produces a circularly polarized pencil beam from any linearly polarized source such as a waveguide horn. It consists of a number of equally spaced, orthogonal, thin metal plates assembled in "egg crate" fashion (see Fig. 1). The polarization vector of the source should be orientated at 45° with respect to the plates.

The plates parallel to an electric field component produce a phase velocity which is determined by their spacing and is greater than the free-space velocity. Hence, the plates act as guides, transmitting the wave for frequencies above the cutoff frequency, $a \geq \lambda/2$. Plates normal to an electric field component have no effect on its phase velocity in this case.

The first section of the lens, consisting of orthogonal metal vanes, is used to obtain a plane wavefront in a conventional manner.[1] The phase shifting section consists of only one set of parallel plates which extend a distance t (see Fig. 2) to produce the 90° differential phase shift between orthogonal components necessary for circular polarization.

The contour of the collimating section of the lens is determined by the principle of equality of electrical path length. Assuming a feed with a spherical wavefront, any path length OPP' must equal the length OQ. Hence[2]

$$\frac{L}{\lambda} = \frac{R}{\lambda} + \frac{L - R\cos\theta}{\lambda_g} \tag{1}$$

* Manuscript received by the PGAP, March 23, 1959.
† Rad. Syst. Sect., Goodyear Aircraft Corp., Akron 15, Ohio.
[1] W. E. Kock, "Metal-lens antennas," PROC. IRE, vol. 34, pp. 828–836; November, 1946.
[2] See for example, J. D. Kraus, "Antennas," McGraw-Hill Book Co., Inc., New York, N. Y., chap. 14; 1950.

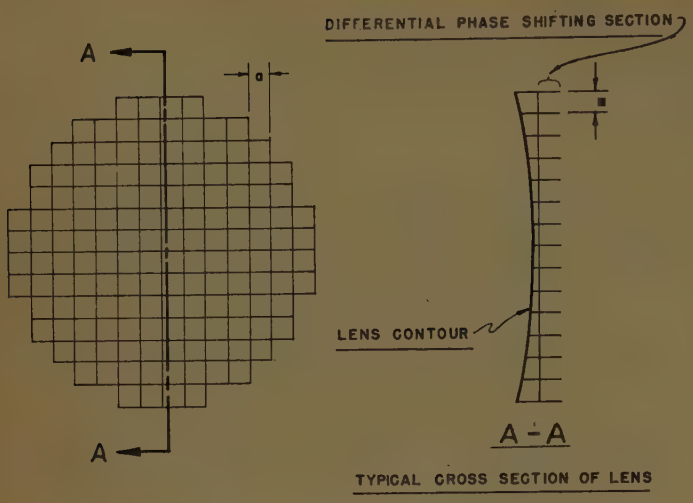

Fig. 1—Configuration of lens.

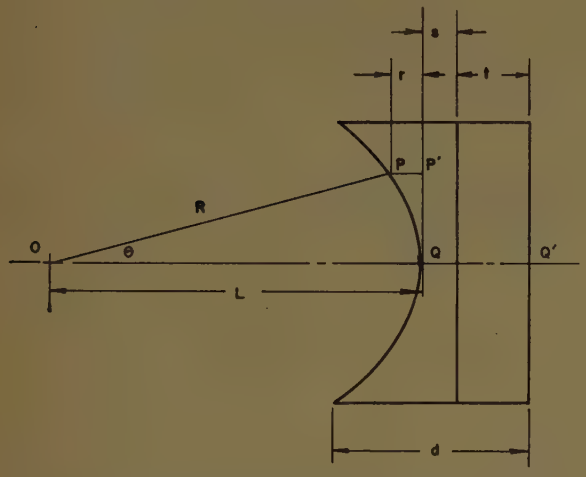

Fig. 2—Coordinate system of lens.

where

L = focal length of lens
λ = free-space wavelength
λ_g = wavelength in lens.

The index of refraction n is determined by the distance a between the plates which are parallel to the electric vector under consideration.

$$n = \frac{\lambda}{\lambda_g} = \sqrt{1 - \left(\frac{\lambda}{2a}\right)^2}. \tag{2}$$

Then (1) may be written

$$R = \frac{(1 - n)L}{1 - n\cos\theta}. \tag{3}$$

Eq. (3) describes the contour of the concave side of the lens where n is given by (2). A three dimensional lens may be obtained by rotating this contour about its axis, OQ'. For this case, equal spacings must be chosen for both sets of plates.

The length of the phase shifting section t is determined by setting the difference in electrical path length between the orthogonal components equal to 90°.

$$\frac{t}{\lambda} - \frac{t}{\lambda_g} = \frac{1}{4}. \tag{4}$$

From (2),

$$\frac{t}{\lambda} - \frac{t\sqrt{1 - \left(\frac{\lambda}{2a}\right)^2}}{\lambda} = \frac{1}{4}$$

or

$$t = \frac{\lambda}{4\left(1 - \sqrt{1 - \left(\frac{\lambda}{2a}\right)^2}\right)}. \tag{5}$$

The distance s may be chosen to optimize the impedance match looking through the lens. The length of this section has no effect on the collimating or differential phase shifting properties of the lens.

A lens of this type is somewhat frequency sensitive. The bandwidth of the collimating portion of the lens is given by Kraus[2] as approximately 5 per cent. The circularity of the beam is similarly frequency sensitive. The tolerances on the lens contour and the plate spacing are given by[2]

$$\Delta r = \pm \frac{0.03\lambda}{1 - n}$$

and

$$\Delta a = \pm \frac{3na\lambda}{(1 - n^2)d}$$

where

a = spacing between plates
n = index of refraction
d = length of plates.

These tolerances are based on a maximum allowable variation in electrical path length in each case of $\lambda/16$.

The lens may be adapted to compensate for other than spherical wavefront illumination by appropriately changing (1). Obviously, the differential phase shifting section which produces the circular polarization can be used with other collimating devices such as waveguide horns, dielectric lenses, parabolic reflectors, arrays, etc.

Abstracts of Papers from the IRE-URSI Symposium Held May 4-7, 1959–Washington, D. C.

The Trade Wind Inversion as a Transoceanic Duct—M. Katzin, B. Y.-C. Koo, J. V. Larson, J. V. Katzin, and H. Pezzner, *Electromagnetic Research Corporation, Washington, D. C.*—The trade wind inversions produce strong elevated ducts capable of trapping VHF radio waves. The persistence of the inversions and their extension in the trade wind belts between major continents suggest that propagation in the trade wind duct may provide a persistent mechanism for transoceanic communication.

This mechanism is explored by means of radiosonde data for stations in the South Atlantic trade wind belt. These records indicate that a duct is present in a majority of the soundings. Since it is known that the radiosonde underestimates ducting because of the slow response of the instrument, it is concluded that a duct is probably present practically all the time. Selected soundings are used to calculate the minimum frequency trapped in the duct. These indicate that frequencies as low as 40 mc can be trapped.

Data are shown on the inversion height and change of refractive index during the year. From these the average trend in duct characteristics is deduced. The effect of a possible "hole" in the duct due to a tropical disturbance is discussed, and its implications with respect to choice of frequency pointed out.

Refractometer profiles taken in the region by Dr. R. M. Cunningham (see next abstract) confirm the deductions made from the radiosonde data. Taken together, the presently available data indicate that the trade wind inversion may provide a highly persistent means of transoceanic radio transmission.

Trade Wind Cloud Forms as Areal Indicators of Duct Strength—R. M. Cunningham, *Geophysics Research Directorate, Air Force Cambridge Research Center*—A study of cloud formations and refractive index profiles associated with the trade wind inversion was made in the area between Recife, Brazil and about 400 miles SE of Ascension I. in a joint project of the Geophysics Research Directorate and the Electronics Research Directorate of the Air Force Cambridge Research Center. Photographs of cloud formations were taken from high altitude and followed directly thereafter by aircraft soundings of refractive index, temperature, and liquid water content through the trade inversion and cloud levels. The area covered by stratocumulus and cumulus clouds was mapped in strips 120 miles wide.

The refractive index profiles obtained in large clear patches are compared with those obtained through sharp cloud tops and through weak cloud areas. A profile, taken east of Ascension I., with a single step of 50 N-units in less than 50 feet of height is shown, illustrating the type measured at the top of a broad solid area of stratocumulus clouds. Multi-stepped profiles measured in clear patches are shown for comparison. Data taken near Recife in this manner show weaker and more complex profiles in more convective cloud situations. Data are also given on horizontal passes through active cumulus which penetrated the inversion by several thousand feet. The relation between cloud form and pattern and refractive index profile is also shown to exist at the western side of the South Atlantic trade.

The results obtained on the relations of cloud structure to refractive index profile indicate that the character of the elevated duct due to the inversion can be obtained in this way over a large region with a small number of profile measurements.

Exploring the Depth of the Surface Layer of the Moon from a Radar Space Observatory—W. E. Fensler, T. B. A. Senior, and K. M. Siegel, *The Radiation Laboratory, University of Michigan, Ann Arbor, Mich.*—A method is suggested for finding the depth of the surface layer of the moon. In essence, the method involves the determination of the power reflection coefficient at different wavelengths, and this coefficient is a function of the number and depth of any layer present, and of the electromagnetic constants associated with this layer. Using the mathematical formula for the reflection coefficient of a layered structure, the above quantities can be calculated from measured values of the power return at different wavelengths.

It is suggested that this experiment be carried out by placing a radar-equipped satellite in orbit around the moon. The data on the power reflection coefficient could be telemetered back to earth for analysis, and the feasibility of the whole system is discussed.

Properties of the Upper Atmosphere Deduced from the Radiation Belt*—S. F. Singer, *University of Maryland, College Park, Md.*—Solar corpuscular radiation can get trapped in the outer regions of the earth's magnetic field. This radiation belt appears to be connected with magnetic storms and aurorae.† In addition, another mechanism has been proposed in which cosmic ray produced neutrons lead to a low altitude equatorial radiation belt which behaves quite differently from the auroral radiation belt.[1] Its dependence with altitude can be calculated and is connected with the density of the atmosphere at each altitude. The equilibrium intensity is determined by the rate at which particles are placed into the trapping region and the rate at which they are removed by collisions with the residual atmosphere. By applying this theory to observed radiation belt intensities we have been able to calculate the atmospheric densities above the exosphere level and have deduced densities of neutral hydrogen up to 10 earth radii. Numerical results will be presented.

Unusual Radio Noise Emission and Absorption—H. W. Wells, *University of Manchester, England*—(No abstract available).

Cesium Beam Frequency Resonator Standard—S. N. Kalra, *Division of Applied Physics, National Research Council, Ottawa, Canada*—A cesium beam frequency resonator has been in use at this laboratory since August, 1958. Details of its construction were described at a previous meeting and so will not be discussed again. Its performance will be discussed particularly with respect to systematic and random errors.

The frequency of the cesium clock is being measured in terms of the astronomical observations of the Dominion Observatory, Ottawa. This standard is also being used to determine the frequency of the transmissions from MSF, WWV, and KK2XEI. This enables international intercomparison of similar standards. Results of these measurements will be presented.

Methods of Describing the Performance of Very Stable Oscillators—R. C. Ward, *Space Technology Laboratories, Los Angeles, Calif.*—Even the most stable oscillators, such as masers and oscillators stabilized with respect to quantum transitions, are corrupted by enough random and periodic frequency modulation to degrade seriously the performance of some systems in which their use is contemplated. At least part of the imperfections of such oscillators can be indicated by their spectra, by the spectra of their instantaneous frequencies, or by other means. The suitability of each of these characterizations is discussed from the point of view of a person who must measure the imperfections and then use this information in systems analysis.

Since some imperfections of stable oscillators have more serious consequences than others, it is important to try to measure them separately. A necessary preliminary is the definition of terms that can be used in describing oscillator performance. Operational definitions are proposed for terms such as agreement, accuracy, inter-unit reproducibility, operational reproducibility, sensitivity, environmental stability, and internal stability.

A Method for Obtaining Dynamic Pattern Data—J. F. Carpenter and R. W. Thille, *Dalmo Victor Company*—In any type of radiating system, the surrounding environment has an effect on the radiation characteristics associated with the source. It therefore follows that the radiation characteristics for a radar antenna will be influenced by its operating environment. Thus, there may be a profound difference between the radiation pattern determined under free space conditions and the actual radiation pattern of the operational radar antenna.

* Supported by the Air Force Office of Scientific Research.

† S. F. Singer, *Trans. Amer. Geophys. Union*, vol. 38, p. 175; 1957.

[1] S. F. Singer, *Phys. Rev. Letters*, vol. 1, pp. 171, 181; 1958.

The purpose of this paper is to describe an antenna patterning system that has been designed and used to determine the shape of the radiation patterns associated with certain large ground based radar antennas in their operating environment. This system, which is completely portable, has a dynamic range of 28 db with flat response from dc to 10 kc and has been designed for a high degree of reliability. It is anticipated that further refinements will increase the dynamic range to over 40 db.

The present system utilizes a CW L-band source mounted in the wing tip of a small aircraft. The source is flown at constant but different altitudes in a circular path around the radar site while the antenna is allowed to rotate and to receive only. The present data has been obtained from both two miles and three miles range. The range will be extended as the system becomes more refined.

Radiation pattern information is received from many different directions and is provided with logarithmic response characteristics to obtain decibel readout and is stored on magnetic tape. The information recorded on magnetic tape is then displayed in visual form through the use of a recording oscillograph.

Automatic Measurement of Dielectric Constant at Microwave Frequencies—W. F. Gabriel, *Microwave Antennas and Components Branch, U. S. Naval Research Laboratory*—It has been found that the dielectric constant of low dielectric materials can be measured accurately, rapidly, and automatically simply by utilizing an automatic microwave impedance instrument of the type which presents its output in Smith chart form; that is, the magnitude and phase of the reflection coefficient. An investigation of the transmission line relationships for a section of line containing a dielectric slug backed by a short circuit reveals that the change in reflection coefficient phase angle, caused by insertion of the dielectric slug, is easily related to the dielectric constant (ϵ') of the slug. In fact, this change in phase angle is precisely the "minimum shift" obtained in the familiar Von Hippel slotted line technique. Consequently, to obtain direct ϵ' readings, it is only necessary to convert reflection coefficient phase angle shifts into dielectric constant, and then construct a suitable chart which has a scale in dielectric constant units. An example of such a chart, calculated for $0.400 \times 0.400 \times 0.900$ slugs in X-band waveguide at 9375 mc, is included. This chart was designed for use with the output devices associated with the NRL automatic impedance instrument; that is, a linear polar recorder and a reflection coefficient phase angle meter. The instrument is capable of phase angle accuracies of $\pm 0.50°$ or better, so that ϵ' measurements are comparable in accuracy to ordinary slotted line measurements. A number of comparison measurements are discussed.

Automatic impedance instruments can also be used to measure the loss tangent of dielectric materials, and a method and chart for accomplishing this will be briefly described. Needless to say, loss tangent is not as easily measured as is ϵ'.

Atmospheric Refractive Index Measurements With a Drop Type Refractometer—A. P. Deam, *Electrical Engineering Research Laboratory, University of Texas.*—A Drop Type refractomer is described which operates at 400 mc and the initial measurements made with it up to elevations of the order of 60,000 feet. The sampling unit contains a Pound stabilized oscillator whose frequency is controlled by a resonant coaxial cavity. This cavity is open to admit the air to be sampled and the frequency of resonance is a function of the index-of-refraction of the air within the cavity. The frequency produced by the stabilized oscillator is radiated to a receiver on the ground or in an aircraft which has a reference oscillator. The frequency difference between the sampling and reference oscillators is a measure of the index-of-refraction.

The initial tests of this refractometer were made at Holloman Air Force Base, N. Mex., by carrying it aloft to 60,000 feet in a balloon and permitting it to fall by parachute. Refractive index soundings were obtained on both the ascent and the descent even when the balloon had drifted 80 miles from the receiver. The index-of-refraction profiles obtained with this instrument are presented.

Fundamental Limitations of External Noise—H. H. Grimm, *General Electric Company.*—The development of low-noise microwave amplifiers prompted the author to re-evaluate noise sources preceding the first low-noise amplifier of a microwave receiver. This report presents design relations or analytical methods which permit approximate evaluation of most noises encountered. Noise sources discussed are those due to the antenna and transmission line components, the atmosphere, the warm earth, and space beyond the ionosphere. The discussion utilizes the concept of excess noise temperature, currently popular in the low-noise receiver art.

Excess noise due to absorbing media at uniform temperatures is shown to be easily evaluated using commonly available information. Noise due to the nonhomogeneous atmosphere is evaluated in an approximate manner for operation with a pencil beam at 400 mc. Noise leakage from the warm earth is also evaluated for an antenna system at 400 mc. An approximate computation is used and the input data requirements are indicated. A brief discussion of radio sky background temperature considerations is given. The need for better absolute background measurements is discussed.

Sferics Monitoring System*—A. L. Whitsen, E. G. Goddard, J. H. Priedigkeit, *Stanford Research Institute, Menlo Park, Calif.*—A sferics monitoring system has been developed and is currently being operated at three arctic sites to study sferic population, the diurnal, seasonal, and auroral effects on VLF propgation, and the locations of sferic sources.

The system is an integrated assembly of electronic, photographic, and electro-mechanical equipment capable of being operated in several different modes to gather the following data:

1) Number of sferics occurring in four 20 db intensity levels in four 6-hour time blocks,
2) Bearing of individual sferics,
3) Waveform of individual sferics,
4) Time integrated bearing patterns, and
5) Noise level and signals in the 12–30 kc range.

A secondary frequency standard at each site is checked against WWV or WWVH daily and provides a common time reference between the records from all sites. A modified Watson-Watt type directional finder system with a unique crossed-loop antenna provides instantaneous bearing. Instantaneous sense is achieved by combining the crossed-loop signals with the signal from an omnidirectional antenna. In addition to the sense function, the latter antenna also provides signal energy to a scanning receiver, a multi-threshold-time-block events counter, and a signal waveform channel.

On the Use of HF Moon Echoes to Determine Cislunar Ion Densities*—V. R. Eshleman, P. B. Gallagher, and R. C. Barthle, *Radio Propagation Laboratory, Stanford University*—At Stanford University we are studying by theory and experiment the ionized medium between the earth and the moon. Of prime interest is the ion density beyond the earth's ionosphere, at distances (several to 60 earth radii) where the interplanetary gas may be dominant. There are two techniques based upon HF moon echoes for measuring the total ion density. The ionospheric part may be determined separately and subtracted from the total.

The moon's radar range exceeds the true range, especially at low frequencies, because of group retardation which is a measure of integrated ion density. (The retardation varies as f^{-2}, being 250 μs at 20 mc for an average cislunar density of $10^9/m^3$.) Range measurements giving density would require high peak power (for pulse ranging) or high stability (for CW ranging); furthermore, the true lunar range is not known accurately.

We employ the full average-power capability of an HS transmitter without regard to high stability or precise lunar range. By transmitting a one-second AM pulse, a reference quantity is, in effect, sent with the measuring quantities. The dispersion of the medium changes the relative phases of the three frequencies, and hence, the character of the modulation. For example, the modulating frequency at which AM is changed to FM should be a direct measure of the integrated ion density.

It may be that path splitting and ion "blobs" will affect relative phases more than does dispersion. Our method would then yield information about time and space variations of ionization. If path splitting affects the modulation conversion measurement, it follows that the ion density could not be measured by the range method. Early studies of HF moon echoes led to the conclusion that the moon was a rough reflector, while more recent studies at VHF and UHF indicate that it is relatively

* This work is under the sponsorship of the Division of Air Force Cambridge Research Center.

* This work is sponsored by the Electronics Research Directorate of the Air Force Cambridge Research Center under Contract AF 19(604)-2193.

smooth. It may be that the moon is smooth, but at HF the cislunar medium is rough.

Measurements of Ionosphere Electron Content by the Lunar Radio Technique—S. J. Bauer and F. E. Daniels, *U. S. Army Signal and Research Laboratory, Ft. Monmouth, N. J.*—(No abstract available).

Ray Patterns of Anomalous Satellite and Round-the-World Signals—M. S. Wong, *Electronics Research Directorate, Air Force Cambridge Research Center, Bedford, Mass.*—Ray patterns portraying the spatial distribution of rays emitted from a radio transmitter are shown for ionospheric layers which vary with height and distance. These patterns are computed with equations which neglect the geomagnetic field but include both the refractive index and, crucially, the index gradients. (The computer used can also handle the geomagnetic field.) With the transmitter near or above ionospheric layers, the following anomalies appear in the patterns: trapping of rays in ionospheric ducts, some extending and others not extending down to ground; regions of reduced radio signal; regions with enhanced, and dense spatial fadings of, signal. These anomalies serve to explain certain features observed in radio signals received from satellites, and predict other features which arise if the receiver were also up in a satellite.

The ray patterns also include ionospheric conditions under which it becomes possible to obtain round-the-world echoes, or signals from a satellite near the antipode.

Measurement of Local Ion Densities by Comparison of Doppler Frequency Curves Obtained from 1957β—W. B. Murcray and J. H. Pope, *Geophysical Institute, University of Alaska, College, Alaska*—During the early stages of the life of 1957β, it was coming out of perigee as it passed over College. As a result, it was in the F region and rising during the time signals were received at the Geophysical Institute. A method was developed for obtaining the ion density at the location of the satellite from the ratio of the 20- and 40-mc Doppler frequencies. Much data remains to be analyzed, but some samples are presented. Evidence for small regions of very high ion densities during aurorae was also obtained.*

Ionospheric Electron Content Determined from Satellite Observations†—O. K. Garriott, *Radio Propagation Laboratory, Stanford University*—When the fading rate due to Faraday rotation of the 20 mc transmissions from the Russian satellites has been observed at middle latitudes, one frequently observed characteristic has been a pronounced drop in rate as the ray path becomes perpendicular to the magnetic field lines. This is readily explained in terms of the Appleton-Hartree equation when propagation becomes "quasi-transverse." At this time the phase path length difference between the ordinary and extraordinary rays is relatively small. The phase path length difference at other times can be determined by simply counting the number of fades due to Faraday rotation starting from the time of Q-T propagation up to the time of interest. One fade, corresponding to a 180° rotation of polarization, indicates a 360° difference in phase path length. Knowing the phase path length difference permits calculation of the integrated electron density in the same manner used in moon echo experiments.

The signals from Sputnik III have been monitored for a number of months by the Stanford Radio Propagation Laboratory. Integrated electron density values obtained from these observations are reported including comparisons with values derived from vertical incidence sounders at times when the satellite was below the level of the maximum electron concentration. Good agreement has been shown on a number of specific occasions.

A Proposed Experiment for the Determination of the Electron Densities Beyond the Ionosphere—J. M. Kelso and C. D. Graves, *Space Technology Laboratories, Inc., Los Angeles, Calif.*—Doppler measurements using two coherent signals transmitted from a rocket or space vehicle form a sensitive and informative method for studying the electron-density variations in the ionosphere.* However, it has been shown that time variations in the ionosphere can sometimes introduce a serious error when the vehicle is at great altitudes where the electron density is low, and it has been proposed that the Doppler measurement be corrected by use of data obtained from a supplemental measurement of the rate of Faraday rotation of the plane of polarization.†

After reviewing and extending the theory of the error in the Doppler measurement, this paper presents the expected magnitude of the error as a function of various ionospheric and magnetic conditions and for several types of vehicle trajectories. Necessary data concerning the time variations of the ionospheric electron density are derived from available theoretical and experimental results. This information is then introduced into the combined Doppler-Faraday experiment to evaluate the net errors caused by the ionosphere. The results indicate that a Doppler-Faraday experiment should yield valuable information concerning the density of electrons in a region where the environment approaches that of solar space.

Density Distribution of Free Electrons in the Upper Atmosphere—D. J. Farmer and W. A. Robinson, *Space Technology Laboratories, Inc., Los Angeles, Calif.*—The distribution of free electrons in the ionosphere has been measured in tests of the Atlas intercontinental ballistic missile by comparing the apparent missile radial velocity, as determined from the Doppler-shifted frequency of a VHF radar, with the radial velocity obtained from accurate trajectory data derived from other measurements. Since, to first order, these two velocities are related through the index of refraction at the missile, the local electron density may be computed with the aid of the Appleton-Hartree equation. Results are compared with approximate true height reductions of terrestrial soundings taken during and after flights at stations in the neighborhood of the missile trajectory. In several flights data were obtained at heights well above the F region maximum and reveal a more gradual decrease of the electron density with height in that portion of the ionosphere than would be expected on the basis of some models.

Ionospheric Scintillation of Satellite Signals—H. P. Hutchinson and P. R. Arendt, *U. S. Army Signal Research and Development Laboratory, Ft. Monmouth, N. J.*—The scintillation of satellite-emitted radio signals has been observed using two different techniques, namely, Doppler-shift frequency measurements and radio direction finding. The variations from a smooth Dopper-shift curve obtained during individual orbits give a measure of the frequency scintillation occurring during the transmission and thus of the roughness of the ionospheric path between the satellite and the observer. As expected, these variations are a function of the received frequency. Examples are discussed of the range in variations of the received frequencies on 20, 40, 108 and 108.03 mc, both as a function of frequency and as correlated with ionospheric disturbances identified from other data.

In particular, a marked disturbance of short-period duration occurring during the reception in the 108 mc band is discussed.

Variations in direction-finder bearings are presented and discussed in relation to the direction finder data and the Doppler-shift frequency variations mentioned above. It is obvious that these measurements correlate with the state of the ionosphere and that the variations, such as the marked disturbance previously discussed, can be localized within the upper atmosphere. Both methods present very sensitive procedures for studies on the hyper-fine structure of the ionosphere.

Frequency Allocations for Radio Astronomy—J. W. Findlay, *Research Equipment Development, National Radio Astronomy Observatory*—A brief review is given of the international situation on getting frequencies allocated for use by Radio Astronomers. The present status of work by the members of the URSI Sub-Commission Ve is presented. This Sub-Commission is attempting to obtain a valuable allocation of frequencies at the forthcoming International Radio Conference to be held at Geneva from August through December, 1959.

Self Calibrating Radiometer for Measuring Noise Temperatures from 0 to 750°K*—F. G. Haneman and T. H. Bridgeman, *Airborne Instruments Laboratory, Mineola, N. Y.*—The design and operating characteristics of a self calibrating radiometer, used for measuring noise temperatures in the 0 to 750°K range, are discussed. This radiometer measures noise power in a 1 mc bandwidth, which is tunable from 405 to 445 mc. The basic system design is similar to that originally proposed by Ryle *et al.*, but includes a novel addition which allows measurement of input noise temperatures below room ambient. Antenna noise temperature

* This work was supported in part by the Rome Air Development Center and by an IGY Grant from the National Science Foundation.
† This work has been sponsored by a grant from the National Science Foundation.

* J. E. Jackson and J. Carl Seddon, "Ionosphere electron-density measurements with the Navy Aerobee-Hi Rocket," *J. Geophys. Res.*, vol. 63, pp. 197–208; March, 1958.
† John M. Kelso, "The measurement of electron densities in the outer ionosphere," Conference on the Propagation of Radio Waves, Liege; October, 1958. (To be published in Proceedings of the Conference.)

* This work was conducted under Air Force Prime Contract AF30(602)-1625.

measurements made on a 60-foot parabolic antenna with this equipment are reported.

A Rapid and Accurate Method for Computing Tropospheric and Ionospheric Refraction Effects on Radio Waves*—S. Weisbrod, and L. J. Anderson, *Smyth Research Associates, San Diego, Calif.*—Computation of the refractive bending of radio waves passing through the earth's atmosphere is a fairly complicated task. Published methods are too tedious for routine application without a computer, or are limited in accurary or in the range of applicability. The method presented here is free of these difficulties and is equally applicable to both the troposphere and the ionosphere, above 100 mc. Furthermore, it can be used directly with the measured refractive index without the necessity of expressing the profile in an analytic form. The profile is represented by linear interpolation between measured points. The only assumptions are that the profile is a function only of height above the spherical earth, and that the height interval between measured points is small compared with the earth's radius.

To apply this method, one chart is required for reduction of the tropospheric data, and a similar chart for the ionospheric data. Refractive bending for a given angle of elevation can be calculated from a ten point profile in about ten minutes. For the case of an assumed parabolic distribution for the ionosphere, an agreement within a fraction of one per cent was obtained between the analytic computation of the bending and the above method, using five equally-spaced points between the vertex and the base of the layer. Similar accuracy is obtained in the troposphere.

An analogous method for computing retardation and the Faraday Rotation is also discussed.

Angular Accuracy of Radio Interferometer Techniques—L. S. Wagner, *Cornell University, Ithaca, N. Y.*—A discussion of radio interferometry as a means of measuring the position of a radio star is presented. Three radio interferometer configurations are considered: 1) the correlation detector interferometer, 2) the total power radio interferometer, and 3) the phase switched radio interferometer. Of these, the correlation detector interferometer and the phase switched radio interferometer are best suited to the angular location of a radio star.

A relationship is developed between the accuracy of measurement of star angle and the output signal-to-noise ratio of a receiver. The relationship between input and output signal-to-noise ratios is presented for the correlation detector and phase switched radio interferometer and these are used to express the accuracy of star angle measurement in terms of the input signal-to-noise ratio. This is further extended so that the accuracy of star angle measurement is expressed in terms of radio star intensity, average brightness of the galactic background, antenna gain, and receiver noise figure.

The analysis of the phase switched radio interferometer indicates that the ratio of input to output signal-to-noise ratio is independent of whether a half-wave linear, half-wave square law or full-wave square law rectifier is used. Results are presented for the standard deviation of error of angle determination for the correlation detector interferometer and for two versions of the phase switched radio interferometer.

A Compound Interferometer—A. E. Covington, *Radio and Electrical Engineering Division, National Research Council, Ottawa, Canada*—The product receiving pattern of a four-element grating and continuous array has been obtained at a wavelength of 10 cm, at the National Research Council in Ottawa. This interferometer system is an extension of the previously described compound interferometer* to an over-all antenna length of 185 meters, and produces a single-lobed fan-shaped radiation pattern of one minute of arc East-West, and 2° North-South. The method of operation will be outlined, and some selected solar drift curves shown.

Application of Digital Data Processing Techniques to Radio Astronomy†—R. Price, *Lincoln Laboratory, Massachusetts Institute of Technology*—Many of the current investigations in radio astronomy employ sensitive radiometers to measure the small power differentials that are produced by the signals of interest. As conventionally built, a radiometer is an assemblage of electronic circuits that perform the functions of filtering, envelope-detecting, and integrating the received signal. Circuit instabilities can introduce serious degradation where observations are being made on extremely weak signals, although cancellation of gain-variation by schemes such as Dicke's switched radiometer technique have had notable success.

With the advent of modern, flexible, high-speed digital data processing machines, together with accurate, high-speed analog-to-digital converters, there is considerable promise of radiometer improvement. Instead of using conventional, analog-type circuit elements to approximate the mathematical operations that describe a radiometer, it is now possible to carry out these operations exactly (except for the negligible effects arising from amplitude and time quantization). It also becomes relatively simple to convert from a radiometer to other types of signal processing if desired.

High-speed digital data recording methods can be a valuable adjunct to digital processing, especially under circumstances where there is only a relatively brief period available for observations, or in which the received signal must be subjected to extensive analysis.

The talk will deal with a novel experiment in radio-astronomy in which these techniques were successfully employed.

Nonlinearity of the Relationship Between F2-Layer Critical Frequencies and Sunspot Number—S. M. Ostrow and E. J. Dutton, *Boulder Laboratories, National Bureau of Standards, Boulder, Colo.*—Examination of the relationship between monthly median f_0F_2 and twelve month running average Zurich sunspot number for thirteen ionosphere stations, each with 14 or more years of observation, shows that the relationship is significantly nonlinear in a large proportion of cases. There seem to be diurnal, seasonal, and geographic differences in significant departures from linearity. It is shown that, for radio propagation predictions purposes, a linear relationship may be used if the nonlinearity is compensated for by arbitrarily assigning all sunspot numbers greater than 150, the value of 150.

Ionospheric Information from Rocket Measurements—H. Friedman, *U. S. Naval Research Laboratory, Washington, D. C.*—Rocket experiments conducted during the IGY have filled in many gaps in our knowledge of 1) the spectrum of ionizing radiations; 2) the variation of electron density with height above the maximum of *F*-region; 3) the distribution of positive ions with altitude up to 820 km; and 4) the conductivity of interplanetary space deduced from observations of scattered Lyman-α radiation in the night sky. In addition to several *D*-region measurements of the short wavelength limit of x-ray flashes during solar flares, information was obtained in one flight about the softer x-ray flare emission absorbed in *E*-region.

The eclipse of October 12, 1958, was observed with rockets measuring x-rays and ultraviolet light. Although the analysis is not yet completed it is apparent that a substantial portion of the x-ray flux persisted throughout totality whereas Lyman-α fell to a low value comparable to the general sky background.

Ionospheric Disturbances following the Flare of August 22, 1958—T. R. Hartz, A. G. Matthews, and J. L. McAlpine, *Radio Physics Laboratory, Defence Research Board, Ottawa, Canada*—A study has been made of the solar and terrestrial effects which were associated with the importance 3 flare of August 22, 1958. The solar disturbance was characterized by large radio noise bursts which were observed over a wide range of radio frequencies. The radio noise data were examined on the assumption that particles of matter were ejected by the flare and that this corpuscular cloud generated each noise burst at a height in the corona where the electron density corresponded approximately to the plasma frequency. The computations yielded two distinct ranges of particle velocities; very fast particles which should have reached the earth in a matter of hours, and slower particles which should have arrived at the earth in about a day and a half. A variety of ionospheric recordings were examined for evidences of the two types of particles, and definite indications of the arrival of the particles were found after about 4 and 34 hours, respectively.

Further data from other flares are presented to show that this sequence of events is not exceptional but is fairly common for certain large solar flares. It is shown that visual and radio measurements of the solar conditions at the time of a flare are sufficient to predict the time, strength, and some of the characteristics of the respective ionospheric disturbances.

Short Wave Radio Fadeouts without Reported Flares—H. DeMastus, *Sacramento Peak Observatory, Boulder, Colo.*, and M.

* This work has been sponsored by Rome Air Development Center, under Contract AF30(602)-1624.

* A. E. Covington and N. W. Broten, "An interferometer for radio astronomy with a single-lobed radiation pattern," IRE TRANS. ON ANTENNAS AND PROPAGATION, vol. AP-5, pp. 247–255; July, 1957.

† The work reported in this paper was performed by Lincoln Laboratory, a center for research operated by Massachusetts Institute of Technology with the joint support of the U. S. Army, Navy, and Air Force.

Wood, *National Bureau of Standards, Boulder, Colo.*—Widespread short wave radio fadeouts (SWF's) were selected which had no reported flares associated with them, in and during which the Sacramento Peak flare patrol was in operation. Sixteen cases of such SWF's were found during the IGY period. The Sacramento Peak flare films covering these SWF times were re-examined in detail. It was found that only one SWF definitely was not associated with unusual optical solar activity. Three cases were questionable, two because of poor observing conditions. The remaining twelve SWF's were strikingly associated with solar active events, typically with marked plage brightenings. One of these twelve cases is of particular interest; a large dark filament, of about 0.4 solar radius in length, disappeared about half an hour before, and suddenly reappeared within a minute of, SWF beginning time. There was no other definite solar activity near the time of the SWF.

E Region Ionization by Cosmic Dust—M. Dubin, *U. S. Air Force Cambridge Research Center*—Recently measurements of the influx rate of cosmic dust into the earth's atmosphere have been made with satellite and lunar rocket vehicles. These measurements have been used to obtain a first order estimate of the rate of bombardment of the E region by the cosmic dust component of extraterrestrial material. By combining these influx rates with cross sections for electron production from collisions at meteoric velocities, the contribution of this component of cosmic dust to the ionization in the E region has been computed. It has been found that this contribution may support an electron density of 10^4 electrons/cc in the presence of a loss mechanism involving a dissociative recombination coefficient. A single correlation of some significance has been found between a "shower" of cosmic dust as measured from the satellite, and a strong sporadic E condition. The methods and results of these measurements will be reviewed in relation to their potential effect upon the structure of the E region. The effect of the cosmic dust upon the E region suggests that the mechanism for maintaining the nocturnal E region as well as the formation of some forms of sporadic E ionization involves ionization by collision from the cosmic dust component of interplanetary matter.

The Formation of an Artificial Ion Cloud-Release of Atomic Potassium at 121 km—F. F. Marmo, L. Aschenbrand, and J. Pressmann, *Geophysics Corporation of America 700 Commonwealth Avenue, Boston 15, Mass.*—An Aerobee rocket was launched from Holloman Air Force Base in New Mexico on November 19, 1957, whereby 150 moles of atomic potassium were released instantaneously at an altitude of 121 km. A brief discussion on the elementary physics on the formation of an artificial ionized cloud as well as the chemistry involved is presented. A description of the results includes positive identification of the ionized cloud by various radar instruments and a vertical incidence ionosonde. Since the cloud was detected for approximately 45 minutes, the data is interpreted to provide details on electron densities, cloud shape and motion vs time, and rate of decay.

Thermal Generation of Artificial Electron Clouds—J. Pressman, F. F. Marmo, and L. Aschenbrand, *Geophysics Corporation of America, 700 Commonwealth Avenue, Boston 15, Mass.*—A Nike Cajun rocket release of atomic cesium during a nighttime hour on May 20, 1958, resulted in a detectable artificially created electron cloud at 101 km. The cloud was generated presumably by thermal ionization of atomic cesium. Both optical and radar detection techniques were utilized. A Stanford University 70 kw pulsed radar detected the cloud for 90 seconds, while the C-3 ionosonde unit located at White Sands Proving Grounds, N. Mex. detected the cloud for about 4 minutes. The generation and decay mechanisms are discussed with correlation of the optical and radar data.

Whistler Propagation in the Presence of Ion Streams—R. E. Barrington, *Radio Physics Laboratory, Defence Research Board, Ottawa, Canada*—The usual theory of whistler propagation predicts that frequencies well below the maximum gyro frequency encountered on the path suffer little absorption, and that the whistler ray direction lies close to the geomagnetic field direction. If whistler propagation is considered in a region in which an ion stream is directed along the geomagnetic field, these conclusions are not always valid. Such a region might exist at times on the lines of force of the earth's field incident in or near the auroral zone. For some values of stream density and velocity, propagation along the field direction is accompanied by large absorption and a large increase in the group refractive index for some frequency components of the whistler. The ray direction is also found to depart markedly from the field direction.

The Behavior of the Transverse Whistler Mode in the Earth's Dipole Field—W. C. Hoffman, *The Rand Corporation, Santa Monica, Calif.*—In classical whistler theory the ray direction can deviate at most 19° 29 feet from the local direction of the geomagnetic field. C. O. Hines,* first pointed out the possibility of whistler mode propagation in arbitrary directions (across as well as along the lines of force) when the presence of ions as well as electrons is taken into account. Hines' analysis holds for the case of a homogeneous ionized medium in the presence of a uniform magnetic field, and thus applies to the ionosphere only locally.

The present paper treats ray-tracing in the equivalent dipole field of the earth using Hines' refractive index formula and an analytic electron density profile which takes account of the principal known characteristics of the ionosphere important to whistler propagation. The ray-tracing equations employed are a transformation of those of J. Haselgrove in polar coordinate form. The conditions for existence of the purely transverse whistler mode, *i.e.*, an orthogonal trajectory of the lines of magnetic force, are investigated, and it is shown that purely transverse whistler mode propagation can persist over any considerable distance only for a very special form of the refractive index. Ray paths for the more general type of whistler mode were computed on the Johnniac for rays starting at latitudes of 10°, 20°, 30°, · · · , 70°, 80°, and 90° for initial angles between the geomagnetic field and the wave normal of 0°, 10°, 20°, · · · , 80°, and 90°, at frequencies of 2 kc and 16 kc.

* *J. Atmos. Terr. Phys.*, vol. 11, pp. 36–42; 1957.

A Survey of Some Promising Methods for the Study of Ray Propagation in a General Medium—J. Brandstatter, *Stanford Research Institute*—This paper will attempt to give a survey of some promising methods for the study of the propagation of rays in nonhomogeneous anisotropic media. Based on an extension of Hamilton's principle, the ray path equations are deduced together with certain properties of the associated wave normals and surfaces. The latter provides an aid in the study of refraction and reflection, particularly in the ionospheric case. It is shown that by the extension of Hamilton's principle stated above, the concepts of dispersion and group velocity appear quite naturally. For the study of dispersion, a perturbation method developed by the author is presented. Finally, it is indicated how a field theory, that is, a diffraction theory, may be constructed. Some of the preceding has already been applied to the study of whistler path phenomena and further applications are already in progress.

Hybrid Whistlers*—R. A. Helliwell, *Radio Propagation Laboratory, Stanford University, Stanford, Calif.*—Whistlers frequently exhibit many well-defined components which are thought to result from the existence of separate paths of propagation. It has been suggested that such paths might be defined by columns of enhanced ionization which are aligned with the earth's magnetic field and which reach from one hemisphere to the other. Another possibility is that whistler energy is permitted to emerge from the ionosphere only at specific locations where conditions are favorable. A test to differentiate these two models would be to excite whistler paths simultaneously in opposite hemispheres from the same source. At a receiver in either hemisphere the result would be the superposition of long and short whistlers—a hybrid whistler. The dispersion ratios of a hybrid whistler and its echoes would be 1:2:3:4:5, etc., if the paths were the same for both directions of propagation. A search of records from the IGY Whistlers-West project has revealed several examples of what appear to be genuine hybrids. Their existence argues strongly for the field-aligned column hypothesis of whistler paths.

The Trapping of Whistlers by Columnar Irregularities in the Outer Ionosphere†—R. L. Smith and R. A. Helliwell, *Radio Propagation Laboratory, Stanford University*, and Irving Yarbroff, *Stanford Research Institute, Menlo Park, Calif.*—Storey showed that whistlers should follow approximately the lines of force of the earth's field because of the anisotropy of the ionized medium. It has been suggested that columns or shells of enhanced ionization aligned with the earth's field might effectively trap the waves as in a waveguide. The conditions for such trapping are developed, assuming that ray theory applies and that the refractive index is large. It is found that waves can be trapped not

* Research supported in part by the Air Force Office of Scientific Research under Contract AF 18 (603)-126.

† Research supported in part by the Air Force Office of Scientific Research under contract AF 18 (603)-126.

only in enhanced columns but also in columns of reduced ionization. The conditions for trapping are given in terms of the ratio of wave frequency to gyro-frequency, the initial wave normal angle, and the degree of enhancement. As an example, a 10 kc ray path is computed for a column with twenty per cent enhancement of ionization with respect to the background level. The path exhibits small snakelike excursions from the axis of the column and satisfies the criteria which have been developed.

Applications of this theory to the interpretation of whistler data are discussed.

Sweep Frequency Observations of the Sun in the Range 25–580 mc/s—A. R. Thompson, *Harvard Radio Astronomy Station, Fort Davis, Tex.*—The sweep frequency equipment for solar radio observations at the Harvard Radio Astronomy Station, Fort Davis, Tex., has recently been extended by the addition of receivers for the bands 25–50 mc and 50–100 mc. The frequency range, previously 100–580 mc, now covers 25–580 mc. The two new receivers are connected to fixed broad band dipoles mounted over a reflecting screen, and solar radiation is received for a period of about 5 hours around noon each day. Interference due to broadcast and communications signals becomes serious below 40 mc, and limits the useful frequency range. The receivers and antenna will be briefly described, and preliminary results of solar observations in the new bands will be given.

On the Region of Origin of Solar Radio Noise Bursts—T. R. Hartz and C. O. Hines, *Radio Physics Laboratory, Defence Research Board, Ottawa, Canada.*—It is frequently assumed that solar radio noise bursts are generated by a plasma oscillation process, in consequence of which each given frequency originates in the solar corona near the level of critical electron density appropriate to that frequency. While this is probably true of the burst as generated, it is probably not always true of the burst as observed. It seems more likely that the observed radio emission arises primarily in a region near the envelope of ray paths drawn from the observing site (the earth) through the ionized solar corona (the so-called escape level), even though the efficiency of energy conversion into radio noise may be low at that region. Except for sources near the central regions of the solar disc, this conclusion can lead to an appreciable change in the interpretation of burst data.

The theoretical and observational bases for the foregoing statements will be presented and discussed.

Disk Distribution of Flares Associated with Solar Radio Bursts of Various Spectral Types—C. Warwick, *National Bureau of Standards, Boulder, Colo.*—The distribution of central meridian distance of Hα flares with beginning times close to the time of solar bursts of spectral types II and III and of inverted U-bursts has been compared to the distribution for all flares. Flares associated with type III bursts are found to be distributed on the disk in very nearly the same way as are all flares. Flares associated with U-bursts, and flares associated with type II bursts are relatively more frequent near the limb, and less frequent near the center of the solar disk compared to all flares.

Correlation of H-Alpha Flares with 10-cm Radio Bursts—S. Edelson, N. J. Santini, R. J. Coates, and T. P. McCullough, *Radio Astronomy Branch, U. S. Naval Research Laboratory, Washington, D. C.*—A previous statistical analysis of solar H-alpha flares and 10-cm radio bursts indicated that on the average the radio peaks occurred about halfway between the start and maximum of the flare. More recently, light curves of H-alpha flares have been compared directly with the NRL 10-cm burst records of McCullough and Bologna. The results from this analysis show that for the type simple 2 bursts the sudden rise in radio flux occurs during the period of rapidly increasing H-alpha intensity and the radio flux reaches a maximum just slightly before the peak brightness in H-alpha.

High Resolution Lunar Measurements at 4.3-mm Wavelength—R. J. Coates, *Radio Astronomy Branch, U. S. Naval Research Laboratory, Washington, D. C.*—Measurements of lunar radiation are being conducted at the Naval Research Laboratory with a 10-foot parabolic antenna (6.7-min. beamwidth) and a Dicke-type radiometer. Many scans have been made across the moon at different times of the lunar month. These scan records are asymmetric, and the amount of asymmetry is a function of the phase of the moon. The sunlit part of the moon's surface is considerably brighter at 4.3-mm than the dark part. The difference between light and dark areas is more pronounced at 4.3-mm than at 8.6-mm wavelength.

The Theory of Ring Arrays—G. Sinclair, *University of Illinois**—There is a renewed interest in ring arrays for possible applications in broadcast stations of very high power. The usual method for analyzing ring arrays was found to be inadequate in a number of respects. A new analysis will be presented which leads to a straightforward design procedure for ring arrays.

A Circular Antenna Array Suitable for Amplitude Scanning†—H. P. Neff, W. T. Patton,[1] J. F. Pierce, and J. D. Tillman, *University of Tennessee, Knoxville, Tenn.*—A circular antenna array is described consisting of several rings of dipoles, with the rings stacked axially. The array is such that it produces a directional beam that can be pointed to any desired azimuth angle. The terminal impedance of all of the dipoles in any one ring is the same, and does not depend upon the pointing of the beam. Further, all of the element currents in any one ring are real, and the currents in successive rings are alternately real and in quadrature. The pointing of the beam thus depends only on the amplitude of the element currents. These properties make it feasible to connect an amplifier to the terminals of each element and electronically control the direction in which the beam is pointed by amplitude modulating the amplifiers by suitable control voltages.

The design of a simple antenna of this type is given, and data are given on currents and impedances. The calculated and measured patterns are presented. The circuit of an amplifier suitable for the required control of the currents is also given.

Method for Estimating Effects of Gaps in Antenna Apertures on Far Field Patterns—V. T. Norwood, *Guided Missile Laboratory, Hughes Aircraft Company*—A problem that has arisen as a result of the many new uses for very long antenna arrays is that of determining the effect of regularly spaced holes in the aperture distribution. This paper provides an expression based upon an approximation which permits one quickly to estimate the position and level of sidelobes caused by such gaps.

The validity of this method is demonstrated by comparison with an exact expression computed on IBM equipment and also by comparison with several far field patterns measured on actual arrays. The estimated sidelobes in one example were 19.1 db down, compared with 19.13 db in the exact calculation.

An Eight Spiral Doublet Electro-Mechanical Scanning Array—J. R. Donnellan, *Microwave Antennas and Components Branch, Electronics Division, U. S. Naval Research Laboratory, Washington* 25, *D. C.*—An eight spiral doublet array, each doublet consisting of a pair of two-wire spirals in the same plane and wound in opposite senses, is used to scan a beam of horizontal polarization over a $\pm 40°$ range by simple rotations of the spiral doublets. The combination of a microstrip ring network and twin lead provides a balanced feed for each spiral in the array. Side-lobe levels are those predicted (25 db) for the broadside pattern and are, in general, below 19 db over the 80° scan. A novel microstrip feed harness which provides isolation between the doublets and serves to absorb most circulating currents is also described. This printed circuit feed structure consists of judiciously-grouped microstrip ring networks and provides the desired feeding coefficients to within ± 0.1 db. An application of the array to tracking purposes is described. A brief discussion of related work planned for the future is also presented.

The Corner Array—A. C. Schell, *Electromagnetic Radiation Laboratory, U. S. Air Force Air Research and Development Command, Air Force Cambridge Research Center, Bedford, Mass.*—An antenna has been designed which represents a combination of the features of a linear array and a reflector surface. The antenna consists of an array located at the bisector of the angle between two intersecting conducting planes. The radiation pattern produced by this structure may be controlled to provide narrow beams with low sidelobes. Two methods of analysis of the field distribution are presented. The first uses physical optics to obtain a solution for the fields along the axis of the corner reflector. The second gives the field from a radiating element on the axis of the reflector. This is extended to yield the field from an array. By manipulating the amplitudes of the element currents, it is shown that the sidelobe level within the reflector sector may be reduced to any desired value. Also, the size of the aperture is shown to correspond to that of other antennas for a given directivity. Finally, results of measurements of the properties of two corner arrays are given, showing a 13°-wide beam from a 60° corner

* Guggenheim Fellow, on leave from the University of Toronto, Can.

† The research reported in this paper has been supported by the Air Force Cambridge Research Center.

[1] Now at the University of Illinois.

array, and an 8° beamwidth from a 30° corner array.

Optimum Gain of Constant Amplitude Linear Arrays—W. W. Gerbes, *Electromagnetic Radiation Laboratory, Air Force Cambridge Research Center*—The problem of determining the conditions for maximum gain of an antenna system in a certain direction is in its general form so complicated mathematically that efforts to solve it have been made for only very simplified arrays, like linear ones.

Hansen, Woodyard and D. G. Reid dealt especially with the optimal endfire-gain of continuous linear arrays of dipoles. But for mathematical reasons one of the papers was restricted to very long arrays, the other gives unlikely high gains for very short arrays and both are in only fair agreement with each other.

In this paper a new attempt is made to clarify this complicated situation with the help of a special tabulated function and the assistance of geometrical methods. The exact condition for optimal end-fire gain is given for all lengths of the array. The Hansen-Woodyard condition appears as the asymptotic form of the general condition for infinitely long arrays. Similar conditions could be derived for an arbitrary angle of maximum radiation, as for broadside arrays. That the supposedly high gains for short arrays do not exist is shown, and the reasons for the disagreements between the above mentioned papers are given.

Numerical Integration Methods for Antenna Pattern Calculations—C. C. Allen, *General Engineering Laboratory, General Electric Company, Schenectady, N. Y.*—A study of numerical integration methods suitable for antenna pattern calculations was conducted for the purpose of determining which method provides a given accuracy with the greatest economy. The accuracy for a given method depends on the number of points at which the integrand is calculated while the cost for a given number of points depends on the complexity of the method. This paper discusses the general principles of numerical integration and outlines four methods in detail. The results of applying these methods on a digital computer to a simple cosine distribution are presented and analyzed. The relation of these results to those obtained for a pattern integral having a nonlinear phase function is discussed. The Gaussian quadratures are shown to have the highest degree of precision and lowest cost in general, while Filon's method is preferable when integrals having a linear phase function are calculated over a large range of pattern angle. The procedure for applying these methods to double numerical integration is outlined.

Forward Scatter from Rain—L. H. Doherty and S. A. Stone, *Radio and Electrical Engineering Division, National Research Council, Ottawa, Canada*—An experimental program to determine the amount of forward scatter from rain at 2720 mc and its effect on tropospheric scatter propagation was conducted during the summer of 1958. The program included a normal 90-mile over-the-horizon path and another path, between the same terminals, established by swinging the antenna beams 10° off-course at each end. The first path receives both atmospheric and rain scatter signals, the latter path a rain scattered signal only. It has been determined that the increase in signal level on the great circle path due to rain is from 5 to 10 db greater than would be expected on the basis of omnidirection scatter from rain drops. The effect of rain on pulse shape, diversity distance and fading-rate is also shown. Some other signal increases are seen to be related to precipitation, in particular with the presence of snow trails, although the mechanism is not yet understood.

Radar Attenuation by Atmospheric Oxygen—L. Blake, *Consultant, Radar Division, U. S. Naval Research Laboratory, Washington 25, D. C.*—The attenuation of radar signals by atmospheric oxygen is calculated for typical long-range-radar frequencies, assuming an antenna location close to the earth's surface, for targets at variable elevation angles and ranges. The basis of calculation is the Van Vleck theory of absorption as a function of oxygen partial pressure and temperature. Tables and graphs of results are presented for the range 100 mc to 10,000 mc. In this range the attenuation due to uncondensed water vapor is relatively negligible, so that in the absence of precipitation virtually all the attenuation is due to oxygen. This is shown to be appreciable for the long atmospheric paths traversed when targets are at great ranges and low elevation angles, amounting to approximately 3.5 db, for instance, at 3000 mc for a ray traversing the atmosphere twice at zero elevation angle.

Analysis Techniques for the Investigation of Short-Time Statistics of Temperature, Refractive Index, and Tropospheric Radio Wave Propagation Data*—F. X. Bostick, Jr., and H. W. Smith, *Electrical Engineering Research Laboratory, University of Texas*—Analysis techniques for investigating the short-time statistical fluctuations of experimental data relating to tropospheric radio wave propagation are described. Statistical parameters include the mean, standard deviation, amplitude distribution and power density spectra of temperature, index of refraction, and 915 mc radio wave propagation data. Results of these analyses are presented and observations relative to the period of stationarity of the power density spectra are made.

A comparison is made between the process of obtaining the power density spectra of signals recorded on magnetic tape with the technique of feeding the signals directly into the power spectrum computer. By the later method fluctuations in the average power density over a given bandwidth may be observed over a period of time. An additional advantage is the increased dynamic range made possible by elimination of all recording and reproduction equipment.

An Analysis of Observed Atmosphere-Induced Phase Variations in Line-of-Sight Microwave Propagation—M. C. Thompson, Jr., H. B. Janes, and A. W. Kirkpatrick, *Radio Propagation Engineering Division, Boulder Laboratories, National Bureau of Standards, Boulder, Colo.*—A knowledge of the statistics of atmosphere-induced variations in the phase of the received signal (*i.e.*, variations in electrical path length) is essential in evaluating the reliability of any system using radio waves for measuring distance and/or velocity. The National Bureau of Standards is studying phase variations in 9400 mc signals caused by atmospheric refractivity fluctuations along the propagation path.

This paper compares the power spectra of phase and refractivity variations observed in the widely differing climates of Hawaii and Colorado. It also discusses the correlation between phase variations and the refractivity observed at the path terminals. Such refractivity measurements offer a means of correcting for at least the longer-term variations in electrical path length.

Methods of Predicting the Atmospheric Refraction of Radio Rays—B. R. Bean, B. A. Cahoon, and G. D. Thayer, *National Bureau of Standards, Boulder, Colo.*—Several new methods of predicting the atmospheric refraction of radio rays have recently been proposed. Two of these, a statistical regression technique and an exponential model of refractive index height structure, require a knowledge of the surface value of radio refractive index at the transmitting point. Comparing the predictions of these methods with values of angular ray-bending calculated for representative refractive index profiles, it is found that both methods will yield results with an rms error less than 10 per cent of the mean bending for all elevation angles above roughly 1/2°. A third method, involving a correction to the values predicted by the exponential model, utilizes as an additional parameter the value of the initial refractive index gradient at the transmitting point and will predict ray-bending down to zero elevation angle with an rms error 10 per cent of the mean bending, or less, even in the case of superrefraction.

The Mechanism of Transhorizon Propagation: Layers vs Turbulence*—A. T. Waterman, Jr., *Stanford Electronics Laboratories, Stanford University*—In transhorizon propagation several models of the troposphere have been proposed as providing a suitable mechanism for microwave transmission. Without making detailed distinctions, these models fall into two broad categories. In one category, the atmosphere is pictured as being a basically turbulent structure which can be described only statistically. In the other category, the atmosphere is pictured as being basically stratified and the role of nearly horizontal layers is emphasized. It is the intent of this paper to examine some experimental evidence for distinguishing between the consequences of the two models.

An experiment having sufficient resolving power to isolate individual scatterers furnishes one criterion. Resolving power in angle can be provided by using a narrow-beam antenna. Resolving power in depth can be provided by transmitting a wide band signal. Resolving power in time can be provided by varying any of the above three dimensions rapidly. The rapid beam swinging experiments at Stanford University have

* The research reported here was supported by the Electronics Research Directorate of the Air Force Cambridge Research Center, Air Research and Development Command under Contract AF 19(604)-2249.

* The research reported in this paper was made possible through the support of the U. S. Army Signal Corps under Contract DA36(039)SC-73151.

provided good resolution in azimuth and time—sufficiently good to isolate individual scatterers in a large number of cases. Results of measurements made over the past year are reviewed. In a predominantly large number of cases they show arriving signals which are not characterized by beam-broadening at any one instant. The changes that occur in the arriving signal are frequently indicative of systematic, rather than random, changes taking place in the atmosphere. This work, together with supporting evidence from results of other experiments, is cited as favoring the layer model of the atmosphere over the turbulent model. The consequences of this conclusion are then discussed.

Vertical Incidence Radar Observations of the Electron Density vs Height Profile of the Ionosphere, and Scatter from the D Region—K. L. Bowles, *Central Radio Propagation Laboratory, Boulder Laboratories, National Bureau of Standards*—As announced informally by Gordon,* NBS has mounted a high sensitivity radar in a brief experiment at 41 mc which has verified the existence of incoherent backscatter by the free electrons of the ionosphere.† The incoherent scatter is found to exhibit a fading spectrum considerably narrower than had been predicted, a fact which suggests that the scatter is due to statistical fluctuations of the density of free electrons in an otherwise homogeneous medium. The implied ionospheric electron density vs height profile up to heights above 500 km is compared with the profile obtained up to the F2 region maximum by true height calculations.

As a second result of the same experiment, echoes are obtained from several strata in the range 70 to 90 km high and are interpreted to bear a close relation to regular VHF ionosphere scatter as observed at oblique incidence. The strength and fading properties of these echoes differ from what might have been expected based on theories of ionospheric scatter presently accepted, and may therefore force a re-evaluation of the theories.

The Scattering of Radio Waves by Free Electrons—B. Nichols, *Cornell University, Ithaca, N. Y.*—Gordon[1] has recently called attention to the possibility that a powerful radar could be used to detect the scatter of radio waves by free electrons. On the basis of an incoherent scattering theory the strength of the radar echo from a given volume would be proportional to the electron density and the frequency spectra of the echo would be a measure of the electron temperature. Bowles[2] has reported an apparent experimental verification of the presence of the expected echo but suggests that the calculation should be done on the basis of the statistical fluctuation of the density of particles on a scale comparable to the wavelength used. This "semi-incoherent scatter," he suggests, will have a frequency spectrum which is broadened only slightly by thermal fluctuations.

In this paper it is shown that both of the approaches mentioned above, when applied to scatter from heights above the *E* region of the ionosphere, lead to similar results both as to the strength of the echoes and their frequency spectra. The effect of the earth's magnetic field on the frequency spectra is also considered.

Investigation of Ionospheric Scatter Propagation at Extreme Distances*—S. C. Goldman, T. J. Goblick, R. Price, *Lincoln Laboratory, Massachusetts Institute of Technology*—This work was motivated by the study made by W. Abel† on the scatter propagation characteristics at 50 mc at very long distances. In these recent experinents a receiver and a tape recorder were carried in an airplane which flew directly away from the transmitting station and recordings were made of the receiver output at ranges of 1600 to 2000 miles. It is within this interval that the transmitter and receiver antennas lose their common scattering volume and a new mode of propagation begins.

These recordings were later used with a radiometer detector similar to the types used in radio astronomy experiments to measure power spectra. This detection scheme was used because at such great distances from the transmitter with a power of 500 kw the signal was too weak to be distinguished and accurately measured by ordinary methods. By this technique, curves of signal strength vs distance from transmitter could be established. The experimental results indicate that in this range interval there is a smooth transition from ionospheric scatter to a mode which resembles just-beyond-the-horizon tropospheric scatter. A geometrical model constructed on this basis has yielded results which agree well with the experimental data.

Further Aspects of 200 mc H-Scatter Signals[1]—J. L. Heritage, S. Weisbrod, W. J. Fay, and L. A. Morgan, *Smyth Research Associates, San Diego, Calif.*—At the fall meeting of USRI, evidence was presented for a 200 mc E layer ionospheric forward scatter propagation mode associated with the earth's magnetic field. Using a sensitive 200 mc system at oblique incidence, H-Scatter signals were observed exhibiting rapid fading and high aspect sensitivity. The H-Scatter signals were observed only from receiving sites—located well south of the transmitter beam great circle—which approached or corresponded to the position for specular transmission via ion clouds strung out along lines of the earth's magnetic field.

In this paper, the analysis of H-Scatter properties is extended to include:

a) Correlation of H-Scatter with simultaneous vertical incidence soundings of the E layer "hot spot" by C-4 ionosonde and by a Stanford University high power 27 mc radar.

b) Comparison of H-Scatter diurnal variation with 50 mc oblique incidence auroral transmission reported by Dyce.

c) Comparison between burst rate and duty cycle of meteor bursts and burst like H-Scatter as a function of time of day and distance of receiver from the great circle path.

A search was made for H-Scatter signals at 55 mc using Channel 2 TV as source. For three field sites, burst rate and duty cycle are given vs azimuth of the directive receiving antenna. It could not be definitely established from these data whether H-Scatter, as known at 200 mc, contributed to the received bursts.

Results of further H-Scatter experiments scheduled for early 1959 will be discussed.

Phase Stability Study of Ionospheric Scatter Medium*—C. M. Beamer, *Collins Radio Company, Cedar Rapids, Iowa*—During October, 1958, an experiment was performed on a 1295 km ionospheric scatter circuit from Long Branch, Ill., to Boulder, Colo., to determine the short-time phase perturbations to a continuous radio wave caused by the medium. Two frequencies, near 30 mc and 50 mc, were used.

A stable CW signal was transmitted which was used at the receiver output to drive keyed mechanical resonators. One resonator was used as the local phase reference, while a second integrated the changes in phase of the signal. The process was reversed at twenty-millisecond intervals. The resonator outputs were compared in a phase detector. In a second test, the resonators, in turn, served as the local reference and the integrated phase was compared in a phase detector directly with the instantaneous phase of the signal.

Distribution curves of the phase changes are generally not log-normal. Close in (near zero degrees), they appear standard but become nonstandard at large perturbations because of meteor and multipath disturbance. RMS values were found from 5 to 25°. The median phase shift was about 10°. Studies of diurnal variations indicate less phase shift at the noon and evening hours than at midnight and early morning, the difference being as much as 2 to 1. Increased phase perturbation at the higher frequency could not be confirmed because of near marginal signal-to-noise operation at 50 mc. Deep fading produced instantaneous phase shifts of as much as 300° in 20 ms and a net of 100° with rates of phase change up to 100,000° per second. Median values were 20 degrees with rms values approaching 50 degrees. Meteors caused similar changes at the onset of trail information. Maximum rate of change observed was over 200,000° per second.

Theory of Spread F—J. Reneau, *Cornell University, Ithaca, N. Y.*—On the assumption that aspect sensitivity plays a major role in the energy backscattered from ionized irregularities elongated along the earth's magnetic field, a formula for the delay time associated with a ray from the ionospheric

* W. E. Gordon, "Incoherent Scattering by Free Electrons with Applications to Space Exploration by Radar," presented to URSI-IRE meeting, Pennsylvania State University, October 22, 1958.

† K. L. Bowles, "Observation of vertical incidence scatter from the ionosphere at 41 mc/sec," *Phys. Rev. Letters*, vol. 1, p. 454; 1958.

[1] W. E. Gordon, PROC. IRE, vol. 46, pp. 1824–1829; November, 1958.

[2] K. L. Bowles, *Phys. Rev. Letters*, vol. 1, pp. 454–455; December 15, 1958.

* The work reported here was performed at Lincoln Laboratory, a technical center operated by Massachusetts Institute of Technology with the joint support of the Army, Navy and Air Force.

† "UHF Signal Level Measurements Along a 2000 Mile Path," presented at the URSI Spring Meeting of 1958.

[1] This research was sponsored by Rome Air Development Center, Air Research and Development Command, Griffiss Air Force Base, New York, under Contract No. AF 30(602)-1624.

* Experiment performed for National Bureau of Standards under Contract CST 7143 by Collins Radio Company.

sounder to the position of perpendicularity in the F region, with allowance for refraction, has been derived.

In the hope that this mechanism may explain the phenomenon of spread F, computation of delay time vs frequency were carried out for several stations located at various magnetic latitudes, and the results compared to observed ionograms. It is concluded that the model does not explain arctic spread F but clarifies the main features of the equatorial spread F.

Observations of F Layer Scatter Near the Magnetic Equator—K. L. Bowles and R. S. Cohen, *Central Radio Propagation Laboratory, National Bureau of Standards, Boulder, Colo.*—At the 1958 Spring URSI meeting* the authors presented a tentative correlation identifying one kind of forward scatter, observed at 50 mc over the 2580 km path from Antofagasta to Guayaquil, as concident with equatorial spread-F over Huancayo. More recent experiments involving height finding by a) variation of antenna radiation patterns and b) oblique incidence pulse delay measurements, demonstrate that the scatter originates in the height region 250 to 600 km. The results of the several types of oblique measurement are compared with both the regular ionospheric sweep frequency soundings and special soundings using a high gain antenna with the C4 at Huancayo, in order to define better the correspondence of the oblique scatter with equatorial spread-F. It is shown that this scatter differs significantly from another type of scatter, attributed to the F region and observed during IGY in the Far East.†

This work has been supported jointly by the U. S. National Committee for the IGY through a grant from the National Science Foundation, by the Voice of America, and by the National Bureau of Standards.

Experimental Study of the Decay of Long Enduring Meteor Echoes—R. V. Gaertner, *Central Radio Propagation Laboratory, National Bureau of Standards, Boulder, Colo.*—The decay characteristics of long enduring echoes from meteor trails have been compared with the decay theories of Booker-Cohen[1] and Manning-Eshleman.[2] The meteor echo data was taken on the NBS, Long Branch, Ill., to Boulder, Colo., oblique incidence circuit at 50 mc and 73 mc. Digital recording and analysis equipment were used. It was found that both theories were represented in roughly equal numbers and that the Booker-Cohen types were generally of shorter duration than the Manning-Eshleman types. The existing decay theories account for less than half of the number of echoes studied. Many of the remaining echoes probably result from conditions somewhat more complicated than the simplified assumptions required in developing the theories.

The Production of Whistlers by Lightning—E. L. Hill, *School of Physics, University of Minnesota, Minneapolis 14, Minn.*—The evidence on the production of whistlers by lightning suggests that conditions over a whole storm area are involved, rather than the properties of individual lighting strokes. This may imply the existence of some type of local ionospheric control by storms having particular characteristics. Possible conditions are 1) very high altitudes for the upper electrical charge distribution, leading to extended general electrical fields, 2) correlation between successive ground strokes, 3) exceptional electrical activity in cloud-cloud strokes, perhaps correlated with cloud-ground strokes.

VLF Radiation Spectra of Lightning Discharges—W. L. Taylor and A. G. Jean, *National Bureau of Standards, Boulder, Colo.*—Spectral analyses are given of the groundwave portion of thirty-three sferic waveforms recorded from cloud-to-ground lightning discharges which occurred at distances ranging between 150 and 600 km from Boulder, Colo. Frequencies of peak energy lie between 5 and 10 kc, which agree favorably with other published results. The average value of energy calculated from the ground-wave pulses was found to be 26,600 joules, which is lower than values derived from other experiments. Various parameters, such as the peak amplitude and duration of the first half-cycle, are related to energy.

Observation of Some Spectral Components of Sferics—R. F. Linfield, *National Bureau of Standards, Boulder, Colo.*—The electromagnetic energy radiated from a lightning discharge is extremely variable. That is evidenced in amplitude and phase variations among the various spectral components. Statistical quantities of sferics having specified characteristics have been measured using equipment developed by the National Bureau of Standards. One such characteristic which has been measured is the amplitude of the pulse formed by a band-pass filter. Pulses whose amplitude exceed a preset triggering level were automatically counted and recorded. Three separate filters were used with center frequencies of 10 kc, 40 kc and 100 kc with bandwidths of 60 per cent, 30 per cent and 30 per cent, respectively. Measurements were made at two geographical locations—Oregon and Colorado, and at two differing periods—summer and fall. The variations observed are attributed primarily to the seasonal change and not the geographical change.

The distribution of sferic rates as a function of triggering level and filter frequency are presented for both omnidirectional and narrow sector measurements.

Observed Time and Directional Variations in Sferic Activity—R. H. Doherty, *National Bureau of Standards, Boulder, Colo.*—Recently, the National Bureau of Standards has made measurements of the number of sferics per second (sferic rate) that exceed a preset level. These sferic rates show temporal variations attributed to thunderstorm activity mainly within the United States. Particularly, diurnal effects in the summer relate to the rise and decay of late afternoon and early evening thunderstorms. Diurnal effects are compared to day-to-day effects for the same periods of time. Seasonal effects are also covered to the extent possible with limited data.

Sferic densities (sferics per degree per second) are plotted on polar paper using a logarithmic scale to show the full range of amplitudes. The effect of seasonal and geographical changes upon the sferic densities is considered. Linear plots are utilized to show typical daily thunderstorm variations.

Sferics observed in a narrow sector are interpreted to represent only one or two thunderstorms. The cumulative distributions of the rate vs amplitude observed in a narrow sector are distinctly different from the corresponding omnidirectional distributions. Amplitude distributions of sferics occurring in a narrow beam are discussed with respect to individual storms.

The Inclusion of Antenna Patterns in Electromagnetic Boundary-Value Problems*—S. Stein, *Hycon Eastern, Inc., Cambridge, Mass.*—Electromagnetic boundary-value problems in three dimensions are usually solved in terms of point sources (the limiting form being incident plane waves). Such solutions are the Green's Functions, from which, in principle, the field resulting from any distribution of current sources may be determined by integrations, although the actual integrations are usually too knotty to ever be carried out. On the other hand, there are theoretical problems in which it would be desirable to calculate the effects in terms of measurable antenna patterns, as for example, when a beam is partially occluded by a large obstacle. The present paper indicates a first step in this direction, namely a systematic technique for establishing such a formulation in problems which can be solved naturally in spherical coordinates. The "classical" spherical-mode wave functions are employed in this representation. The discussion includes a description of appropriate representations for fields and antenna patterns, and of the wave-function addition theorems necessary for establishing the formulation.

Generalized Snell's Law—K. S. Kelleher, *Aero Geo Astro Corporation, 1914 Duke Street, Alexandria, Va.*—Snell's Law, as applied to constant refractive index media, provides a basic condition on ray directions. In media of variable refractive index, it is desirable to have a similar condition.

This paper employes a vector approach to yield a derivation of a generalized condition on ray path directions. The derivation gives a relationship at a point on the ray path between the rate of change of the ray tangent and the gradient of the refractive index. It is therefore independent of any particular coordinate system. This condition is then applied to several coordinate systems by setting up a differential equation in the particular system of interest and showing solutions useful for lens design. As expected, the rectangular index variation yields the familiar $n \sin \alpha = \text{constant}$ and

* This research was performed as part of studies under contract NOnr-2632(00) with the Office of Naval Research.

* R. Cohen and K. L. Bowles, "50 mc Oblique Transmission Experiment Near the Magnetic Equator," presented to URSI-IRE meeting, Washington, D. C.; April, 1958.

† R. Bateman, J. Finney, E. Smith, L. Tveten and J. Watts, "International Geophysical Year Observations of F-Layer Scatter in the Far East," in publication.

[1] H. G. Booker and R. S. Cohen, "A theory of long-duration meteor-echoes based on atmospheric turbulence with experimental confirmation," *J. Geophys. Res.*, vol. 61, no. 4, p. 707; 1956.

[2] L. A. Manning and V. R. Eshleman, "Discussion of the Booker and Cohen paper, 'A theory of long-duration meteor-echoes based on atmospheric turbulence with experimental confirmation'," *J. Geophys. Res.*, vol. 62, no. 3, p. 367; 1957.

the media of spherical symmetry has the condition $nr \sin \alpha = \text{constant}$.

Critical Pressure and Power for High-Frequency Breakdown—A. S. Dunbar, *Missiles and Space Division, Lockheed Aircraft Corporation, P.O. Box 504, Sunnyvale, Calif.*—The condition known as breakdown in high-frequency antennas and components is the result of a gas discharge in the air in or surrounding the antenna or component. It should be remarked at the outset that there are two aspects of the breakdown phenomenon, both of which are called breakdown but which are different in nature. The electric arc discharge which occurs at high RF power and at air pressure ranging from a fraction of one atmosphere to several atmospheres is one aspect. The glow discharge, or corona, which occurs at relatively low power and low pressure is less well known and is the aspect of breakdown of most concern in missile antenna technology.

The mechanism which produces corona is essentially the same as that which leads to the arc discharge. So long as the pressure is high enough or the power low enough that the energy imparted to the gas is not sufficient to initiate ionization in considerable quantity, discharge will not occur. However, as soon as sufficient ionization by collision does begin to occur, the corona will begin to be visible, for then numbers of ions and electrons are produced and excitation of the gas is the result. When gas atoms or molecules are excited by energetic collisions, they give off light of characteristic frequencies, which for air appears purple. For this reason the breakdown is called a glow discharge. The glow discharge may become an arc discharge under certain conditions of power, pressure, and geometry.

Experiments have shown that there can be found a critical pressure for which the RF power necessary to cause the glow discharge is minimum. For either higher or lower pressure, more RF power must be supplied to cause the discharge. Furthermore, it has been found that this minum is proportional to the frequency, at least in the case in which diffusion is the predominal loss mechanism.

It is the purpose of this paper to present a discussion of the conditions for critical breakdown and to establish the fundamental relations among pressure, power, and frequency. The theoretical analysis shows that the ratio of the RF electric field to the pressure is a constant, independent of frequency, and that the critical pressure is a linear function of the frequency. Curves of critical pressure and power as a function of frequency are shown, together with experimental results.

Use of the "Q" Concept in Antenna Evaluation—J. R. Gruber and J. A. Kuecken, *AVCO Manufacturing Corporation, Crosley Division, Cincinnati 15, Ohio.*—An exposition of the concept of "Q" as applied to antenna equivalent circuits is presented. Use is also made of the concept of fractional de-tuning and a novel modification of the Smith Chart presented to permit direct transformation of impedance data into terms of antenna "Q" in the classical circuit sense. The value of this concept as a "figure of merit" for comparison of varying types of antenna data is developed with representative experimental data given. This approach is shown to be a powerful tool, particularly in the development of antennas with dimensions small compared to a wavelength.

Excitation and Propagation of Surface Waves—F. C. Karal, Jr., and J. B. Keller, *Institute of Mathematical Sciences, Division of Electromagnetic Research, New York University*—A geometrical theory is developed for the analysis of surface wave excitation and propagation. The surfaces along which the surface waves propagate may be either curved or flat, and may have either constant or variable properties. The theory is based on the concept of a complex or imaginary ray. The excitation coefficient which enters the theory is determined from the solution of a canonical problem—that of a line source over an impedance plane. Then the theory is applied to the surface wave excited by a line source, on a wedge with variable surface impedance. The result agrees precisely with the asymptotic form of the exact solution. Another application is made to the surface wave excited on a cylinder by a line source. The result also agrees with the exact solution.*

Surface-Wave Propagation on an Elliptical Dielectric Rod—J. C. Wiltse, *Electronic Communications, Inc., Timonium, Md.*—A formal solution has been obtained for the problem of electromagnetic wave propagation on a straight dielectric rod of elliptical cross-section, and several general conclusions have been drawn from the resulting field equations. In general the field expressions for possible modal solutions cannot be described in terms of single orders of the Mathieu functions (if elliptic cylinder coordinates are used) or of sinusoids and Bessel functions (if circular cylinder coordinates are used). An exception to this statement occurs when the eccentricity of the ellipse is zero. Except for the case of a circular cross-section it is very difficult and time consuming to obtain specific values of guide wavelengths, cut-off frequencies, and other numerical data. The theoretical results are in contradiction with information given in a previously published paper, but the latter is shown to contain several significant errors.

In a companion experimental investigation the attentuation and approximate field extent have been measured for several dielectric image lines at frequencies near 35 and 70 kmc. Various semi-elliptic cross-sections were used for the dielectric materials. As anticipated, attenuation was found to be a function of the shape of the cross section; for certain eccentricities the attenuation can be reduced below that for a semicircular dielectric cross section with the same area. Several structures for shielding a dielectric image line will also be described.

Ohmic Losses in Conducting Wedges—R. M. Chisholm, *Queen's University, Kingston, Ontario, Canada.*—The electromagnetic boundary conditions which must be imposed at the faces of imperfectly conducting wedges are examined carefully. The "surface impedance" condition used in calculating waveguide wall losses can produce fields which do not satisfy the Meixner edge condition and which yield very high ohmic losses near the tip of the wedge. An exact analysis shows the losses near the wedge tip to be small and the "surface impedance" condition, therefore, is modified to give an approximate solution to wedge problems in which the perfectly conducting solutions are known.

A simple waveguide having a circular cross-section, a sector of which is occupied by a metal wedge, is used as an example. The tangential magnetic field variations along the surface of the wedge are shown graphically, demonstrating a large deviation in the magnetic field from the perfectly conducting solution near the tip of the wedge.*

Radio Phase Distortion—A Mechanism for Transhorizon Radio Propagation—J. B. Smyth, *Smyth Research Associates, San Diego, Calif.*—The phase front of a radio wave propagated at small grazing angles to the earth's surface is distorted by inhomogeneities in the refractive index of the atmosphere. The new propagation wave-numbers generated by this distortion carry energy forward parallel to the earth's surface in the lower regions of the troposphere. This mechanism has been singularly successful in describing certain phenomena associated with the diffraction of light, and its extension to transhorizon radio wave propagation is discussed.

Weather Dependence of Fast Fading Spectra at 915 mc—J. A. Bradshaw, *General Electric Research Laboratory, Schenectady, N. Y.*—Spectra of envelope records of CW signal transmitted at 915 mc from Bedford, Mass., to Schenectady, N. Y., have been taken and analyzed in cooperation with the University of Texas over a period of more than a year. These spectra show relatively slow variations in the "knee" of the curve and the slope beyond the "knee." These variations can be correlated to some extent with changes in the weather over the path of transmission. Implications of these correlations for the study of the mechanisms of transmission will be discussed.†

The Correlation of Meteorological Observation with the Signal Received in Tropospheric Propagation—L. G. Abraham, *General Electric Research Laboratory, Schenectady, N. Y.*—There has been considerable interest in the past in being able to predict the performance of radio propagation paths using meteorological parameters. Such ability would be an invaluable aid to the system designer. Some success has been achieved by Bean and Meaney of NBS using monthly median values of the received signal and surface index of refraction.[1] But the problem remains of predicting the hour-to-hour variations in path loss.

* The research reported in this paper has been sponsored by the Electronics Research Directorate of the Air Force Cambridge Research Center, Air Research and Development Command, under Contract No. AF-19(604)-1717.

* The research reported herein is from a Ph.D. thesis submitted to the University of Toronto by the author and supported by Extramural Grant No DRB 5540-02 from the Defence Research Board of Canada.

† The research reported in this paper has been sponsored by the Electronics Research Directorate of the Air Force Cambridge Research Center, Air Research and Development Command. The publication of this paper does not necessarily constitute approval by the Air Force of the findings or conclusions contained herein.

[1] B. R. Bean and F. M. Meaney, PROC. IRE, p. 1419; October, 1955.

A multiple regression analysis has been made of the radio and weather data collected during one year on a Bedford, Mass., to Schenectady, N. Y., propagation link. (This radio link was about 135 miles long and was operated at a frequency of 915 mc. As such, it represented a short, over-the-horizon tropospheric propagation path.) Hourly median values of received radio signal were used. Radiosonde runs at Albany and Boston supplied the corresponding weather parameters. The best fit of the data had a 0.75 correlation between predicted and observed hourly median radio signal level as expressed in dbm.

Statistical tests of the regression fit revealed that the most significant meteorological variables, among those available, were water vapor content and stability index. There was evidence that the predominant radio propagation mechanism alternated between two choices.*

Reflection from Rounded Foreground Terrain†—L. J. Anderson, *Smyth Research Associates, San Diego 11, Calif.*—Comparison of experimental height-gain data with a simple ray treatment, in the case of rounded foreground terrain features, results in good agreement when the features are reasonably smooth. Six different cases have been compared over diffraction paths, and the ray model has been found to yield heights of maximum and minimum which are in close agreement with observation. In the case of scatter paths, the patterns are largely smoothed out. This is shown to be consistent with the model, because the energy arrives over a range of angles.

The studies were made in southwestern Arizona over path distances from 14 to 84 miles, and at frequencies from 1700 to 3300 mc.

The Effects of Elevated Horizons and Antenna Height on Tropospheric Scatter Transmission—J. A. Holladay and K. F. Wright, *Collins Radio Company, Cedar Rapids, Iowa.*—It is well known that the transmission loss on a tropospheric scatter circuit is considerably increased by elevated horizons. A family of curves has been developed which relates elevated horizon loss to combined horizon angles and path length. The curves are based on the fact that transmission loss varies with both scatter angle and height of intersection. Considerable experimental data has been gathered in support of the elevated horizon loss curves, and they have proved a very useful aid to predicting scatter circuit performance.

The effect of antenna height on transmission loss has been studied on a 172-mile scatter circuit. A 15-foot parabolic antenna was moved from ground level to 200 feet above ground and compared with a second 15-foot antenna at ground level. The data offered some interesting problems of interpretation due to an apparently uncorrelated long-term fade which existed at times between the two antennas. The combined results of many tests showed no decrease in transmission loss due to increased antenna height. Thus, there was no height gain observed on the circuit.

An Exact Earth-Flattening Procedure—B. Y.-C. Koo, *Electromagnetic Research Corp., Washington, D. C.*—An earth-flattening procedure which yields an exact solution to the differential equation of the height-gain function for arbitrary spherically stratified atmosphere over spherical earth is developed. This involves the use of an exponential height scale (first suggested by E. T. Copson to M. H. L. Pryce). From this procedure it turns out that a given solution of the usual height-gain equation is equivalent to the same solution of the exact equation with a slightly modified index profile. This is illustrated for the case of the standard atmosphere. As a result, it is suggested that the definition of the standard atmosphere be modified so as to be a linear function in the exponential coordinate system.

Separation of Specular and Scatter Content in Pulse Radar Return at Near-Vertical Incidence—F. J. Janza, R. K. Moore, and B. D. Warner, University of New Mexico, Albuquerque, N. Mex. (No abstract available).

Results on Critical Frequency Studies for the Northern Hemisphere—G. E. Hill, *AVCO Manufacturing Corp., RAD, Wilmington, Mass.*—Monthly medians of f_0E and f_0F_2 for January, March, and June, 1957, were collected from all available Northern Hemisphere ionospheric sounding stations. The data was arranged according to G.M.T., in 3-hour intervals, plotted on polar stereographic maps and analyzed for isopleths of the critical frequencies (8 maps per month). Instantaneous synoptic data from the I.G.Y. network, including f_0E_s, was handled similarly for July 11–15, 1957 (8 maps per day).

The monthly maps show the following: As expected the daytime f_0E essentially follows a cosine dependence on the solar altitude. The f_0F_2 generally decreases toward high latitudes forming a "polar low." This polar low is more extensive in winter than summer. This polar low moves around the globe at high latitudes following the sun, the winter radius being about twice the summer radius. The high daytime winter values of f_0F_2 in auroral latitudes are related to the position of the polar low. Evidence of solar tidal effects is found (the polar low becomes a complex of three lows).

The synoptic series in July show that the features evident on a monthly average are present on a daily basis also. The strong regularity of the E layer appears daily as well as monthly. The daily features of f_0F_2, however, show some important departures from the monthly median variations. These departures, or disturbances, have characteristic velocities ranging from about zero to several hundred meters/seconds. There exit preferred areas of development, but these areas are not permanent. Depressions occur at all times of the day and frequently about noon. The occurrence of sporadic E in temperate latitudes is mainly in a broad belt nearly encircling the earth. A minimum is found at early morning longitudes. At night E_s is found in northern latitudes. During the five-day period wide departures from this simplified picture for E_s occur. There appears to be some correspondence between patterns of f_0F_2 and of E_s occurrence.

The effect of the ionospheric general circulation is discussed, although no specific circulation model is presented.*

Electron Density Along the 75°W. Meridian Station Chain—J. W. Wright and G. H. Stonehocker, *National Bureau of Standards, Boulder, Colo.*—Investigation of the electron density (in terms of plasma frequency, f_N) as a function of height for a chain of stations on or near the 75°W. meridian for several quiet days in September, 1957, has been accomplished. The station chain includes Chimbote and Talara, Peru; Bogota, Colombia; Panama, Canal Zone; Puerto Rico; Grand Bahama Is. and Ft. Monmouth, N. J. The method of investigation was to reduce hourly ionograms to give true heights of reflection at 0.2 mc frequency intervals from 1.6 mc to f_0F_2. The method after Budden was used in an IBM 650 computer program. Another computer program was used to interpolate the values of electron density at fixed heights, compute height of the maximum, and integrate the electron density up to h max. The data is presented in the form of diurnal curves of the heights of f_N for each station and cross-section plots of heights of f_N through the normalized 75°W. meridian for each two hours of the day. The results of this investigation present several areas of further work, including extension of the chain into higher latitudes and more extensive coverage within. The investigation is a continuing project of the true height group at the National Bureau of Standards.

A Study of the F2-Layer During Eclipses—T. E. VanZandt, R. B. Norton, and G. H. Stonehocker, *National Bureau of Standards, Boulder, Colo.*—The electron density vs time at 10 km height intervals has been computed from ionograms taken during the eclipses at Baguio and Guam on June 20, 1955, and at Danger Islands on October 12, 1958.

The continuity equation with transport neglected and with various hypotheses about the photochemical processes has been solved using the Danger Islands electron density curves, which are so simple and regular as to suggest that transport is of little importance. In every case the derived loss times have been found to be considerably smaller than the attachment times determined by other workers who used various methods on both eclipse and nighttime data. However, the results of most workers involve the same scale heights: about 50 km and 300 km and somewhat larger at 400 km. These results are also in good agreement with the recent atmospheric scale heights derived from satellite data.

It is shown by synthesis from the electron density profile at totality, using the derived loss times, that the eclipse F1½-layer, which was strong at Baguio and Danger Islands, is essentially due to the decrease of the rate of electron production with height.

* The research reported in this paper has been sponsored by the Electronics Research Directorate of the Air Force Cambridge Research Center, Air Research and Development Command. The publication of this paper does not necessarily constitute approval by the Air Force of the findings or conclusions contained herein.

† This work was sponsored by the Signal Communications Dept., Army Electronic Proving Ground, Fort Huachuca, Ariz.

* This study was conducted under contract AF 19(604)-4092 with the Electronics Research Directorate, Air Force Cambridge Research Center, Bedford, Mass.

The Determination of Consistent Ionospheric Parameters for Region *F* from Electron Density-Height Profiles*—D. Grant and E. R. Schmerling, *Ionospheric Research Laboratory, Pennsylvania State University, University Park, Pa.*—Present theories of region *F* favor a Chapman-like electron production function, a height-dependent attachment-like loss term and a vertical drift velocity. Considerable uncertainty exists at present regarding the parameters q_0, h_0, and H which enter into the electron-production function. An attempt has been made to obtain consistent values of these from data for a number of different ionospheric sounding stations.

We assume that electron-production and loss are the most important factors governing the day time behavior of region *F* at moderate latitudes, and that the effect of electron movements is superposed as a perturbation. From the diurnal variation of the electron density, N, we estimate, to a first order, the unperturbed values of N at noon, and construct an electron density-height profile. Using values of loss-cofficient evaluated independently,† a process of curve fitting enables q_0, h_0 and H to be found.

For the stations Washington, Talara, Panama and Slough we obtain consistent values of h_0 and H of the order 180 km and 45 km approximately, with q_0 of the order 650 electrons per cc per second for summer 1957, in good agreement with values obtained independently from *F*1 region data.

Diurnal Variation of Vertical Drift in the *F* Region[1]—S. Chandra, J. F. Gibbons, and E. R. Schmerling, *Ionosphere Research Laboratory, Pennsylvania State University, University Park, Pa.*—Vertical drift velocities for electrons in the *F* region have been computed from experimentally obtained electron-density-height profiles. Assuming an attachment type of loss term and a reasonable Chapman model for electron production,[2] it is possible to integrate the continuity equation and evaluate v at any height and time. The night time values of v are computed on the assumption of zero electron production. To give continuity during the day, limits must be assigned to Q.

Computation of v for the three equatorial stations—Panama, Talara and Huancayo, shows periodic variation during 24 hours with an amplitude of the order of 25 m/second. The velocity is downwards during the night and upwards during the day.

Electron Density Determination in a Non-Uniform Ionosphere from Rocket Dispersion Measurements—J. S. Nisbet, *Ionosphere Research Laboratory, Pennsylvania State University, University Park, Pa.*—This paper describes an improved method of computing the electron density-height profile of an ionospheric layer deduced from Faraday rotation fading patterns of high frequency signals radiated from ascending long range missiles.

A previous paper has shown how the profile can be deduced by means of a computing program assuming that the ionosphere is horizontally stratified in the region of interest. Here methods are discussed for establishing correction factors and error limits for the effects of latitude and longitude variations using reduced ionograms from the launch point and down range sounding stations.

Ionospheric electron density-height profiles deduced from the launch records of IGY satellites are given.

High Electron Density Gradients Observed with Rockets—J. Carl Seddon, *National Aeronautics and Space Administration, Washington 25, D. C.*—The data records for eight rocket flights at New Mexico and Manitoba, Canada, have been reviewed with particular attention to electron density gradients. Evidence for such gradients between 66 and 200 km is presented. One gradient is always found to be present near the mesopause. The others are variable in occurrence and altitude, except for *E*-region gradients which have a strong tendency to occur at the particular altitudes of 100, 105, 110, 117, and 129 km. The gradients are mostly associated with thin layers, the maximum thickness being 2 km. In the latter case, the gradient was approximately 10^6 electrons per cc per km. A comparison is shown of the profile of a New Mexico sporadic-*E* condition with the profile obtained by the British at Woomera, Australia, which reveals a striking similarity. The difference between spread-*F* gradients and lower altitude gradients is briefly discussed.

Rocket Measurements of Electron Densities Through an Aurora—J. E. Jackson and J. C. Seddon, *National Aeronautics and Space Administration, Washington 25, D. C.*—An Aerobee-Hi rocket, instrumented to measure electron densities, was fired at Fort Churchill, Canada, directly into an overhead auroral display. The rocket was launched at 0025 CST on November 24, 1958, and reached an altitude of 207 km. The CW propagation method was used, and electron densities were measured at altitudes between 50 and 150 km. The higher altitude data are unusually irregular due to variations in the total electron density content along the rocket-to-ground propagation path. The ionization present at night in the absence of auroral activity was determined by a previous rocket flight, launched at 0017 CST, on February 4, 1958. Since both experiments were conducted at the same location, in 1958, at dates nearly symmetrical with respect to the summer solstice, and at the same time of night, only one parameter was significantly different, namely the auroral activity. Both flights show virtually no ionization (less than 1000 el/cc) up to an altitude of 84 km. Between 100 and 150 km, the flight with no aurora indicates an average density of about 10^4 el/cc, whereas the flight with aurora reveals an average density at least 10 times greater. The electron density profile for the auroral flight exhibits three peaks at approximately 128, 138 and 152 km, where densities exceeded 4×10^5 el/cc. The *P'-f* records taken during this flight reveal high electron density gradients at approximately the same altitudes. Other correlations with the *P'-f* records are discussed.

Some Applications of Dynamic Programming to Statistical Communication Theory—R. Bellman and R. Kalaba, *The RAND Corporation, Santa Monica, Calif.*—The purpose of this paper is to describe some applications of the functional equation technique to dynamic programming to the study of various multistage stochastic decision processes arising in the statistical theory of communication.

The point of departure is a generalization of the well-known Kelley model of a communication system in which the user seeks to maximize the utility of a noisy channel. This provides an opportunity to reinterpret the Shannon concept of channel capacity. It leads to a discussion of optimal usage of channels having statistical properties that are initially unknown, but which can be more precisely determined in the course of the communication process.

Other applications to modulation theory and feedback communication systems are indicated, the aim throughout being to show how quite general communication processes can be treated in unitary fashion by the functional equation technique of dynamic programming.

An Example and Extension of Capacity Calculation of a Certain Discrete Channel with Memory*—S.-H. Chang and P. G. McHugh, *Northeastern University, Boston, Mass.*—In a previous paper† the capacity of a certain asymmetrical binary channel is studied under the following conditions: 1) Blocks of binary digits are used as the transmitting symbols. 2) The channel resumes its quiescent state at the beginning of each block. 3) The memory of the channel is characterized by the dependence of the noise probabilities for each digit upon the preceding digit or digits in the same block. To illustrate the application of the method some calculations are made in the present paper on a hypothetical channel which reveal certain relations between the effects of the signal-to-noise ratio and the bandwidth (upon which the memory depends) on the capacity of the channel. It is found that the capacity may be increased if the interdigital interference is tolerated to a much greater extent than commonly allowed in practice. Also, by using special weightings of binary pulses the effect of memory on the capacity can be minimized. This is due to a better matching of the waveform with the channel. The method of calculation is also extended from the binary channel to the m-nary channel.

Single Error Correcting Codes for Asymmetric Binary Channels[1]—W. H. Kim and C. V. Freiman, *Department of Electrical Engineering, Columbia University, N. Y.*—In a highly asymmetric binary channel it

* The research reported in this paper is sponsored by the USA National Committee for the IGY under Project No. 6.9.

† J. A. Ratcliffe, *et al.*, *Phil. Trans.* A, vol. 248, p. 621; 1956.

[1] The research reported in this paper has been sponsored by the USA National Committee for the IGY under Project No. 6.9 and by the Geophysics Research Directorate of the Air Force Cambridge Research Center, Air Research and Development Command, under Contract AF 19(604)-4563.

[2] Ratcliffe, Schmerling, Setty and Thomas, *Phil. Trans. Roy. Soc.*, vol. 248, pp. 621–642; March, 1956.

* This research was made possible through the support of the Electronic Research Directorate of the Air Force Cambridge Research Center, Air Research and Development Command.

† Sze-Hou Chang, "Capacity of a Certain Asymmetrical Binary Channel with Finite Memory." Scheduled for publication in the December, 1958 issue of IRE TRANSACTIONS ON INFORMATION THEORY.

[1] This work was supported by National Science Foundation Grant G3676.

may be sufficient to correct only those errors which result from incorrect transmission of one of the two code elements. The minimum distance requirement for pairs of single error correcting code characters in such a case is weaker than in the case of a symmetric channel. This weaker requirement is used to generate codes which generally contain more code characters than similar length single error correcting codes designed for use in a symmetric channel. The asymmetric code is symbol-correcting but not systematic. In the coding scheme, the first $[n/2]$ positions of the n-length code characters is specified independently and a single error correcting code of length $n-[n/2]$ is used to generate the remaining positions. The method of error correction is described and examples of generation and correction are included. Minimum weight-distance requirements for multiple asymmetric error correcting codes are included. Correct transmission of equiprobable messages is discussed briefly and the code which yields the highest average probability of correct transmission of four equiprobable messages through a highly asymmetric channel is included as an example.

On Band-Limited Signals with Prescribed Arbitrarily Spaced Samples—B. F. Logan, *Bell Telephone Laboratories, Inc., Murray Hill, N. J.*—An exposition is given of recent results pertaining to the construction of band-limited signals with prescribed arbitrarily spaced samples. Two implications of these results are examined in some detail.

First, it is noted that the time intervals between any finite number of prescribed samples may be arbitrarily small, suggesting the possibility of signalling over an ideal low-pass channel at an arbitrarily high rate for any finite length of time. However, it is demonstrated that the apparent high-frequency content of such signals is the result of near cancellation of extremely large low-frequency signals; and for this reason, signalling at higher than Nyquist rates is impractical.

Secondly, it is noted that for sufficiently large n, the nth derivative of any finite message is completely characterized (to within a scale constant) by its zero crossings. The behavior of functions having only real zeros is considered. Practical difficulties encountered in zero-crossing encoding and decoding are discussed. Some experimental results are included.

The Compatibility Problem in Single-Sideband Transmission—K. H. Powers, *David Sarnoff Research Center, RCA, Princeton, N. J.*—Through the use of the concept of the analytic signal, the relation between the inphase and quadrature components and the instantaneous envelope and phase of a single-sideband signal are considered. A theorem of Paley and Wiener is shown to be directly applicable to the study of the compatibility problem in single-sideband transmission. For example, if an envelope is assumed to be bandlimited, then any modulated wave with single-sided spectrum having that envelope must necessarily occupy a spectral width equal to or greater than twice the bandwidth of the envelope. This result shows clearly that a truly compatible single-sideband system cannot possibly be achieved with the spectral economy of conventional single-sideband.

On the other hand, it is also shown that the bandwidth of the square of the envelope of a single-sideband wave is exactly equal to the spectral width of that wave. The necessary relation that must exist between the envelope and phase is shown to lend itself to circuit instrumentation. A hybrid amplitude- and phase-modulation system is described that has the spectral economy of conventional single-sideband but distortionless reproduction is achieved with a square-law envelope detector. The operations that must be applied to the original intelligence signal in the generation of this hybrid wave are described in detail.

On the Statistical Theory of Optimum Demodulation—J. B. Thomas and E. Wong, *Department of Electrical Engineering, Princeton University, Princeton, N. J.*—The multidimensional demodulation problem is considered from the point of view of maximum likelihood estimation. Correlated signals and noises are treated. This formulation yields a set of two matrix integral equations which must be solved for the optimum estimates.

For amplitude modulation the problem reduces to that of finding a set of time varying filters which are, again, solutions to a matrix integral equation. Special cases such as two-receiver systems, quadrature modulation, and single-sideband have particularly simple representations and are considered in some detail.

For nonlinear modulation, FM, PM, etc., explicit solutions for the optimum estimates of the signals usually cannot be obtained. However, if feedback is allowed, this approach yields the form of the optimum demodulation system for limiting cases.

An inherent assumption that poses difficulties in practice is that the phases and amplitudes of the carriers are known. Practical schemes for estimating phases and amplitudes generally introduce further errors in optimum estimates of the signals.

A Synchronously Switched Binary Communication System—K. K. Clarke, *Department of Electrical Engineering, Polytechnic Institute of Brooklyn, Brooklyn, N. Y.*—A binary communication system having several novel features is considered. The system embodies synchronized switching and coherent detection. These imply the assumption that the receiver is able to maintain synchronization of local oscillators both with the bit rate and with the carrier frequency.

The use of synchronized switching reduces the effects of impulse interference, removes the effects of interbit interference, and increases the signal to noise ratio of the output during the build-up period. A practical signal is then proposed for transmission.

The statistics for the buildup of white noise is double energy circuits are developed. These are coupled with the method of signal energy build-up to derive the behavior of the signal to noise ratio during the build-up period. This behavior is studied both for ideal sine wave bursts, and for practical, band limited signals.

The signal to noise information is combined with proposed detection criteria to derive error probabilities, which are then compared with the ideal error rates obtainable through the use of Fourier Transform criteria filters. Comparisons are again made for both ideal and practical signals.

Certain results from an experimental version of the proposed system are presented and compared with theoretical predictions. On the basis of this comparison a multi-sample detection procedure is proposed which appears to yield a lower error rate than the single, final sample, Fourier Transform filter approach.

On Scattering of Waves by the Infinite Grating of Circular Cylinders—V. Twersky, *Sylvania Electronic Defense Laboratory, Mountain View, Calif.*—The new functional equation for scattering by a grating of relatively arbitrary elements* is specialized to circular cylinders. This specifies the problem in terms of a set of algebraic equations involving only the known scattering coefficients of the isolated circular cylinder, and certain series of elementary functions.† The special results for normal incidence are identically those obtained originally by Ignatowsky;[1] as a check, we also extend his separation of variables procedure to arbitrary angles and transform the results to those obtained directly by our Green's function approach. The equations are then applied to obtain various closed form approximations for both polarizations, for conducting and dielectric cylinders, for arbitrary angles of incidence; and appropriate results are compared with those of Lamb, Gans, Lewin, and Marcuvitz. Simple closed forms for low frequencies (which take account of packing, or coupling, effects up to multipoles of order 2^5) are applied numerically and graphically. We also show that to a first approximation the packing effects for H parallel to the axes merely increase the dipole moment of the isolated circular cylinder: in this range the circular cylinder within the grating is equivalent to a unique isolated elliptic cylinder (*i.e.*, whose size and shape is independent of angle of incidence).

On Scattering of Waves by the Grating of Elliptic Cylinders—J. E. Burke and V. Twersky, *Sylvania Electronic Defense Laboratory, Mountain View, Calif.*—The new functional equation for scattering by a grating of relatively arbitrary elements[2] is applied to elliptic cylinders. This specifies the problem in terms of a set of algebraic equations involving the known scattering cofficients of an isolated elliptic cylinder and certain series of elementary functions. Closed form approximations (which include in general up to quadrupole-quadrupole interactions explicitly) are obtained for both polarizations, for conducting and dielectric cylinders, and for arbitrary angle of incidence. Results are also given for the limiting cases such that the ellipses reduce to lines (*i.e.*, strip elements) parallel or perpendicular to the plane of the grating.

* V. Twersky, IRE TRANS. ON ANTENNAS AND PROPAGATION, vol. AP-4, pp. 330–345; July, 1956; URSI-Michigan Symposium on Electromagnetic Wave Theory, June, 1955.

† V. Twersky, "Elementary Function Representations of Schlömilch Series," Rep. No. EDL-E24, Sylvania Electronic Defense Lab., 1958.

[1] W. v. Ignatowsky, *Ann. Physik*, vol. 44, p. 369; 1914.

[2] V. Twersky, IRE TRANS. ON ANTENNAS AND PROPAGATION, vol. AP-4, pp. 330–345; July, 1956.

Angular Scattering from Random Volume Distribution of Spheres—C. I. Beard and V. Twersky, *Sylvania Electronic Defense Laboratory, Mountain View, Calif.*—In a previous paper* we described the development of a "dynamical macroscopic gas" and a 5-mm scattering range, and gave experimental and theoretical results for the forward, time-averaged, transmitted intensity and phase as functions of the concentration of scatters. (We used 1.36″ diameter styrofoam spheres, and concentrations ranging from 50 to 1000 in a styrofoam "gas container" approximately 10″ by 10″ by 20″). In the present paper we give corresponding data and calculations for the time averaged coherent intensity and phase, and for the corresponding incoherent scattering (differential cross section) as functions of angle of observation and concentration.

On the Theory of Scalar Diffraction and its Application to the Prolate Spheroid†—N. D. Kazarinoff and R. K. Ritt, *Department of Mathematics and the Radiation Laboratory, Department of Electrical Engineering, University of Michigan, Ann Arbor, Mich.*—Scalar scattering of a plane wave by a perfectly reflecting body whose surface is a level surface in a coordinate system in which the scalar wave equation is separable is considered. A general method for the computation of the surface distribution is described. This method reduces the problem of finding the surface distribution to that of evaluating a certain contour integral. The distribution induced on a prolate spheroid by an axially symmetric plane wave is specifically computed. The evaluation by residues of the contour integral, given by the general theory, leads to the expected "creeping wave" interpretation of the residue series. Contrary to expectation, it is found that the attenuation of the "creeping waves" depends upon ωR, where ω is the wave number and R is the radius of curvature at the tip of the spheroid in exactly the same way as the attenuation in the case of the sphere of radius a depends upon ωa. The surface distribution is computed over the entire shadow region including the tip.

Near-Zone Back Scattering from a Large Perfectly Conducting Sphere—V. H. Weston, *Radiation Laboratory, University of Michigan, Ann Arbor, Mich.*—The near-zone problem of back scattering for the case of a plane harmonic wave incident on a perfectly conducting sphere, is considered for the small wavelength region. The effect of considering the observer at a finite distance from the scattering body rather than the usual infinite distance is as follows. The creeping wave terms contribute most in the far field. As the observer approaches the sphere, the creeping wave terms diminish in magnitude. The terms representing the purely reflected field vary slowly with change in distance from the center of the sphere. For very large spheres there is very little difference between being in the far or near field.

The Scattering of Electromagnetic Waves by a Corrugated Sheet—T. B. A. Senior, *Radiation Laboratory, University of Michigan, Ann Arbor, Mich.*—The physical optics method is used to determine the scattering of a plane wave by a perfectly conducting sheet having sinusoidal corrugations. The only approximation is that concerning the current distribution excited on the sheet and the scattered field appears as a spectrum of plane waves whose amplitudes are given by a simple integral expression.

Scattering of a Plane Scalar Wave by Fundamental Surfaces with Mixed Boundary Conditions—H. Unz* and F. B. Sleator,† *Radiation Laboratory, University of Michigan, Ann Arbor, Mich.*—The problem of scattering of an arbitrarily directed scalar incident plane wave by a fundamental surface of orthogonality with general mixed linear boundary conditions is solved for arbitrary separable coordinate system. From the generalized Fredholm integral equation of the second kind derived from Helmholtz solution:

$$u(S) - Ae^{i\vec{k}\cdot\vec{r}}|S + \frac{1}{4\pi}\oint\!\!\oint_{S'}\left[u(S')\frac{\partial G(S,S')}{\partial n'} - G(S,S')\frac{\partial u(S')}{\partial n'}\right]dS \quad (1)$$

a simple linear relationship is found between the unknown coefficients of the expansion of $u(S')$ and of $\partial u(S')/\partial n'$ in terms of the eigenfunctions of the separable coordinate system $(\xi_1; \xi_2; \xi_3)$ over the fundamental surface of orthogonality $\xi_1 - \xi_1$.

By applying the general mixed linear boundary conditions over $\xi_1 - \xi_1$°:

$$au(S') + b\frac{\partial u(S')}{\partial n'} - F(S') \quad (2)$$

where a, b are arbitrary constants and $F(S')$ is a given function, another set of linear relationships between the coefficients is found. From the two sets of linear equations the unknown coefficients may be determined and the scattered field calculated. The above method may be applied to both Laplace and Helmholtz equations and since we require only the free space Green's function expansion, the problem of finding the Green's functions of the first and the second kind is eliminated.

Scattering of Radio Waves on Short Tropospheric Paths Due to Small Scale Refractive Index Fluctuations—A. Adey, W. Heikkila, C. May, and S. Penstone, *Defence Research Telecommunications Establishment, Defence Research Board, Ottawa, Canada*—This paper is a summary of studies of scattering of UHF radio waves on short tropospheric paths, that have been made at DRTE during the past three years. These studies have revealed the existence of weak sidebands on the received signal due to the scattering, with smooth energy spectra extending up to some tens of cycles per second. These scatter contributions place limits on the accuracy of certain applications of radio techniques, such as the accurate measurements of distance.

In an effort to obtain more detailed information on the nature of the irregularities causing the scattering, a beam-swinging experiment on a 3-mile path has been conducted. Marginal sensitivity of the experimental arrangement has limited the accuracy of the results. However, the scattering measurements obtained permit a qualitative understanding of the phenomenon.

Measurement of rapid temperature and refractive index fluctuations have also been made. Spectra extending up to 100 cps and correlation functions up to 50 feet have been determined.

Another Aspect of Antenna-to-Medium Coupling on a Tropo Scatter Circuit—H. Staras, *RCA Laboratories, Princeton, N. J.*—The concept and characteristics of Antenna-to-Medium Coupling loss have already been discussed in the literature in some detail. These earlier analyses show that the coupling loss is not significant unless the beamwidth of the antenna becomes equal to or less than the angular width of the scatter volume as seen from the antenna. An inverse phenomenon occurs if one tries to design an antenna null to protect a given location beyond the horizon; namely, if the width of the null is narrower than the angular width of the scatter volume, the null can be filled in by off-path scattering and the desired protection might not be achieved. This paper outlines the analysis used in evaluating the "filling-in" of the antenna null by off-path scattering and presents curves which should prove useful in obtaining quantitative estimates.

An examination of the interrelation between the scattering process and the free-space antenna pattern reveals that the scattering process averages the free-space antenna pattern, the averaging interval being of the order of several degrees. Thus a qualitative conclusion can be drawn that if it is desired to protect an installation with a 40 db null, this null must be maintained over at least several degrees in order to be effective. A cosine squared pattern is not satisfactory.

Experimental Swept Frequency Tropospheric Scatter Link*—W. E. Landauer, *Airborne Instruments Laboratory, Mineola, N. Y.*—An experimental swept frequency tropospheric scatter link has been established in France with a path length of 190 miles. The transmitter (designed by Compagnie Generale de Telegraphie Sans Fil) sweeps in a nearly linear manner from 3100 to 3600 mc and back to 3100 mc at about 10 cps. The average transmitted power is 250 watts. The receiver and data display (designed by Airborne Instruments Laboratory) sweep in synchronism with the transmitter, the synchronizing signal being derived from the carrier frequency of a broadcast station (Paris-Inter). The receiver is designed so that it tracks the swept signal at levels down to about 4 db above noise level, and after severe fades reacquires signals larger than 6 db above noise level in about 1 to 2 msec. Received signal amplitude is presented as a simultaneous function of frequency and time.

Preliminary data obtained from the link indicate that at all times there are privi-

* C. I. Beard and V. Twersky, "Propagation through random distributions of spheres," WESCON Convention Record, pt. I, pp. 87–100; 1958.

† The research reported in this paper has been sponsored by the Air Force Cambridge Research Center, Air Research and Development Command, Contract AF-19(g04)-1949.

* Elec. Eng. Dept., University of Kansas, Lawrence, Kans.

† Science Dept., Univ. of Puerto Rico Rio-Piedras, Puerto Rico.

* This work was supported under Signa Corps Contract DA-36-039-sc-73276.

leged transmission frequencies present in this band where the transmission is about 10 db above the median for this band.

The preliminary data gathered from the link are described, as well as general design features of the system.

Effective Bandwith of Tropospheric Propagation—L. G. Abraham, *General Electric Research Laboratory, Schenectady, N. Y.*—The popular theory of over-the-horizon, tropospheric propagation, due to Booker and Gordon,* is based on radiowave scattering from a turbulent atmosphere. Because this explanation was essentially a multipath process, it has been suggested by Gordon† that the modulation bandwidth would be limited. A more refined treatment by Staras‡ includes the effects of dielectric constant variations as well as the geometry of the multipath. Interestingly enough, the estimate of effective bandwidth given by Staras is more than a factor of seven smaller than that by Gordon. Recent experiments conducted on a propagation path between Bedford, Mass., and Schenectady, N. Y., seem to agree more closely with the theoretical work of Staras. This is a pertinent investigation since past tropospheric communication systems designs have employed the more optimistic bandwidth figures due to Gordon.

The aforementioned experiments were in the 915 mc band and of the multi-frequency variety. (This radio link was almost 135 miles long. As such, it represented a short, over-the-horizon tropospheric propagation path.) Amplitude cross-correlations were obtained as a function of frequency spacing. At a separation of 2 mc, the correlations had a mean value of about ½. Plans will be outlined as to how information on phase fluctuations of the frequency differences is to be obtained.

Knowledge of the amplitude cross-correlations does not define the effective bandwidth in itself. Possible definitions employing the correlation will be discussed. An alternative approach to the problem will be given in terms of the ratio of envelope amplitudes.[2]

Studies of "Airplane" Doppler Patterns[3]—J. Bradshaw, *General Electric Research Laboratory, Schenectady, N. Y.*—"Airplane" Doppler patterns occur frequently in the envelope record of the CW signal transmitted at 915 mc over the 134 mile path from Bedford, Mass. to Schenectady, N. Y. Assuming the plane flies a straight path at constant velocity, one can remove effects of the plane's motion and determine from the pattern the time variations in the "normal" RF path length. These data indicate that the fading period of phase fluctuations is similar to the period of amplitude fluctuations of signal received by the normal path. Simultaneous records of sidebands transmitted with the 915 mc signal show similar "airplane" patterns. However, the phase fluctuations at a sideband separation of one mc appear to be little correlated.

Carrier-to-Noise Requirements for Teletype Communication via Steady or Fading UHF Carriers—A. D. Watt, E. F. Florman, and R. W. Plush, *National Bureau of Standards, Boulder, Colo.*—A description of FM and SSB multichannel systems loaded with FSK teletype subcarriers is presented, including transmitter peak to average power considerations and bandwidth requirements. Either system will of course be capable of multichannel telephone operation. Steady carrier teletype performance of each system is determined and presented as per cent teletype errors vs carrier to noise.

Amplitude-time characteristics of tropospheric forward scatter carriers are shown by cumulative distributions of amplitude and fade duration, and the effects of propagation path parameters on fading is discussed.

Fading carrier nondiversity performance is calculated for both FM and SSB systems. Following a discussion of diversity types and combining techniques, the calculated system performance with typical diversity schemes is shown.

The results of the calculation of system performance and required transmitter powers over typical paths are compared with measured system performance.

Measured Statistical Characteristics and Teletype Message Error Rates on Tropospheric Systems—E. F. Florman and R. W. Plush, *National Bureau of Standards, Boulder, Colo.*—Measurements were made on two tropospheric systems differing considerably in path length, antenna beamwidths, and frequency. The results are presented in a manner which permits direct comparison of the carrier statistical characteristics of each system; these results are also useful in calculating system performance.

Teletype message error measurements are given in terms of signal-to-noise ratios and bandwidths.

Direction of Arrival of Ionospherically Propagated Radio Waves—E. C. Hayden and E. C. Jordan, *University of Illinois*—Some characteristics of ionospherically-propagated radio waves have been studied, with particular reference to the directions of arrival of the various modes and components, under conditions where multipath propagation is possible. A special double-pulse transmission was used, on a 450 km east-west path, at a frequency of 5155 kc. Receiving equipment was developed to display and measure simultaneously the bearing and polarization of any selected portion of the complex signal, as well as the relative time of arrival of the various components.

Information was obtained on both the long-time and short-time directional fluctuations of signals propagated in both the one-hop nighttime E layer mode and the one-hop F layer mode, including information on the behavior of the individual magneto-ionic components of the latter mode.

The nighttime E layer signals were found to have remarkably stable directional characteristics. The two magneto-ionic components of the F layer mode were next in order of stability, but showed persistent deviations from the great circle path, the ordinary component arriving about 9° to the north, and the extraordinary component about 4° to the south of the great circle path.

Observations were also obtained on widely-deviated auroral and sporadic E modes, both on a narrow aperture system, and on a wide aperture system about 1000 feet in diameter.

The D_1, D_2 Layers and the Absorption of Radio Waves*—G. C. Rumi, *Geophysical Institute, University of Alaska, College, Alaska*—The present study is concerned with the absorption of radio waves in the D region of the ionosphere. Firstly, it is shown that, if the absorbing region is split into two layers, the curve of absorption vs frequency is characterized by a point of inflection. Experimental data on absorption reported in the literature are shown to fit the theoretically derived curve. Secondly, it is shown that, if the absorbing region is composed of two layers, the f_{min} measured with an ionospheric sounder should present a discontinuous behavior. f_{min} plots obtained at College, Alaska, are shown to behave as expected under the hypothesis of two layers in the absorbing region. It is concluded that absorption data lead to an interpretation that the D region is composed of two layers, D_1 and D_2.

A second section of the paper is devoted to an investigation of the electron collision frequency in the D region. The electron collision frequency is directly related to the point of inflection in the absorption vs frequency curve discussed in the first part of the paper, and to the discontinuity presented by the f_{min} plots. Experiment Aurora data (Experiment Aurora is a plurifrequency and pluripath experiment which was carried out in Alaska from 1949 to 1955) are interpreted as an indication that the point of inflection in the absorption vs frequency curve for a high latitude ionosphere is displaced during disturbed periods with respect to quiet periods; such a displacement is equivalent to an increase in the electron collision frequency. A similar displacement is observed in the discontinuity that affects f_{min} plots at College, Alaska, when quiet period and disturbed period data are compared. It is deduced that the electron collison frequency in the D region increases during disturbed periods at auroral latitudes.

VHF Radio-Wave Absorption in Northern Latitudes†—G. C. Reid and H. Leinbach, *Geophysical Institute, University o Alaska, College, Alaska*—Periods of strong radio-wave absorption at a frequency of about 30 mc as observed in northern latitudes are discussed. It has been found that most of these periods can be classified roughly into three distinct types, one of which (Type I) is the normal SID event which accompanies some solar flares. Type II events are almost invariably associated with visible auroral and magnetic activity, and can appear at

* H. G. Booker and W. E. Gordon, PROC. IRE, p. 401; April 1950.
† W. E. Gordon, PROC. IRE, p. 23; January, 1955.
‡ H. Staras, PROC. IRE: October, 1955.
[2] The research reported in this paper has been sponsored by the Electronics Research Directorate of the Air Force Cambridge Research Center, Air Research and Development Command. The publication of this paper does not necessarily constitute approval by the Air Force of the findings or conclusions contained herein.
[3] The research reported in this paper has been sponsored by the Electronics Research Directorate of the Air Force Cambridge Research Center, Air Research and Development Command. The publication of this paper does not necessarily constitute approval by the Air Force of the findings or conclusions contained herein.

* This work was supported by the Geophysics Research Directorate of the Air Force Cambridge Research Center.
† This work is part of the IGY program and is supported by a grant from the National Academy of Sciences.

any point on the earth at which active aurora is visible. Type III events always appear to follow a major solar flare after an interval of a few hours, and may persist for two or three days after the occurrence of the flare. These phenomena appear to be confined to geomagnetic latitudes greater than than 60°. Both Type II and Type III absorption give rise to the "polar blackout" phenomenon when observed at HF.

A brief discussion is given of possible mechanisms causing these events, and Type III absorption is tentatively attributed to the emission of charged particles (ultra-soft primary cosmic rays) from the sun during a solar flare.

Investigations of the Lower Ionosphere Over South Africa—J. A. Fejer* and R. W. Vice, *National Institute of Telecommunications Research, Johannesburg, Union of South Africa*—Investigations of the lower ionosphere by the National Institute of Telecommunications Research at Johannesburg are described.

Three distinct methods were employed. The observation of weak echoes from the *D* region and the measurement of ionospheric wave interaction were used to determine electron densities and collision frequencies for heights below about 85 km while measurements of ionospheric absorption near 2 mc gave information about the same quantities for heights of about 95 km.

The distribution of electron density with height in the *D* region and the dependence of this distribution on the solar zenith angle are tentatively determined. The present results are based on more extensive observations than the results of previous work of the same nature and should therefore be considerably more reliable.

An Experimental Study of Pulse Amplitude Focusing Near the MUF—R. K. Salaman, *National Bureau of Standards, Boulder, Colo.*—The effect on pulse amplitude of focusing near the MUF has been examined experimentally using sweep-frequency transmissions over a 2400-km east-west path. Measurements were made primarily near the F2 MUF in the daytime and at night during summer months. "A-plan" photographs of the received pulse group were made at 25 kc intervals, while the frequency was changed at the rate of about 60 kc. The pulse-width dependence was tested by using pulse widths of 20 and 500 μsec, 20 and 50 μsec or 20 and 100 μsec, on alternate 7½ minute sweeps through the MUF, and by switching between pulse widths of 20 and 100 μsec for alternate samples with a sweep. Because of interference, fading, uncertainty in the calibration of the records (and possibly also to the relatively coarse sampling intervals), an enhancement of less than about 6 db could not be reliably detected. With this qualification, it can be stated that no appreciable focusing was observed for any of the pulse widths used. Some additional records made during one winter night with the sampling interval decreased to 2.5 kc showed a tendency for the amplitude to increase slightly (not more than 6 db) within 50 to 100 kc of the MUF.

* Now at the Radio Phys. Lab., Defence Res. Board, Ottawa, Canada.

F*-Layer Transmissions on Frequencies Above the Conventionally Calculated MUF—W. G. Abel and M. L. Phillips, *Lincoln Laboratory, Massachusetts Institute of Technology*—Transmissions made on frequencies of 18 to 38 mc, over distances from 2150 to 3200 km, where the transmission frequency usually exceeded the conventionally calculated MUF, showed that continuous successful communications could be maintained on such frequencies most of the time. For observation periods of these tests (10 to 20 minutes) comparisons of median, upper, and lower decile values of received field strength indicate approximate log normal distribution for low field strengths and nondirective antennas, and Rayleigh distribution for high field strength and directive antennas. A nearly linear positive correlation was found between received field strength in db and the logarithm of the MUF, with greater change in received field strength (db) with change of log MUF for the higher frequencies. Little change in this slope was observed with distance. Less slope was observed for ionospherically disturbed times than for quiet. Such variations seem compatible with the assumption that received power is proportional to the spatial probability of the existence of reflection conditions near the path midpoint. For these tests, values of standard deviation pertinent to normal distributions of MUF in this region are about 1 to 2 mc and 4 mc respectively, for quiet and disturbed conditions.

Experimental data for this analysis were obtained from a series of measurements conducted jointly by Massachusetts Institute of Technology, Lincoln Laboratory and the Army Signal Research and Development Laboratory (USASRDC). These experiments were reported in part in a paper entitled "Long Distance High Power Radio Propagation at Frequencies Exceeding the MUF," by W. G. Abel and M. L. Phillips, presented at the USRI–IRE Spring Meeting, 1956.

A Method of Computing Ionospheric Focussing of Radio Waves Using Vertical Ionograms—D. B. Muldrew and E. S. Warren, *Defence Research Telecommunications Establishment, Shirley Bay, Ottawa, Canada*—A method is given enabling field intensity distributions due to ionospheric focussing to be calculated from the appropriate vertical ionogram. These are presented as a function of frequency for a given distance and as a function of distance for a given frequency. A number of examples are presented to indicate the peculiar forms often taken by these distributions and to show the relative importance of focussing and absorption. Other factors determining the field intensity distribution are discussed briefly. It is shown that the focussing effect explains the distribution of field intensity of some sweep frequency back scatter signals.

New Geometrical Properties and Their Usefulness for Ionospheric Radio Propagation—K. Toman, *Geophysical Research Directorate, 415 Summer Street, Boston, Mass.*—If one chooses an arbitrary point P inside of two concentric circles other than their center, a normal s upon the diameter, both through P, forms a segment Δs which is one-half of the difference between the secants of both circles. Δs diminishes if s is rotated on P in either sense. For the conditions stated above Δs is a maximum.*

This property applies not only to linear but also to circular and to any arbitrary ray paths through a uniformly stratified ionosphere. If the path length of a ray in passing through the ionosphere is a measure of absorption, maximum absorption is strictly obtained at zero elevation angle Δ. For highly elevated antennas this maximum lies within the observation range. The absorption distribution is found to be symmetrical relative to $\Delta=0$.

The symmetry of a minimum property of the angle of incidence of a ray upon a spherical ionosphere leads to an extension of the MUF-concept for highly elevated antennas.

Impedance, Power and Noise Transformations by Means of the Minkowski Model of Lorentz Space—E. Folke Bolinder, *Electromagnetic Radiation Laboratory, Air Force Cambridge Research Center, Bedford, Mass.*—It is shown how the Minkowski models of two-, three-, and four-dimensional Lorentz space can be used geometrically in transforming impedance, power, and noise quantities through bilateral two-port networks. The transformations constitute direct generalizations of some earlier geometrical methods that have been applied in the complex impedance plane, the complex reflection-coefficient plane, and the Cayley-Klein models of two- and three-dimensional hyperbolic space.

The geometric operations performed in the Minkowski models of the Lorentz spaces are put into analytic form by means of matrix algebra. This standard treatment is compared with a treatment by means of an associative, but noncommutative, algebra called "Clifford Algebra." This elegant and powerful mathematical tool is briefly outlined.

The application of the geometric-analytic theory in network theory is illustrated by means of several numerical examples.

Problems on the Borders of Electromagnetic Theory—W. S. Ament, *U. S. Naval Research Laboratory, Washington 25, D. C.*—We discuss concepts applicable to the mathematical formulation of four problems:

1) Down an ideal transmission line, A transmits messages, B transmits jamming, with powers W_a, W_b. With full knowledge of the jamming statistics, A chooses coding and frequencies to achieve maximum information rate, R. What fixed jamming spectrum S and modulation should B have chosen to minimize R?

2) A lossless filter of mass m slides freely along a closed loosless transmission line of length L containing standing EM waves. The filter is accelerated by radiation pressure and redistributes the frequencies by the Doppler principle. For a given (conserved) total energy, what average wave-spectrum S and kinetic energy $\frac{1}{2}kT$ of the filter hold for the ergodic equilibrium?

* The work reported here was performed at Lincoln Laboratory, a technical center operated by Massachusetts Institute of Technology with the joint support of the Army, Navy and Air Force.

* K. Toman, "A maximum property of two concentric circles." (Accepted for publication by the *Mathematical Gazette*.)

3) A tapered matching section of electrical length L joins lines of impedances Z, Z', the mismatch having power reflection coefficient $R(\omega)$. For assigned signal band $B(\omega) \geq 0$, what is the impedance-taper such that $\int_0^\infty B(\omega)R(\omega)d\omega$ is minimum?

4) A lossless closed rectangular box contains EM standing waves of total energy E. By the slow slice of an ideal knife-edge, two ideal closed boxes are formed, containing total EM standing-wave energy E'. In the general case, what is $E'-E$?

In 1) (and in 2) when $L \to \infty$) S must be the (Planckian) spectrum of emission from a hot matched load.

Steady State Transmission Through a Network Containing a Single Time Varying Element*—C. A. Desoer, *Department of Electrical Engineering, University of California, Berkeley, Calif.*—This paper presents a thorough discussion of the steady state analysis of a linear network, of arbitrary degree of complexity, containing a single periodically varying element. The fundamental and all the side band amplitudes and phases are the unknowns of this problem. This formulation leads to an infinite set of linear algebraic equations. The proposed method of solution makes full use of circuit theoretic ideas, such as impedance matching and tearing apart, and of iterating techniques which are particularly suitable for automatic computation. The proposed method has the additional feature of leading to the amplitude and phase of all side-bands and of getting a bound on the error if the iterations are stopped at any particular point. In particular, it is shown that provided the impedance seen by the time varying element becomes capacitive at high frequencies, the complete solution can be found within an arbitrary accuracy.

The Cumulative Correlator—L. S. Schwarz, *College of Engineering, New York University, N. Y.*—The use of cross-correlators in the detection of radar and communication signals has received increasing prominence in recent years. However, conventional correlators make inefficient use of the available information by always making their decision as to whether the input signals are correlated or uncorrelated after a prescribed correlation time. Cumulative correlators overcome this difficulty by making a decision as soon as sufficient information is accumulated to assure its reliability. Analytic methods analogous to those used in the general random flight problem show the performance of the cumulative correlator to be significantly superior to that of a conventional correlator for almost any input signal statistics. The classical difficulty of sequential observer techniques of this type, namely that occasional excessively long decision times are required, can be avoided by truncating the decision process at only a small cost in performance.

As an example of the benefits obtainable with cumulative correlators, the results of the analysis are applied to a system with fixed total input power and a prescribed minimum usable snr. A reduction in average decision time of as much as 85 per cent is obtained as compared with a conventional correlator of equal reliability.

A Wide-Range Adaptive Frequency Domain Filter for Satellite Tracking—B. E. Keiser, *Missouri Research Laboratories, Inc., St. Louis, Mo.*—The frequency-domain separation of a desired signal from unwanted disturbances has always presented a challenge to the communication engineer. Most frequently the desired signal occupies a portion of the frequency spectrum different from that of the noise, and separation by means of fixed parameter elements is feasible. However, if either the signal or the disturbance is a function with a time-varying spectrum, such as the Doppler return from an earth satellite, and if the long-time spectra of the signal and the disturbance overlap considerably, a more effective separation may be obtained with an input-controlled variable-pass network, here referred to as an adaptive frequency-domain filter.

Although such devices have been described in the literature previously, none has been constructed to cover the 1600:1 frequency range of the unit described here, nor have such wide-range devices been analyzed to any extent.

The paper includes the design criteria for adaptive frequency-domain filters, and in particular, shows how bandwidth, tracking rate, and tracking loop integration time are related to one another.

Methods for preventing adaptive filters from pulling over to an undesired signal are discussed, together with the dynamic response of the filter to a step change in input frequency.

Analysis of Periodic Filters with Stationary Random Inputs—H. Urkowitz, *Philco Research Division, Philco Corporation, Philadelphia, Pa.*—A periodic filter is one whose frequency characteristic is periodic in frequency. Examples are delay-line cancellers for moving-target indication and delay-line sweep integrators. z-transform techniques have proved useful in the analysis and synthesis of these filters when determinate inputs are involved. The determination of the mean square output and other statistical properties with random inputs has heretofore usually involved numerical integration, even for fairly simple cases. This paper presents formulas for computing the mean square value and other statistical properties of the output when the input is a stationary random function. The formulas involve the values of the input auto-correlation function at integral multiples of the basic delay and the sums of product pairs of the coefficients in the z-transform power series. Simple algebraic forms result, making slide-rule computation feasible. The effects of internal noise are also considered by means of the same techniques. Specific formulas are derived for single and double cancellers, velocity-shaped cancellers, and sweep integrators.

An Analysis of the Hybrid Correlator—T. Kaliszewski and W. F. Higgins, *Applied Research Laboratory, Sylvania Electric Products, Inc., Waltham 54, Mass.*—In an effort to simplify and improve the performance of the correlation systems, a new scheme, called a hybrid correlator, which utilizes both coherent and noncoherent detection, was devised.

The hybrid correlator has the advantage over the purely noncoherent type in that it reduces considerably the detector loss, especially in the region of low input snr. The detector loss of the hybrid correlator is somewhat higher, however, than that of a purely coherent type. Still, the over-all performance of the new scheme is improved since by reducing the number of output filters, the probability of false alarm is likewise reduced. In addition to simplicity, the new device may also relax rather severe conditions of time delay compensation and spectral alignment.

Assuming Gaussian statistics for both the input signals and the additive noise, which is assumed to be statistically independent of the signal, the following expression is obtained for the normalized correlation function $\chi(\tau)$:

$$\chi(\tau) = \frac{1}{(1+\sigma_1^2/A_1^2)(1+\sigma_2^2/A_2^2)} \cdot \frac{\sin^2 \pi\alpha\tau}{2\cdot\pi^2\alpha^2\tau^2}.$$

In the above expression, the symbols have the following meaning:

α = bandwidths of signal (and noise) at the input to the multiplier.
τ = time delay of signal (or noise) at the input to Channel 1 and 2.
σ_1^2, σ_2^2 = noise power in Channel 1 and 2 respectively.
A_1^2, A_2^2 = signal power in Channel 1 and 2 respectively.

The function $\chi(\tau)$ is normalized with respect to the product of total power in Channel 1 and 2 and corresponds to the action of AGC in each channel.

In deriving the above expression for $\chi(\tau)$ it was assumed that the correlation function of the signal (or noise) envelope is of the form

$$\sigma_{ij} = \chi_{ij} \frac{\sin \pi\alpha\xi}{\pi\alpha\xi}$$

where χ^{ij} is the coefficient of the cross-correlation ($i \neq j$) and auto-correlation ($i=j$) functions and α is the bandwidth of the pre-multiplication signals, *i.e.*, filters. The frequency function $H(\omega)$ of the post-multiplication was chosen to be

$$\left.\begin{aligned} |H(w)^2| &= 1 \\ &= 0 \end{aligned}\right\} \begin{aligned} &\text{for } -\Delta\omega < \omega < +\Delta\omega \\ &\text{elsewhere.} \end{aligned}$$

The method employed to obtain the output snr consists of deriving the power spectrum of the output of the post-multiplication filter and assuming the input to the squaring device to be still Gaussian. This is quite a reasonable assumption, which simplifies considerably the calculations.*† With the above, the snr at the input to the squaring device is

$$\left(\frac{S}{N}\right)_i = \frac{\alpha}{2\Delta f} \cdot \frac{1}{(1+\sigma_1^2/A_1^2)(1+\sigma_2^2/A_2^2)}$$

* This research was supported by the United States Air Force through the Air Force Office of Scientific Research of the Air Research and Development Command, under Contract No. AF 18(600)-1521.

* R. W. Smith, "The Relative Advantages of Coherent and Incoherent Detectors" Mono. No. 6 of the *IEE;* August 15, 1957.

† S. O. Rice, "Mathematical Theory of Random Noise," Selected Papers on Noise and Stochastic Processes, N. Wax, ed., Dover Press; 1954.

and at the output,

$$\left(\frac{S}{N}\right) = \frac{2\cdot\left(\frac{S}{N}\right)_1\cdot\left(\frac{S}{N}\right)_2\left\{\frac{1}{2}+\frac{\Delta f}{\alpha}\left(1+\frac{\sigma_2^2}{A_1^2}+\frac{\sigma_2^2}{A_2^2}\right)\right\}^2}{2\left(\frac{S}{N}\right)_2+1}.$$

In the above

$$\left(\frac{S}{N}\right)_1 = \frac{\alpha}{2\Delta f_e}\cdot\frac{1}{\left(1+\frac{\sigma_1^2}{A_1^2}\right)\left(1+\frac{\sigma_2^2}{A_2^2}\right)}$$

$$\left(\frac{S}{N}\right)_2 = \frac{\alpha}{2\Delta f}\cdot\frac{1}{\left(1+\frac{\sigma_1^2}{A_1^2}\right)\left(1+\frac{\sigma_2^2}{A_2^2}\right)}$$

where Δf_e is the effective passband of the integrator and (S/N) is the signal-to-noise ratio for conventional coherent correlator.[1]

For $\Delta f \ll \alpha$ and $2(S/N_2) \gg 1$ we can write

$$\left(\frac{S}{N}\right)_0 = .25\left(\frac{S}{N}\right)_1$$

which implies 6 db of loss in the output snr over the conventional coherent correlator (for equal input and output filter bandwidths).

For comparison purposes we plot expression (S/N_0) for the hybrid correlator along with similar results for purely coherent* and noncoherent correlators. The advantages associated with the hybrid correlator over a noncoherent are apparent, especially in the region of low snrs.

Diffraction by an Elliptic Cylinder—B. D. Levy, *Institute of Mathematical Sciences, Division of Electromagnetic Research, New York University, New York City*—The boundary value problem corresponding to a cylindrical wave incident upon an acoustically soft or acoustically hard elliptic cylinder is formulated and solved by the usual separation of variable technique. This solution is then asymptotically expanded for large values of $kh = 2\pi h/\lambda$, where λ is the wavelength, and h is one half the interfocal distance of the generating ellipse of the cylinder. The short wavelength expansion of the field is also obtained by applying the newly developed geometrical diffraction theory, and compared with the asymptotic expansion of the diffracted field. For both the soft and hard cylinders it is shown that the geometrical solution is the leading term of the asymptotic expansion of the exact solution.†

Diffraction by a Prolate Spheroid—J. B. Keller and B. D. Levy, *Institute of Mathematical Sciences, Division of Electromagnetic Research, New York University, N. Y.*—The short wave length asymptotic expansion of the field diffracted by an acoustically soft or acoustically hard prolate spheroid is obtained both analytically and by the geometric theory of diffraction in the shadow of the spheroid. The geometric solution is shown to be in agreement with the leading term of the asymptotic expansion of the exact solution. The solutions so obtained, however, differ from a previous analysis of the same problem. Errors are pointed out in the previous work which lead to the discrepancy in results.

The geometric theory is also used to obtain expressions for the back-scattering cross section of the spheroid in both the scalar and vector (electromagnetic) cases.*

On the Theory of Diffraction by a Composite Cylinder—R. D. Kodis, *Division of Engineering, Brown University, Providence, R. I.*—Formulas are developed for the diffracted field around a perfectly conducting cylinder with a dielectric sleeve of arbitrary thickness. These formulas represent the field due to a unit electric line source parallel to the cylinder (either inside or outside the dielectric sleeve) as a discrete spectrum of radial eigenfunctions. It is shown that if the source is outside the sleeve, the representation of the total field everywhere in this region can be transformed to a linear superposition of two terms. The first of these is the discrete spectrum representation of the diffracted field in the region exterior to a perfectly conducting cylinder with radius equal to the outer radius of the dielectric sleeve; the second term, which involves the inner radius and the properties of the dielectric, is an integral that converges rapidly at high frequencies and permits accurate approximation to the dielectric "correction." The correspondence with optical results in some special cases is shown.

A Line Source on the Interface Between Two Media—V. A. Papadopoulos, *Brown University, Providence, R. I.*—By the assumption of dynamic similarity we are able to solve a number of electromagnetic problems which involve pulse fronts. A method is described for finding the field associated with the sudden setting-up of a line source on the plane interface separating two distinct media.

Halo Effects in the Diffraction of Electromagnetic Waves—J. R. Wait and A. M. Conda, *National Bureau of Standards, Boulder, Colo.*—In many cases, the observed behavior of the light to shadow transition for optical and microwave diffraction can be explained by the Kirchhoff theory. However, when the radius of curvature of the diffracting edge becomes large, the Kirchhoff diffraction pattern appears to be shifted by an amount which depends on polarization, electrical characteristics of the surface, and distances of the source and observer. For a perfectly conducting surface, the effect of the shift amounts to a virtual displacement of the diffracting edge. This case has been investigated by Artmann in 1950, Rice in 1954, Bachynski and Neugebauer in 1958, and Wait and Conda in 1958,* all using different approaches.

In the present paper, an electomagnetic theory of the phenomenon is outlined which removes the restrictions of perfect conductivity and perfect smoothness. (At the same time, certain discrepancies in Artmann's work are resolved). The calculated diffraction patterns clearly illustrate the influence of the electrical properties of the diffracting surface. In certain cases the concept of a virtual displacement of the diffraction edge may still be retained.

The practical significance of this phenomenon is discussed briefly in connection with a) ground wave propagation over a spherical earth near line-of-sight, b) diffraction by hills, c) diffraction of ionospherically reflected radio waves by the earth's bulge, and d) radiation from antennas in the vicinity of convex surfaces.

Fresnel Diffraction by Convex Surfaces—N. A. Logan, *Missile Systems Division, Lockheed Aircraft Corporation, Sunnyvale, Calif.*—The mathematical problem of predicting the Fresnel diffraction effects of a convex surface in the problem of propagation of radio waves around the earth and past curved crests of hills is the same as that of predicting the effects of rounded edges of apertures in optical diffraction experiments. Contributions to the study of the Fraunhofer diffraction fields have been made by White (1922), Fock (1950), Artmann (1950), Rice (1954), Kear (1955), Wu and Rubinow (1955), van de Hulst (1956), Wu (1956), Jones and Whitham (1957), and Neugebauer and Bachynski (1958).

In 1950 Fock indicated how one could treat Fresnel diffraction effects in the propagation of radio waves around the curvature of the earth. The first study of the effects of the curvature of the crests on the Fresnel diffraction in the propagation of radio waves past curved hills was made in 1958 by Neugebauer and Bachynski.

In the present paper the earlier work of Fock is generalized to permit one to study Fresnel diffraction effects subject to the condition,

$$kh > \frac{(ka)^{1/3}}{2} > 1$$

where $k/(2\pi)$ is the wavelength, a is the radius of curvature and h is the distance of the source or receiver from the obstacle. In the earlier work by Fock the results were valid only for

$$ka \gg kh > \frac{(ka)^{1/3}}{2} > 1.$$

These conditions are satisfied in the study made by Fock of propagation around the earth. The classic Fraunhofer results ob-

* P. E. Green, Jr., "The output signal-to-noise ratio of correlation detectors" IRE TRANS. ON INFORMATION THEORY, pp. 10–18; March, 1957.

The authors wish to express their appreciation to Dr. D. B. Brick for suggesting this analysis and helpful discussion and to Dr. L. S. Sheingold, Manager of the Applied Research Laboratory, for permission to publish these results.

† The research reported in this paper has been sponsored by the Electronics Research Directorate of the Air Force Cambridge Research Center, Air Research and Development Command, under Contract No. AF-19(604)-1717.

* The research reported in this paper has been sponsored by the Electronics Research Directorate of the Air Force Cambridge Research Center, Air Research and Development Command, under Contract No. AF-19(604)-1717.

* J. R. Wait and A. M. Conda, "On the Computation of Diffraction Fields for Grazing Angles," Proc. of the Conference on Radio Wave Propagation, Liege, Belgium, October, 1958, Academic Press. (Gives references to earlier work.)

tained by Artmann and Rice require the condition

$$h \gg \frac{a^2}{h}$$

and therefore correspond to the optical problem of diffraction by an edge of a screen or the radio problem of diffraction by rounded hills when the transmitter and receiver are very far from the hill in comparison to the radius of curvature of the crest. In the work of Neugebauer and Bachynski, the condition $h>a$ is implied and therefore the work of these authors is not directly applicable if $h<a$.

The simplicity of the present results can best be appreciated by considering the final results for the case of a cylindrical wave

$$u^i = \sqrt{\frac{2}{\pi kR}}\, e^{i(kR-(\pi/4))}$$

in which case the total field in the presence of the obstacle is given by

$$u = u^i - \left(\frac{ka}{2}\right)^{1/3} \sqrt{\frac{2}{\pi kR_1}} \sqrt{\frac{2}{\pi kR_2}} \cdot e^{ik(R_1+R_2-S)-i(\pi/4)} \left\{ \mu f(-\mu\xi) + g(\xi) - \frac{i}{4\mu^2} g''(\xi) \right\}$$

where

$$f(\alpha) = e^{-i\alpha^2-i(\pi/4)} \int_\alpha^\infty e^{ix^2}\,dx$$

is the Fresnel integral, and $g(\xi)$ is the integral

$$g(\xi) = \frac{e^{i(\pi/4)}}{\sqrt{\pi}} \int_0^\infty e^{i\xi t} \frac{v'(t) - qv(t)}{w_1'(t) - qw_1(t)}\,dt + \frac{e^{-i(\pi/12)}}{\sqrt{\pi}} \int_\Gamma e^{-\xi t/2(\sqrt{3}+i)} \cdot \frac{v'(t) - qe^{i(2\pi/3)}v(t)}{w_2'(t) - qe^{i(2\pi/3)}w_2(t)}\,dt$$

where $v(t)$ and $w(t)$ are Airy functions. Tables of $g(\xi)$ as a function of ξ are presented for $q=0$ (vertically polarized wave) and $q=\infty$ (horizontally polarized wave). The quantities R_1, R_2, and S are defined by Fig 1.

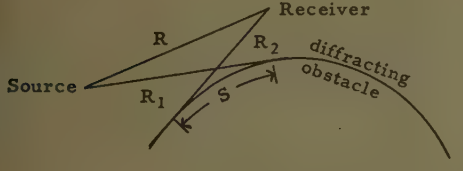

Fig. 1.

The parameters ξ and μ are defined by

$$-\xi = \left(\frac{ka}{2}\right)^{1/3} S,$$

$$\frac{1}{\mu^2} = \left(\frac{ka}{2}\right)^{2/3} \left(\frac{2}{kR_1} + \frac{2}{kR_2}\right)$$

In the shadow region we omit the term u^i, replace S by $(-S')$ and μ by $(-\mu)$.

The terms involving $f(\alpha)$ are those contained in the classic problem of diffraction by a knife edge. All effects of the convex surface are contained in the integral $g(\xi)$.

A Convergent "Farfield" Expansion for Two Dimensional Radiative Wave Functions—S. N. Karp, *New York University, N. Y.*—Radiative solutions of the three dimensional Helmholtz equation

$$\Delta u + k^2 u = 0$$

are known to be representable in the form

$$u = r^{-1} \exp(ikr) F\left(\frac{1}{r}, \theta, \phi\right)$$

with

$$F\left(\frac{1}{r}, \theta, \phi\right) = F_0(\theta, \phi) + \sum_{n=1}^{\infty} F_r(\theta, \phi) r^{-n},$$

where the series is both asymptotic and convergent. In fact $F(1/r,\theta, \phi)$ is known to be an analytic function of $1/r$ for $|r|>a$ provided all the singularities of u are contained in the sphere of radius a. On the other hand, in two dimensions, the corresponding farfield expansion

$$u = r^{-1/2} e^{ikr} \left[f_0(\theta) + \sum_{n=1}^{\infty} f_n(\theta) r^{-n} \right]$$

is asymptotic, but is not convergent. We remedy this defect by showing that any radiative solution of the two dimensional Helmholtz equations can be written in the form

$$u = H_0^{(1)}(kr) E\left(\frac{1}{r}, \theta\right) + H_1^{(1)}(kr) 0\left(\frac{1}{r}, \theta\right),$$

where the functions E and 0 are analytic functions of $1/r$ for $|r|>a$. Here a is the radius of the smallest circle containing the singularities of u. Furthermore we show how to deduce $E(0, \theta)$ $0(0, \theta)$ from the customary farfield datum namely $f_0(I)$. The generalization to n dimensions is given, and the special simplicity of the three dimensional result is explained.

The convergence of the new formula may by useful in converting indoor measurements into farfield patterns.*

On the Characteristics of UHF Signals Reflected from the Moon and Traversing the Auroral Zone†—*Staff Members of Lincoln Laboratory, Massachusetts Institute of Technology, Stanford Research Institute, and Defence Research Telecommunications Establishment, Ottawa, Canada*—An experimental investigation of UHF propagation into outer space through an aurorally disturbed ionosphere was accomplished by utilizing reflections from the moon. This experiment was a cooperative program involving personnel and facilities of the Massachusetts Institute of Technology, Lincoln Laboratory, the Stanford Research Institute, and the Canadian Defence Research Telecommunications Establishment, Defence Research Board.

A 440 mcps CW signal was transmitted to the moon from the SRI site located at the Geophysical Institute, College, Alaska. The reflected signal was received at the DRTE site at Shirley Bay, Ontario, and at the MIT, Lincoln Laboratory Millstone Hill Radar Station, Westford, Mass. The Doppler shift, fading rate and the amplitude of the two orthogonal components of the received signal were measured simultaneously at the receiving sites during the periods that the moon was simultaneously visible at all sites. Observation commenced on September 15, 1958 and continued through the winter of 1959. During this period, data were also obtained on auroral backscatter activity of VHF and UHF, magnetic disturbances, and occurrences of visual aurora at the Alaskan site. The influence of auroral disturbances on the received signal was ascertained by comparing the predicted and measured behavior of the Doppler frequency shift, the change in the polarization angle, and the libration fading rate. The prediction system has been successfully employed in a similar test conducted at low latitudes.* Several occurrences of auroral disturbance of the UHF signals were observed in which the character of both the libration fading rate and the polarization angle was substantially altered. The average amplitude of the signal remained constant during these occurrences. There was no evidence to indicate attenuation of the signal when the transmission path to the moon was well above the horizon.

UHF Radar Propagation Research at Ottawa—B. C. Blevis, *Defence Research Telecommunications Establishment, Ottawa, Canada*—During construction of an auroral radar system for continuous operation on two frequencies in the UHF band, 488 and 944 mc a number of ad hoc experiments have been performed. Preliminary information has been obtained on echo depth in range, spatial distribution of auroral returns, Doppler frequency spectrum, and relative occurrences on the two frequencies. In addition, the radar system has been used to investigate radio echoes from the moon.

The equipment consists of large polar-mounted paraboloidal antennas, low-noise narrow-band receivers, and transmitters having an available peak power of 10 kw. The frequency stability required for the experiments is maintained by the use of crystal standards to determine both the transmitter frequency and the receiver local oscillator injection frequencies.

Auroral echoes have been obtained over a region of ±35° in azimuth about magnetic north and over a range of elevation angles from 0 to 13°, indicating off-orthogonal angles of up to 4° at the 100 km level. Doppler components, measured at 488 mc, of as much as 3 db above noise have been observed at frequencies as far removed as ±4 kc/s from the carrier frequency. Implied east-west velocities from such measurements are of the order of 1 km/second. On one

* The research reported in this paper has been sponsored by the Electronics Research Directorate of the Air Force Cambridge Research Center, Air Research and Development Command, under Contract No. AF 19(604)1717.

† The work reported here was performed at Lincoln Laboratory, a technical center operated by Massachusetts Institute of Technology with the joint support of the Army, Navy and Air Force.

The work at Stanford Research Institute was sponsored by the Rome Air Development Center of the Air Research and Development Command under contract AF 30(602)-1762. This work was performed at the Defence Research Telecommunications Establishment under Project No. PCC D48-38-01-11.

* S. J. Fricker, R. P. Ingalls, W. C. Mason and M. L. Stone, "Comparison of measured and computed values of the rapid fading-rate of ultra high-frequency signals reflected from the moon," *Nature*, vol. 182, pp. 1438–1439; November 22, 1958.

occasion during simultaneous operation on the two frequencies a 10 to 15 db difference in signal amplitude was recorded. This indicates a wavelength dependence for received power of about λ^4 on the assumption that the radar beam is not filled with scattering centers.

The preliminary results obtained with the system are consistent with those of other workers with general agreement on such things as observed east-west drift motions, wavelength dependence of the scattered energy, and aspect sensitivity.

UHF Auroral Investigations*—R. I. Presnell, R. L. Leadabrand, R. B. Dyce, J. C. Schlobohm, and M. R. Berg, *Stanford Research Institute, Menlo Park, Calif.*—The results of radar investigations of the auora at frequencies of 216.4, 398, and 780 mc are presented. The various characteristics of the echoes that have been obtained are:

Range	Heights
Depth in Range	Strength
Bearings	Times of Occurrence
Elevation Angles	Duration of Echoes

Polarization Effects

Two distinct types of echoes have been shown to exist: "discrete" and "diffuse." They differ mainly in that the discrete echoes occur during the nighttime and the diffuse echoes occur during the daytime. In addition, the diffuse echoes arise from a much larger reflecting region than the discrete echoes.

Comparison of the echoes with visual aurora, magnetic activity, earth potentials, 41-mc auroral radar data, and auroral absorption has been made. An indication of the aspect sensitivity of the auoral reflections has been obtained. Crude estimates of the wavelength dependence of reflected echo power have been obtained for the reflections using nonsimultaneous data at three frequencies.

For discrete echoes:

$$\frac{P_{f_1}}{P_{f_2}} \alpha \left(\frac{\lambda_1}{\lambda_2}\right)^{6\pm 2}$$ (assuming the target does not fill the antenna beam).

For diffuse echoes:

$$\frac{P_{f_1}}{P_{f_2}} \alpha \left(\frac{\lambda_1}{\lambda_2}\right)^{4\pm 2}$$ (assuming the target fills the antenna beam).

Doppler spectra of 398-mc auroral reflections were obtained for both discrete and diffuse echoes. With the system sensitivity used, the maximum Doppler shifts are ± 6 kc. In addition to being shifted, the spectrum of the auoral signal is also spread by as much as 3 kc.

Simultaneous Auroral Observations at Two Ultra High Frequencies†—M. L. Stone, R. P. Ingalls, C. H. Dugan, and L. P. Rainville, *Lincoln Laboratory, Massachusetts Institute of Technology*—A dual frequency high powered radar facility designed for high resolution measurements of backscatter from the aurora was installed at the Massachusetts Institute of Technology, Lincoln Laboratory Field Station, South Dartmouth, Mass., in September, 1958. This equipment operates at 425 and 675 mcps and utilizes pulse widths of 6 μsec. The two high powered radars are diplexed into a 60-foot diameter rotatable paraboloidal antenna providing comparable beamwidths at the two frequencies.

A description is given of experimental techniques and preliminary results of the auroral backscatter observed on this system from regions 400 to 900 miles north of the radar location. Some tentative data are presented on the spatial distribution, wavelength dependence, and character of the reflections from aurora.

Simultaneous Auroral Echoes at VHF*—W. A. Flood, *Cornell Aeronautical Laboratory, Buffalo, N. Y.*—Three low power auroral radars, operating at 49.7, 143.5, and 226 mc and using scaled antenna systems have been used to obtain simultaneous auroral echoes. On many occasions the returns at the higher frequencies occur at greater ranges than the returns at 49.7 mc. On the basis of Booker's theory of auroral returns, one would expect that echoes at all three frequencies would maximize at the same range. A possible explanation of these data will be advanced.

Ionospherically Propagated Ground Backscatter at 48.5 mc/s—A. G. McNamara, *National Research Council of Canada, Ottawa, Canada*—A by-product of the IGY auroral radar chain in Canada has been the observation of ionospheric propagation at a frequency and at distances not commonly encountered. The four radar stations at latitudes of 45°, 52°, 64°, and 74°, permit data to be obtained over a great area. The phenomenon has been observed for three years, occurs only in the winter months, and is a daytime effect. The diurnal variation of occurrence at Ottawa and Saskatoon is bimodal, with the peaks occurring in the morning and afternoon. Since the radar utilizes a quasi-rotating antenna system, the propagation direction may be followed. The echoes are observed at ranges of 3000 to 4500 km and are interpreted as single-hop F-layer-propagated ground backscatter. The relatively large signal strength at these ranges suggests that a strong focussing mechanism may be operative.

By correlation with auroral echo occurrence on the same radars, a distinct nonlinear correlation has been found, the occurrence of auroral activity exerting a repressing effect on the ionospheric propagation. Evaluation of the cross correlation function shows the reaction to be greatest in the 24 hours immediately following the auroral echoes, and the reaction falls off rapidly on subsequent days.

Interpretation of Some Backscatter Echoes in Terms of Field-Aligned Irregularities in the F Region—P. Weaver, *Cornell University, Ithaca, N. Y.*—Long range echoes at 14 mc which seem to be explicable in terms of direct backscatter from field aligned irregularities in the F region have been regularly observable in the evening hours from Ithaca, N. Y. The echoes appeared at ranges of 1000 km and beyond, were spread in range, had "auroral fading rates," and seemed to be correlated with the occurrence of "spread F."

Direction finding measurements placed the apparent points of reflection in the F region, with no fast fading echoes coming from azimuths radically different from north.

Contours of off-perpendicular angle with respect to the earth's magnetic field indicated that the observed echoes were coming from an area of near perpendicularity (as low as 9°). Because of refraction in the F region, all northward ray paths from Ithaca which would be "reflected" back to earth are bent into perpendicularity at some point along their trajectory. The assumption is therefore made that the observed echoes arise from backscattering by irregularities in the F region elongated along the earth's magnetic field. Calculations on this basis, allowing for refraction and delay in the F region, lead to echoes at about the observed range.

Measurements of Ionospheric Electron Content by the Lunar Radio Technique—*S. J. Bauer and F. B. Daniels, U. S. Army Signal Research and Development Laboratory, Fort Monmouth, N. J.*—Measurements of the Faraday rotation of lunar radio echoes on a frequency of 151 mc are used to determine the time variation in the total ionospheric electron content. Absolute values of ionospheric electron content are determined from these measurements in conjunction with information on the electron content below the F_2 peak computed from vertical-incidence sounding data. Diurnal, day-to-day, and seasonal variations in the total electron content are presented. The ratio $n_a:n_b$ of the number of electrons above the F_2 peak to that below is found to be in the order of four to five during three summer nights (June) before sunrise and about equal to three after sunrise. For two days in November the ratio $n_a:n_b$ is found to be equal to about three, both before and after sunrise. Possibilities of inferring other characteristics of the upper ionosphere from observed variations in the total electron content are briefly discussed.

* This work was sponsored by Rome Air Development Center under contract AF 30(602)-1762. Cooperation of the staff of the Geophysical Institute of the University of Alaska is gratefully acknowledged.

† The work reported here was performed at the Lincoln Laboratory, a technical center operated by the Massachusetts Institute of Technology with the joint support of the U. S. Army, Navy, and Air Force.

* This work has been performed under Air Force contract AF 19(604)-2454 Geophysical Research Directorate, Air Force Cambridge Research Center.

ANNOUNCEMENT

URSI Fall Meeting
El Cortez Hotel, San Diego, Calif.
October 19, 20, 21, 1959

SUBSCRIBE NOW

TORONTO SYMPOSIUM PROCEEDINGS

The special issue of the PGAP TRANSACTIONS covering the proceedings of the URSI International Electromagnetic Theory Symposium, which was held at the University of Toronto, Canada, June 15–20, 1959, may be ordered now. This issue will be available at the end of the year.

A similar document, the *Proceedings of the Michigan Symposium*, published two years ago, has proven to be a standard reference. The Toronto Symposium consisted of invited papers by carefully selected authors and its proceedings will undoubtedly also command great respect.

It will comprise 450 pages and contain over 50 papers. As an example, it may be noted that the portion of the volume devoted to Surface Waves contains contributions by the following authorities:

Carlos M. Angulo
H. M. Barlow
H. Bremmer
J. Brown
A. L. Cullen
L. B. Felsen
Bernard Friedman
K. Furutsu
George Goubau
A. Hessel
A. E. Karbowiak
A. A. Oliner
Gerhard Piefke
S. A. Schelkunoff
James R. Wait
F. J. Zucker

Send for your copy today. The rates are: PGAP member $8.00; Libraries $12.00; IRE members $12.00; Nonmembers $16.00.

Mr. Delmer C. Ports
Jansky and Bailey
1339 Wisconsin Avenue, N. W.
Washington 7, D. C.

Enclosed is a check in the amount of $_____. Please send me _____ copy copies of the *Proceedings of the 1959 Toronto Symposium.*

Name: _____

Address: _____

_____

Contributors

Wallace L. Anderson (M'58) was born in Adams, N. D., on September 2, 1922. During World War II, he served as an officer in the Airways Communications System of the Air Force. He received the B.S. degree in electrical engineering from the University of North Dakota, Grand Forks, in 1948, and the M.A. degree in physics from Rice Institute, Houston, Tex., in 1957.

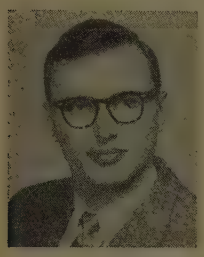

W. L. Anderson

He worked for the McCollum Exploration Company of Houston, Tex., for several years, doing field and research work. He is presently a research associate in the Electrical Engineering Division of the University of New Mexico Experiment Station, and is a doctoral candidate in the Department of Electrical Engineering.

Mr. Anderson is a member of the Society of Exploration Geophysicists, Sigma Tau, and Sigma Xi.

❖

Carlos M. Angulo (S'50–A'52–M'52–SM'56) was born in Pinto (Madrid), Spain, in 1921. He received the degree of Ingeniero de Telecomunicacion from the Escuela Oficial de Telecomunicacion in Madrid, Spain, in 1946; the M.E.E. degree in communication engineering in 1951 and the D.E.E. in electrophysics in 1955, both from the Polytechnic Institute of Brooklyn.

C. M. Angulo

From 1946 to 1948, he worked as an assistant technical director of Transradio Espanola S. A. in Madrid in radio telegraphy and radio telephony. In 1947 he became a research associate of the Spanish Council of Scientific Research in Madrid and worked in electroacoustics.

He joined the Polytechnic Institute of Brooklyn as a research associate in 1949 and as instructor of electrical engineering in 1950; his research during this period was in microwaves. He became an assistant professor of engineering in 1952 and associate professor in 1955 at Brown University, Providence, R. I., where he is at present doing research in antennas and propagation, and teaching. During the summer of 1956, he was a visiting research associate professor at the Control Systems Laboratory of the University of Illinois, working in propagation problems.

Dr. Angulo is a member of Tau Beta Pi, Sigma Xi, and the American Association for the Advancement of Science.

Norman J. Beyers was born in Pana, Illinois, on February 12, 1929. He received the B.S. degree in meteorology and climatology from the University of Washington, Seattle, in 1956.

N. J. Beyers

From 1948 to 1952 he served in the United States Navy and worked in naval aerology. He joined the United States Army, White Sands Signal Agency, in 1956 and has been engaged in research in microwave propagation and atmospheric electricity.

Mr. Beyers is a member of the El Paso Chapter of the American Meteorological Society.

❖

William S. C. Chang (S'56–M'58) was born in Kiangsu, China, on April 4, 1931. He received the B.S. and M.S. degrees in engineering in 1952 and 1953, respectively, from the University of Michigan, Ann Arbor, and the Ph.D. degree in electrical engineering from Brown University, Providence, R.I., in 1957.

W. S. C. Chang

At Brown University he was associated with the theoretical research on dielectric antennas. From 1957 to 1959 he was a lecturer and a research associate at the Stanford Electronic Laboratories, Stanford, Calif., engaged in the research of solid-state masers. At present he is an assistant professor and associate supervisor at the Antenna Laboratory of The Ohio State University, Columbus.

Dr. Chang is a member of Sigma Xi, Tau Beta Pi, and American Physical Society.

❖

Maurice G. Chernin (SM'57) was born in El Paso, Texas, on June 21, 1923. He received the B.S.E.E. degree from the University of Texas, Austin, Texas, in 1944. He received the M.S.E.E. degree from Stanford University, in Stanford, Calif., in 1947. He served in the United States Navy during World War II working primarily in navigation, tactical radar, and attack boats.

M. G. Chernin

He was employed by the Airborne Instrument Laboratory, Inc., from 1947–1951. Since 1952 he has been employed by the Hughes Aircraft Company, Culver City, Calif. His main fields of experience include ground control intercept radar, moving-target indicators, strategic bombing radars, timing circuits, millimeter-wave antenna techniques, and flush-mounted microwave antennas. During the Berlin airlift in 1948, he participated in establishing radar traffic control of allied aircraft.

Mr. Chernin is a member of RESA, the New York Academy of Sciences, and the American Institute of Physics.

❖

W. A. Cumming (S'47–A'48–M'50–SM'57) was born in Detroit, Mich. on July 16, 1926. After receiving the B.S. degree from Queen's University, Kingston, Ontario, Can., in 1947, he joined the staff of the Radio and Electrical Engineering Division of the National Research Council of Canada, Ottawa. Since that time he has been a member of the Microwave Section, working in the field of antenna design and development.

W. A. Cumming

Mr. Cumming is a member of the Professional Institute of the Public Service of Canada, and the Association of Professional Engineers of the Province of Ontario.

❖

B. M. Fannin (A'49–M'55–SM'55) was born June 9, 1922, in Midland, Tex. He received the B.S., M.S., and Ph.D. degrees in electrical engineering from the University of Texas, Austin in 1944, 1947, and 1956, respectively.

B. M. Fannin

From 1944 to 1946 he served in the USNR. He was a research associate in the Electrical Engineering School of Cornell University from 1948 to 1951 and was employed at the Electrical Engineering Research Laboratory of the University of Texas from 1951 to 1956. The next two years he was an associate professor of electrical engineering at the University of New Mexico and assumed the same position at the University of Texas in the fall of 1958.

He has been active in tropospheric propagation research since 1948 and is a member of U.S.A. Commission II of URSI.

Jack M. Fiskin was born in Augusta, Kan., on August 27, 1923. He received the B.A. degree in physical science from Kansas State College, Manhattan, Kans., in 1947 and is working on the M.S. degree in physics at Long Beach State College, Long Beach, Calif.

J. M. Fiskin

From 1948 to 1949 he was an experimental thermodynamicist in the Chemical Engineering Department of the California Institute of Technology. In 1949 he joined the Atomic Energy Department of North American Aviation as a nuclear engineer. Since 1952, he has been a member of the research staff of the Douglas Aircraft Company working in the general field of applied physics.

❖

Raymond F. Goodrich was born in Chicago, Ill., on May 20, 1924. He received the Ph.D. degree in physics from the University of Illinois, Urbana, Ill., in 1954. He joined the University of Michigan, Radiation Laboratory, Ann Arbor, Mich., in September, 1954. He has done research on the scattering matrices associated with the radar cross section of the B-47 and has served as a consultant from the Radiation Laboratory to other projects. He has recently been successful in extending the Russian Physicist Fock's method of solving diffraction problems to three-dimensional bodies and specifically to the cone as a major contribution.

R. F. Goodrich

Dr. Goodrich is a member of the American Physical Society, Sigma Xi, the American Institute of Physics, and the American Association of Physics Teachers.

❖

Fumio Ikegami (M'57) was born on February 17, 1926, in Manchuria. He received the B.S. degree in electrical engineering in 1947, and the D.Sc. degree in engineering in 1956, both from Kyoto University, Kyoto, Japan.

F. Ikegami

From 1947 to 1949 he worked at Radio Wave Section, Radio Wave Bureau, Ministry of Communications, in the field of VHF propagation. From 1949 until 1953 he was engaged in researches of microwave propagation in connection with designing microwave relay links at Radio Wave Section, Electrical Communication Laboratory, Ministry of Electrical Communications. Since 1953 he has continued researches on tropospheric propagation, including radio meteorology, as a senior engineer at Radio Wave Propagation Section, Electrical Communication Laboratory, Nippon Telegraph and Telephone Corporation, Tokyo. Since 1958 he has been an instructor in radio wave propagation at Tokai University, Tokyo.

Dr. Ikegami is a member of the Institute of Electrical Communication Engineers of Japan and the Society of Terrestrial Magnetism and Electricity of Japan.

❖

Ralph E. Kleinman was born in Bronx, N. Y., on July 27, 1929. He received the M.A. degree in mathematics from the University of Michigan, Ann Arbor, Mich., in 1951. He has worked in the Radiation Laboratory since 1951, with the exception of a two year period of service in the U. S. Army. He has made significant contributions to the understanding of the special functions needed in the study of radar cross sections and to the solutions of radiation and scattering problems from simple shapes. His primary interest is in applied mathematics, particularly in electromagnetic theory.

R. E. Kleinman

Mr. Kleinman is on Fulbright leave for the year 1958–59, studying at the University of Delft, The Netherlands. He is a member of the American Mathematical Society.

❖

Tingye Li (S'55–M'58) was born in Nanking, China, on July 7, 1931. He received the B. S. degree in electrical engineering from the University of Witwatersrand, Johannesburg, South Africa, in 1953, and the M.S. and Ph.D. degrees in electrical engineering from Northwestern University, Evanston, Ill., in 1955 and 1958, respectively.

T. Li

While at Northwestern University he was associated with the Microwave Laboratory and worked on microwave antennas and small-diameter helical antennas. Since November, 1957, he has been a member of the technical staff of Bell Telephone Laboratories, Inc., engaged in microwave antenna and propagation studies.

Dr. Li is a member of Sigma Xi and Eta Kappa Nu.

Shiu-Chang Loh (M'58) was born on September 3, 1932, in Shanghai, China. He received the B.S. and Ph.D. degrees in electrical engineering from the University of Leeds, Eng., in 1955 and 1957, respectively.

S. Loh

In 1957, he was awarded a fellowship by the National Research Council of Canada and is now employed in research studies in the Microwave Laboratories in Ottawa.

❖

Andrew L. Maffett received the B.A. degree in mathematics from Gettysburg College, Gettysburg, Pa., in 1943. He received the M.A. degree in mathematics from the University of Michigan, Ann Arbor, Mich., in 1948.

A. L. Maffett

He worked for the University of Michigan, Radiation Laboratory, from 1951–1952, returned to Gettysburg College as Assistant Professor of Mathematics from 1952–1954, and rejoined the Radiation Laboratory in 1954 to 1957. He is now with the Bendix Systems Division, Bendix Aviation Corp., Ann Arbor, Mich.

Mr. Maffett is a member of Sigma Xi and the American Association of University Professors.

❖

Charles E. Phillips (S'53–A'54–M'57) was born in San Jose, Costa Rica, on March 10, 1929. He received the B.E. degree in 1953 and the M.S. degree in 1956, both from Ohio State University, Columbus, and both in electrical engineering.

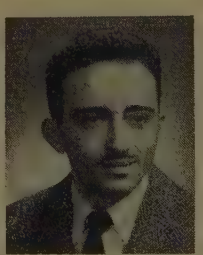

C. E. Phillips

From June, 1953 to January, 1957, he held the position of research associate at the Ohio State University Antenna Laboratory. Since 1957, he has been with the San Diego Division of Convair, where he now holds the position of assistant research group engineer in the Microwave Group. On a part time basis, he has been instructor in the Department of Electrical Engineering at the Ohio State University, and lecturer in physics at San Diego State College.

Mr. Phillips is a member of Tau Beta Pi, Eta Kappa Nu, and an associate member of Sigma Xi.

Robert E. Plummer was born in Fort Wayne, Ind., on September 26, 1928. He served in the United States Navy from 1946–1949, working in radar equipment and instrumentation in Airborne Electronics Maintenance School. In 1953 he received the B.S. degree in electrical engineering from the University of Florida, Gainesville, Fla. He received the M.S. degree in electrical engineering from the University of Southern California, Los Angeles, in 1957. In June, 1953, he joined the technical staff of the Microwave Laboratory, Hughes Aircraft Company, Culver City, Calif. He has since been engaged in antenna research and development, and is presently head of the nose-cone group of the antenna research department.

R. E. Plummer

Mr. Plummer is a member of Phi Kappa Phi, Sigma Tau, and RESA.

❖

Craige E. Schensted received the B.S. degree in physics from the University of Minnesota, Minneapolis, Minn., in 1950. He has taken courses in engineering at the University of Nebraska, Lincoln, and University of Wyoming, Laramie, in 1945 under the Army Specialized Training Program. He joined the Radiation Laboratory in 1951 and did research in applied mathematics, particularly boundary value problems. He transferred to the Computation Group of Willow Run Laboratories in 1958.

C. E. Schensted

❖

Dipak L. Sengupta was born in Bengal, India on January 16, 1931. He received the B.S. degree with honors in physics in 1950 and the M.S. degree in radiophysics and electronics in 1952, both from Calcutta University, India, where he worked as a government of India senior research scholar until the end of September, 1954. During that time he worked on a special type of transmitter and receiver in the VHF range. He received the Ph.D. degree in electrical engineering in November, 1958, from the University of Toronto, Canada, where he also worked as part-time research assistant in the Electrical Engineering Department. He designed and developed the antenna assembly of the radiotelescope which is in operation at the University of Toronto, and from November, 1958 until January, 1959 he worked on high gain antennas.

D. L. Sengupta

He joined the Gordon McKay Lab of Harvard University in February, 1959 where he is presently engaged as a research fellow in electronics in the Division of Applied Physics and Engineering. His principal interests are in field theory, antennas, and microwave theory and technique.

❖

Howard E. Shanks was born in Temple City, Calif., on January 28, 1933. He attended Pasadena City College from 1950–1952, transferring to the California Institute of Technology in Pasadena, where he received the B.S. degree in electrical engineering in 1954. He then joined the Hughes Aircraft Company, Culver City, Calif., under the M.S. Fellowship Program. He received the M.S. degree in physics from the University of California at Los Angeles in 1956.

H. E. Shanks

He has been with the antenna research department at Hughes for the past five years, working on UHF, VHF, antennas, circular aperture antennas, scattering, cross sections, flush-mounted high-speed radar antennas, pattern synthesis methods, and advanced antenna techniques.

Mr. Shanks is a lecturer in electrical engineering at the University of Southern California. He is a member of Tau Beta Pi and RESA.

❖

Keeve M. Siegel (SM'57) was born in New York, N. Y., on January 9, 1923. He received the B.S. degree, and in 1950 the M.S. degree in physics, both from the Renssalaer Polytechnic Institute, Troy, N. Y.

K. M. Siegel

In October, 1948, he joined the Engineering Research Institute, University of Michigan, Ann Arbor, Mich., as a member of the upper atmosphere physics group, subsequently becoming head of the group. Later he was placed in charge of the Theory and Analysis Department at the Institute. In January, 1957, he became head of the Radiation Laboratory. In June, 1957, he was appointed professor of electrical engineering at the University.

He is a member of the New York Academy of Sciences, American Mathematical Society, American Physical Society, American Institute of Physics, Institute of Aeronautical Sciences, AAAS, and Sigma Xi.

William B. Sisco (M'52) was born in Bardstown, Ky., on November 8, 1920. He received the B.S. degree in 1942 and the M.S. degree in 1948, both in electrical engineering, from the University of Kentucky, Lexington. In 1952 he received the Ph.D. degree in electrical engineering from the University of Texas, Austin. While in graduate school, he held teaching fellowships at both the University of Kentucky and University of Texas.

W. B. Sisco

During 1942 to 1946, he served as a civilian engineer and radar officer in the U. S. Army Signal Corps. In the years 1946 and 1948 he was a research scientist at the NACA, Langley Field, Va. Since 1952, he has been employed by the Douglas Aircraft Company as a research engineer and staff consultant in applied physics.

❖

Osamu Tukizi was born in Takamatu, Japan, on December 17, 1915. He received the B.S. degree in physics from the University of Kyusyu in 1944.

O. Tukizi

He then joined the Physical Institute of Radio Waves in Tokyo which was reorganized in 1949 into the Electrical Communication Laboratory, where he has been engaged in the theoretical research of tropospheric propagation.

From July, 1955 to January, 1956, he took an advanced study of propagation at the Laboratoire National de Radioélectricité in France.

Mr. Tukizi is a member of the Physical Society of Japan and the Society of Terrestrial Magnetism and Electricity of Japan

❖

C. P. Wang (S'56) was born in Peiping, China, in 1931. He received the B.S. degree from the National Taiwan University, Republic of China, in 1954 and the M.A. degree from the University of Toronto, Can., in 1956.

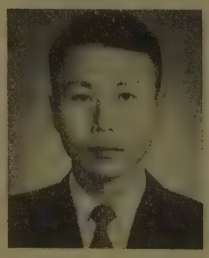

C. P. Wang

During the summer of 1957 he worked for the National Research Council of Canada. Since then he joined the Stanford Electronics Research Laboratories as a research assistant and is currently working towards the Ph.D. degree at Stanford University, Calif.

ELECTRICAL ENGINEERS AND PHYSICISTS

....with an orientation toward antenna design and development ...space communication

Vast new missile and space projects have created outstanding opportunities at Douglas for qualified engineers and physicists with advanced degrees (B.S. also considered). Areas involved are analysis and development in UHF and microwave regions (including communication system analysis and antenna design development), and research in high frequency breakdown and in wave propagation in ionized gases.

For full information write to Mr. C. C. LaVene, Box 621-C, Douglas Aircraft Company, Inc., Santa Monica, California.

DOUGLAS

The most respected name in aircraft, missile and space technology

STAVID

ADVANCES NEW TECHNIQUES IN MICROWAVE ANTENNA DESIGN

When long-range detection devices are required, STAVID is in the vanguard creating and advancing the state-of-the-art. STAVID's continued expansion provides several excellent career opportunities for engineers who wish to contribute and demonstrate technical proficiency in Microwave Antenna Design.

Candidates who wish to be considered on this dynamic team should possess a BSEE with a minimum of 4 years' experience in design and development of UHF-Microwave Radar & Communication Antennas; RF rotary joints and radar receiving and duplexing systems; microwave monopulse antenna systems for military search, guidance and tracking radar applications; lens antennas and radar antennas of parabolic horn, slot array, polyrod and pillbox types.

Investigate these exciting career opportunities immediately by sending a complete resume in confidence to:

Mr. J. R. Clovis,
Personnel Dept. M,

STAVID ENGINEERING, INC.

U. S. Highway 22 Plainfield, N.J.

For Information Concerning

ADVERTISING RATES

Contact

MR. DELMER C. PORTS

Jansky and Bailey, Inc.

1339 Wisconsin Ave., N.W.

Washington 7, D. C.

Telephone: Federal 3-4800

FILED IN STACKS

INSTITUTIONAL LISTINGS

The IRE Professional Group on Antennas and Propagation is grateful for the assistance given by the firms listed below, and invites application for Institutional Listing from other firms interested in the field of Antennas and Propagation.

ANDREW CORPORATION, 363 E. 75th St., Chicago 19, Ill.
Antennas, Antenna Systems, Transmission Lines, Development and Production.

ANTLAB, INC., 6330 Proprietors Rd., Worthington, Ohio
Antenna Pattern Range Systems—Recorders & Mounts.

BLAINE ELECTRONETICS, INC., 14757 Keswick St., Van Nuys, Calif.
Antennas, Paraboloids, Scale Models, Antenna Radiation Pattern Measurement Towers.

COMMUNICATION PRODUCTS COMPANY, INC., Marlboro, N. J.
Fixed Station and Vehicular Antennas and Associated Cable Systems

DEVELOPMENTAL ENGINEERING CORP., 1001 Conn. Ave. N.W., Washington, D. C. and Leesburg, Va.
Research, Development, Installation of Antennas and Antenna Equipment for Super Power Stations.

DORNE AND MARGOLIN, INC., 29 New York Ave., Westbury, L. I., N. Y.
Research, Development, and Manufacture of Airborne Antennas and Systems

THE GABRIEL LABORATORIES, Div. of the Gabriel Co., 135 Crescent Road, Needham Heights 94, Mass.
Research and Development of Antenna Equipment for Government and Industry.

HUGHES AIRCRAFT COMPANY, Culver City, Calif.
Research, Development, Mfr.: Radar, Missiles, Antennas, Radomes, Tubes, Solid State Physics, Computers.

I-T-E CIRCUIT BREAKER CO., Special Products Div., 601 E. Erie Ave., Philadelphia 34, Pa.
Design, Development and Manufacture of Antennas, and Related Equipment.

JANSKY & BAILEY, INC., 1339 Wisconsin Ave. N.W., Washington 7, D. C.
Radio & Electronic Engineering; Antenna Research & Propagation Measurements; Systems Design & Evaluation.

MARK PRODUCTS CO., 6412 W. Lincoln Ave., Morton Grove, Ill.
Multi Element Grid Parabolas, Antennas for Two-Way Communications, R & D.

THE RAMO-WOOLDRIDGE CORPORATION, Los Angeles 45, Calif.

TRANSCO PRODUCTS, INC., 12210 Nebraska Ave., Los Angeles 25, Calif.
Res., Design, Dev., & Mfr. of Antenna Systems & Components for Missile, Aircraft & Ground Installations.

WEINSCHEL ENGINEERING COMPANY, INC., Kensington, Md.
Antenna Pattern Receivers; Bolometer Amplifiers; Modulated Microwave Sources; Insertion Loss Measuring Systems

WHEELER LABORATORIES, INC., 122 Cutter Mill Road, Great Neck, N. Y.
Consulting Services, Research and Development, Microwave Antennas and Waveguide Components.

WIND TURBINE COMPANY, West Chester, Pa.
Complete Antenna Systems and Towers

The charge for an Institutional Listing is $25.00 per issue or $75.00 for four consecutive issues. Application may be made to the Technical Secretary, The Institute of Radio Engineers, 1 East 79th Street, New York 21, N. Y.